Floating Sensor Arrays for Wave Measurement

Brian Gordon Sellar

THE UNIVERSITY
of EDINBURGH

A thesis submitted for the degree of Doctor of Philosophy

May 2013

Abstract

This research aims to improve the quality and availability of wave field information available to the developers and operators of wave energy converters (WECs) to aid in their design and operation. Applications relate to improving performance in varying wave climates, reducing extreme and fatigue-causing loads and reducing risk in critical marine operations through providing access to array-based and near-real-time surface elevation information.

This Thesis describes a design process, leading from conceptual design, through to critical review. Design, assembly, commissioning and testing of multiple novel sensors involved technical work spanning mechanical, electrical, communications, signal processing and manufacturing disciplines. This required project management of areas including budget, procurement, IPR and programme scheduling.

Three experimental procedures are outlined which were used to test the feasibility of a novel instrument conceived to meet the potential requirement for improved surface elevation data in large hydraulic test facilities and at sea. The first involves a method in the laboratory to assess the physical ("mechanical-only") surface tracking ability of long, floating, ribbon-like sensor elements that are aware of their position in two dimensions. Showing mean errors in wave height tracking of 6% and wave period tracking errors of 0.1% in irregular waves, across the widest available test range, results from surface tracking tests justify the subsequent testing of actual sensor implementations. Two approaches are taken: the first involves the modification and testing of a sensor technology comprising position-aware optical fibres with the second approach involving the design, fabrication and testing of floating sensors based on micro-electro-mechanical (MEM) sensor technology.

Whilst wave period errors (individual time domain wave-by-wave comparisons) remain low for the optical fibre system at approximately 1% with standard deviations of approximately 10%, wave height errors are significant. Mean wave height error (depending on processing technique) range from -6% to 4% with standard deviations of 18% to 25% across irregular sea states. Performance is shown to be affected by wave steepness with wave trough tracking showing higher performance compared to wave crest tracking.

Preliminary testing of the MEM-based sensor ribbons (in array form capable of measuring position in three dimensions) show wave height errors in regular waves to be on average 1.3% with standard deviations of relative error of 8.4%. Wave period errors and their standard deviations were below 1%. In irregular waves, mean significant wave height is under-predicted, across a range of directional seas, by 3% with standard deviation, across the tests and individual ribbons forming the array, of 7.5%. Peak wave period is under-predicted by 1.3% with standard deviation of 2.2%. Time domain statistics are not reported but it is expected that - as with the optical fibre system - performance degradation would occur when moving to irregular seas.

Wave height error magnitude excludes the application of the developed sensors from small-scale tank testing where mm levels of accuracy are required. With further work, however, sensors based on this concept could potentially be used in larger scales and at sea where spatial wave field information is necessary, where wave period is critical and where other sensor techniques require baseline data.

Declaration

I declare that this thesis was composed by myself and that the work contained therein is my own, except where explicitly stated otherwise in the text.

(*Brian G Sellar*)

Acknowledgements

Thank you to my colleagues at the Institute for Energy Systems for their support and to the wider team of the School of Engineering and in particular the mechanical workshop and IT and finance departments.

Thank you Measurand Inc. of New Brunswick, Canada.

I also appreciate the advice, assistance and good company of the academic staff and researchers who enabled tank testing at Aalborg University, the GWK facility, Hannover and Heriot-Watt University.

The support of the EPSRC for both indirect funding of this PhD thesis and direct funding of a related project is gratefully acknowledged.

Thanks go to my supervisors, Tom Bruce and Robin Wallace, for allowing me the freedom to try things...

And to the following family and friends for their various encouragements, threats and incentives to finish things: Lauren, Mum, Dad, Karen & Jamie, Hazel & Alan, Eileen & Allan Tutty, Tom Davey and all the boys from home. Thank you.

Contents

List of Figures

List of Tables

Nomenclature

η surface elevation. The height of the free water surface above or below (signified by a negative number) a specified mean water level. [m]

λ wavelength. [m]

ω angular frequency. [radian s^{-1}]

ρ density of water. [kgm^{-3}]

σ_{1p} standard deviation of the directional distribution, the directional spreading (at the peak of the spectrum). [degrees]

θ_{1p} mean wave direction (at the peak of the spectrum). [degrees]

GW gigawatt. Unit of electric power equal to one billion watts.

GWh gigawatt hours. Unit of electrical energy.

k wave number. [m^{-1}]

kW kilowatt. Unit of electric power equal to one thousand watts.

kWh kilowatt hours. Unit of electrical energy.

A wave amplitude. Height of wave from MWL to wave crest. [m]

AMF filtering technique. Arbitrary Magnitude/Response filtering.

b bend. Interchangeable with "curvature" and the inverse of the equivalent radius of curvature. [radian m^{-1}]

BF filtering technique. Basic filtering with look up table.

d water depth. [m]

$D(f,\theta)$ angular spreading function.

EU European Union.

fps frames per second. Number of images recorded by a video camera in one second.

g acceleration due to gravity. [ms^{-2}]

Gb gigabyte. Unit of data storage capacity equal to one billion bytes.

H wave height. [m]

H_{m0} significant wave height calculated from zeroth spectral moment. [m]

H_m time domain mean wave height. [m]

H_s significant wave height. [m]

Hz Hertz. Frequency/number of cycles per second. [Hz]

Mb megabyte. Unit of data storage capacity equal to one million bytes.

MWL mean water level. Mean water level in the absence of waves.

PTO power take off.

R correlation coefficient.

r radius of curvature. [m $radian^{-1}$]

R^2 correlation coefficient squared.

RT1 filtering technique. Real time filtering with on-the-fly adjustable filter weights.

RT2 filtering technique. Real time filtering with look up table.

S wave steepness. H / λ.

s arc length. [m]

$S(\omega)$ spectral variance density. [m^2s]

$S(f)$ spectral variance density in terms of frequency. [m^2s]

$S(f,\theta)$ directional spectral density. [m^2s]

Std standard deviation.

T wave period. The time it takes, at a fixed position, for two wave peaks to pass that position. [s]

T_e wave energy period. [s]

T_m time domain mean wave period. [s]

T_p wave peak period. [s]

WEC wave energy converter.

WG wire resistance wave gauge.

CHAPTER 1

Introduction

1.1 Research Motivation

This thesis has been funded and produced because of increasing international focus on Marine Renewable Energy. The marine environment may offer solutions to some of the major challenges we face during this century. These include the consequences of increasingly expensive energy supply (economically, environmentally and politically) and increasing demand for minerals, fresh water and food. If we are to turn to the seas and invest in developing technologies to exploit them we will need to increase knowledge of this frontier, creating infrastructure and tools to facilitate exploitation and to monitor the effects of our efforts.

The aim of this research is to increase knowledge of the dynamics of water waves by designing and testing a sensor that can provide wave field information at unprecedented levels of detail over a wide area. This wave field information could have impact on the fields of oceanography and offshore renewable energy by offering opportunities to either benchmark or improve existing sensor technologies or by providing information that can be used to design better technological solutions for the extraction of useable energy from the seas.

1.2 Research Objectives

Experiments were conducted at the University of Edinburgh, Aalborg University, Denmark, Heriot-Watt University, Edinburgh and the GWK facility, Germany to address the following specific research objectives:

1. To test the ability of a buoyant ribbon-like or rope-like element to mechanically track the water/air interface.
2. To define confidence levels for these element's tracking abilities across a range of sea states
3. To construct an active sensor suitable for performance testing in two dimensions in the Edinburgh 20 metre Flume (*approx* 1:50 scale).
4. To construct an active sensor to allow performance testing in larger wave flumes and basins to study the scalability of the system.
5. To construct an active sensor array at a scale suitable to test the performance in *three* dimensions.
6. To highlight which design and deployment parameters most influence sensor performance.

This work is structured around three central sections. The first concerns the design of an experimental procedure to assess the ability of floating ribbon-like structures to track the water/air interface with the second and third sections investigating two implementations of the concept. These core sections form Chapters 4, 5 and 6 as shown in the thesis roadmap in figure 1.1.

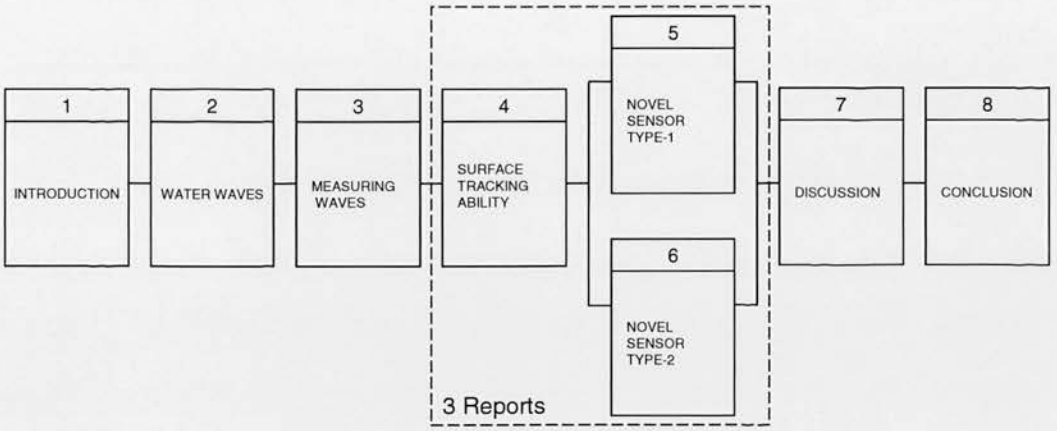

Figure 1.1. Thesis chapter structure.

1.2.1 Applications in Measuring and Modelling the Marine Environment

Traditional methods of measuring the wave field at sea have relied on human observation or buoys equipped with motion sensors and telemetry equipment. Whilst these provide information suitable for categorising weather conditions they were never designed to provide the level of detail that may be required as our uses of the seas evolve. Over the last decade satellite measurements of the sea surface have provided significantly improved global descriptions but at a spatial resolution that cannot provide information on specific locations and in particular are limited when their orbits pass near coastal regions - where much of our new marine activity may occur.

If a sensor can be developed that can rapidly measure surface elevation across a wide area our ability to reliably describe the useable energy content will improve and additionally, new studies of wave field dynamics can be conducted. At a smaller scale this sensor could be used in controlled environments (i.e., large scale hydraulic test facilities) to study wave dynamics and may assist investigation of wave group behaviour, wave coherence versus wave direction, amplitude, frequency, roughness etc., with further uses in reflection analysis. If reflections can be confidently defined

then control strategies can be employed to mitigate their effects making for more reliable and efficient hydraulic testing of coastal structures and marine machines.

1.2.2 Applications in Wave Energy Converter Control

Harnessing the sea's energy by means of wave energy conversion or tidal stream conversion for example would reduce our reliance on imported fossil fuels and reduce CO_2 emissions. Machines produced to operate in the marine environment will be designed for a specific deployment location. With better advanced knowledge of this location the machine design will be better optimised to operate around the mean condition and to cope with the predicted extremes. With continuous knowledge of this location's wave field the now operating machine can tune its behaviour, in any number of ways, in response to the inputs received. Major benefits are expected in terms of economic viability (encompassing costs of manufacture, deployment, operation, maintenance and price per unit electricity) when more is known about the deployment environment. This research aims to improve knowledge of this environment.

1.2.3 Summary of Applications

- investigation of wave shape
  - effects on structures
  - current/wave interactions
  - wave group dynamics
- control strategies for wave energy converters
- deterministic sea wave prediction
  - reduce risk in marine operations near offshore structures
- reflection analysis in large scale hydraulic facilities
- investigation of wave directionality

1.3 Wave Energy

Marine Renewable Energy: A Brief Introduction

The demand for energy both globally and within the UK continues to rise. This growing need combined with dwindling hydrocarbon supplies from the British sector of the North Sea tipped the UK into becoming a net importer of gas in 2004 [1] (ahead of government predictions) and soon, a net importer of oil [1, 2]. In the four years of forming this thesis, energy issues, which form part of the climate change debate, have soared up the political agenda and in some form are rarely out of the media. Within this rapidly evolving sphere new elements continue to develop; security of supply is now a major, if not top, priority for policy makers globally, surmounting the previous theme of CO_2 emission reduction. This has now been seen on several occasions in Europe where the relationships and actions of EU members, the major gas producers and subsequent transit countries affect energy policy decisions.

Energy produced from technologies deployed at sea may help meet these two challenges. A diversified portfolio of energy sources including wave, tidal and offshore wind would significantly improve the UK's exposure to risk whilst providing low CO_2 electricity with the lower priority (at present) welcomed side-effect of securing industrial jobs in traditionally under performing geographical areas. [2]

There are many proposed energy conversion mechanisms for producing useful power from the seas. These include taking advantage of salinity and temperature gradients, using the momentum of tidal streams or the potential energy of tidal elevation changes and coupling an electrical generator to the motions of the sea surface itself. This latter category, hereby labelled *Wave Energy*, is the mechanism considered in this work.

[1] Depending on pricing, extraction rates and demand the UK oscillates between net importer and net exporter although the trend is towards a net importer.

[2] Since this thesis commenced a severe global recession has occurred which may again change the prioritisation of energy and industrial policy.

1.3.1 Wave Energy: Advantages and Opportunities

The seas around the UK and particularly in the west coast of Scotland have long been proclaimed as having one of the best wave energy resources in the world, [3, 4] and there has been significant research into methods of converting this energy into electricity for the Grid [5, 6]. Approximately 10% of Europe's wave power, $14GW$, is located off Scotland's coasts [7, 8]. It is estimated that Wave and tidal stream energy together could meet 15% to 20% of current UK electricity demand [9]. A recent report published by a group established to evaluate the potential of UK offshore renewable projects points to the creation of 145,000 new UK jobs with between 2 to 5 GW of installed capacity predicted by 2050 [10]. [3]

It is well known that it is increasingly difficult to achieve planning consent to build industrial equipment and execute civil engineering programmes (power stations, wind turbines, power lines, pipelines) on land (particularly in small countries like the UK where the stakeholder density is large)[11, 12]. Offshore plant could potentially meet less opposition and will have lower environmental impact than traditional electricity generation technologies [13, 9, 14, 15].

1.3.2 Wave Energy: Challenges

Ocean waves are slow oscillatory systems which vary in amplitude, frequency and power. In the context of electricity generating WECs this input must be coupled to electrical generators that are legally obliged to provide electrical power within regulated amplitude and frequency tolerances. This is an engineering challenge and may be tackled via, for example, novel designs of generator including linear designs, power conditioning electronics or intelligent control of an individual WEC, or by extension, realising a global averaging effect by using an array of WECs (and possibly intelligently controlling each individual). In addition, ocean waves are created by winds blowing in different directions at different locations and at different times. Being able to operate in and take energy from these multi-directional, multi-frequency sea states is another facet to the engineering challenge and has consequences on

[3] Modest scenario (2GW) and mid-level scenario (5GW).

WEC geometry, array design and importantly mooring design [16].

With the high costs associated with vessels, equipment, insurance, personnel and developing and maintaining HSE [4] commitments, designing devices to require as minimal maintenance as possible will be needed for economic viability. However, whilst steps can be taken at the design stage experience of deployment, operation and recovery will be needed to improve designs iteratively over the time span of years. This applies to installation techniques and design as well as recovery / decommissioning.

Again with economic viability in mind, any deployed devices will need to operate for a given period through greatly varying weather conditions. There will be an inevitable premium paid in designing in safety factors in constructing a device capable of surviving the environmental rigours of the ocean.

Areas of electrical use have grown up around coal mines and rivers. Unfortunately the wind, wave and tidal resource resides/frequents locations hundreds of miles away from the areas where coal was found in the last two centuries and hence population and industrial centres. Planning permission issues and moreover the cost of fabricating, installing and integrating new electricity carrying cables mean that intervention will be required at a governmental level [12, 17, 18, 19].

Recently on a continental level, EU power companies, funding councils and governments have been proposing a connected "Super-Grid" which would allow renewably generated power to flow around the North Sea (and in the future further afield to Middle-East and North Africa), reducing the cost to individual stake holders whilst offsetting variability [20].

In addition, supply chain issues will effect the contribution Renewables make to the UK economy and should not be underestimated [21, 22].

Wave power is a variable resource. In order for the grid to viably cope with wave climates that change both temporally and spatially, some form of back up power generation - either external to the wave energy system or internally - is required. The timescales for this storage depends on the costs to the generator of intermittency. The

[4] Health and Safety and Environment

generator could be causing problems (and thus receiving charges) to the network with perturbations of the order of seconds or the network as a whole could be unable to meet demand for a period of days during unusually high demand and low renewable input.

Another consequence of the variability of the ocean is that a system design must be able to cope with forces and motions arising from waves many times more energetic than the mean, around which the device's power generation is optimal. This adds to the engineering challenge and the cost.

Significantly, not enough is known about the environment in which the renewable devices will reside. Increasing our knowledge of and quantifying the *resource* has been a major focus in the most prominent and recent research consortia including SuperGen-Marine I and II, the UKERC's *Roadmap* and the EU FP7 Equimar project [23, 24, 25]. Securing finance for marine renewable energy plants will require good estimates of the expected energy yield and the yield fluctuations over the lifetime of the projects [26].

> There are still many knowledge gaps for floating devices, these include knowledge of the ways waves behave and how the resource is characterised as well as on the magnitude of the loads caused by the marine environment.
>
> Report by the European Thematic Network on Wave Energy, 2003 [27].

1.3.3 Addressing Challenges through the Development of an Improved Wave Sensor

This work hopes to test the ability of a new type of sensor to assist with this challenge to the industry. By gaining more knowledge of the operating environment both investors and designers can make better project decisions, improving the likelihood of technical success and the magnitude of economic success.

1.4 WEC Design, Optimisation and Control

> In order for an oscillating system to be a good wave absorber it should be a good wave generator.
>
> J. Falnes

1.4.1 WECs Require Control Strategies

Wave Energy Converters will have a frequency of oscillation at which they are resonant. When this frequency is matched by the driving frequency of incident waves the device's output power will be at a maximum. WEC design including geometry and power take off system will most likely be based around the most dominant wave frequency at the deployment site but for the majority of the time the resonant condition will not be met. As real seas comprise many different frequencies and exhibit non-linearity (as opposed to nice simple sine waves) controlling WEC mechanical behaviour in response to these varying disturbances will be necessary in order to maintain sufficient output power. The increase in efficiency or economic viability resulting from control strategies is as yet unknown. It has been estimated that improvements will be significant, [28, 29], with one author suggesting 1.5 to 3 times increased average energy production [30]. This estimated range has been corroborated with performance gains in the range of 100-330% found in a recent review of a variety of types of control strategies [31].

Survivability and Performance

It is easy to imagine the benefit of advanced prior knowledge of the wave field when considering survivability and reduced fatigue loading. Instructions based on this information could be delivered to the WEC to take actions to reduce the risk of damage, possibly increasing damping of the PTO or changing the relationship with the mooring system or, for example, self-submerging by the use of using buoyancy/ballast tanks.

Control Strategies

Wave field information will likely improve, and in some cases enable, WEC control. Early wave energy research highlighted the potential for control strategy implementation. It is present in the original works of Budal in Trondheim, Norway and Salter in Edinburgh, UK and has continued to be an integral part of the research field [28, 32, 29]. For a more thorough introduction to WEC control strategies, their histories and their implementation good starting places can be found in the publications of the Edinburgh Wave Power Project and the research of Falnes, Budal and Hals, Barbarit and Clement, Korde, and a recent review-led PhD Thesis on these topics by Price [16, 30, 33, 34, 35, 36, 37, 38, 39, 40, 41, 42]. A brief history of wave power and review of some of the leading control strategies that could make wave power viable can be found in Appendix C.

A Note on Causality

It has been shown that the response of a WEC to multi-frequency waves is non causal and that information of the future wave state is needed to properly predict the interactions [43]. However, the impact of acausality can be diminished by the fact that moving upstream in a wave field can be thought of as moving ahead in time, i.e., the experienced perturbation is the result of a wave that can be measured some distance ahead/upstream that moves with a known velocity. Provided that at the frequencies under investigation the coherence length of the wave field is sufficient then the disturbance upstream at some starting point in time should be similar in form to the disturbance downstream some distance away at a time in the future. Here downstream is used loosely to imply that a WEC lies behind a measuring point and in the mean direction of the wave field [40, 44].

1.4.2 Control Strategy in the Context of this Work

It is the author's opinion that optimal control is, at present, a distraction since a WEC exposed to any type of wave other than a perfectly linear, sinusoidal wave (which does not exist in the laboratory let alone the outside world) and in the presence of imperfect information relating to wave field, body motion and other physical quantities, will not behave in the way predicted by a model.

Indeed, more pragmatic approaches are emerging concentrating on deployment, operation and final cost per kw as opposed to maximum efficiencies and maximum theoretical controllability [45]. And the design of the Pelamis, the industry leading design puts survivability as the primary design goal [46].

> The device must be designed with survivability as the key objective, then effective ways of improving power capture must be found.
>
> Richard Yemm, Pelamis Wave Power Ltd.

1.4.3 Control Strategies Require Improved Wave Field Measurements

Designing a sensor array that can provide device designers and operators with improved information on the wave field in which their devices will operate could prove one stage in the process of continued improvement of WEC technology and associated control strategies.

1.5 Existing Measurement Techniques for the Provision of High Resolution Surface Elevation Data

With the predicted demand for surface elevation information in the Wave Energy sector identified, a survey of existing measurement techniques was carried out. Discussed more fully in Chapter 3, a brief summary is outlined below. Key limitations of the technology - specifically related to Wave Energy - are highlighted in bold.

Table 1.1. Summary of advantages and disadvantages of leading candidate technologies.

Wave Buoy	
Advantages	Established technology Calibration techniques well understood If correctly installed and calibrated provides good time-elevation data and statistical wave data. Above surface telemetry possible Can be deployed for long durations (years with servicing)
Disadvantages	Reduced reliability in steep waves Careful mooring consideration required Prone to storm damage, vessels, vandalism Not a fixed point (Lagrangian measurement). Buoy moves across and around waves as well as moving in heave. **Single point measurement - no spatial information** (steepness, shape, non-linearity), no wave evolution, difficult to infer directional information particularly in multi-modal sea states.
Bottom Mounted ADCP	
Advantages	Being located on the seabed can reduce likelihood of damage (in some cases) Array based measurement allows directionality of waves to be measured Good measurement of co-located currents which can be incorporated into wave measurement analysis Wide range of emitted frequencies to suit deep water to shallow water applications
Disadvantages	**Difficult to deploy for long duration** (at high frequencies required and as required for wave-field monitoring).(1 month is typical deployment) **Below surface telemetry required** (low bandwidth, increased expense) and frequent marine operations: retrievals and deployments **Depth attenuation** of pressure signal used in wave measurement algorithms Require heavy (up to 3000kg) seabed frames in energetic sites or being anchored to seabed in surf zone. Depth of deployment sets maximum resolvable wave lengths and directional resolution (beam spread angles at surface plus pressure gauge attenuation).
X-Band Radar	
Advantages	Not a single point measurement. Grid of data covering 100's metres to kms is possible at 10m-100m grid spacing. Good statistical wave properties achievable. Non-contact with the marine environment
Disadvantages	Emerging technology. Further trials required and are ongoing. Permit likely required for use (EM Spectrum, siting of radar tower etc.) **Individual wave-by-wave analysis more challenging.** Site specific filters required. **Complex calibration** and configuration at each site and when changing sampled region. **Poor temporal resolution** ($\approx$2.5s)

1.6 Thesis Roadmap

1.6.1 Introduction, Motivation and Existing Technologies

Chapter one served as an introduction to the field and to highlight the motivation for this work. Chapter two, *The Environment*, introduces water waves with a brief outline of theory and relevant physical properties before discussing more realistic and often encountered waves at sea and the commonly used methods of parameterising their characteristics. Chapter three, *Measuring the environment*, discusses the wide variety of measurement techniques used to characterise water waves both at sea and in hydraulic laboratories.

1.6.2 Meeting Research Objectives: Three Reports

Chapters four, five and six are near stand-alone reports. Chapter four, *Surface Tracking of a Ribbon*, describes the experiments conducted to meet objectives one and two (surface tracking abilities) and contains a description of the experimental procedures and a summary of results and conclusions. The report in Chapter five, *A Novel Sensor - Type I - Optical Fibre*, describes the steps taken to meet objective three (two dimensional sensor) via use of a novel optical fibre sensor technology. Again experimental procedures, results and conclusions are contained. Chapter six, *A Novel Sensor - Type II - Inertial Sensors*, describes an alternative approach to sensor construction with the intended aim of meeting objectives four, five and six (towards a three dimensional sensor array). Due to the increased scope of this report it has been subdivided in to several sections. These consider testing in two and three dimensions across a variety of scales and lead to a discussion of the newest sensor construction - a 1:12 scale fully marinised sensor designed to withstand testing at sea.

1.6.3 Summary, Discussion and Further work

Chapter seven *Conclusions and Further Work*, brings together the summaries from each of the three report sections and discusses to what extent the research objectives have been met. Elements identified as *further work* are discussed.

CHAPTER 2

Water Waves

2.1 Water Waves

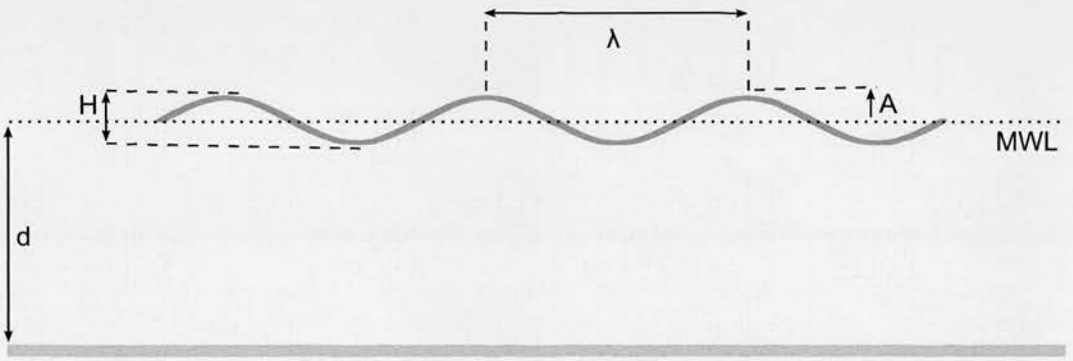

Figure 2.1. Schematic of water wave and associated parameters.

A schematic of a water wave is seen in Fig. 2.1. The wavelength, λ, is the distance from one wave peak to the next wave peak. Wave height, **H**, is the difference from a wave's peak to its trough and wave amplitude, **A**, is the distance from the Mean Water Level (**MWL**) to the wave peak. The water depth, **d**, is the distance from the (**MWL**) to the sea bed (or floor of a wave basin/flume).

Other commonly used parameters:

- T , Wave period. The time it takes, at a fixed position, for two wave peaks to pass that position. [s]
- η , Surface elevation. The height of the free water surface above or below (signified by a negative number) a specified MWL. [m]
- $\omega = 2\pi/T$, Angular frequency. [radians s^{-1}]
- $k = 2\pi/\lambda$, Wave number. [m^{-1}]
- $c = \lambda/T$, Phase velocity or celerity. [ms^{-1}]
- $s = H/\lambda$, Wave steepness.
- $E = \rho g H^2$, Energy of wave train per unit area.[J]

where ρ is water density (taken as $1000kgm^{-3}$ for fresh water and $1020kgm^{-3}$ for sea water) and g is gravitational acceleration taken as $9.81ms^{-2}$.

2.2 Water Wave Generation

There are three causes of water waves in a body of water: wind, tides and sudden disturbances arising from either geological, astronomical or human/biological activity (e.g., ships, marine mammals etc.).

Wind-generated waves are surface waves that have been created by the action of the moving air stream over the free surface. As the air roughens the surface, positive feedback occurs due to the now increased area for the wind to act upon, and waves grow in amplitude and wavelength.

At a larger scale the gravitational attraction of the Moon and Sun cause the tidal motions of the free surface. The range of tides (the difference in water level between successive maximum and minimum) and the time between one extreme of level and the next vary greatly depending on location on the planet. In several locations, generally in semi-enclosed areas, tidal ranges can be greater than ten metres in height

such as in the Bristol Channel in the UK and in the Minas Basin in the Bay of Fundy in Canada [47]. Tides and their associated water dynamics will not be considered in this thesis other than in the role they would play in the deployment and operation of sensor networks which is discussed briefly in chapter 6, section 6.3.4.

Water waves are also generated when there is a sudden disturbance in the body of water. A passing ship will cause a wake and the impact of an asteroid or a mass of land sliding in to the sea could generate a wave with wavelengths of kilometres with heights of tens to hundreds of metres. This work deals with disturbance waves (of a more benign nature) as they are the mechanism in the laboratory for creating waves. Using hinged paddles water is accelerated to mimic the effect of low amplitude wind-generated water waves (see Fig. 2.2).

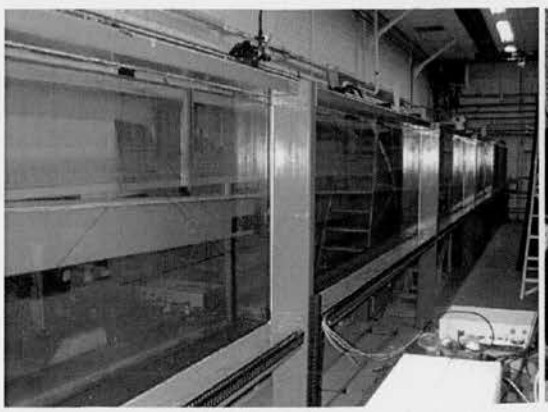

(a) The 20m Edinburgh Flume, hinged-flap type wave maker

(b) 15mx18m Aalborg Basin, piston type wave maker

(c) The 307m, 800kW GWK Flume, piston type wave maker

Figure 2.2. Wave making facilities used in this thesis.

Table 2.1. Wave types

Period (s)	Wavelength	Type
0-0.2	≈ cm	capillary
0.2-9	up to $\approx 130m$	wind sea
9-15	<500m	swell
15-30	1000s of m	long swell
30-hours	up to 1000s of km	long period waves
12.5h, 25h etc.	thousands of km	tides

Hinged wave paddles when combined with a feedback controller and an opposing wave absorbing beach allow the generation of repeatable waves where reflections are minimised. The paddles take as an input a wave time series which can be made up of simple, low amplitude sine waves or complex combinations of sine waves resulting in scaled water wave outputs of varying complexity in two dimensions (flumes) or three dimensions (basins).

In reality waves co-exist and interact with currents which themselves vary temporally and spatially. Wave-current interaction is an ongoing important area of research and has impacts on WEC station keeping, loadings and resource characterisation and capture but is considered outside of the scope of this work.

2.3 Linear Wave Theory

Linear Wave Theory [48], is used throughout science and engineering to describe gravity water waves. It is a solution, given various simplifying conditions, to the Laplace equation (which is used heavily in time-independent problems involving electrostatic, gravitational and fluid velocity potentials.) These simplifying assumptions are listed below:

- the fluid is homogeneous and incompressible implying constant density.
- the fluid is ideal - zero viscosity
- vorticity is zero - the water particles do not rotate
- air pressure above the water surface is constant

- the Coriolis force is neglected
- wave amplitude is small with respect to wavelength
- there is a solid, unmoving, horizontal bottom boundary

2.3.1 The Dispersion Relation

The dispersion equation, which relates angular frequency to wavenumber (and wavelength), can be written as

$$\omega^2 = \left(gk + \frac{\sigma k^3}{\rho}\right)\tanh(kd) \tag{2.1}$$

where g is acceleration due to gravity, σ is the surface tension of water, ρ is water density and d is water depth. Throughout this work very small amplitude waves (less than 1cm) are ignored thus the term in equation 2.1 involving the surface tension, σ is neglected. Also, when water depth is sufficiently large relative to a given wavelength the deep water condition brings $\tanh(kd)$ equal to one. The deep water condition can be invoked when $\frac{d}{\lambda} \geq \frac{1}{2}$.

This leaves:

$$\omega^2 = gk \tag{2.2}$$

2.3.2 Wave Velocities

Whilst a wave appears to be moving at the phase velocity, c, the water particles do not travel with the wave, instead following circular paths whose amplitudes fall off exponentially with depth.

Waves are said to be dispersive since wave components contributing to a given disturbance will propagate at a speed dependent on their wavenumber and are therefore likely to separate in phase from one another or *disperse*.

Phase Velocity

The phase velocity c (also known as celerity) is the speed of propagation of the disturbance and depends on wavenumber (with longer waves travelling faster than shorter waves):

$$c = \frac{\lambda}{T} = \frac{\omega}{k} = \sqrt{\left(\frac{g}{k} + \frac{\sigma k}{\rho}\right)\tanh(kd)} \tag{2.3}$$

Again neglecting surface tension, σ, and assuming deep water gives

$$c = \sqrt{\frac{g}{k}} \tag{2.4}$$

For shallow water where the waves experience strongly the bottom boundary the $\tanh(kd)$ term in equation 2.1 can be approximated as kd and the celerity expressed as

$$c = \sqrt{gd} \tag{2.5}$$

Group Velocity

The group speed, C_g, can be thought of as the velocity with which the overall shape of the wave's amplitudes propagate through space and is also commonly described as the velocity at which the energy in a monochromatic wave travels. Group speed is defined as:

$$C_g = \frac{\partial \omega}{\partial k} \tag{2.6}$$

In deep water the group speed and energy in a wave group travels at half of the celerity/phase velocity, c. In shallow water the group speed is equal to the phase velocity.

2.4 Waves at Sea

Waves at sea can look very dissimilar to the waves produced in the laboratory. Composed of waves generated by wind and tides that have arrived from varying locations together with the locally generated waves they are extremely complex and dynamic. These seas can be considered to be a superposition of many waves of differing heights, periods and directions. Quantifying various parameters of a sea can be achieved by analysing a time series record on a wave by wave basis or in terms of its frequency content. Figure 2.3 illustrates the concept of complex sea states being composed of simpler underlying sine-wave-like components.

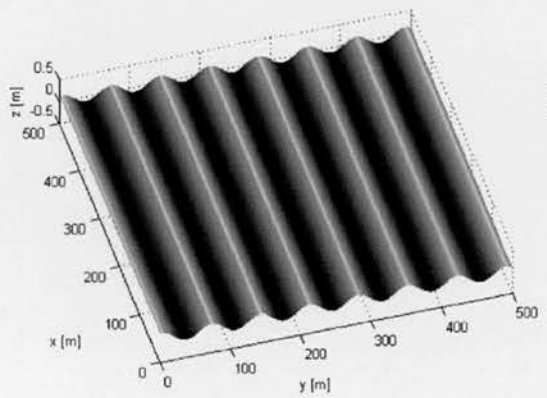

(a) Regular

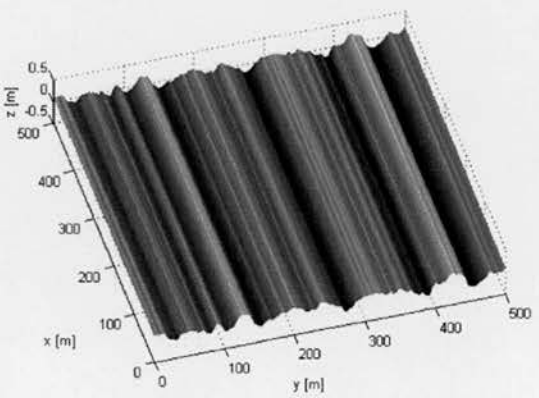

(b) Irregular long-crested

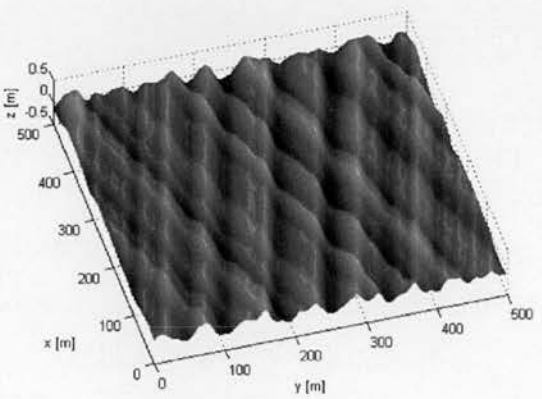

(c) Irregular short-crested

Figure 2.3. Increasing complexity of wave fields from regular/sinusoidal (*a*), long-crested (JONSWAP) (*b*), to short-crested mixed directional waves (*c*).

2.4.1 Frequency Content Analysis: the Energy Spectrum

The distribution of energy as a function of frequency leads to the energy spectrum which is traditionally also referred to as the wave spectrum. Two types of wave spectra are used: discrete spectra where Fourier analysis of a recorded time series gives the spectral density at discrete frequencies; and parametric spectra where the energy content is described as a function of frequency. Parametric spectra are used when only minimal global parameter statistics are known (no wave elevation time series for example) and an attempt is being made to obtain further characteristics based on the spectral shape governed by these basic inputs and also when a comparison between the two spectra has revealed similarities allowing the parametric spectra to be used as a representative model [25]. By recording wave elevations at many locations globally, deriving the discrete spectra and checking the fit of the observed spectra to a parametric model, the validity of the various parametric spectra have been assessed. Examples of parametric spectra include Bretschneider, JONSWAP, Pierson and Moskowitz, Mitsuyasu and Ochi and Hubble. These have been adjusted over the years to better fit prototype data and to include site specific factors such as wind fetch [49].

$S(\omega)$, the spectral variance density in $m^2 s$ is given by,

$$S(\omega) = \frac{1}{2}\frac{A^2(\omega)}{\delta\omega} \tag{2.7}$$

In terms of frequency, f, $S(f) = 2\pi S(\omega)$.

In practice the spectral variance density is found by performing a Fast Fourier Transform (FFT), the computationally optimised Discrete Fourier Transform (DFT), on a digitised, sampled signal. Fourier analysis requires that the wave elevation signal is periodic around it's length (in time) and thus modifications or taper windows are implemented at the beginning and end of the signal. In this work, frequency domain analysis was conducted using the Wavelab 2.0 software where the default taper settings of a *cosine squared* taper with 20% overlap and 20% width were used unless otherwise stated.

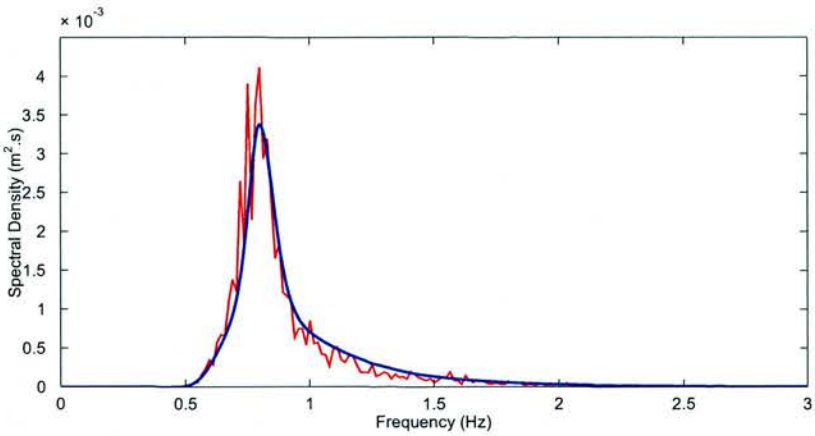

Figure 2.4. Discrete spectra produced from wave gauge data of an irregular wave during flume test (red) and corresponding parameterised JONSWAP spectra (blue) (with γ set to 3.3).

For a list of sea state parameters recommended for use in the wave energy field see table 2.2 and [50].

2.4.2 Wave by Wave Time Series Analysis

An alternative approach to quantifying wave elevation time histories is to analyse the signal on a wave by wave basis. This involves determining starting points and finishing points for regions of the signal and measuring their properties. The overall statistics are based on the aggregate of these individual wave events.

Figure 2.5 illustrates the method of identifying an individual wave based on the point in time at which the elevation crosses the mean water level (MWL) from a positive elevation to a negative elevation (zero down crossing). An alternative approach, zero up crossing, is to identify where a wave crosses the MWL with a positive gradient. The differences in overall statistics that these alternative methods lead to are small and are not considered in this thesis. In practice, due to infrequent discretised sampling, the zero crossing point is determined by an interpolation scheme. Figure 2.5 also highlights the sensitivity of the process to small errors in elevation where wave number 3 may have been better described as a shorter period, small elevation wave as there is a turning point that almost exists below the MWL. This issue has consequences on wave time series analysis and comparison of multiple elevation

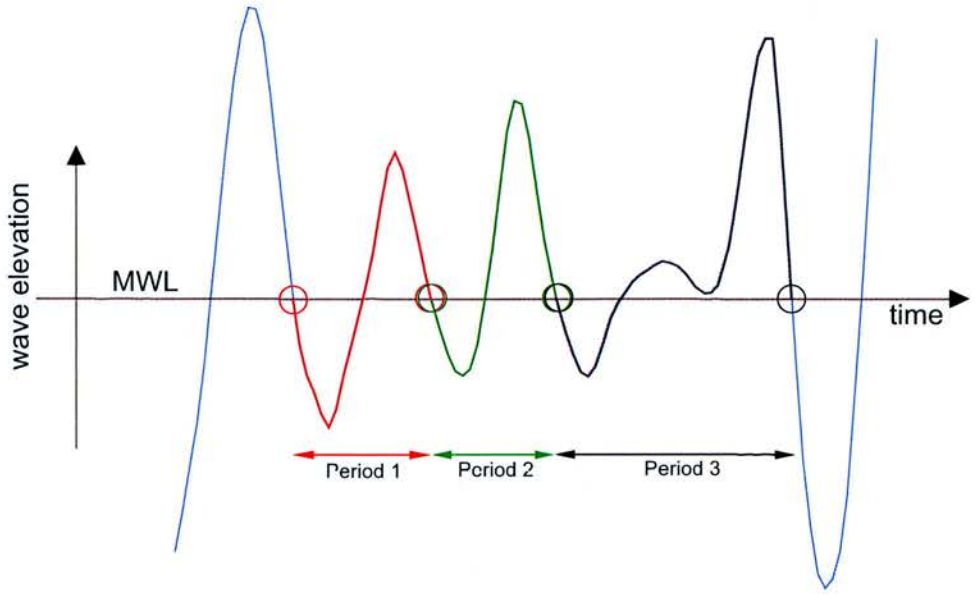

Figure 2.5. Schematic showing wave zero-down-crossing method

measurements and is discussed further in chapter 4, section 4.2.3.

2.4.3 Wave Steepness

Wave steepness is a ratio of wave height divided by the length of the wave (wavelength). Waves with relatively high amplitude and short wave length have high steepness. As wave steepness increases the validity of linear wave theory reduces. Behaviour varies between deep and shallow water conditions (and is further complicated by interaction with underlying currents), but in deep water, once steepness increases beyond approximately 1/7 (0.14), waves break [51]. Wave breaking events are generally categorised as either Spilling, Plunging or Surging with varying geometries, surface mixing abilities and levels of energy dissipation. Experimental testing within this work does not include wave breaking. Tests were, however, conducted at high steepnesses in order that as broad a test range as possible could be delivered (subject to the specification limitations of test facilities used). In reality, in large non fetch-limited and deep water sea-states (well described by the Pierson-Moskowitz equation) significant steepness (using significant wave height and mean wave period terms) remains constant at approximately 1/20 (0.05) [52].

2.4.4 Directionality

A directional wave spectrum not only takes in to account the distribution of energy with respect to frequency but also the distribution of energy as a function of direction. In reality, most sea states (other than long-crested waves where the crest lines are straight and parallel) are composed of multi-directional waves thus the directional wave spectra offers the most comprehensive statistical wave field description. With full directional spectral analysis the drivers of a sea-state can be separated and identified. Good understanding of the directional spectrum is an important factor in the design and functioning of coastal and offshore structures and is critical in assessing the effects of reflected waves near structures [53, 54]. The directional spectrum is key in the field of wave modelling and air-sea interaction; and affects the forces experienced by piles and offshore structures including vessels and platforms; and plays a role in coastal erosion, sediment transport and pollution dispersal [55].

Figure 2.6. Fishing boat returning to the port of Vlissingen, Netherlands in storm (force 10) conditions on January 18th 2007. ©Ed Francissen.

The directional spectral density, $\mathbf{S}(f,\theta)$, builds on equation 2.7,

$$\mathbf{S}(f,\theta) = S(f)D(f,\theta) \tag{2.8}$$

where $S(f)$ is the unidimensional spectrum (expressed as a function of frequency) and $D(f,\theta)$ is introduced as the angular spreading function. $D(f,\theta)$ is dimensionless and normalised by setting its integration, over angle, from 0 to 2π equal to 1,

$$\int_0^{2\pi} D(f,\theta)d\theta = 1 \tag{2.9}$$

Quantifying Directional Seas

The primary directional sea state parameters are the mean wave direction (at the peak of the spectrum) θ_{1p}, and the standard deviation of the directional distribution, the directional spreading (at the peak of the spectrum) σ_{1p}. The latter describes the distribution of wave energy around the mean value. Unlike the more stable (in terms of analysis method) spectral parameters such as H_s and T_p, both θ_{1p} and σ_{1p} can be defined as functions of frequency.

There are several routes to identifying the key directions and frequencies contained in a wave field each with associated advantages and disadvantages and dependencies on the instruments used to supply the raw data. As improved and less expensive oceanographic instruments become available and subsequently more directional wave data is accrued, defining and executing appropriate analysis methods is increasingly important. Ideally, to provide the full directional spectrum, without the use of prior information and assumptions, numerous high-resolution instruments would be deployed in an array over a wide area in order that all spatial scales of waves and their corresponding directions may be captured. The E.U COST report suggests coverage of at least $1km$ with a spatial resolution of $1m$ and sampling set at $1Hz$ [55]. Current technology remains well below this specification and as such methods are used (and assumptions are incorporated) which aim to maximise the use of sparse, and in some cases, low-resolution and noisy information.

The most widely used method to quantify directional seas makes use of the Fourier expansion method [56]. Use of the first pair of Fourier coefficients has been proven to adequately describe θ_{1p} and σ_{1p} in relatively simple sea-states but insufficient to describe more complex wave fields. Where multiple wave directions comprising

similar frequencies are present in a wave field or where there are combined sea-states with varied frequencies the accuracy of the Fourier-based method reduces [57, 55]. Enhanced methods to obtain the directional spectrum have been developed including Extended Maximum Entropy Method (EMEP), Extended maximum Likelihood Method (EMLM), Bayesian Direct Method (BDM) and Iterated Maximum Likelihood Method (IMLM) [58] The traditional Fourier method remains the least computationally intensive method but offers relatively poor directional resolution and is sensitive to errors in the data. The BDM, whilst potentially capable of providing the best estimates is computationally intensive. The EMEP method is considered the best all-rounder providing high resolution, generally fast, error-tolerant results. [59, 60]. However, the presence of artificial double peaks in the spectra produced by the EMEP method has been noted and choosing the most appropriate method of realising directionality requires consideration of the measurement programme [61]. In addition, it has been suggested that a combination of methods may be required to conclude on the best estimate of directionality [62].

2.4.5 Non-Linearity

A disadvantage of the energy spectrum lies in its inability to provide information on parameters important to the design of marine structures, such as shock loads, which arise due to the *shape* of individual waves and wave groups [63].

One of the most obvious non-linearities in waves is the increasing asymmetry of the wave between trough depth and crest height, through the mean water level, as waves get larger in amplitude. Wave-wave interaction at a particular location causes non-linearity in addition to the non-linear evolution of a group of waves over time and wave breaking events [64]. Increasing effort is being directed to the effects of currents on wave characteristics and on the effects of wave motion to turbulent variation of mean current flow. These interactions are another source of non-linearity. In the laboratory when creating focused wave groups, for example, the presence of non-linear effects leads to uncertainty when predicting the spatial and temporal location of wave focusing and the amplitude of the focused wave.

The scope of this work largely avoids having to either segregate or mitigate non-linearity as the aim is to measure the behaviour of a sensor instrument in a large variety of sea states from low amplitude linear waves to complex mixed and likely highly non-linear sea states. However, as discussed in Chapter 7, Section "Further Work", any advancement of the sensor data processing or indeed integration into a wider measurement system would likely take advantage of the known physics of linear wave systems whilst also implementing strategies to deal with inherent non-linearity.

2.4.6 Widely Used Wave Field Parameters

The term significant wave height, H_s, has had an interesting career and can cause confusion. It was traditionally determined by averaging the wave heights of the highest one third of waves in a wave time series, often labelled $H_{1/3}$. In addition it has been assigned to the variance of the wave time series. An alternative definition stems from the frequency domain gives H_{m0}, where the significant wave height is related to the zeroth spectral moment (or proportional to the square root of the area under the spectral graph).

$$H_{m0} = 4\sqrt{m_0} \tag{2.10}$$

Where the n^{th} spectral moment is calculated from,

$$m_n = \int_0^\infty \omega^n S(\omega) d\omega \tag{2.11}$$

where $n = 0, 1, 2, 3, ...$

The mean wave period as obtained from zero crossing analysis, $T_z = T_{02}$ is defined as the mean of the individually determined wave periods in the record.

From the wave spectra the average wave period, T_{02} and the energy period, T_e, can be defined, respectively, by

$$T_{02} = \sqrt{\frac{m_0}{m_2}} \tag{2.12}$$

$$T_e = \frac{m_{-1}}{m_0} \tag{2.13}$$

The energy period, T_e, is used in wave energy studies as it provides knowledge of the energies associated with the longer waves (lower frequency) in a wave spectrum and can be approximated as,

$$T_e = 1.2T_z \tag{2.14}$$

Table 2.2. Wave field parameters used in this work.

Symbol	Label	Description/Formula	Units
$S(\omega)$	Spectral (variance) density	$S(\omega) = \frac{1}{2}\frac{A^2(\omega)}{\delta\omega}$	m^2s
$S(f)$	Spectral (variance) density	$S(f) = 2\pi S(\omega)$	m^2s
$\mathbf{S}(f,\theta)$	Directional spectral density	$\mathbf{S}(f,\theta) = S(f)D(f,\theta)$	m^2 s deg^{-1}
H_{m0}	Significant wave height	$H_{m0} = 4\sqrt{m_0}$	m
T_{02}	Average wave period	$T_{02} = \sqrt{\frac{m_0}{m_2}}$	s
T_e	Energy period	$T_e = \frac{m_{-1}}{m_0}$	s
P	Wave power per metre wave crest	$P = \frac{\rho g^2}{64\pi} {H_s}^2 T_e$	Wm^{-1}
S	Wave steepness	$S = \frac{H}{\lambda}$	-
H_m	Mean wave height	Sum of zero-crossing-defined wave heights divided by number of waves	m
T_m	Mean wave period	Sum of zero-crossing-defined wave periods divided by number of waves	s

2.5 The Energy Resource

For a sinusoidal wave,

$E = k_E H^2$ where $k_E = \rho g/8 = 1.25 kW s/m^2$

The energy on this horizontal square metre of the water surface is divided between potential energy due to the mass of water lifted to a wave crest and kinetic energy due to the water's velocity. A $3m$ linear wave would therefore represent 11.25kW.s/m^2.

In terms of wave power a commonly used parameter is power per metre wave crest (expressed in W/m). It is calculated by,

$$P = \frac{\rho g^2}{64\pi} {H_s}^2 T_e \tag{2.15}$$

Assuming commonly used values of $\rho = 1000 kg/m^3$ and $g = 9.81 ms^2$ gives,

$$P = 0.577\, H_s^2\, T_e \tag{2.16}$$

in kW/m.

Global estimates of available wave power expressed in this way can be seen in figure 2.7a. Estimation of incident power available to a WEC, the measurement of captured power and the ratio of these quantities will be one of many parameters used in the assessment of control strategy effectiveness.

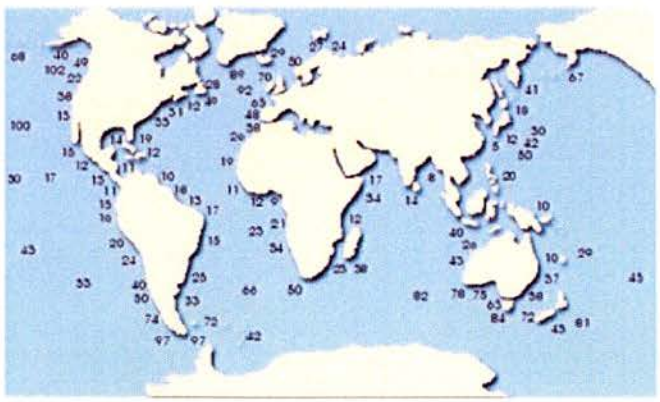

(a) Global annual mean wave power estimates (kW/m).

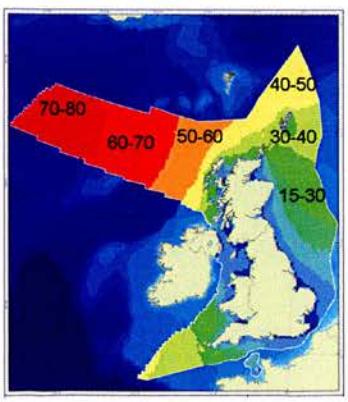

(b) UK annual mean wave power estimates (kW/m)

Figure 2.7. Global and UK wave power estimates.

a) Website of Pelamis Wave Power,
b) Adapted from the Atlas of UK Marine Renewable Energy Resources. ©. Crown copyright.

2.5.1 Resource Assessment

Choosing a site for an individual WEC or WEC farm is a complex task with many considerations which include:

- a "suitable" wave climate for a particular device
- station keeping considerations - mooring ability, depth, bathymetry
- array interactions
- access to the electricity network
- avoidance/mitigation of stakeholder conflicts e.g., military, fisheries, ecology, shipping, oil and gas, tourism.

In reality compromises will have to made across all of these considerations.

2.5.2 Defining the Resource in terms of WECs

The wave resource can be described with parameters featuring increasing spatial and temporal detail from average energy over a region of tens of square kilometres in deep water to twenty minute statistical descriptions in coastal regions in the vicinity of a measuring device such as a wave buoy. Whilst financial investment will depend heavily on the resource (and predicted energy yield) being characterised over ten to twenty years, elements of device performance, such as reliability due to fatigue or extreme loadings may require more detailed information about the environment than regional wave models can provide.

Large scale wave resource assessments are based on computer modelling using large scale wind-wave models from which wave power statistics can be computed. [4]

Due to the added complexity of coastal sites due to changing bathymetry, reflections, shallow water effects the low spatial resolution data of a global or mesoscale wind wave model may not be sufficient to ascertain the power available at this locality. Here, wave measuring equipment, usually wave buoys, can be used along with the

large scale models to drive more detailed, higher resolution coastal models. Existing data sets however tend to be acquired from point measurements and frequently contain no directionality information of the wave field or where this data is provided it can be difficult to interpret. Since spatially varying parameters such as the direction of waves and their associated spreading will likely play a role in the performance of a WEC, new technologies may be required to measure these parameters.

CHAPTER 3

Measuring the Environment

3.1 Overview

Measuring water waves has been a historical challenge in the fields of oceanography, hydrodynamics, maritime engineering and a variety of laboratory studies. At sea a multitude of solutions have evolved that float on the surface, lie on the sea bed or are mounted on vessels. In the laboratory where attachment points are much more readily available measurements tend to be of the *fixed* rather than floating type. Each of these methods fall into one of two categories as noted by MS Longuet-Higgins:

> Surface waves can be recorded in two kinds of ways, either with a fixed (Eulerian) probe or with a free-floating (Lagrangian) buoy.
>
> MS Longuet-Higgins [65]

If our use of the seas are to increase and taking with it the monetary value of operations conducted at sea (ship to ship connections, increasingly complex oil and gas operations, deployment of renewable energy devices and autonomous vehicles for example) then traditional measurement techniques may require upgrading or rethinking. Generally their limitations lie in the number of points where measurements are taken (spatial density and area of coverage), in their sampling rate in time, in their maximum telemetry data rates or in their overestimation or underestimation

of parameters under certain sea conditions.

The following sections summarise the main operating principals, uses and limitations of the main technology types currently used to measure waves.

3.2 Techniques at Sea

Current technologies for obtaining ocean surface elevation include wave buoys, Acoustic Doppler Profilers (ADPs) and several types of Radar. Each method has associated advantages and disadvantages. See table 5.1 in Chapter 5 for a summary of leading-technology characteristics relevant to this work and table 3.2 for a manufacturer-supplied summary specification comparison [55, 66, 67, 68, 69].

Wave buoys

(a) Benchmark - Hippy-40

(b) An example of MEM IMU

(c) Datawell Waverider MKIII

Figure 3.1. Typical motion measurement payloads of wave buoys

c) ©Datawell BV Oceanographic Instruments

Since the pioneering work of Longuet-Higgins buoys have been deployed for monitoring the wave field and meteorology over the ocean [56].

Buoys provide good quality wave height, period and often direction measurements but suffer from poor spatial coverage. Whilst proven technology, wave buoys remain

expensive to build, deploy and operate. Deployment, maintenance and removal involves vessel rental which is extremely expensive and in the case of large buoys vessel scheduling and pricing can be dominated by oil and gas industry conditions. In addition, buoys are exposed to shipping, fishing and storm damage/loss.

Wave buoys intended for long open ocean deployments are usually of diameter of several metres. The large diameter arises from having to carry a large payload (instruments and moreover power supply) whilst supporting heavy mooring lines. These buoys suffer from lower resolution compared with small buoys such as the Datawell Waverider, as their ability to track the moving surface is hindered by higher inertias and mooring influences [70]. Smaller buoys intended for shorter period deployments can be lightly moored on elastic, compliant moorings. Even so incidents involving buoys becoming detached from their moorings are not uncommon.

The recent availability of micro-electro-mechanical sensors (MEMS) offers the ability to reduce the volume and weight of a buoy sensor payload therefore reducing the diameter of floatation material needed. Previous buoys contained a large mechanised platform which adds undesired weight and load on the power supply. The Hippy 40 sensor package is an example of this type of sensor package and forms the benchmark device against which new buoys are measured [71]. The reference platform for the pitch and roll measurements is a gravity-stabilized disc surrounded in a liquid inside an aluminium cylindrical can. The Hippy electronically double integrates acceleration measured at its isolated and suspended cantilever arm to produce vertical displacement.

Buoys have been traditionally deployed for marine weather forecasting for the shipping/fishing industry and for storm warnings. The time series generated are processed on board the buoy and the summary statistics of a selected period (typically 20 minutes to meet the requirement of pseudo-stationarity for spectral processing) are transmitted. This level of data may not be sufficient for the marine renewable sector where access to the time series is needed, either in near real-time or after a deployment for post processing. The quality of these time series has been noted to be variable and can require extensive post processing [60].

Notable international buoy networks currently in operation include the NOAA-NDBC

(National Data Buoy Network) covering East and West coasts of the USA, the Gulf of Mexico and the Hawaiian Islands and the Indian National Data Buoy Programme. This network, unlike it's American counterpart, use buoys capable of directional measurements as standard.

In summary, buoys are the standard method for providing spectral parameters (including directional information) at a *point* in the ocean and the recently completed Equimar project recommends their use in offshore renewable resource assessment [25]. Further advances in buoy technology may be required for the renewable sector leading to smaller and lighter buoys capable of supplying full raw data via high bandwidth telemetry. By residing on the surface and therefore having access to through-air telecommunication frequencies buoys have an advantage over their submerged competitors and can access cellular, radio or satellite communication networks.

Acoustic Doppler Profilers

Whilst measuring the Doppler shift of suspended particles in a water column and inferring the surrounding fluid's velocity was originally intended for use as a tool in current flow measurement this principal is being increasingly used to measure waves. Being situated on the seabed reduces the risk of shipping damage to an ADP but large forces remain which can lead to data loss and sensor damage (as was experienced in Denmark during 1999,[72]). Design and implementation of the locating frame are critical to an ADP's deployment and operation. Experiences such as during the Strangford narrows programme suggest that frames have to be extremely robust to survive, leading to installation difficulties for diver teams [73]. Figure 3.3a shows the configuration of a Nortek AWAC (ADCP) on a tripod frame with auxiliary battery and data storage canister attached as used by the author in the recent £13 *M* "ReDAPT" project - Reliable Data Acquisition for Tidal Power [74].

Some ADPs give directional wave data using software to convert orbital velocity measurements into wave frequency and directionality. The software makes use of linear wave theory to derive elevation. The Nyquist theorem dictates a maximum bed

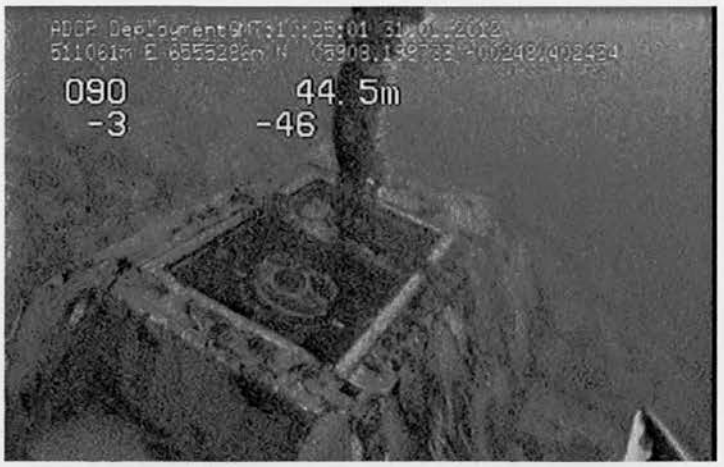

(a) ADCP deployed by author (as Client) in Orkney, UK April 2012.

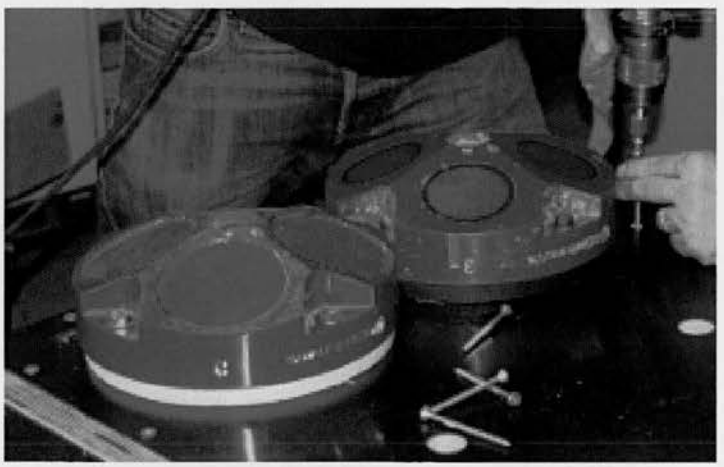

(b) Author constructing ADCP installation frame

(c) ADCP's deployed in 307m long, 7m deep GWK, Hannover.

Figure 3.2. Acoustic Doppler Profilers (ADPs)

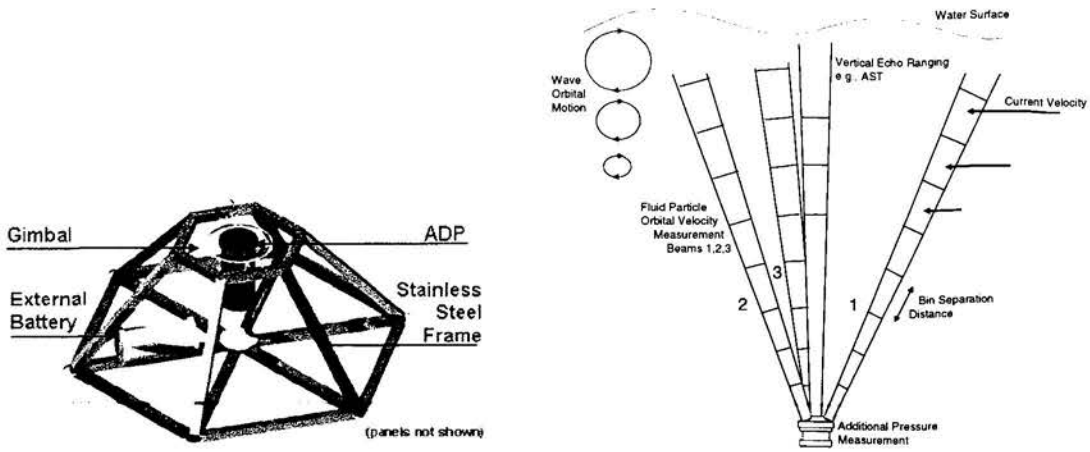

(a) CAD schematic showing RDI ADCP configuration on the ReDAPT Project, 2011

(b) ADP (Nortek AWAC) Working Principal Schematic

Figure 3.3. Typical installation method of ADPs (a) and working principal (b)

depth for a required surface wavelength resolution. At 50m depth and dependent on beam alignment an ADP can resolve only waves above approximately 3.5 seconds and, in terms of the directional spectrum, approximately 6 to 9 seconds [75, 76].

Nortek systems are one of the leaders in the field of current profilers along with Teledyne systems and SonTek. Their AWAC with Acoustic Surface Tracking (AST) measures wave direction, surface elevation (wave height) and current in one almost all-plastic instrument. The AST echo-ranges to the surface using a vertically orientated (if the instrument is deployed flat) transducer. This allows the measurement of short period, locally-generated waves and can output either time series histories of surface elevation or the summary statistics as produced by wave buoys.

ADPs often store the data on board with battery life of the order of six months to a year depending on configuration. This data is retrieved at the end of the deployment after instrument recovery. If data is required on-the-fly there are several methods to achieve this including a cable to shore (up to 5km) [77], acoustic modems to shore or acoustic modems or cables to a surface platform which can then relay via radio/satellite/GSM.

Radar

X-Band Radar

Commercially-available X-Band Radar can be installed on fixed (e.g. offshore oil installations) or moving (e.g. vessel-based) platforms. Operating on the principle of measuring the backscatter of radar energy from the ocean surface they offer massive spatial coverage improvements over Buoys with a typical system being able to cover a swept area of radius 2km at a spatial resolution down to 10m. Systems include Miros, WAVEX and OceanWaves WaMoS II. Shorter range, higher resolution set-ups exist, using a system covering an area of 20x20m with a resolution of 0.4m [78]. For spectral sea-state parameters H_{m0}, T_p , etc. X-Band Radar has been shown to give excellent agreement with other measurement techniques such as Buoys [79] (estimated accuracies, as revealed by in-situ testing, are shown in table 3.1, [80]). However, these are averaged parameters and do not give information about individual waves. Recent software developments such as the DWFA algorithm in WaMoS II can pick out individual waves from a radar image by using linear wave theory as the basis of an inversion technique leading to colour-coded wave elevations. Typical systems suffer from poor temporal resolution (Δt=2.5s) limited by the rate of rotation of the radar emitter and the number of images required for analysis and in addition may not be able to pick out wave heights below 0.5m [79]. Recently, an X-Band radar in conjunction with the inverting software was used to measure sea surface elevations. The results were compared to a co-located wave buoy with the sampling rate of this buoy reduced to allow comparison to the radar and software system. Although there is general agreement, large errors are present particularly in wave amplitude [81]. Since the heights are picked out by an algorithm this could possibly be tuned to reduce errors but importantly a benchmark data set would be required. This has been supported in discussions with the radar company OceanWaves GmBh [82].

Table 3.1. Summary of reliability of WaMos II / X-band radar sea state parameters based on in-situ testing.

Wave parameter	Range	Standard deviation
Significant wave height	0.5 - 20 m	10 %
Peak wave period	3 - 50 s	5 %
Peak wave direction	0 - 360°	± 10°

Table 3.2. Summary specification (manufacturer-supplied) of leading ocean wave measurement technologies.

a) Wave Buoy			
Typ. Sample Rate	1.28Hz		
Typ. Coverage	Single Point		
Parameter	**Range**	**Res**	**Accuracy**
Heave	± 20 (m)	0.01 (m)	<2%
Wave Period	1.5-33 (s)	0.1 (s)	<2%
Wave Direction	0-360 (°)	1 (°)	3 (°)
b) Bottom Mounted ADCP			
Typ. Sample Rate	2Hz		
Typ. Coverage	Array Based Measurement Covering < 1 λ		
Parameter	**Range**	**Res**	**Accuracy**
H_s	10 (m)	0.01-0.1 (m)	1 %
Wave Period	1/3/5* - 100 (s)	0.1 (s)	n/a
Wave Direction	0-360 (°)	0.1-0.5 (°)	2 (°)
c) X-Band Radar (WaMoS II)			
Typ. Sample Rate	<1Hz		
Typ. Coverage	Array Based Measurement Covering > 1-10λ		
Parameter	**Range**	**Res**	**Accuracy**
H_s	0.5-20 (m)	0.1 (m)	10 %
Wave Period	3-18 (s)	0.1 (s)	± 0.5 (s)
Wave Direction	0-360 (°)	1 (°)	2 (°)

*Increasing minimum detectable wave period for reporting of:
single point η; non-directional η and directional sea-state.
Increasing depth increases minimum observable wavelength and increases attenuation of pressure signal.

HF Radar

High Frequency (HF) Radar emits radio waves from ground base stations with wavelengths in the range 10-100m and can sense from 10km out to 200km with resolutions decreasing with range to a maximum of a few hundred metres for short range set-up [83]. Whilst it operates under the same principal as X-Band systems the longer electromagnetic wavelength explains the greater range but reduced spatial resolution. Accuracy of the directional spectrum and derived wave parameters depends on radar power spectrum frequency resolution, temporal and spatial variability in the measurement cell, angle between two radar look directions, antenna sidelobe levels, wave height, noise and interference levels [84]. Algorithms have been developed to process the radar images to extract sea-state parameters. HF Radar's use as a current measurement device is well established but there is some debate as to its ability to measure accurately these sea-state parameters. Radio Frequency (RF) Licensing, interference and planning issues also affect the implementation of the technology [79, 81].

HF radar comprises two types: phased-array radar e.g., ocean current surface radar (OCSR) and Pisces, and direction-finding radars e.g., coastal ocean dynamics application radar (CODAR) and SeaSonde [84].

Experience from the 2003-2005 trial of dual Pisces deployment (intersecting beams from north Devon and South Wales) suggests that significant wave heights below 1m are unreliable [84].

There may be scope for improved radar performance by altering the frequency based on the changing environmental parameters including interference and wind, precipitation, wave climate. Using the WERA radar system which is a hybrid of both phased-array and direction-finding radar, the EU-funded EuroROSE experiment in Fedje, Norway suggests that HF radar may have limitations in its ability to cope with sudden changes in wave climate. This limitation may be a result of minimum reliably measured wave frequency of 0.35Hz inherent to the system's scanning frequency [83].

LIDAR

Light Detection and Ranging systems (LIDAR), whereby light of a choice of frequencies (from Ultra-Violet (UV) to near infra-red) is used to highlight a surface and report the range to that surface, have been used widely in atmospheric and terrain mapping fields. In the context of oceanography they were first developed for aerial surveying of coastal bathymetry and were later used in underwater obstacle detection tasks [85]. These LIDAR were operated at a near normal angle to the surface. A more practical installation for the use in measuring wave fields in the shipping, oil and gas and renewable sector would be vessel mounted LIDAR systems which would negate the inability of moving systems to continuously measure a fixed region. These would be able to monitor the vicinity around a vessel, rig or WEC but would be operating at much shallower angles (limited by the tower height). Difficulty arises in the signal processing of the very weakly returned and heavily scattered light. In one trial processing power is dynamically allocated depending on the distance from the optical radar and the condition of the signal [85]. This study used line scans where the wave field is sampled at various points in a line away from the radar. This system would be upgraded to a planar scanning one where the emitter and receiver would sweep a field of view and build up a wave field from many line scans.

Evidence to support the utility of remote sensing technologies (both radar and laser systems) in the field and in the absence of absolute references comes from the WACSIS (Wave Crest Sensor Intercomparison Study) project [86] where good agreement was found between wave measurements taken via collocated laser and radar instruments - despite their varied measurement techniques [87].

Other Techniques

Global wave models

Large scale wave resource assessments are based on computer modelling using large scale wind-wave models from which wave power statistics can be computed. Global wave models can be used as the starting point for a more detailed, coastal assessment

of wave climate. The global model provides the boundary conditions for a computer program (3rd generation spectral model such as WAM, SWAN and Mike21-SW) that incorporates local bathymetry and provides higher resolution outputs [88]. A recent publication on the use of local wave models at a site in Orkney, UK - of particular interest to the sector due to the establishment of a wave and tidal test site - suggests that simple spectral parameters alone may not be sufficient in the wave and tidal sectors and highlights the necessity for a re-modelled wave resource parameter that takes in to account the resource-power production interactions [89].

Satellite Altimetry

The TOPEX/Poseidon satellite (see Fig. 3.5b), launched in 1992, uses radar altimetry to measure sea-level height with a repeat period of 10 days. Time of flight return trip measurements are used in addition to satellite position information and knowledge of instrumental and atmospheric effects provides the distance to the sea surface.

Satellites such as the European Space Agency's ESR1 and ESR2 and NASA's Jason 1, launched December 2001 and placed on the same orbit as TOPEX/Poseidon and one minute ahead, can measure sea surface elevations to within 4cm with a goal of below 2.5cm. Jason 1 completes a scan comprising 90% of the oceans' unfrozen surface every ten days. These measurements are useful for large time-span averaged values and give information on global sea levels. Wave buoys are used in the calibration procedure of these satellites [90]. OSTM/Jason-2, the follow-on to Jason-1 mission, launched in June 2008. One of Jason-2's goals is to maintain the accuracy of significant wave heights to 0.5m or 10% of the value (whichever is greater). Jason-1 will be moved into a parallel orbit to make way for Jason-2 and will form one half of the new joint mission.

Satellite deployments tend to focus on measuring rising global sea levels and large ocean/atmosphere phenomena such as El Nino and long time scale climate oscillations [91]. With reductions in the cost of satellites, the development of mini-satellites and moreover the advances in operating them in arrays (currently in a co-operating pair as with the TerraSAR-X and TanDEM-X programme [92]) improved ocean mea-

surements from space are likely in the future.

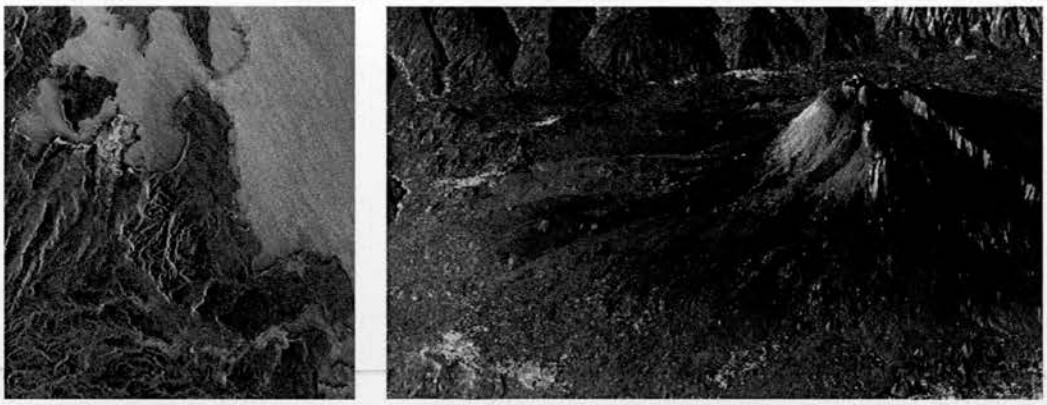

(a) Image showing elevations North of Madagascar showing sea surface roughness reductions in the bottom-left of image.

(b) Image showing Mount Etna, Italy produced from the first bi-static joint data-set from TanDEM-X and TerraSAR-X

Figure 3.4. Advancing satellite technology - TanDEM-X and TerraSAR-X.
Images from Astrium website. ©Astrium 2010.

Fixed Installations

Fixed installations such as those on a pier or oil rig offer several advantages. Access, repair and maintenance is easier as there is a permanent crew near the sensor. Ships and helicopters routinely transit to and from the rig and moreover, the difficult part - the moorings - have already been funded, designed and installed [93].

Disadvantages include disruption to the measured wave field by fixed structure itself and the requirement to be able to withstand harsh environments.

In 2007 a custom wave gauge, consisting of long wires fixed to the ramp of the prototype Wavedragon device, was trialled in the field. Following successful trials in the laboratory this capacitance based measurement system failed due to a combination of mechanical damage and marine bio-growth. This highlights the difficulty in finding robust solutions to the measurement of air/water interface that can survive and operate when taken from the laboratory to the ocean [94].

Pressure Transducers

Bottom mounted pressure transducers have been used for a long time (since around 1947) to measure surface elevation. They benefit from being out of harms way regarding surface traffic and comprise relatively cheap components. As information from the surface is attenuated through the water column accuracy falls off with depth. However, nonlinearity of the surface profile is stronger in shallow water and careful handling of the pressure data to reveal surface elevation is needed in this regime to maintain accuracy [95]. Pressure transducers are often used to provide complimentary data to other methods (such as acoustic surface tracking) where there disadvantages are offset by their reliability and insensitivity to sources of acoustic noise such as bubble formation from breaking waves.

Visible Spectrum Imaging

(a) ATSIS for measuring 3D breaking waves (Wanek and Wu, 2006)

(b) TOPEX/Poseidon, NASA

(c) Image generated from WaMoS II and X-Band Radar

Figure 3.5. Remote sensing techniques. Visible and radar imaging

Visible spectrum imaging may allow wide area wave characterisation at low cost. In particular, passive imaging methods, where no externally applied light source is used (a strategy usually applied in laboratories), could prove useful. The main methods of inferring wave characteristics from a series of images are through light reflection off of the surface, sun glint, photogrammetry and polarimetry. All the methods have advantages and disadvantages. The reflection method requires low wave steepness, sun glint methods do not provide direct surface elevations and polarimetry methods

have thus far only been used under a limited range of atmospheric and sea conditions. Photogrammetry methods (see Fig. 3.5a) rely on the calibration of images via known geometric features or physical behaviours along with comparing images from multiple positions. This research area also has applications in robotics. Historically stereoscopic vision systems have proved challenging to implement however advances in computational power and analysis techniques could offer quicker and cheaper access to wide area surface elevation data [96, 97].

3.3 Techniques in the Laboratory

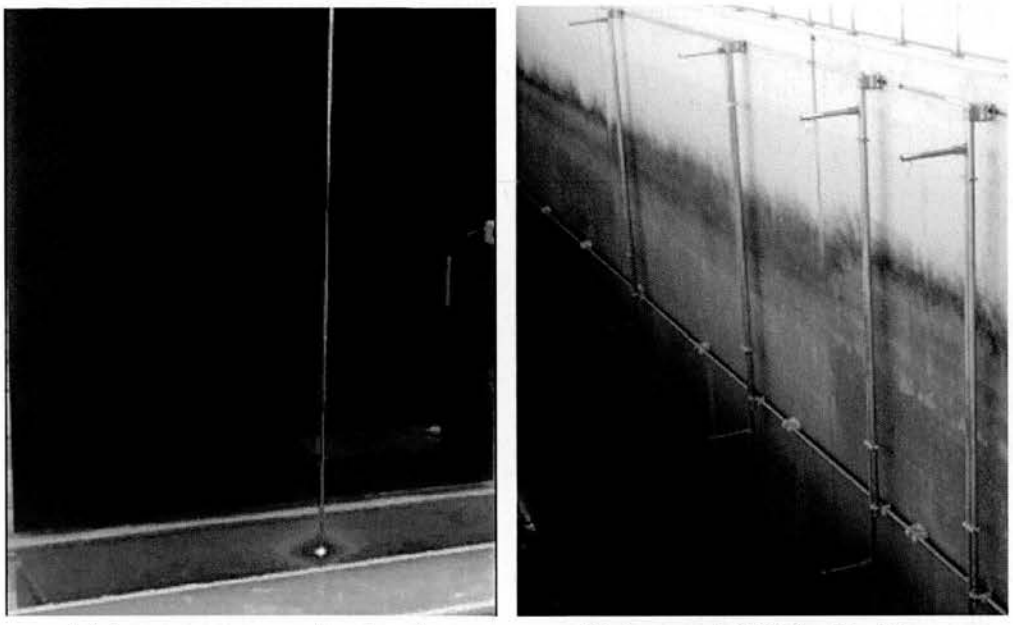

(a) Laser wave gauge developed under SuperGen Marine II (Payne, 2011)

(b) Image of GWK facility, Hannover showing resistance wire wave gauges

Figure 3.6. Laboratory wave measurement techniques.

Resistance Wire Wave Gauges

Resistance wire wave gauges are the benchmark tool used in hydraulic test facilities for measuring surface elevation at a point. They consist of two parallel thin rods (usually of several mm diameter) and measure the resistance between the two rods

when immersed in water (see Figs. 3.6 and 3.7. As the water level between the probes varies the resistance changes. This relationship has been shown to be extremely linear. Alternating current (AC) is used to prevent build up of charged particles at what would be the anode and cathode if direct current was used. Circuitry which changes the frequency of the AC is necessary to avoid cross contamination of the resistance measurements between probes in the tank. Off the shelf data acquisition equipment can then sample the probes which output a varying voltage proportional to the wave elevation.

Changes in the conductivity of the wave flumes and basins effect the resistance measurements which can arise through temperature changes and mixing of contaminants due to wave action. Careful and time consuming calibration is therefore essential when using these gauges. Some laboratories which make heavy use of these gauges have invested in automated systems for raising and lowering the probes to aid calibration. In addition, in wide or deep basins, wave gauge placement can become a labour-intensive task or may require special mountings to be fabricated and positioned, either suspended above the water or surface piercing from the bottom of the tank. For studies at small scale and involving waves of relatively high frequency or small amplitude resistance wire wave gauges may not provide the accuracy required.

Other Techniques

Laser Wave Gauges

When very high levels of accuracy are required optical methods using lasers and cameras can be employed. These installations tend to be customised to a particular project. One example (see Fig. 3.6a) comprises a vertically orientated laser which affects a spot of laser light onto the water/air interface. This spot is imaged by an above and angled camera and through careful calibration (via moving the laser through known displacements) and image processing (involving sub-pixel interpolation and noise rejection) the centre of the spot is transformed to a wave height. Whilst this particular method provides sub-millimetre precision, further work is required to develop this technique further to improve deployability and reduce cost.

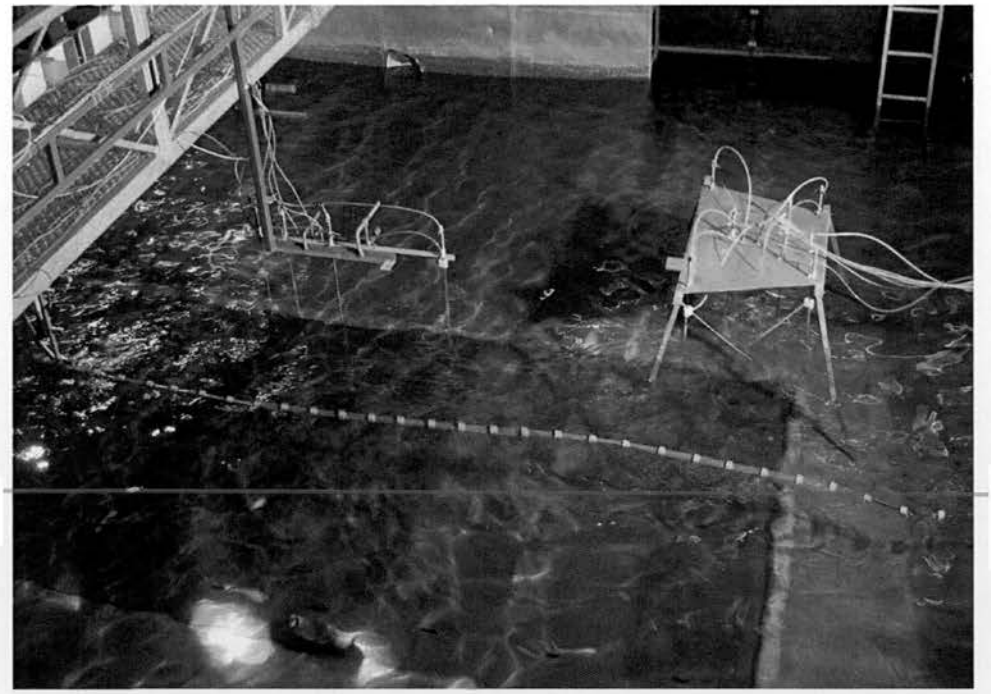

Figure 3.7. Shape Tape and wire resistance wave gauge arrays installed in Aalborg University Tank.

Ultra Sonic Position Sensors

Often used in automated production lines in factories ultra sonic position sensors can precisely measure the distance to objects placed above or below them. There is potential for them to be used as wave gauges in hydraulic facilities. A limited trial was conducted on their use in very large scale test facilities at the Grosser Wave Kanal (GWK), Hannover during the testing programmes of summer of 2009. The outcomes have not yet been published.

Visual Imaging Techniques

The visual imaging techniques referred to in the field measurement section above can be adapted for use in wave flumes and wave basins. However, their advantages in the field are diminished in the laboratory by the ability to hard-wire and locate other, simpler, more reliable measurements - although they offer spatial information that the standard point-measurement technologies can not.

A cost effective method of measuring surface elevation across one or more wave-

lengths is possible in wave flumes which have one or more transparent side panels. This technique has been used in this work (see Chapter 4). Off the shelf cameras can be used and combined with open source software, e.g., ImageJ or with proprietary software such as the image processing toolbox for MATLAB. A large variety of set-ups can be used including point and diffuse lighting (of a variety of colours) and dyes in the water [98]. The consistent aim is to provide an area of enhanced contrast between the surface elevation and the background. Even without transparent walls camera-based techniques can provide wave data via oblique angles although accuracy declines as the camera/s are moved away from perpendicular to the flume walls [99]. Extending the use of visual imaging techniques is discussed in the further work section.

3.4 Measuring Directionality

Directionality information can be obtained by either measuring the same parameter at multiple points or by measuring different parameters at the same point. The latter is the technique used in directional wave buoys where the parameters of heave, pitch and roll are measured and the measurements are all co-located. An alternative approach would be, for example, an array of bottom mounted pressure transducers.

Single point systems measure several varied properties of waves from the same location. The most common system is the heave-pitch-roll buoy. Other systems include PUV triplets comprising pressure reading (vertical axis) and two horizontal velocity components, current meters with three dimensional velocity measurement capability and inertial measurement units measuring triplets of orthogonal accelerations. Arrays comprise of multiple sensors at fixed and separate locations and can measure one or more (in combination) wave parameters such as elevation, pressures and currents. Remote-sensing systems, where a snapshot of an area is taken at a given time and the surface profile inferred by filtering can also be used to provide the directional spectrum. Examples of these systems include visible-spectrum imaging, land and sea-based HF-Radar and the radar systems found on satellites as discussed in section 3.2. An advantage of wide area measurement, such as radar and visual

imaging techniques, lies in the ability to select array positions from a large choice of data points. Selection of these data points has been shown to affect the outcome of directional wave analysis or in other words you can move virtual sensors whereas for a fixed seabed array, for example, the array separations and orientations are fixed.

The directional spectra S(f,θ) can be revealed by a variety of analyses of the measured data. They are divided in to two categories: stochastic and deterministic. Stochastic methods treat the wave field as a superposition of many components with random phases and these components are independent of each other.

Experimentally derived data analysis in this work has been implemented using the stochastic approach, more specifically using the extended maximum entropy principle (EMEP) method. In this analysis, outlined in Chapter 6, the software toolbox for Matlab, DIWASP, has been used to analyse sensor outputs and provide directionality estimates of the measured sea states.

3.5 Deterministic Sea Wave Prediction (DSWP) Models

Deterministic sea wave prediction (DSWP) models are an area of interest in the oil and gas, shipping and search and rescue fields. Having detailed and short term predictions of the incident wave field could enable otherwise dangerous or impossible operations such as landing a helicopter on a moving deck. Another recent development is the requirement to access the predicted large number of offshore wind turbines for inspection and maintenance. It is currently recognised that the complexity and non-linearity of the wave field will limit predictions to the order of several tens of seconds but that this limited future knowledge could be of benefit. Typically DSWP models are concerned with long period swell waves that underlie the incident wave field (as opposed to locally generated highly non-linear wind-waves, capillary waves, breakers etc.) and can lead to large excursions in vessel pitch or heave. To generate output predictions of wave motion the models require information on the wave field in the vicinity to the area of interest.

One challenge, (depending on sensor array set up), is that the measured points may

not be stationary and thus not provide data sampled at spatially uniform sites - a condition which is necessary for traditional discrete spectral techniques [100, 101]. In the case of LIDAR techniques polynomial interpolation in space of the data on to uniformly sampled sites brings with it the disadvantage of requiring a higher sampling rate (several times the Nyquist minimum) which in turn would reduce the time-aperture for receiving an already weak signal.

The novel sensor array (or a future derivative) described in subsequent chapters may be well suited to informing a computer algorithm about sea surface perterbutations in the immediate vicinity of a marine operation. The computer algorithm's role would likely be to provide estimates of future perturbations at a given location with a certain degree of confidence. By having access to array (as opposed to single-point) data whose spatial and temporal densities can be tuned (based on constraining factors of sensor deployment and computer processing power) the algorithm should have an improved ability to predict future surface elevations. In addition, the methods by which these models propagate water wave dynamics could play a role with the data acquisition and processing system itself through instrument calibration and optimisation. Whilst these deterministic methods are outside the scope of this work they are included to highlight both motivation for acquiring improved measurements and as a possible aid to securing these measurements.

CHAPTER 4

Design Concept Feasibility Study: Surface Tracking of a Ribbon

4.1 Preliminary Feasibility Study: Optical Tracking

4.1.1 Motivation

This aim of this thesis is to investigate both the ability of ribbon-like, flexible and floating instruments to physically track a moving water/air interface and the ability of an instrument based around this ribbon concept to measure and report its position in three-dimensional (3D) space.

In order to test the ability of a ribbon configuration to remain *mechanically* close to the water/air interface whilst under the influence of waves an optical test procedure was devised and implemented and is outlined in this chapter. This optical tracking technique involves using off-the-shelf camera equipment to provide insight into the *potential* of long, flexible ribbon-like elements to accurately measure waves. Both regular and irregular wave tests were conducted in the Edinburgh 20m wave flume with various floating structures trialled. Following these tests on purely mechanical wave-tracking ability, active measurement instruments configured as floating ribbon-like elements were trialled under the same wave conditions presented here. These

electronically active sensors and the methodology of their testing are discussed in chapters 5 and 6.

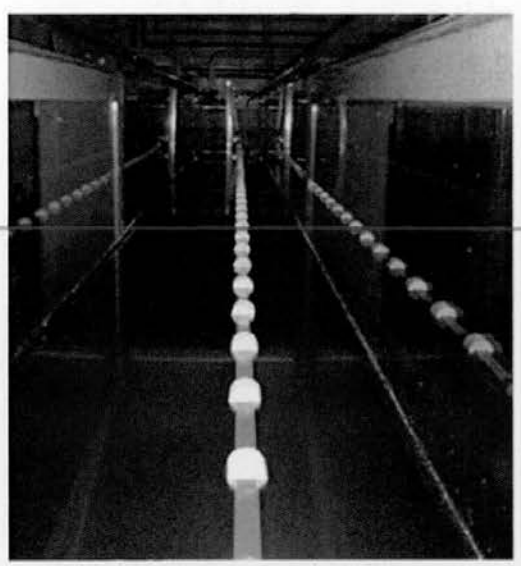

(a) Optical fibre-based floating ribbon in Edinburgh Flume

(b) Inactive floating ribbon (as array) in Edinburgh Curved Tank

(c) MEM-based floating ribbon in GWK, Hannover Flume.

Figure 4.1. Three implementations of the floating ribbon sensor concept

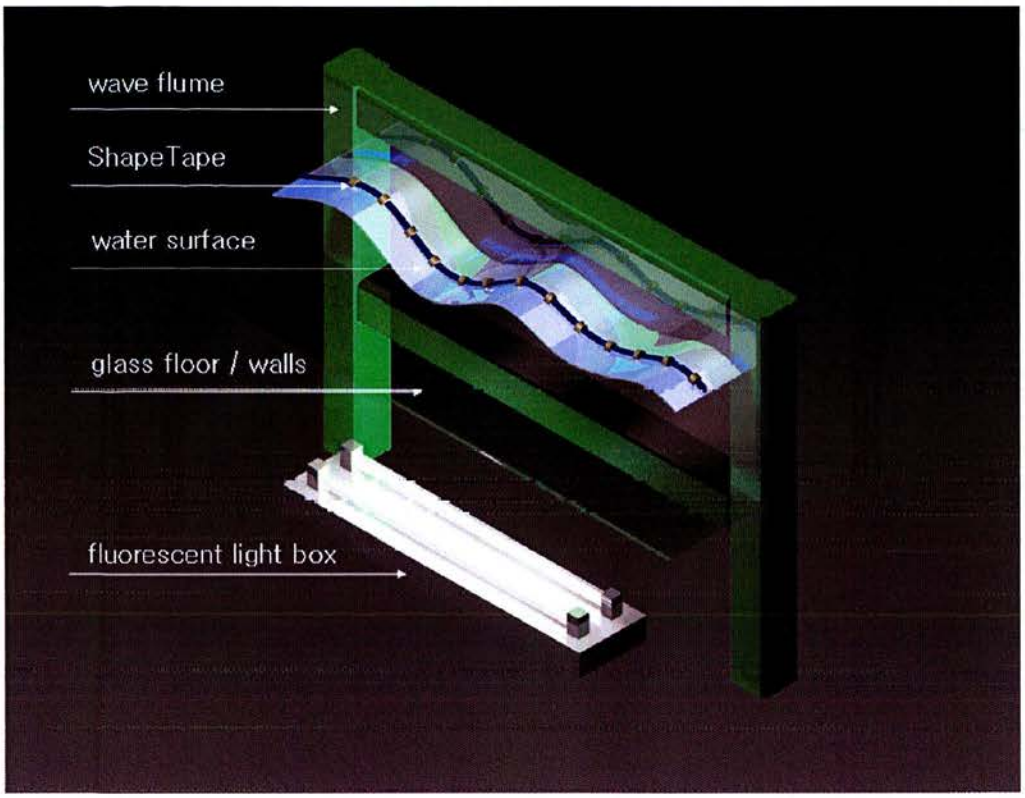

Figure 4.2. CAD sketch showing one 3m flume section with ShapeTape floating in incident irregular wave.

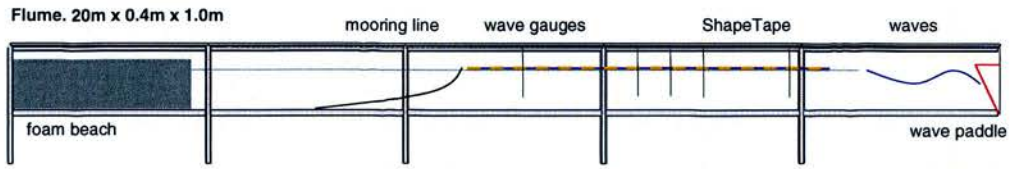

(a) Diagram of experimental set up

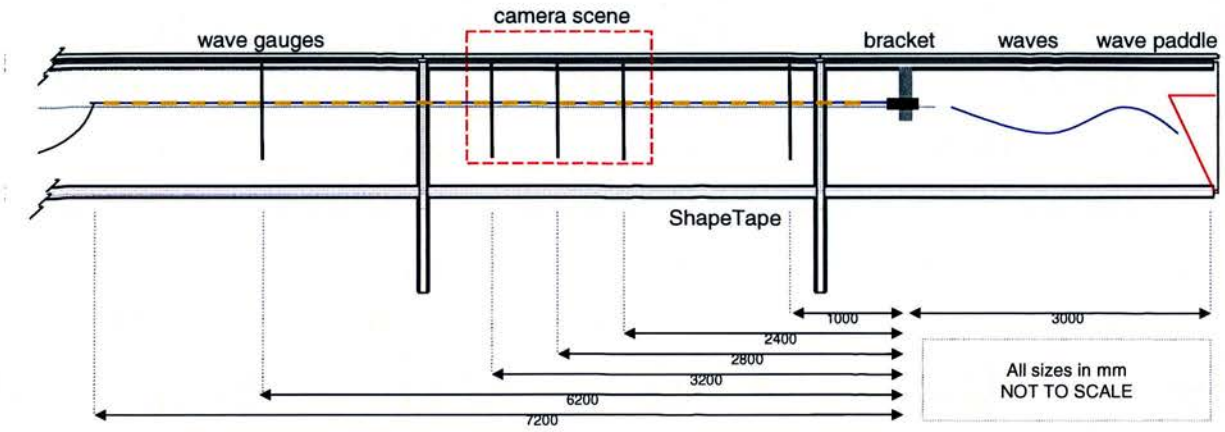

(b) Diagram of experimental set up

Figure 4.3. Experimental set-up showing positions of wave gauges, ShapeTape and camera field of vision

4.1.2 Experimental Procedure

Investigation of available technology

An investigation was conducted on available technologies that could, in theory, be integrated in to floating ribbon-like arrangements. This revealed several candidate technologies: the first comprising existing, off-the-shelf, long, thin and flexible sensors manufactured by a technology company in Canada based on fibre-optics and the second comprising integration of various Micro-electro-mechanical systems (MEMS). Given that the optical fibre technology could provide an integrated solution, i.e., the sensors and the ribbon structure are combined as a single pre-fabricated system, experimentation in to the surface-tracking ability of such as system could be carried out immediately and hence this option was selected.

Testing of an off-the-shelf "Demonstrator" technology

A demonstration ribbon 7m long, 15mm wide and 3mm deep, comprising spring steel and optical fibres and coated in a thin layer of Polyvinyl chloride (PVC) was supplied by Measurand Inc. of Canada. The width and depth dimensions are fixed due to product specification. The length of 7m was selected due to this being the longest ribbon offered by the company at the time of research. This measurement device was designed for use in motion capture procedures and will be detailed in subsequent chapters. Its mechanical behaviour in a wave flume is investigated here. A Computer Aided Design (CAD) rendering of a typical experimental set up is shown in figure 4.2. This ribbon exhibited typical physical properties of the company's Shape Tape ™ product but by being inactive electronically cost only the price of shipping. Buoyancy aids, spaced 150mm apart, were added along the length of the ribbon to keep it flat across the water/air interface. Without these buoyancy aids the ribbon would sink. The spacing was selected after experimentation to allow the optimal surface contact of the ribbon whilst adding the least amount of buoyancy and inertia to the system.

Testing via optical tracking

Filming of the ribbon in a variety of wave conditions and subsequent image analysis provided estimates on the ability of the ribbon to surface-track.

There is a strong tradition of using optical techniques in wave flumes to measure parameters such as turbulence, vorticity, mixing and particle velocity and a large variety of choices of implementation. A common theme in these techniques is the care required in experimental set up. In this particular set up the tank glass walls, and the water within, needed to be clean of surfactants and debris caused by rusting of various components of other users' experiments and the use of pollen (which subsequently decays) for particle motion experiments. Testing a large number of lighting configurations resulted in suitable under-tank lighting in terms of the lighting position, types and intensity. A dual fluorescent tube arrangement was trialled and then adopted to provide general up-lighting of the surface meniscus against the glass, with a series of spot bulbs used to *fill-in* any low intensity areas. In order to aid analysis, an above tank ultra-violet (UV) tube lamp was used to highlight the floats - which were coated in UV reactive paint. The large contrast between the floats (blue) compared to the highlighted meniscus (white) can be seen in the stills of figures 4.4, 4.5 and processed image, figure 4.6. It is assumed throughout that the central position of the meniscus represents the surface elevation of the water waves. Whilst 3D effects in the flume (and surface tension at the glass) may result in this edge meniscus being offset with respect to the surface elevation as measured at the centre of the wave field it is assumed that this offset remains constant. It should also be noted that the procedure is looking for *relative* differences between the central float positions and the central meniscus as this value determines the level of *surface-tracking* that is being achieved by the floating sensors. Quantifying the effect of the meniscus as a measure of surface elevation is discussed further in the Discussions section. With further experience in image processing the stringent requirements of test set up were able to be reduced. For example, denoising filters can be applied to remove bubbles or smears thus reducing the requirement for cleaning or repeating tests.

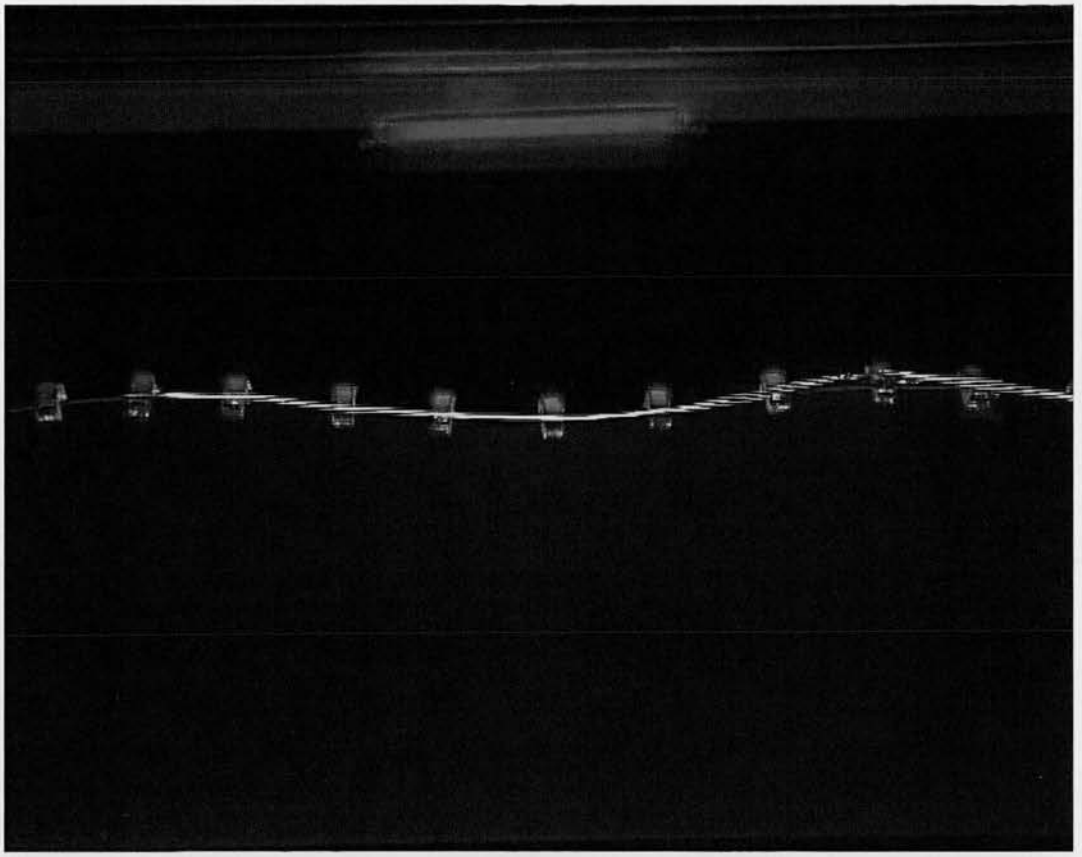

Figure 4.4. Frame of preliminary optical tests

A preliminary batch of testing was carried out (and subsequently analysed) using images shown in figure 4.4. To improve the resolution of float displacement measurements a second batch of tests were carried out with the camera closer to the flume walls, as shown in figure 4.5.

Image Processing Procedure

The procedure for image capture and analysis is summarised below

- Sony 3 CCD captures images at 25 frames per second (fps), PAL format at 720x576 pixels on to DV video tape.
- Movie files are extracted using Adobe Premiere and converted to sequence of thousands of 1.1Mb bitmap files.
- Folders of images are batch processed using ImageJ in the following way:

  - Crop image to remove top and bottom unnecessary sections.
  - Optimise image contrast.
  - Threshold the image using colour information in images to produce two images: one containing floats; and the other containing the water/air interface.
  - Make images binary (black and white only)
  - Particle track floats outputting particle summaries (corner locations, centres, area etc.) to text file.

- MATLAB batch processes folders of surface binary images and curve-fit to produce surface location in x and y axis.
- MATLAB pairs surface positions with float positions and outputs error between the two.

ImageJ is open source software (based on the Java programming language) which is used extensively in the medical imaging field. Processes can be run as click-recorded macros or as coded plug-ins of which there are many hundreds made available to download by the ImageJ community [102]. An alternative method of image analysis to ImageJ became available in 2009 when the University of Edinburgh opened the license for the MATLAB Image Processing Toolbox to multiple users. [1]

Initially a small number of tests using Jonswap irregular wave spectra were conducted using the varying peak frequency, T_p and significant wave height, H_{m0}, shown in table 4.1.

Table 4.1. Preliminary Irregular Wave Test Matrix

Label	H_{m0}(m)	Peak Period, T_p (s)	Duration (s)
1	0.016	1.02	1024
2	0.077	1.02	1024
3	0.037	0.99	1024
4	0.072	1.32	1024

[1] Since the completion of these experiments ImageJ has continually grown and received funding council support in the USA. A major new release ImageJ 2.0 is now available and is being used in undergraduate, masters and postgraduate student projects in the Edinburgh Flume.

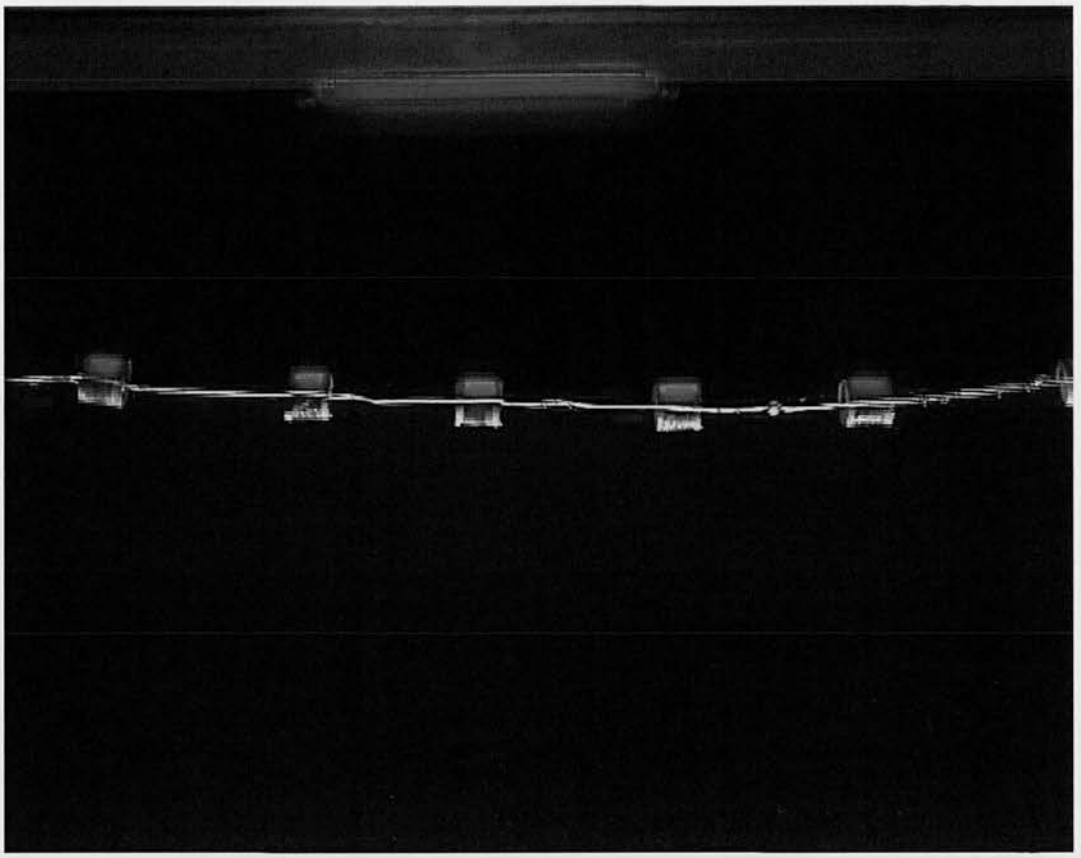

Figure 4.5. Frame of zoomed-in optical tests

Figure 4.6. Processed movie frame

4.1.3 A Note on the Use of R and R^2

Throughout this thesis the correlation coefficient, R, features in many plot legends. It has been used as an estimate of the agreement between the measurements of two independent instruments (in a line-of-best-fit sense) and moreover, as a subsequent parameter to base post-processing algorithm tuning on, as opposed to offering

robust statistical meaning. Errors between prototype sensor and traditional baseline measurements are generally reported in terms of absolute error between the two instruments and/or relative errors in terms of percentage. Negative percentages are included (the error having not been squared then subsequently square rooted) in order that any trends and bias in sensor performance could be more readily highlighted. Where error analysis involves the parameter R^2 this has been included to highlight trends in any errors reported, for example in showing the sensitivity of measured wave height error to the experienced wave steepness. Again, as with R, the parameter is not used in its strict statistical sense but as a tool to assist post-processing, error-reduction, calibration error mitigation and sensitivity studies.

4.1.4 Results

Irregular Waves

Figure 4.7 shows a typical comparison of the float position and surface elevation for test number two during two 30 seconds periods of the test, chosen to show typical/representative behaviour.

Surface elevations were processed in the time domain by a zero up-crossing/down-crossing method using both WaveLab 2 [103] and an internally available MATLAB routine, *TimeDomainStats5.m* [104], which makes use of the Wave Analysis for Fatigue and Oceanography, (WAFO) toolbox [105]. Figure 4.7 shows a wave record with high correlation (>0.96 based on normalised coefficient returned by cross correlation) but whose wave-by-wave comparison produces large individual errors. It was identified during these limited tests that a more thorough and robust method of analysing the elevation data would be required. Subsequent to these preliminary tests effort was focused on improving image processing routines to allow a greater number of further High Definition tests to be conducted with increased automation. A limited post processing procedure was used in these early tests with more weighting put on the overall trends in the elevation - time traces.

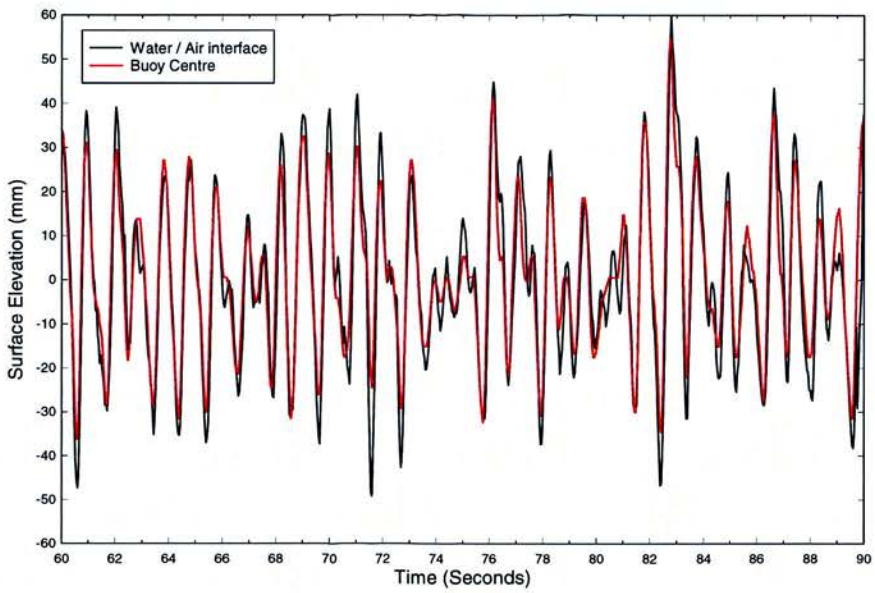

(a) 30 second interval. $H_{m0} = 0.077m$, $T_p = 1.0sec$

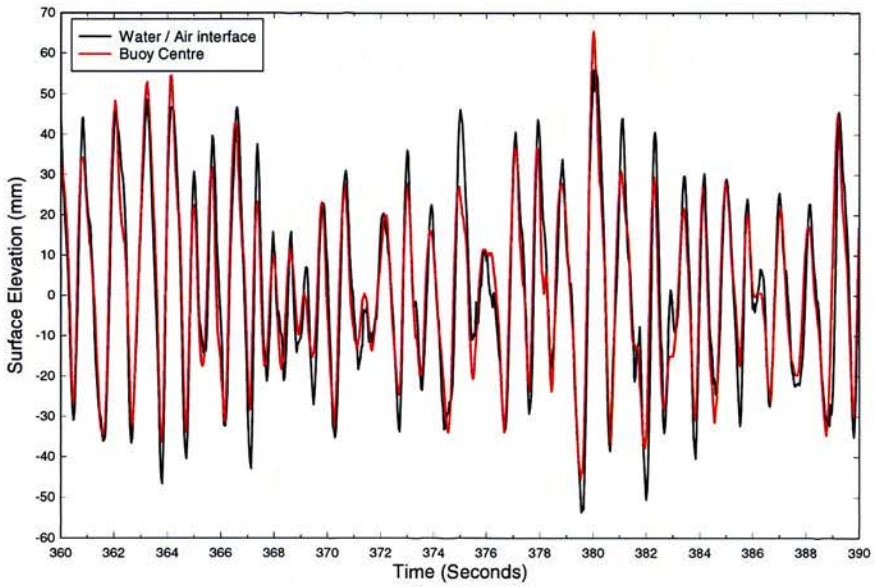

(b) 30 second interval. $H_{m0} = 0.077m$, $T_p = 1.0sec$

Figure 4.7. Irregular test number 2 - wave elevation time series

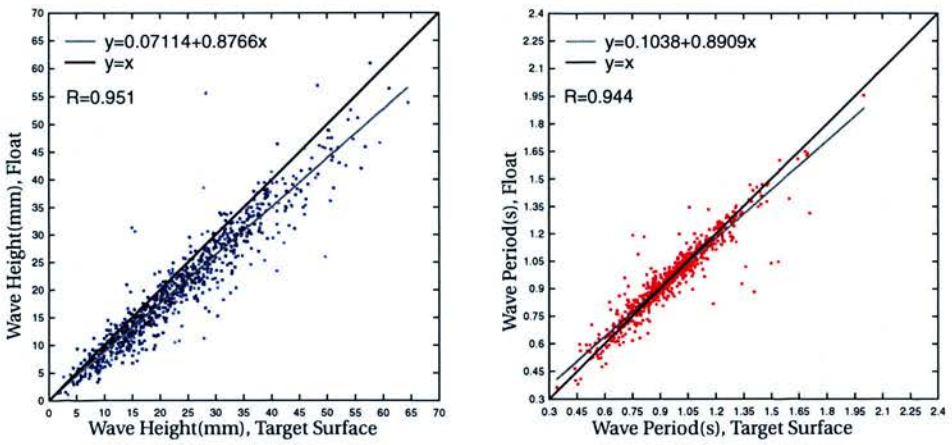

(a) Wave Height (b) Wave Period

Figure 4.10. Original irregular test number 3. Float-tracked wave heights and wave period compared to wave gauges.

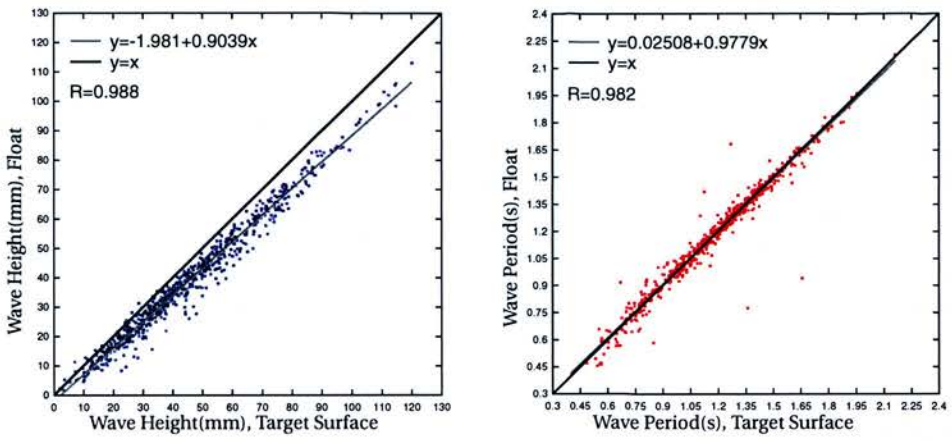

(a) Wave Height (b) Wave Period

Figure 4.11. Original irregular test number 4. Float-tracked wave heights and wave period compared to wave gauges.

Results from these tests were based on the dynamics of the central float (with respect to camera field of vision). No comparison was made between the various floats along the ribbon. This was due to time constraints and the intermittent availability of edge floats as they come in and out of each image frame. From visual inspection of the tests, video footage and the time elevation comparisons it was concluded that for a significant range of waves in a irregular sea conditions (although for a limited quantity and type of sea state) a floating ribbon remains closely coupled to the water/air interface. Therefore, based on these exploratory tests and after discussion with the manufacturers, a fully active and customised ShapeTape was purchased.

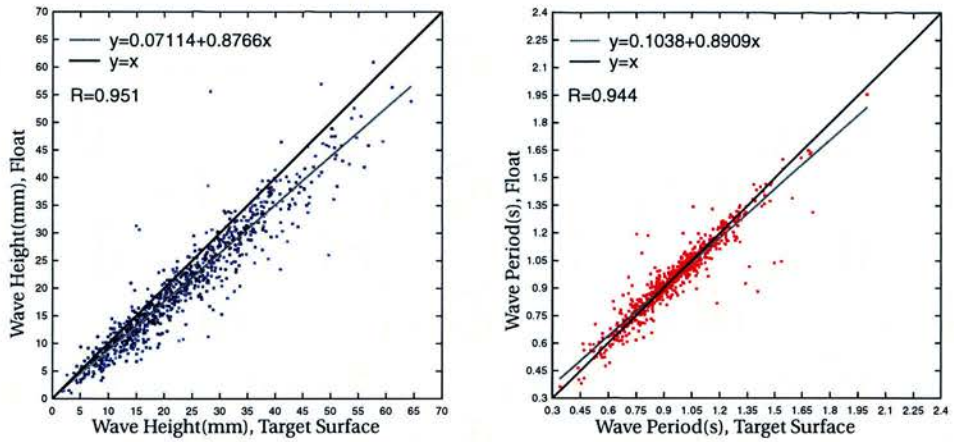

(a) Wave Height (b) Wave Period

Figure 4.10. Original irregular test number 3. Float-tracked wave heights and wave period compared to wave gauges.

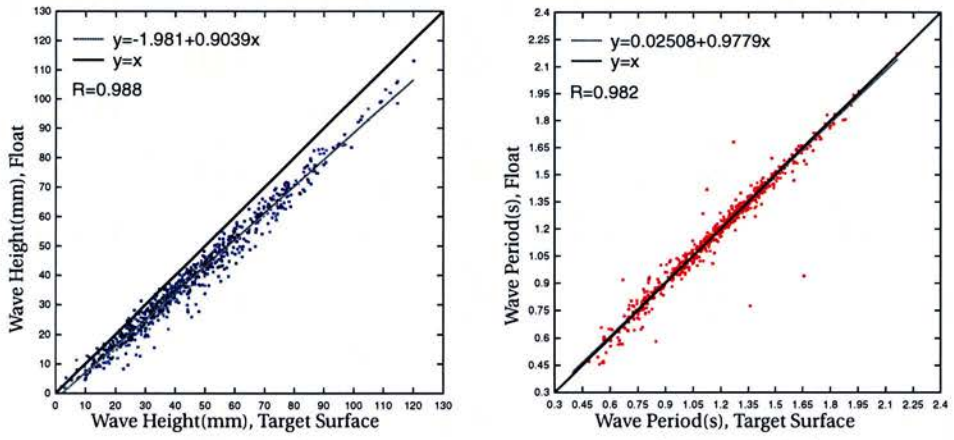

(a) Wave Height (b) Wave Period

Figure 4.11. Original irregular test number 4. Float-tracked wave heights and wave period compared to wave gauges.

Results from these tests were based on the dynamics of the central float (with respect to camera field of vision). No comparison was made between the various floats along the ribbon. This was due to time constraints and the intermittent availability of edge floats as they come in and out of each image frame. From visual inspection of the tests, video footage and the time elevation comparisons it was concluded that for a significant range of waves in a irregular sea conditions (although for a limited quantity and type of sea state) a floating ribbon remains closely coupled to the water/air interface. Therefore, based on these exploratory tests and after discussion with the manufacturers, a fully active and customised ShapeTape was purchased.

Summary of Conclusions:

- Surface tracking based on early test results together with qualitative visual inspection was encouraging and merited further investigation
- Surface tracking performance improved for tests comprising longer wavelength, higher period waves as shown in figures 4.8 to 4.11.
- To test the ability of thin, lightweight and flexible ribbons to track the water air/interface high resolution more robust optical tracking experiments were required.
- Improved post-processing routines/algorithms were required to assess the results of further testing.

Follow on tests were implemented and are described in the following section.

4.2 Feasibility Study: Improved Optical Tracking

4.2.1 Motivation

To quantify the surface tracking ability of a thin, flexible and lightweight ribbon more tests were needed along with careful post processing of tank test footage. Having taken delivery of the electronically active sensor, optical tests became a lower priority but were revisited in later active ribbon tests and a new method of image capture, post processing and analysis applied. This process is outlined in the following sections.

4.2.2 Experimental Procedure

A Canon Legria HF HD consumer-class video camera (recording in "High Definition") was used which produces a 25 frames per second (fps) movie comprising images with almost four times as many pixels as the previous set up. In order to streamline the time consuming processing and analysis all processing was carried out in MATLAB using the Image Acquisition Toolbox (as opposed to ImageJ as in previous tests).

Figure 4.12 shows a typical image (with wire resistance wave gauges overlaid for visualisation purposes).

Image Processing Procedure

Image processing was conducted as explained below:

- "DGAVCIndex" software was used to create a movie file wrapper (.MTS to .avs) (allows greater range of software to access the movie file)
- "VirtuaDub" software used in preliminary processing
  - open converted movie file and strip out images (for later batch processing)
  - frame cropping (file size reduction)
  - deinterlacing (to reduce motion induced artifacts)
- 15,000 4.6Mb bitmap images created per 512 second test
- MATLAB Image Toolbox and the code from the Matlab Particle Tracking Code Repository, [106]
  - various filters trialled, optimised and implemented
  - image multiplication/addition/subtraction across the 3 RGB (red, green, blue) images
- MATLAB Curve Fitting Toolbox, Optimisation Toolbox and SLM toolbox [107] used to spline fit to the water/air interface. [2]
- MATLAB Image Toolbox used in edge detection of the float positions
- MATLAB custom script used to search for anomalies, investigate and fix where appropriate.

The various stages of image processing can be seen in figure 4.12. Figure 4.12a shows the water/air interface having been separated from the background image and

[2] from SLM - Shape Language Modeling by John D'Errico - Least squares spline modeling.

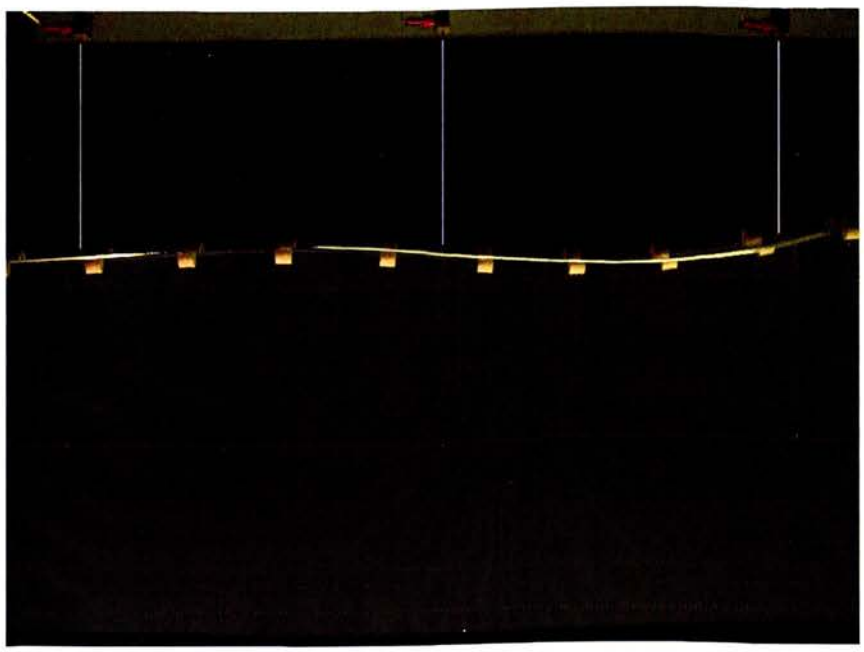

(a) Original frame from movie file (1440x700 pixels)

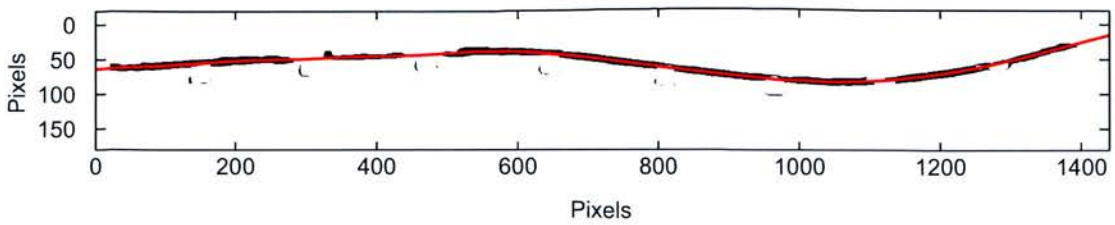

(b) Water/air interface highlighted and data points used to fit spline.

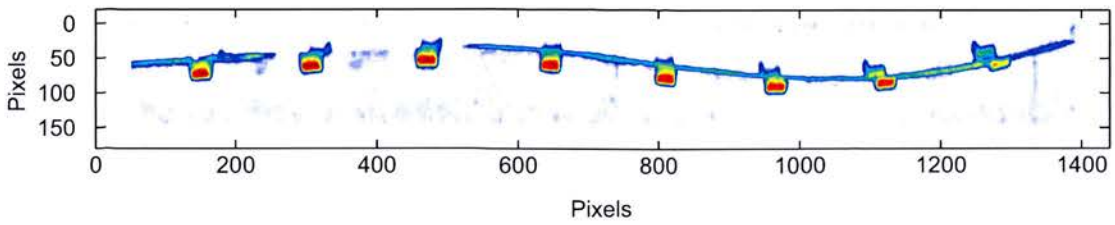

(c) Floats along ribbon highlighted.

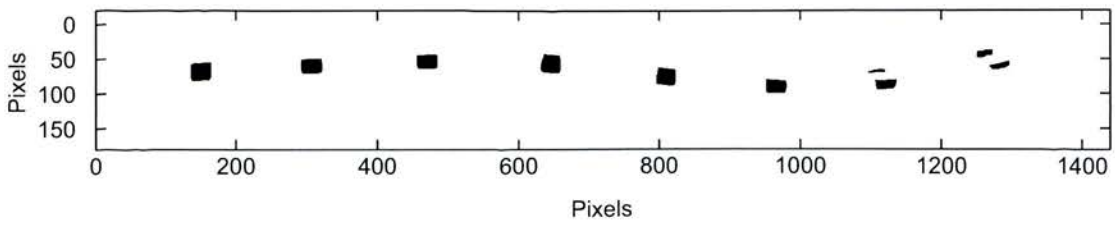

(d) Floats separated from image.

Figure 4.12. High Definition (HD) image processing

a cubic spline having been fitted to the data. Examples of this fitting can also be seen in figures 4.32 to 4.34. In these screenshots the three wave gauges have been filtered out of the image (they are barely visible in grey) and are subsequently indicated for clarity. The surface tracking algorithm's estimate of surface elevation is marked in cyan whilst the algorithm's estimate of floats visible below the surface are outlined in red. Regarding the surface-fitting, the SLM toolbox offers exceptional flexibility and control over the "shape" of the least-squares fitting cubic spline. Among the many control parameters are: adaptive "knot" placement; regions to ignore; end conditions; maximum/minimum derivatives and maximum/minimum values. In particular, end condition control is useful due to the ability to set the value to be within a specified range based on previous images (in time). This improves immunity to noise for end curvatures where the lower contrast and more error prone edges of the images could *(and did)* otherwise cause problems. Before curve fitting a custom Matlab script analyses the density of pixels along the region of interest and if the data passes a certain threshold then these data points and their neighbours are included in the curve fitting process. During processing frames were monitored for unusual activity and these frames labelled for further automatic (sub-routine) or manual processing.

Image Processing Time Cost

Whilst the HD camera offers many more pixels and thus a higher spatial resolution it comes at a large cost - computational time in processing the images. Using the best set up available (limited by software license availability, computer availability, network speeds and hard disk drive space etc.) the times to process the footage can be seen in table 4.2. 240,000 images were processed in these tests.

As data folders are processed, interruptions and errors occur due to experimental issues. For example lighting changes, breaking waves and large build up of surfactants on the glass. In addition, computational issues can break the algorithms such as memory allocation errors or losing a tracked particle for several frames.

Table 4.4 shows the test matrix used in these high definition tests. The range was

Table 4.2. Time and Data cost of video processing

Process	Time Cost (hours) Initial	Running	Outcome Data Size (Gb)
Filming	several	N/A	14.4[1]
Camera to PC	1/2	1/2	14.4
Movie to Frames	8	67[2]	1000
Process Frames[3]	100	83[4]	2.5

[1] 9600 seconds of filming @ MPEG2 compression of 1.5Mb/s = 14.4 Gb.
[2] 9600 seconds @ 25fps = 240,000 frames. Processed @ 1fps = 67 hours.
[3] 240,000 frames processed @ 0.8 seconds = 83 hours.
[4] Depending on processing error frequency.

chosen to suit the operating range of the tank from large long waves to short steep waves. Test 5 proved to be at the edges of the tank's operating range and contained many large breaking waves. It was halted 280 seconds in to the test. The footage was processed and included in the analysis.

4.2.3 Results

Regular Waves

Wave gauge consistency

Five wire resistance wave gauges were installed in the flume as can be seen in figure 4.3. Wave gauge number 1 and wave gauge number 5 were distant from the field of view of the camera and the ribbon / floats compared with the centrally positioned wave gauges 2, 3 and 4. Figure 4.13 shows the mean values of all 5 wave gauges over the 64 tests. It can be seen that there is greater variance in the gauge readings for higher frequency waves. There is less deviation around the mean if analysis is limited to the three central gauges and gauges 1 and 5 are neglected. During image analysis the optically tracked surface is matched with the gauge that is closest to it at any given time.

Figures 4.14 to 4.16 are intended to highlight any trend in the wave gauge measurements. It appears that whilst there is no correlation of error (within this test range) against wave height, increasing wave period and wave steepness seem to affect a

Table 4.3. Regular wave test matrix

Test #	Wave Height (m)	Period (s)	Test #	Wave Height (m)	Period (s)
1	0.01	1.43	33	0.06	1.00
2	0.02	1.43	34	0.07	1.00
3	0.03	1.43	35	0.08	1.00
4	0.04	1.43	36	0.09	1.00
5	0.05	1.43	37	0.01	0.91
6	0.06	1.43	38	0.02	0.91
7	0.07	1.43	39	0.03	0.91
8	0.08	1.43	40	0.04	0.91
9	0.09	1.43	41	0.05	0.91
10	0.01	1.25	42	0.06	0.91
11	0.02	1.25	43	0.07	0.91
12	0.03	1.25	44	0.08	0.91
13	0.04	1.25	45	0.01	0.83
14	0.05	1.25	46	0.02	0.83
15	0.06	1.25	47	0.03	0.83
16	0.07	1.25	48	0.04	0.83
17	0.08	1.25	49	0.05	0.83
18	0.09	1.25	50	0.06	0.83
19	0.01	1.11	51	0.07	0.83
20	0.02	1.11	52	0.08	0.83
21	0.03	1.11	53	0.01	0.77
22	0.04	1.11	54	0.02	0.77
23	0.05	1.11	55	0.03	0.77
24	0.06	1.11	56	0.04	0.77
25	0.07	1.11	57	0.05	0.77
26	0.08	1.11	58	0.06	0.77
27	0.09	1.11	59	0.07	0.77
28	0.01	1.00	60	0.01	0.71
29	0.02	1.00	61	0.02	0.71
30	0.03	1.00	62	0.03	0.71
31	0.04	1.00	63	0.04	0.71
32	0.05	1.00	64	0.05	0.71

Table 4.4. Irregular wave test matrix

Test #	H_{m0} (m)	Peak Period, T_p (s)	Duration (s)
1	0.112	1.32	512
2	0.069	1.05	512
3	0.046	0.85	512
4	0.036	0.76	512
5	0.119	1.33	280 of 512
6	0.080	1.07	512

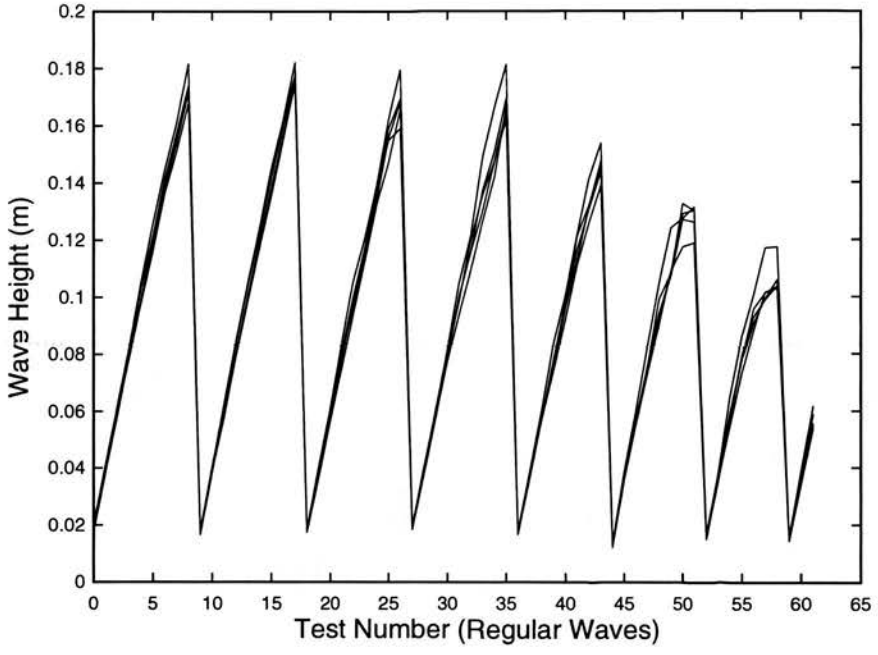

Figure 4.13. Wave gauge consistency. Wave heights reported by 5 wave gauges for 62 regular wave tests.

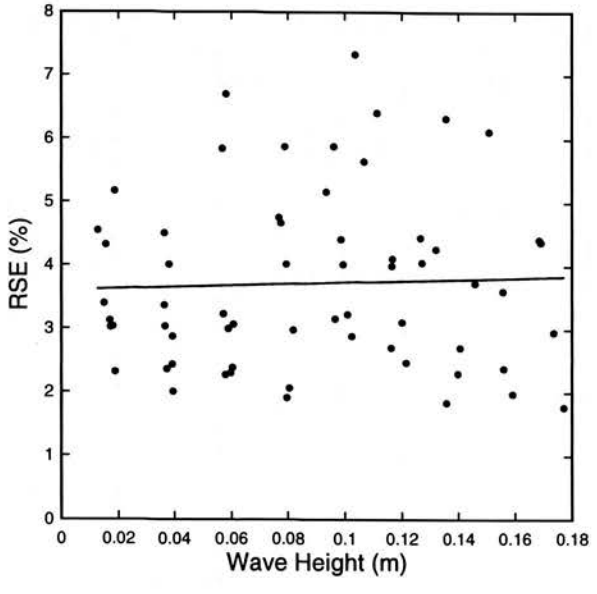

Figure 4.14. Relative Standard Error (%) versus wave height (m) of 5 wave gauges

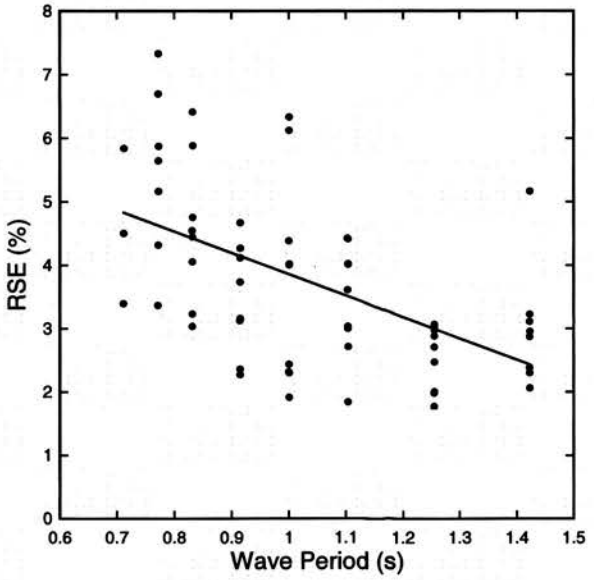

Figure 4.15. Relative Standard Error (%) versus wave period (sec) of 5 wave gauges

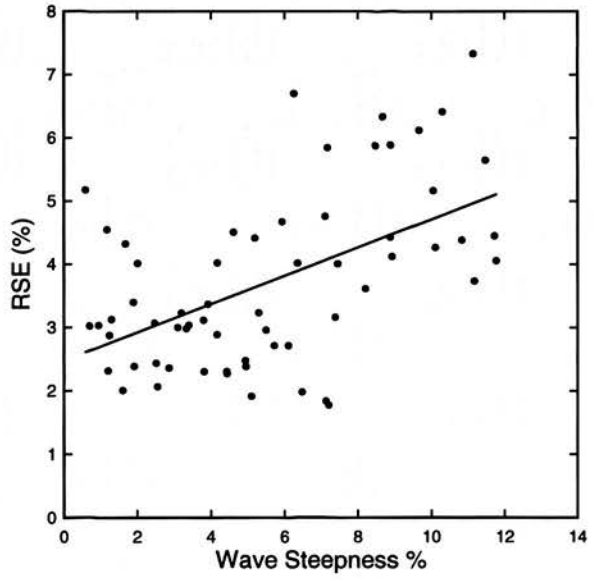

Figure 4.16. Relative Standard Error (%) versus wave steepness of 5 wave gauges

greater *error*, or more accurately, difference between wave gauge measurements.

Optical Tracking - Surface vs Wave Gauge

Figures 4.17a and 4.17b show high correlation (R^2 = 0.992 for wave heights and R^2 = 0.998 for wave periods) between measured surface elevation using wire resistance wave gauges and the surface elevation reported after image processing. This gives confidence in the method of using estimates of float centres versus imaged surface as a description of surface tracking ability for those regions distant from a wire resistant wave gauge. If the surface imaging produced large errors only floats near a wire resistance wave gauge would be able to be tracked.

Optical Tracking - Float Centre Position

Figures 4.18 and 4.19 show the results from regular wave test numbers 1 to 57. Due to high wave steepness and surface roughness the image processing routines could not function adequately for tests 58 to 64. Figure 4.18 shows the mean error across centre positions of floats 2 to 7 (excluding the two outermost pods) as a percentage of the mean wave height measured by the three nearest wire resistance wave gauges. Also shown is the Relative Standard Error (RSE) or standard deviation of the mean wave height measurements across floats 2 to 7 as a percentage of the traditionally measured mean wave height. Figure 4.19 displays the same parameters in terms of wave period. It can be seen that mean wave period errors remains unchanged (and very small) with increasing steepness whilst the standard deviation of the errors across the sensor region increases with steepness. It should be noted that this measure of error still remains below approximately 2%.

Irregular Waves

Table 4.5 shows time domain zero-crossing analysis of the six irregular wave tests. It should be noted that this table shows the standard deviation of the mean across the 8 pods as opposed to the standard deviation across the many data points of each pod's signal. A large standard deviation implies that the wave-by-wave matching process

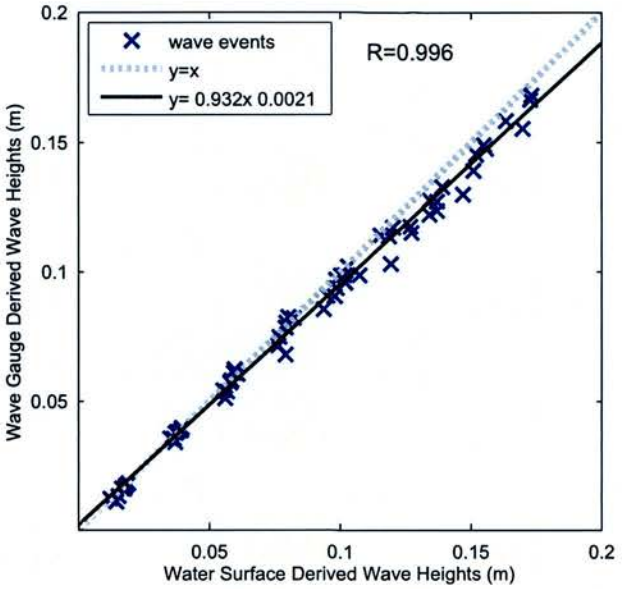

(a) wave elevations

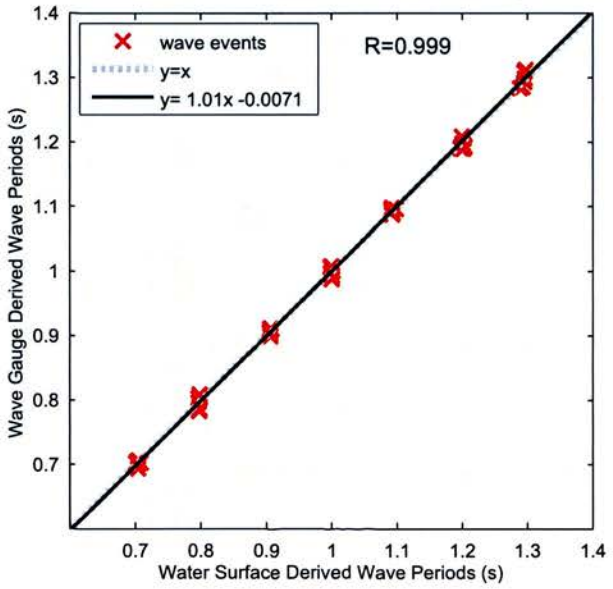

(b) wave periods

Figure 4.17. Wire resistance wave gauge measured versus optically tracked surface parameters

showed large variation across the sensor / camera field of view. The labels Matched, Unmatched, Processed and Error>20 are detailed below:

- *Matched*: The number of waves in the wave gauge elevation time series that have been identified and paired (matched) with the corresponding wave from

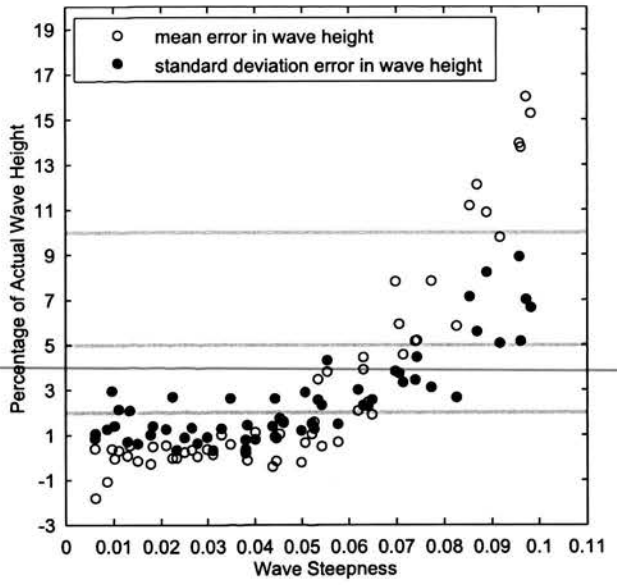

Figure 4.18. Errors in float-centre measured wave height vs steepness

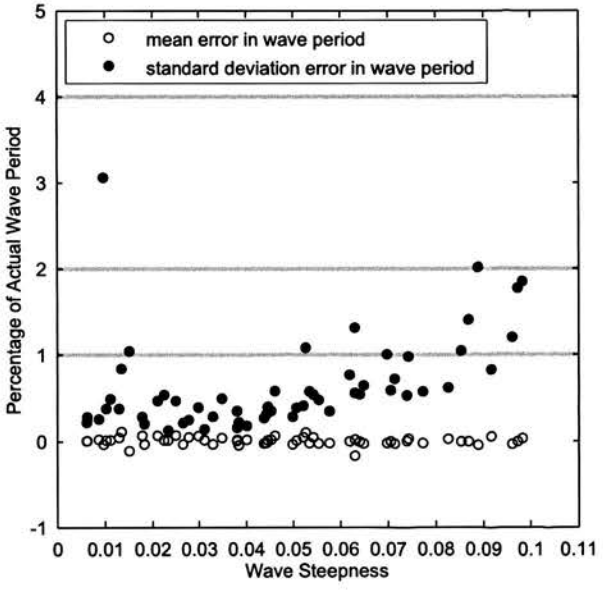

Figure 4.19. Errors in float-centre measured wave period vs wave steepness

Table 4.5. Time domain wave events

Test	Number and Type of Event							
	Matched		Unmatched		Processed		Error > 20	
	Mean	Std.	Mean	Std.	Mean	Std.	Mean	Std.
1	424	3.1	7.6	3.1	5.4	2.1	4.8	2.1
2	470	3.8	5.1	3.8	6.0	1.8	3.8	1.9
3	580	9.4	16.9	9.4	11.0	4.4	11.9	4.9
4	590	2.7	3.0	2.1	3.0	1.3	4.5	2.1
5	233	8.4	6.9	8.4	3.0	1.3	2.0	1.6
6	468	9.0	7.1	9.0	4.1	2.2	2.9	2.2

the float-centre elevation time series.

- *Unmatched*: Wave events that were flagged as having greater than 20% error between wave gauge period and float-centre tracked period.

- *Processed*: Wave events that with minor modification (adjusted wave height of < 0.02m) produce matched wave events.

- *Error>20*: Wave events that contain errors of magnitude greater than 20% between wave gauge and float-centre tracked period.

It should be noted that given the high level of agreement of wave period comparisons, wave period agreement is used as the initial threshold value, with wave-height being introduced in the subsequent steps. An example of the individual wave event "processing" can be seen in figure 4.20 which shows an event that has been flagged during the overall image processing routine. Large errors in period trigger a secondary analysis routine which ascertains if the error is due, in part, to the zero downcrossing method of defining waves. If the tracked surface time-series reports a very small wave/s and the corresponding float position time-series lies within a small distance from the MWL an adjustment to the float data is proposed (see Fig. 4.20 around the 95 second position). The adjustments are flagged in the algorithm and are only included in the statistical analysis once they have been manually checked during post-processing. If the adjustments are too bold or unwarranted they are discarded on a correction-by-correction basis. This is made possible by simultaneously displaying each investigated event and the routines' suggested alterations and due to the

fact that each 512 second irregular wave train show only between three and eleven outlier events averaged across the eight tracked floats, as can be seen in table 4.5.

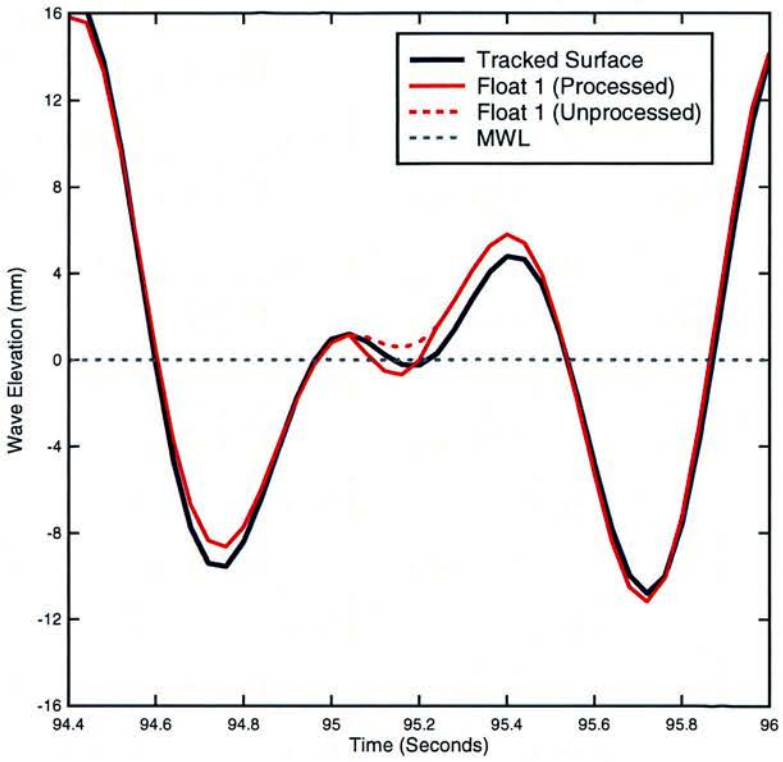

Figure 4.20. Example of zero-downcrossing processing

Figures 4.21 and 4.22 show two representative time series snapshots from irregular test no. 3 and irregular test no. 5. Each subplot (a-c) shows the surface elevation from two adjacent float centres and the corresponding local surface elevation. The level of coherence in the long wavelength, large amplitude, irregular seas of 4.22 is clearly greater than in the higher frequency sea-state of test no. 3 where the behaviour of two adjacent pods is comparatively less similar. This could indicate a wave flume with poorer wave absorption qualities in high frequency sea-states. The cause of this would require further specific testing on both the force-feedback mechanism of the wave generator (which seeks to actively damp reflected waves) and the flume's synthetic "beach" (which passively damps waves).

Figure 4.23 show the correlation between wave heights and wave periods as measured at float central positions and local surface elevations. Test 1 and floats 2,4,6 and 8 are shown.

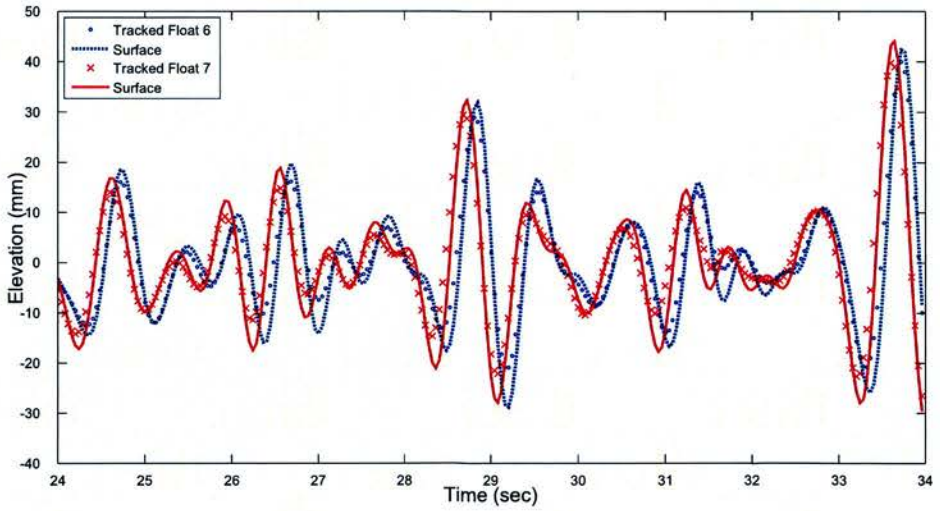

(a) Surface elevation as reported by surface tracking and float numbers 6 and 7.

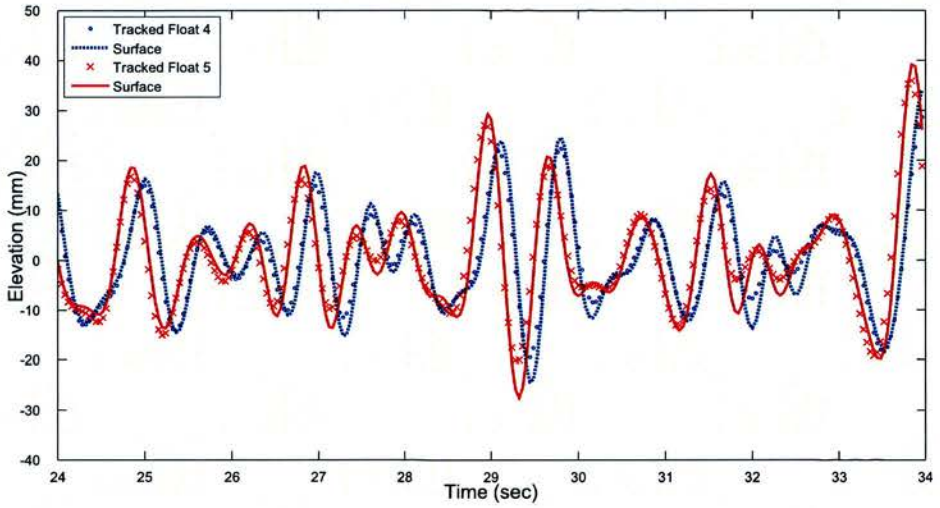

(b) Surface elevation as reported by surface tracking and float numbers 4 and 5.

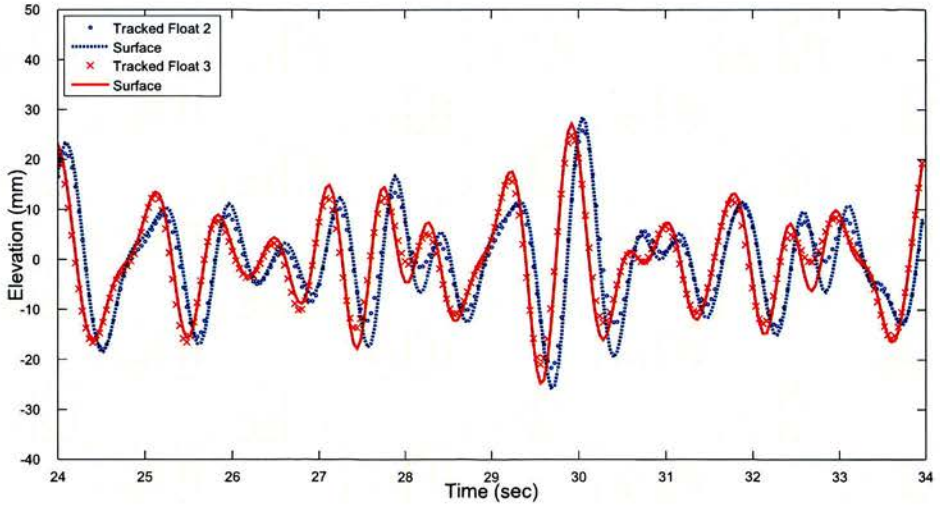

(c) Surface elevation as reported by surface tracking and float numbers 2 and 3.

Figure 4.21. Optical tracking during irregular test number 3

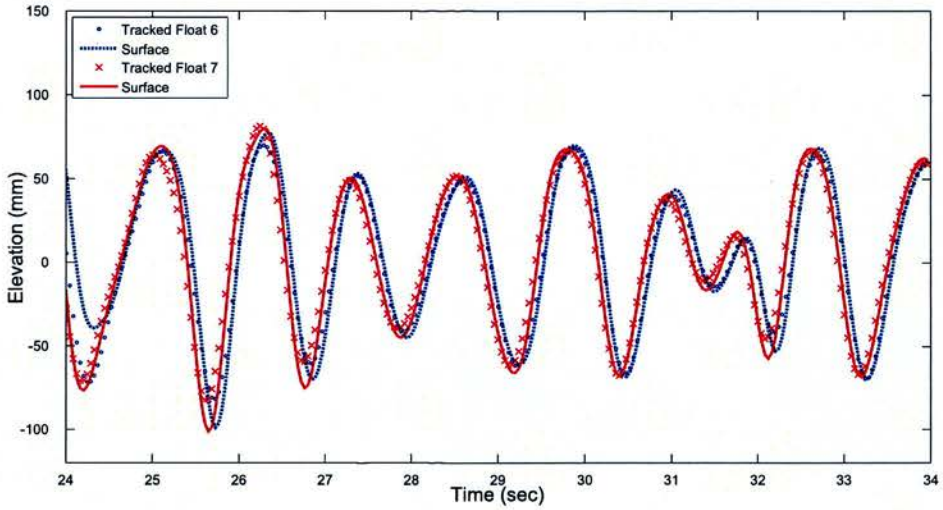

(a) Surface elevation as reported by surface tracking and float numbers 6 and 7

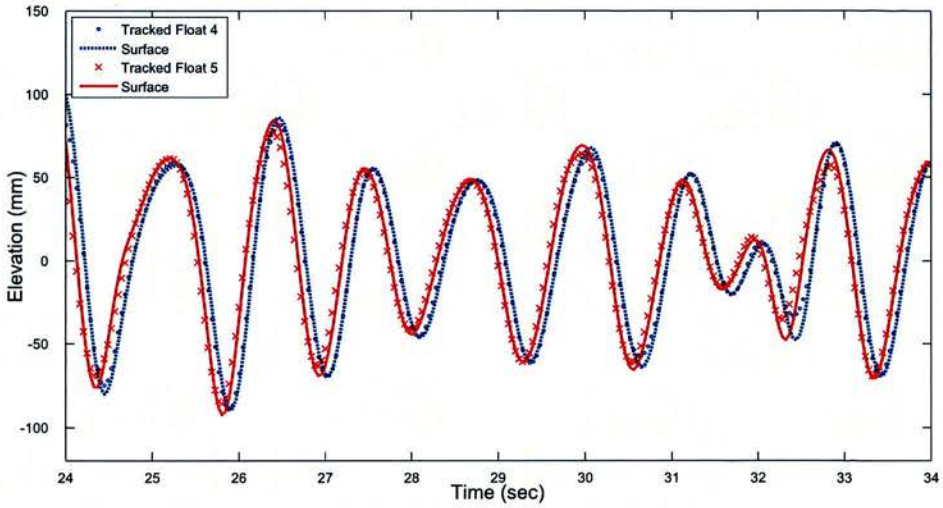

(b) Surface elevation as reported by surface tracking and float numbers 4 and 5

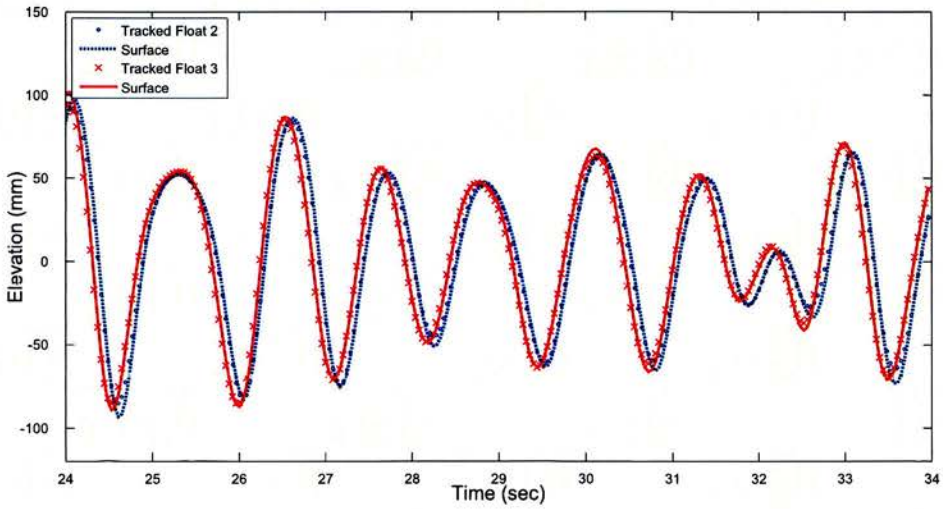

(c) Surface elevation as reported by surface tracking and float numbers 2 and 3

Figure 4.22. Optical tracking during irregular test number 5

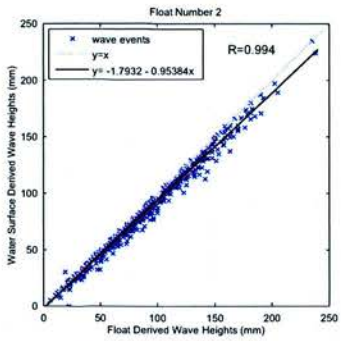

(a) Float 2 - wave height

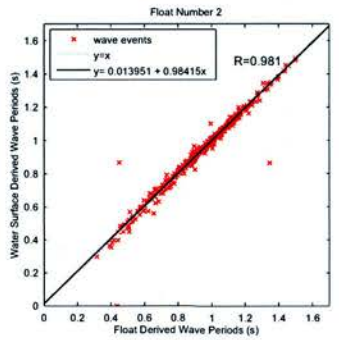

(b) Float 2 - wave period

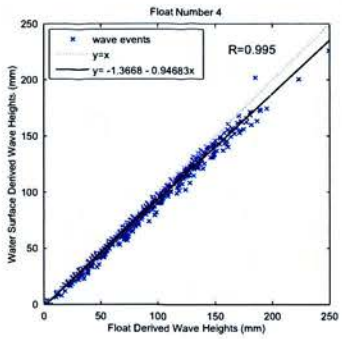

(c) Float 4 - wave height

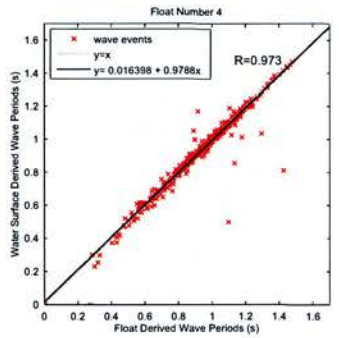

(d) Float 4 - wave period

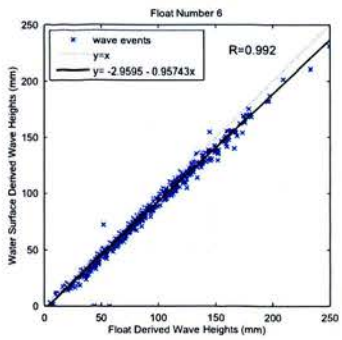

(e) Float 6 - wave height

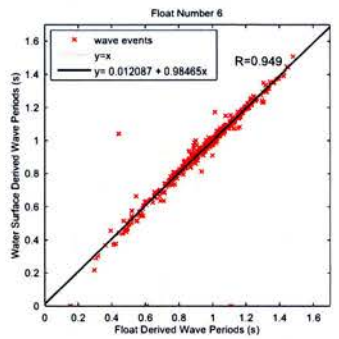

(f) Float 6 - wave period

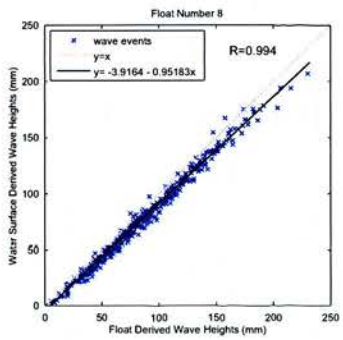

(g) Float 8 - wave height

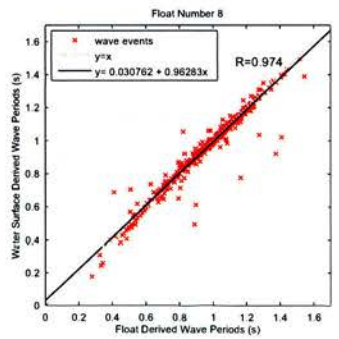

(h) Float 8 - wave period

Figure 4.23. Irregular test 1. Included as representative test comparison of intra-ribbon float numbers 2,4,6 and 8.

Figure 4.24 shows longer test sequences and overall comparison between the centrally positioned float no. 4 and the local surface elevation.

Figures 4.25 to 4.28 show the correlation between wave heights and wave periods as measured at float central positions and local surface elevations measured via wire resistance wave gauges. Floats in closest proximity to each of the wave gauges as testing progressed were used. These plots indicate increasing under-prediction of surface elevation by the floats as wave height increases and better relative agreement as test peak wave-period increases (with tests 3 and 4 showing lower correlation than the longer period tests). Increased correlation between measurements with increased peak period also holds for wave period with the level of correlation high across all tests, as can be seen in figures 4.27 and 4.28.

Figure 4.29 captures the trend (which was visible in the wave-by-wave plots of figures 4.25 to 4.28) of decreasing measurement correlation (wave height and wave period) with decreasing wavelength.

Figure 4.30 indicates the relative improved performance of the method in terms of tracking wave crests compared to tracking wave troughs.

As is suggested by the plots of wave-by-wave events (in terms of their agreement in magnitude and the level of correlation), spectral descriptions of the wave gauges and visually tracked surface are in good agreement. This is shown in figure 4.31.

Figure 4.36 collates all irregular wave tests and reports wave heights and wave periods as measured at float central positions and local surface elevations for float numbers 2 to 7. End-floats (numbers 1 and 9) are neglected due to the greater likelihood of errors arising from camera position and their transition in and out of frame. 16,600 individual wave events are captured.

Frequency Domain Results

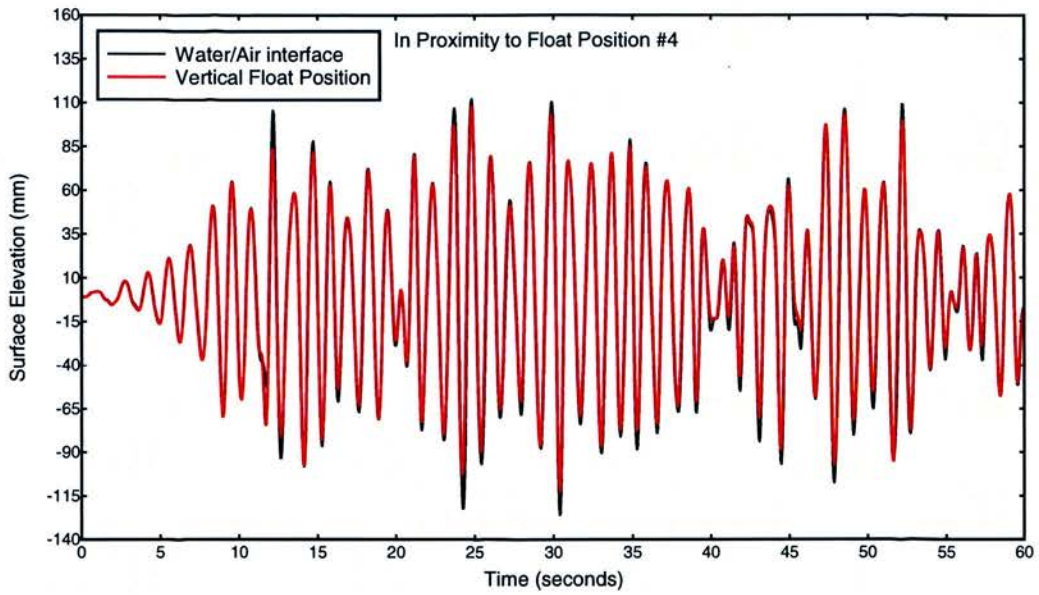

(a) First 60 seconds

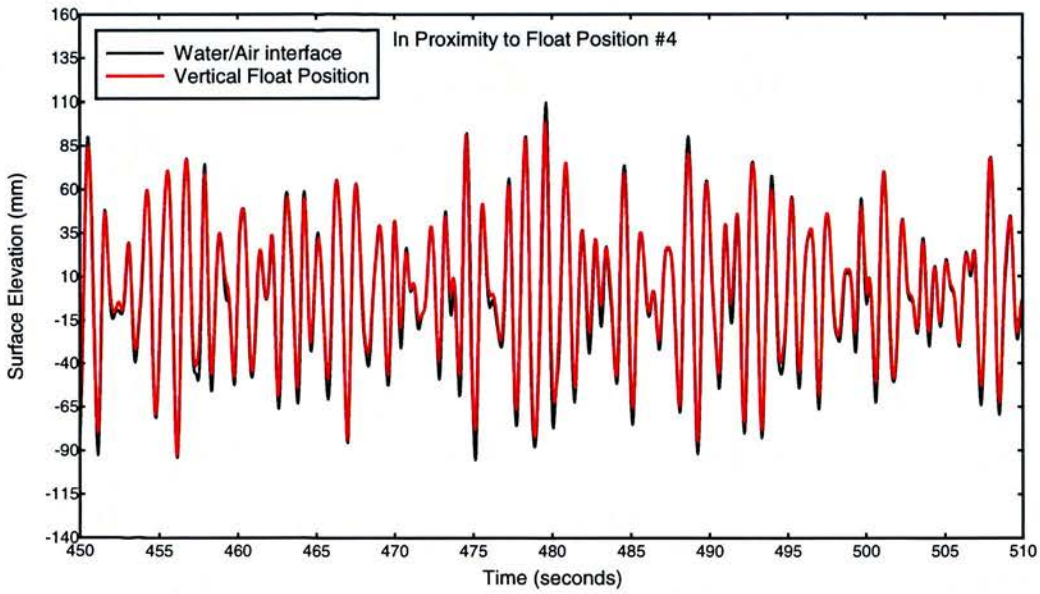

(b) Last 60 seconds

Figure 4.24. Surface elevation vs time. Irregular test 1

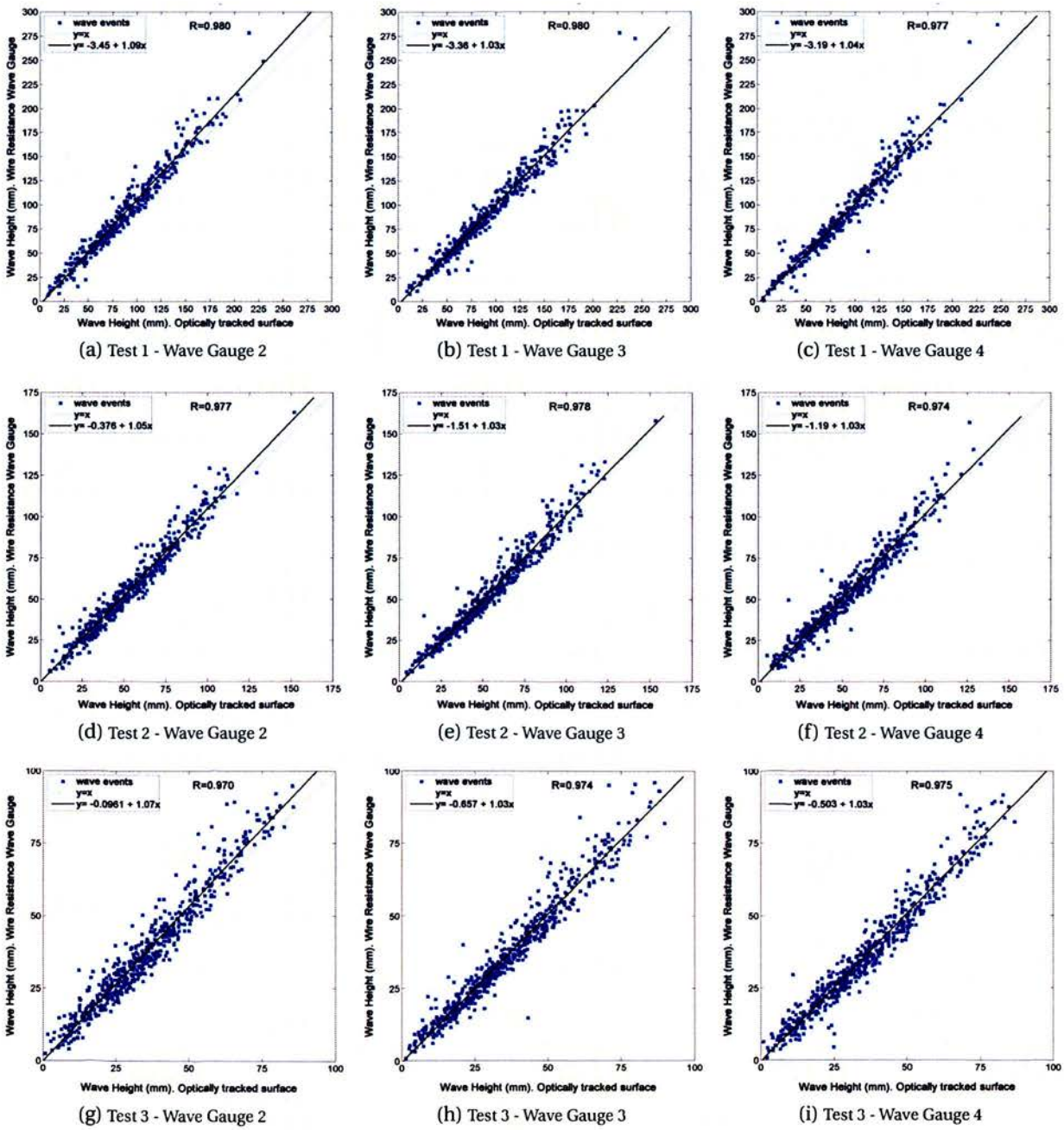

(a) Test 1 - Wave Gauge 2 (b) Test 1 - Wave Gauge 3 (c) Test 1 - Wave Gauge 4

(d) Test 2 - Wave Gauge 2 (e) Test 2 - Wave Gauge 3 (f) Test 2 - Wave Gauge 4

(g) Test 3 - Wave Gauge 2 (h) Test 3 - Wave Gauge 3 (i) Test 3 - Wave Gauge 4

Figure 4.25. Irregular tests 1 to 3. Wave gauge vs optical surface tracking wave heights

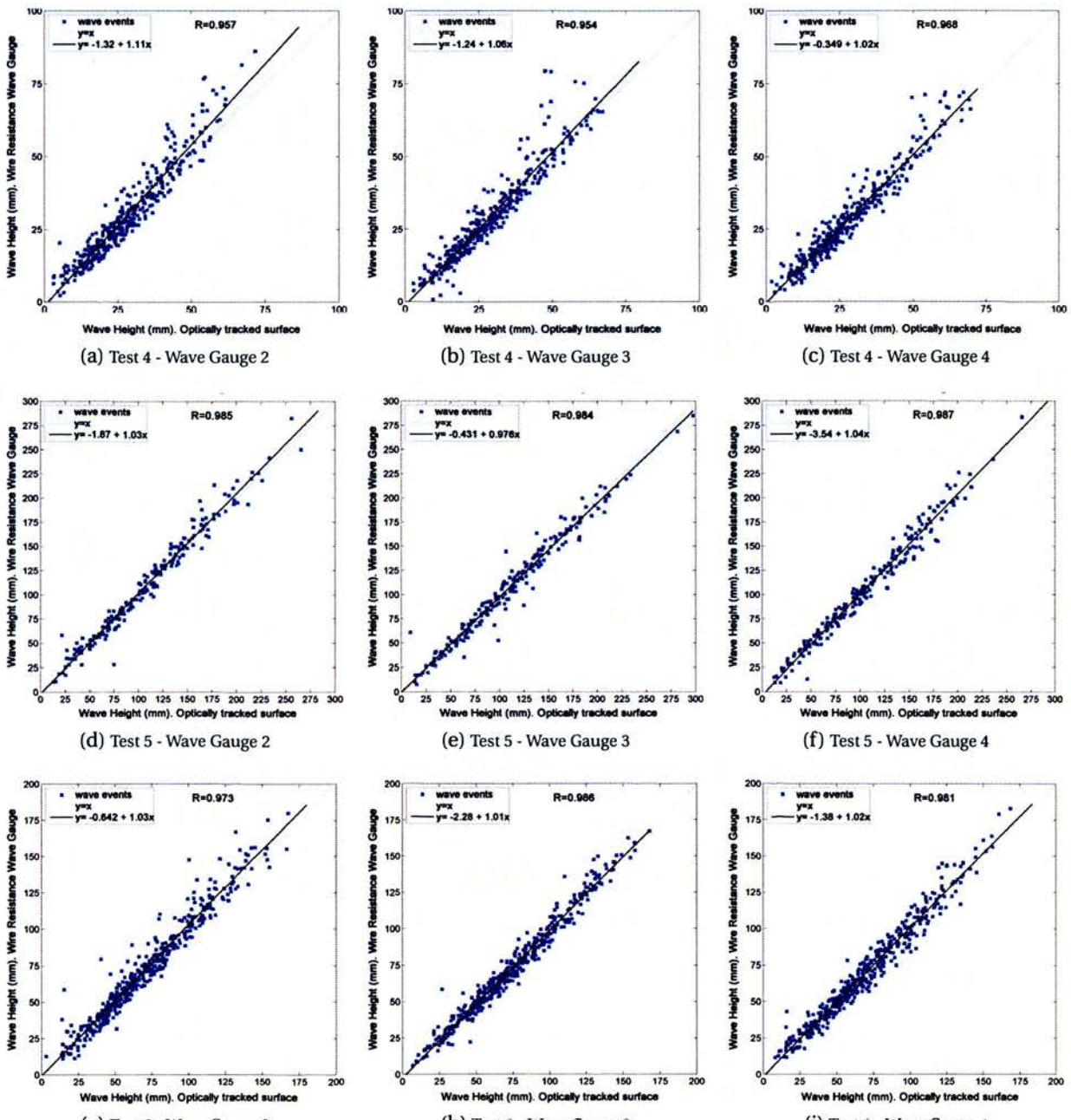

(a) Test 4 - Wave Gauge 2 (b) Test 4 - Wave Gauge 3 (c) Test 4 - Wave Gauge 4

(d) Test 5 - Wave Gauge 2 (e) Test 5 - Wave Gauge 3 (f) Test 5 - Wave Gauge 4

(g) Test 6 - Wave Gauge 2 (h) Test 6 - Wave Gauge 3 (i) Test 6 - Wave Gauge 4

Figure 4.26. Irregular Tests 4 to 6. Wave gauge vs optical surface tracking wave heights

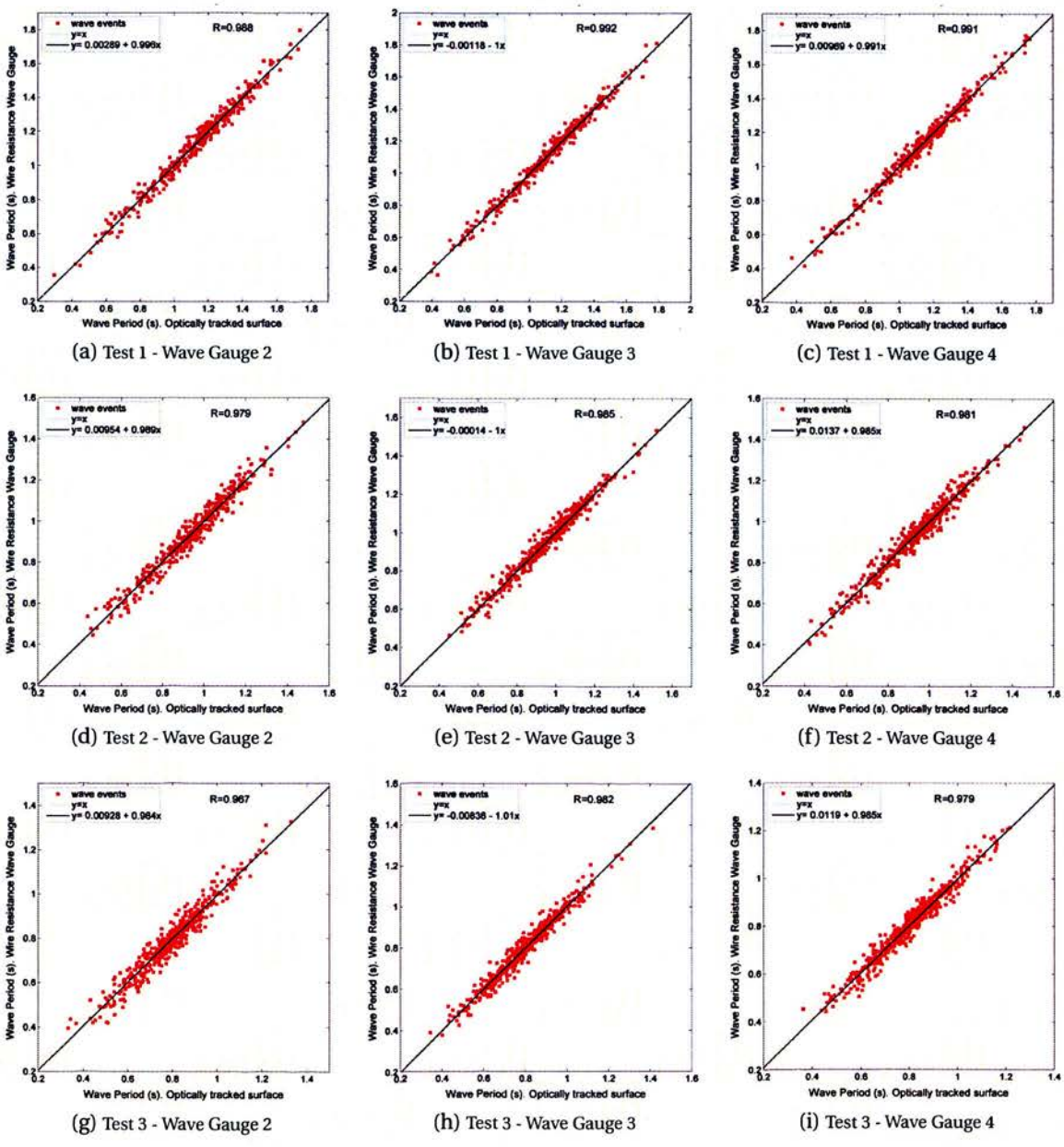

(a) Test 1 - Wave Gauge 2 (b) Test 1 - Wave Gauge 3 (c) Test 1 - Wave Gauge 4

(d) Test 2 - Wave Gauge 2 (e) Test 2 - Wave Gauge 3 (f) Test 2 - Wave Gauge 4

(g) Test 3 - Wave Gauge 2 (h) Test 3 - Wave Gauge 3 (i) Test 3 - Wave Gauge 4

Figure 4.27. Irregular tests 1 to 3. Wave gauge vs optical surface tracking wave periods

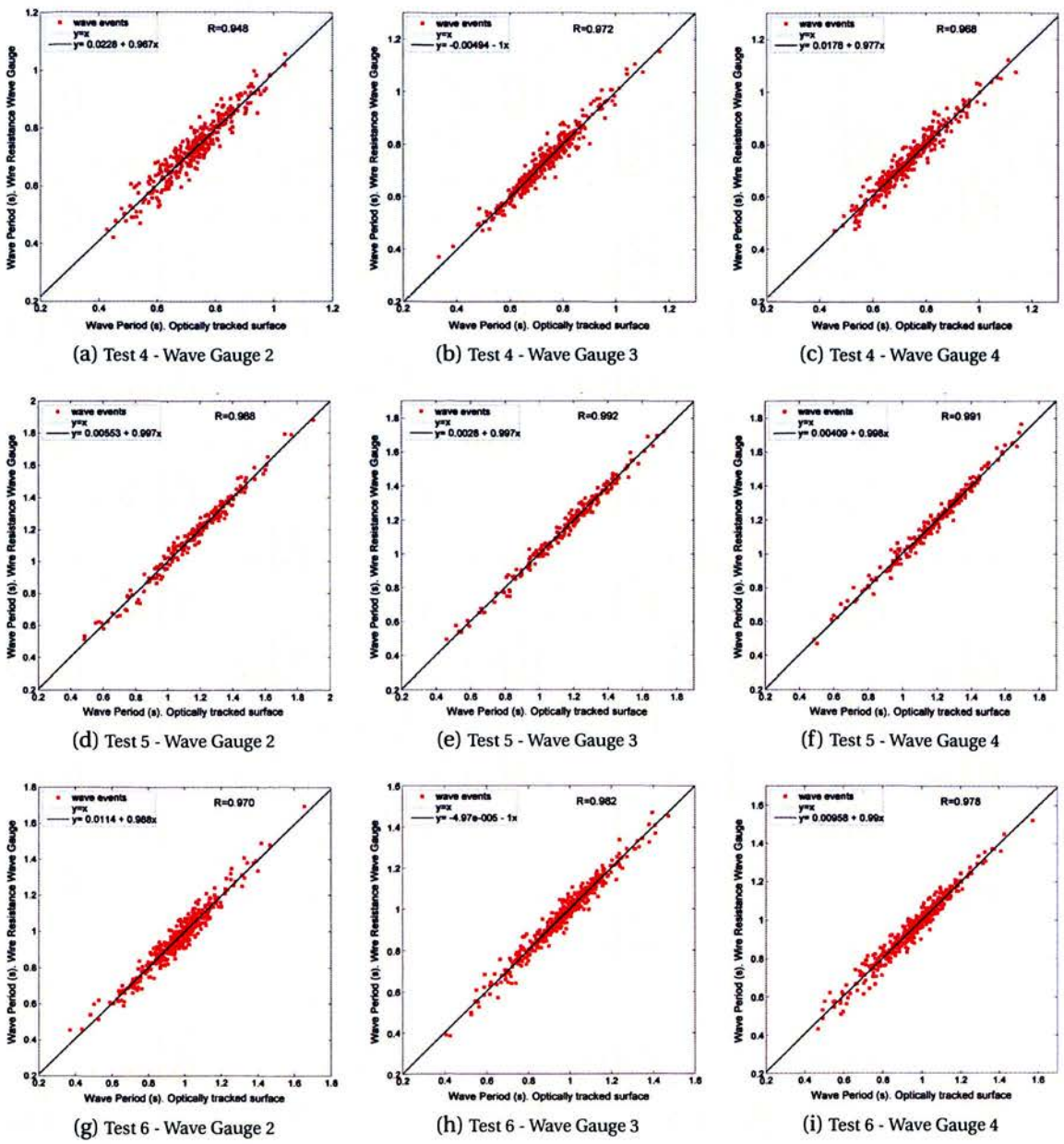

(a) Test 4 - Wave Gauge 2 (b) Test 4 - Wave Gauge 3 (c) Test 4 - Wave Gauge 4

(d) Test 5 - Wave Gauge 2 (e) Test 5 - Wave Gauge 3 (f) Test 5 - Wave Gauge 4

(g) Test 6 - Wave Gauge 2 (h) Test 6 - Wave Gauge 3 (i) Test 6 - Wave Gauge 4

Figure 4.28. Irregular tests 4 to 6. Wave gauge vs optical surface tracking wave periods

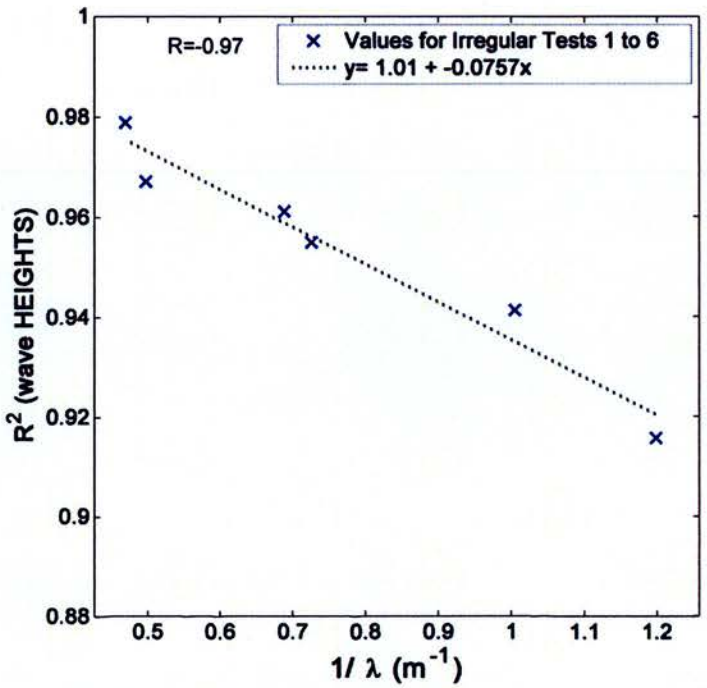

(a) R^2 values of the comparison of wave gauge wave heights to surface-tracked wave heights versus $1/\lambda$ for the six irregular tests

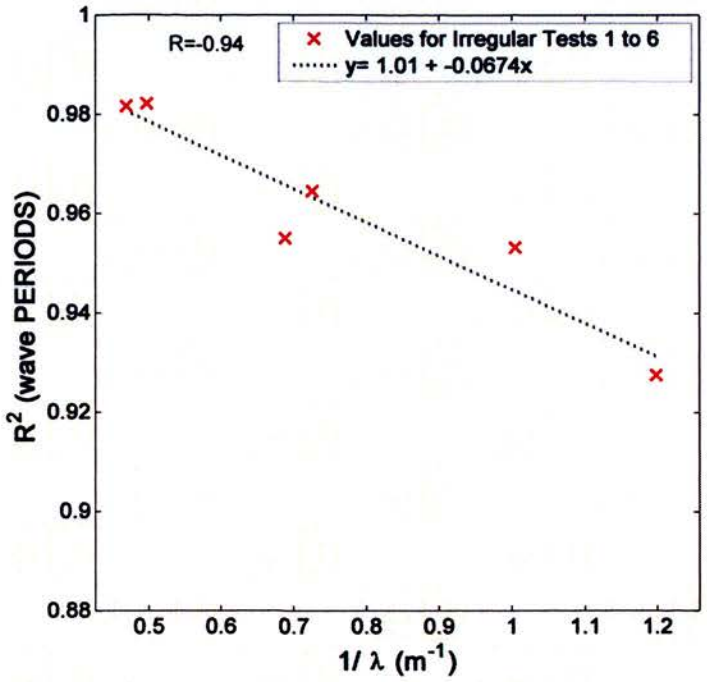

(b) R^2 values of the comparison of wave gauge wave periods to surface-tracked wave periods versus $1/\lambda$ for the six irregular tests

Figure 4.29. Variation of R^2 of wave heights and wave periods with the mean test wavelength, λ

Table 4.6. R^2 values of matched wave events from time series for optically tracked surfaces versus wire wave gauge tracked surfaces. And the standard deviation of R^2 values across the camera field of vision/floats.

Test No.	H_{m0}(m)	T_p (s)	Mean R^2 value	STD R^2 value
1	0.112	1.32	0.9672	0.0026
2	0.069	1.05	0.9549	0.0020
3	0.046	0.85	0.9413	0.0120
4	0.036	0.76	0.9156	0.0189
5	0.119	1.33	0.9789	0.0036
6	0.080	1.07	0.9612	0.0124

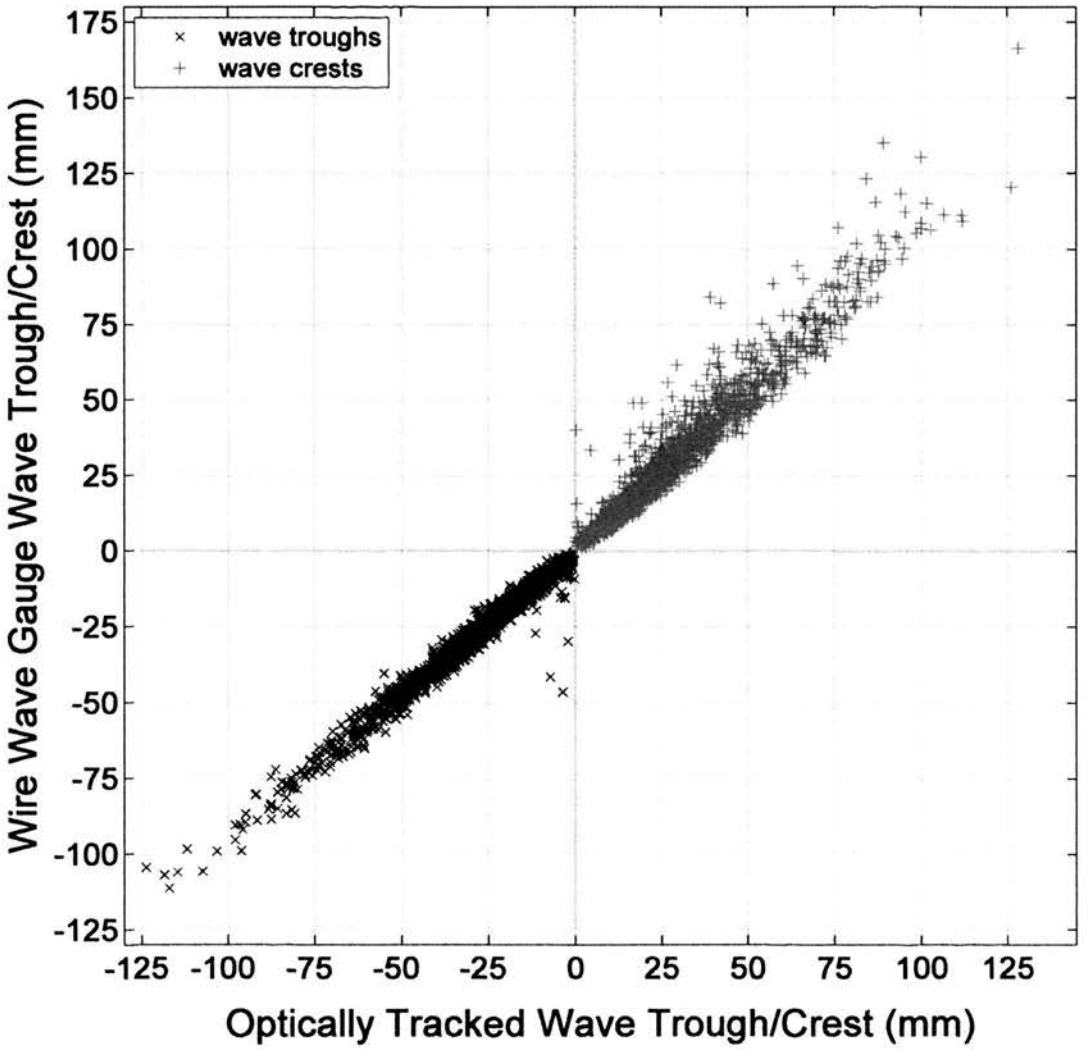

Figure 4.30. Wave trough and wave crest tracking performance

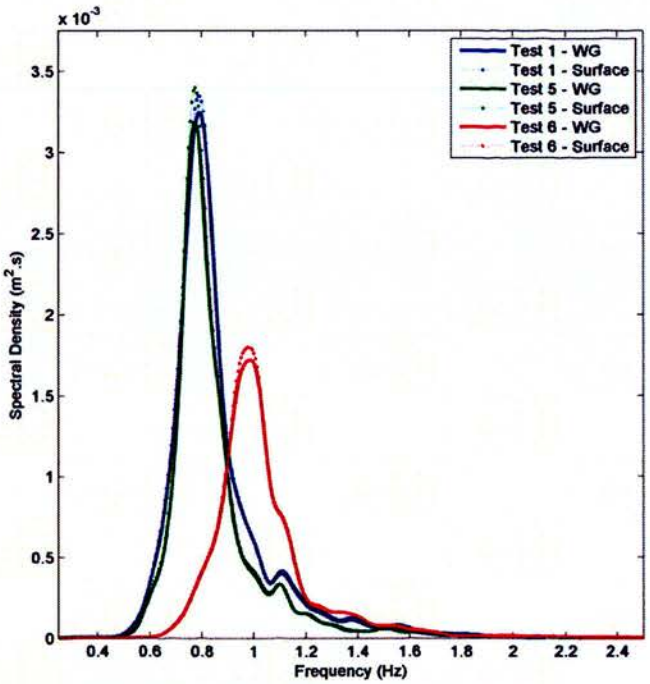

(a) Irregular Tests 1,5 and 6 (large amplitude)

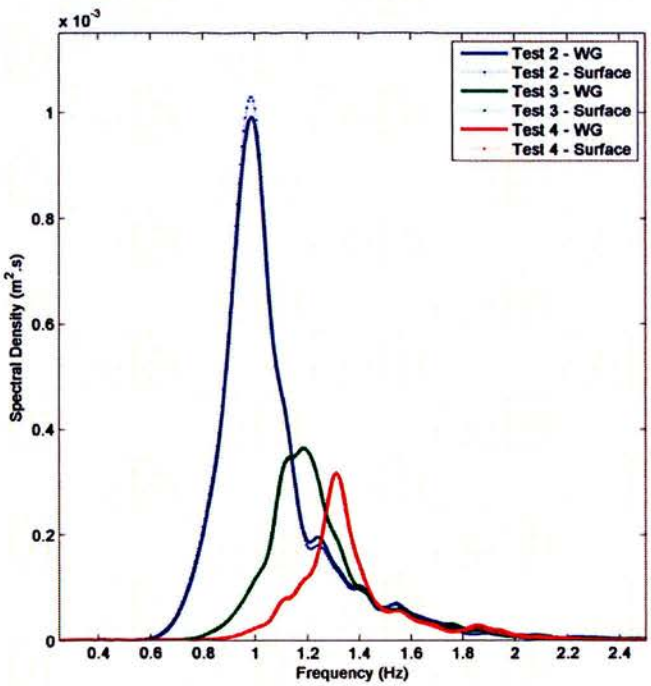

(b) Irregular Tests 2,3 and 4 (low amplitude)

Figure 4.31. Wave spectra produced from Irregular tests 1 to 6.

Table 4.7. Summary of spectral values

Test		H_{m0} (mm)			T_p (s)		
		WG	Surface	Floats	WG	Surface	Floats
1	Mean	107.6	104.0	97.4	1.322	1.280	1.280
	Std	2.1	1.4	2.0	0.024	0.000	0.000
2	Mean	66.0	63.8	58.6	1.054	1.024	1.027
	Std	2.2	0.8	1.4	0.043	0.000	0.009
3	Mean	44.8	42.5	37.6	0.876	0.837	0.890
	Std	2.6	0.5	1.3	0.037	0.027	0.000
4	Mean	35.2	33.0	32.0	0.762	0.759	0.759
	Std	2.9	0.5	0.9	0.000	0.000	0.000
5	Mean	131.3	127.0	117.1	1.291	1.311	1.311
	Std	5.4	1.8	1.8	0.024	0.028	0.028
6	Mean	80.5	81.0	73.0	1.068	1.050	1.050
	Std	2.5	1.2	1.4	0.038	0.000	0.000

4.3 Discussion and Further Work

To look for trends in the response of the floats, Kernel Density Estimators (KDE), a non-parametric method to extract probability density functions, have been used instead of histograms due to the latter's dependence on bin end points and unsmooth representation of the data. These plots are qualitatively useful by allowing the visualisation of symmetrical or unsymmetrical features/trends in the data. The contours on a KDE plot represent probabilities or likelihoods linking the parameters on each axis [108]. The WAFO toolbox provided the "kde.m", MATLAB function.

Figure 4.35 shows a KDE containing composite information from over 16,000 wave events which were extracted via time series analysis of the irregular wave tests. The plot shows a joint distribution of wave steepness and relative wave height (a) and relative wave period (b) error. It can be seen that as wave steepness increases the optically-tracked float centres report waves with smaller wave heights than the measured surface elevation.

Table 4.8 provides summary statistics of percentage errors for 16,400 combined wave events for floatation positions two to seven. The first float and last float (floats one and eight) have been excluded due to the fact that they come in and out of shot during tests which the algorithm cannot suitably deal with.

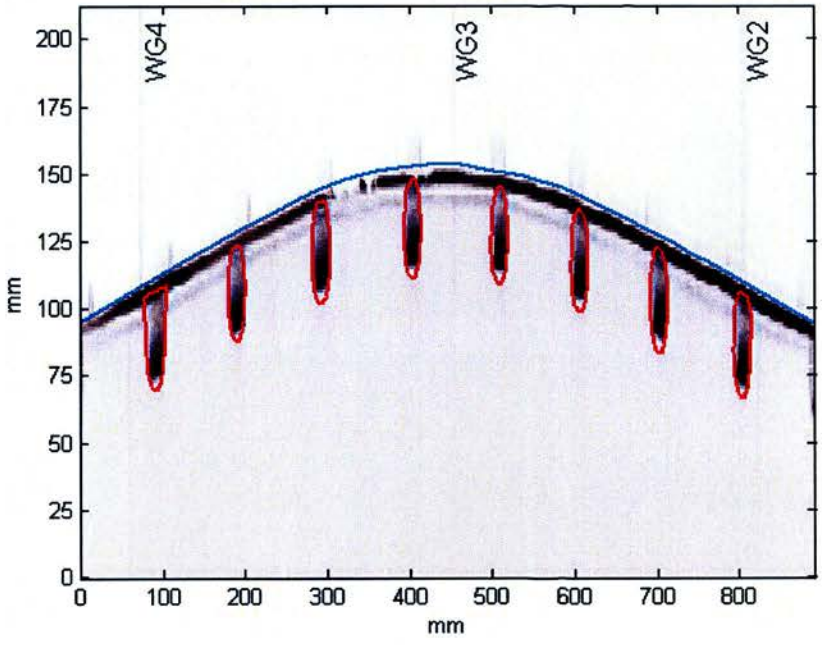

Figure 4.32. Screenshot of a processed low amplitude wave

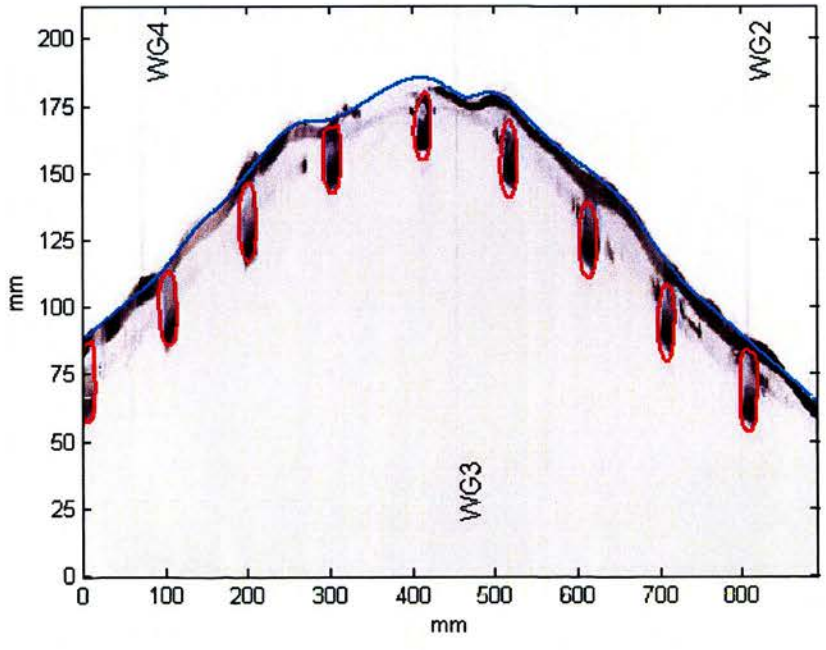

Figure 4.33. Screenshot of a processed medium amplitude wave

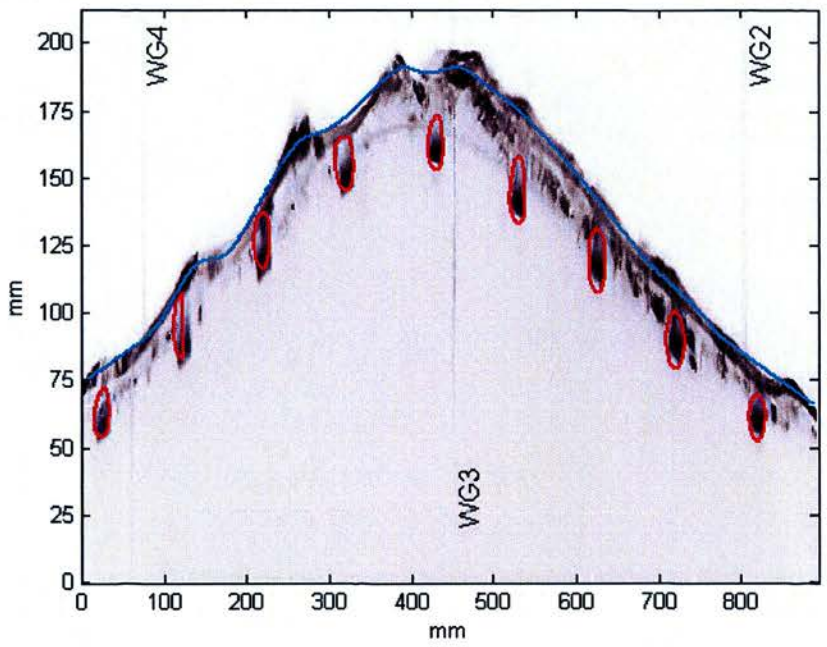

Figure 4.34. Screenshot of a processed high amplitude wave

4.3.1 Optical Tracking of Water/Air Interface

Regular Waves

Results from the regular wave tests show strong agreement between surface tracked wave elevation and the wire resistance wave gauges and furthermore between surface tracked wave elevation and central float position. Above a wave steepness of 0.07 there is an increase in mean divergence of the centre of the floats compared to the surface with the average difference rising from below 5% to approximately 15% by a steepness of 0.1 - as shown in figure 4.19. Differences in measured wave period were below 2% for all but one test and remained generally below 1%. The standard deviation of reported periods across each floating pod increased with wave steepness with the mean of the pod values remaining below 1% for all steepness encountered in regular wave testing.

Figures 4.18 and 4.19 show that the ribbon can track the water/air interface well in steepness ranges of 0.01 to 0.1. Below steepness of 0.083 the centre of the floats is on average within 8% of the wave gauge reported mean wave height and below 0.5%

of the wave gauge reported mean wave period. As steepness increases the tracking ability reduces (as does the image processing methodology which is discussed later). At a steepness of 0.1 the centre of the floats is on average within 15% of the wave gauge reported mean wave height and remains below 0.5% of the wave gauge reported mean wave period although the standard deviation across the floats rises to around 2%.

Irregular Waves

For the irregular wave tests the wave gauge measurements compared to tracked surface measurement agree less than expected with 10% error on average and greater than 10% for large waves. This could be due to several factors: limitations in the camera set up where large waves create a large angle between the lens and the meniscus - the camera is now looking up and under the wave. This should produce a bias towards higher tracked surfaces than the WG. False tracking of the reflected or rear interface could also play a role.

Overall the image processing tests and analysis highlight the large extent to which a floating ribbon can track the air/water interface. As steepness increases the floats spend more time off centre of their equilibrium point (i.e., resting at mid-float-depth on the surface of the air-water interface), thus an ideal sensor co-located here would under or over predict the actual wave height. However, with further processing, the magnitude of a sensor's position error could perhaps be mitigated by, for example, building up a look-up table of behaviour versus wave height, frequency and steepness. Even if correlation between the errors and a single or set of detected wave parameters proved too low for adequate error correction knowledge of the magnitude of the likely error in a given sea state remains an advantage.

Summary of Errors

Over all six irregular wave tests comprising 16,600 matched wave events the comparison of surface floats to surface-tracked position resulted in the following summary statistics.

- Mean Relative Error - Wave Heights
  - 6.3% for waves below steepness of 0.12
  - 5.7% for waves below steepness of 0.12 and periods above 0.6 seconds
- Mean Relative Error - Wave Periods
  - -0.1% for waves below steepness of 0.12
  - -0.1% for waves below steepness of 0.12 and periods above 0.6 seconds
- Standard Deviation of Relative Error - Wave Heights
  - 8.6% for waves below steepness of 0.12
  - 7.4% for waves below steepness of 0.12 and periods above 0.6 seconds
- Standard Deviation of Relative Error - Wave Periods
  - 2.5% for waves below steepness of 0.12
  - 2.3% for waves below steepness of 0.12 and periods above 0.6 seconds

Sources of Error

There are multiple sources of error:

- Diffracted waves from the floating pods produce ripples with amplitude of tens of mm in height (see Fig. 4.34) which when reaching the glass walls cause increased disturbance.
  - This could be a main source of error and could also be one that has a relationship with wave height, period and steepness.
  - These effects could be reduced via optimisation of floatation aids, for example by having more distributed floatation or more rounded floatation.
  - Improved filtering of these ripples could improve performance.
  - Implementation of dynamic allocation and positioning of knots for spline fitting improved performance.

- The angle between the camera lens and the extremity of the field of view plays a role in object detection. This should be investigated further.

- Further enhancement of camera configuration and calibration.

- An additional error checking loop should check to make sure that false (or rear) menisci are not being tracked.

    - For example, an improved algorithm that monitored the change in rate of the position of the predicted surface could assist in the prevention of false surface tracking.

Wave gauge consistency

Wave gauge Relative Standard Error analysis (between the 5 wave gauges) suggests increased difference between each of the gauges as wave steepness increases. However, with steepness corresponding to an increase with time (due to experimental schedule) a proportion of the wave gauge "error" could feasibly be due to the gauges drifting off calibration in addition to reflection and physical interference caused by the presence of the ribbon. Due to daily mixing of the tank, daily calibration of the wave gauges and stable environmental conditions wave gauge drift was rejected as a significant source of error.

It is expected that increased wave steepness and hence complexity and non-linearity would cause reduced coherence of time series down the tank and thus across the longitudinally separated wave gauges. The increasing variance in the wave gauge measurements as wave steepness and wave period increases could lead to an increased expectancy of increased variance in floating ribbon measurements.

Given the large source of unknowns and uncertainty around the surface tracking behaviour of a mechanical floating ribbon and the inherent ability of the measurement device to internally estimate 3D position it was assumed for the remainder of the tests that values measured at a wire resistance wave gauge represent the true physical position of the surface.

Image Processing Overhead

Whilst optimisation of image processing routines in terms of computational time was never a priority subsequent experience with image analysis, and in particular checking outlier or strange results and quality assurance has revealed that expedient access to the processed images and fitted parameters is essential. Of the various routines tried, the average time to process one image - with the output being a spline representing the surface and a set of polygons describing the shape and positions of the pods - was one second. Using the latest revamped approach this time was reduced to 0.5 seconds. Further advances in reducing the time would require moving away from the MATLAB programming environment or re-engineering the MATLAB code to take advantage of the Parallel Computing Toolbox, multi-core CPU's and/or taking advantage of one or more Graphical Processing Units (GPUs). The latter was trialled and saw reductions in processing times of the pre-filtering (2D filters designed to emphasise the pods in one case and the surface in the other) of approximately 30%.

Table 4.8. Summary of percentage errors for 16,600 combined wave events across the field of vision of the camera. End floats from each end of the frame are excluded due to the intermittency of their appearance in shot.

	Mean of % Error	STD of % Error
Wave Height	6.3	8.6
Wave Period	-0.1	2.5

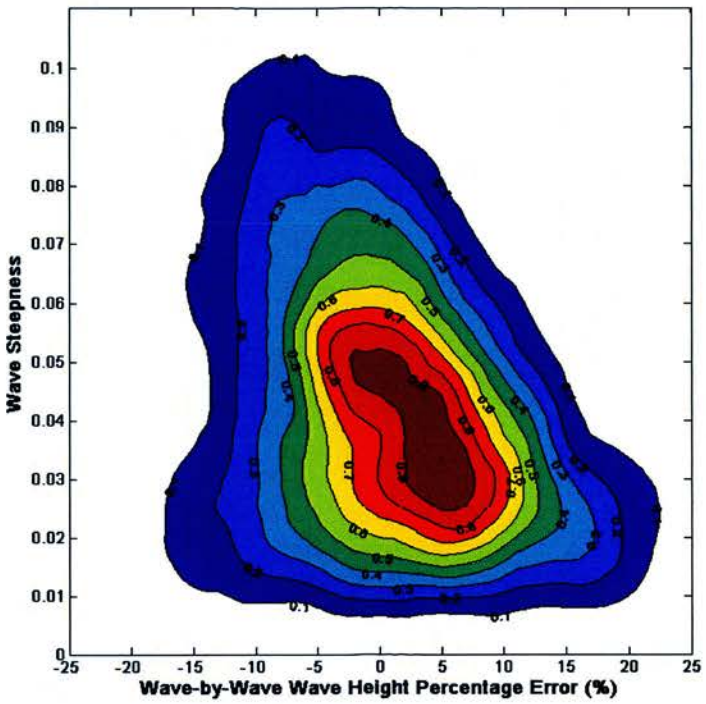

(a) Wave Height

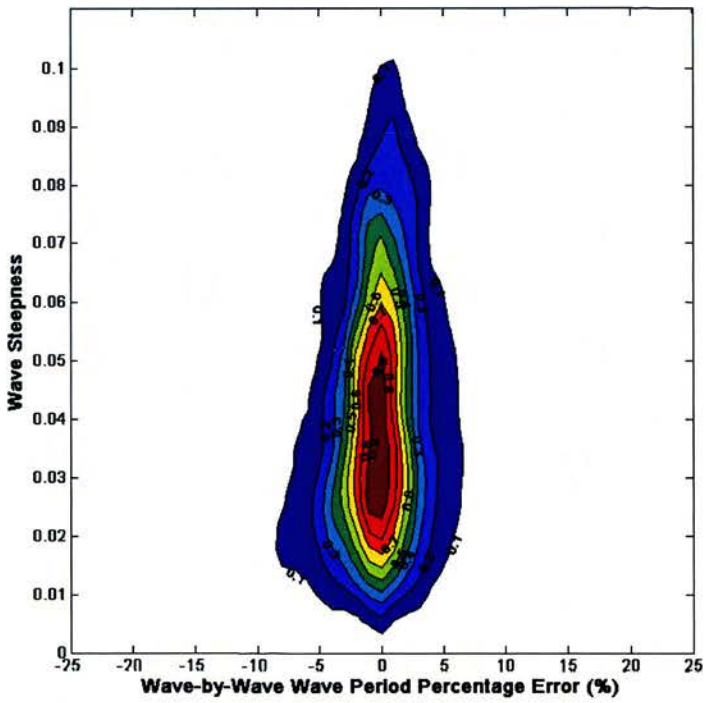

(b) Wave Period

Figure 4.35. Kernel Density Estimate (KDE) for combined irregular wave tests (16400 waves extracted via time series analysis) showing joint distribution of wave steepness and relative wave height error(a), and relative wave period error (b).

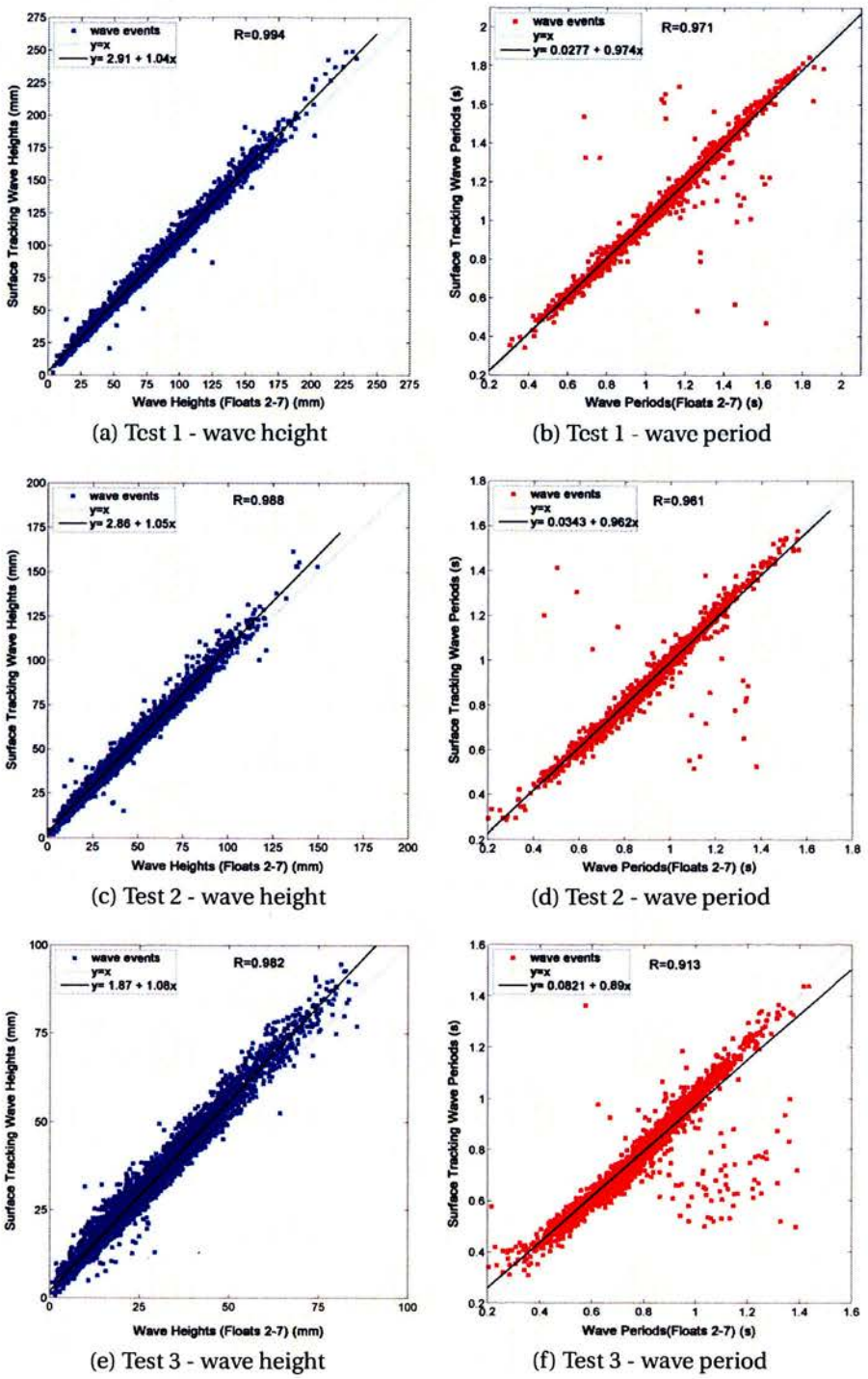

(a) Test 1 - wave height

(b) Test 1 - wave period

(c) Test 2 - wave height

(d) Test 2 - wave period

(e) Test 3 - wave height

(f) Test 3 - wave period

Figure 4.36. Irregular wave tests. All wave events reported by Floats 2 to 7 (of 8)

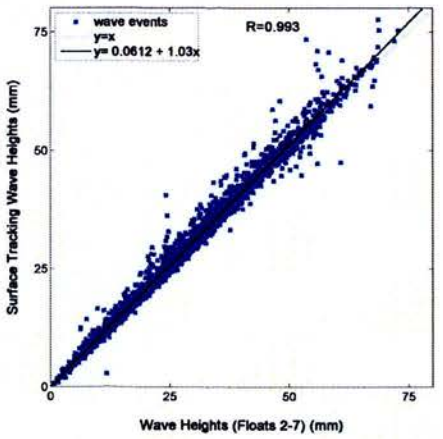

(g) Test 4 - wave height

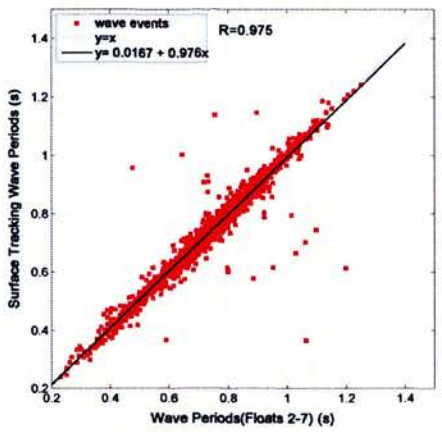

(h) Test 4 - wave period

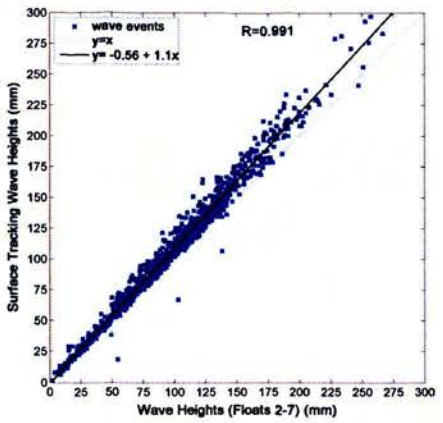

(i) Test 5 - wave period

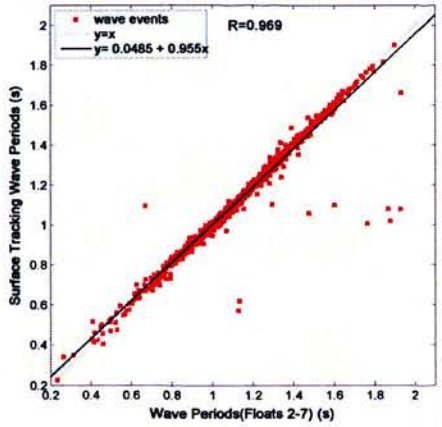

(j) Test 5 - wave period

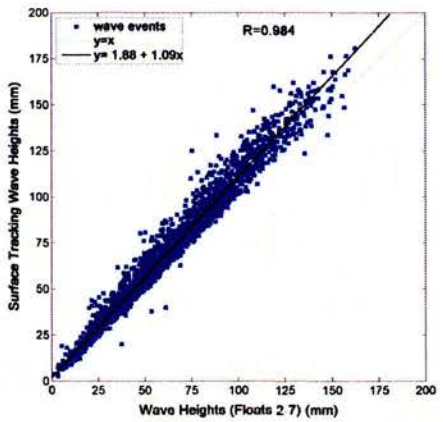

(k) Test 6 - wave height

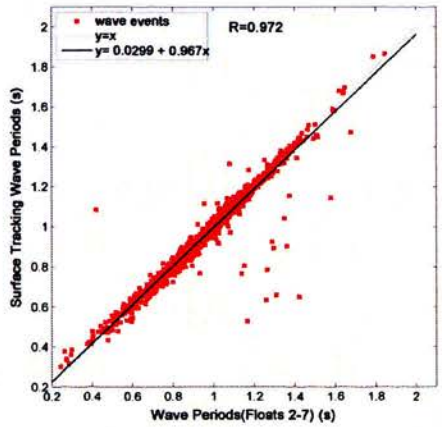

(l) Test 6 - wave period

Figure 4.36. Irregular wave tests. All wave events reported by Floats 2 to 7 (of 8)

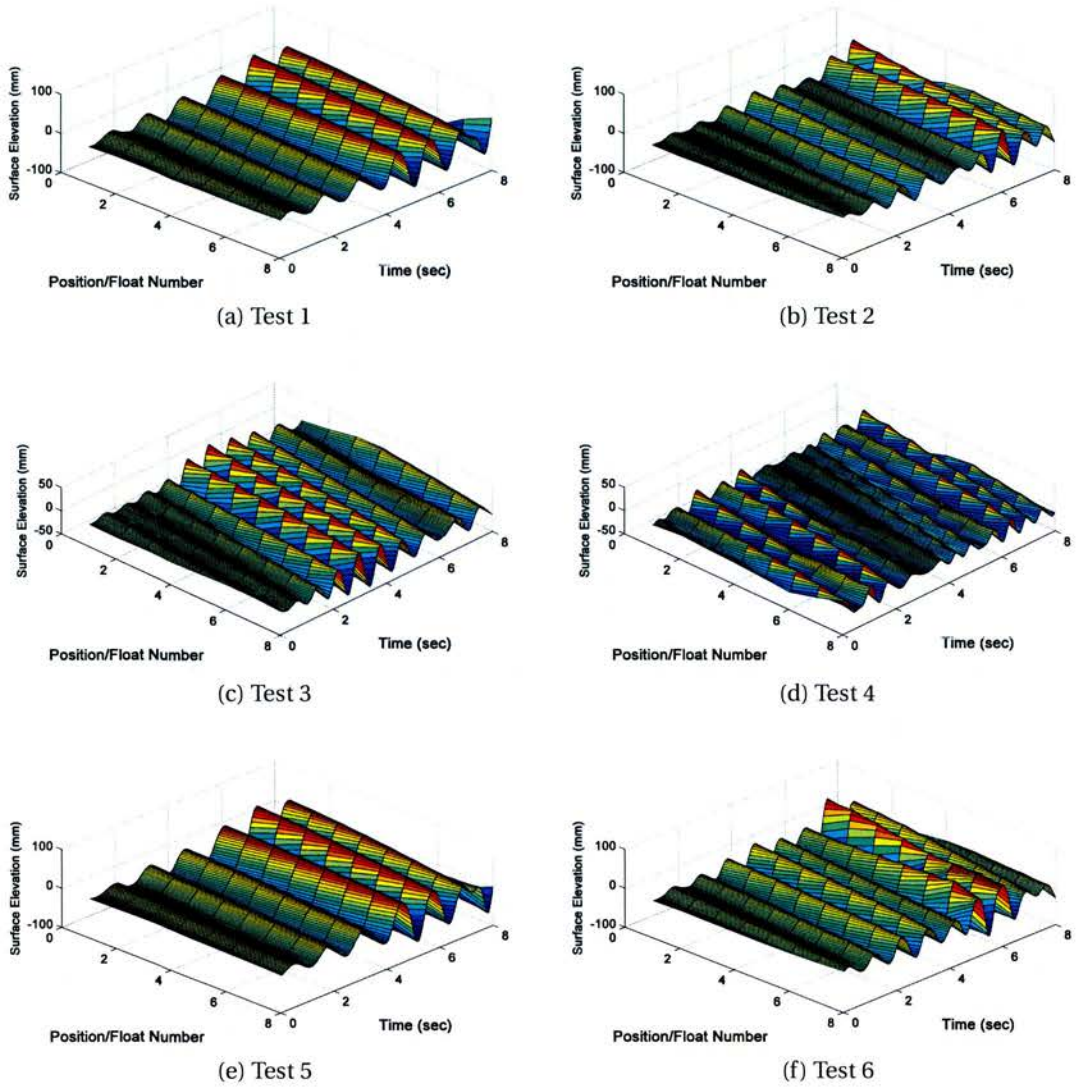

(a) Test 1

(b) Test 2

(c) Test 3

(d) Test 4

(e) Test 5

(f) Test 6

Figure 4.37. Surface elevation as tracked by camera system. Spatial time series for irregular tests 1 to 6.

4.4 Conclusion

An experimental procedure, based around testing in laboratory glass-walled wave flumes, to track the water/air surface and to track buoyant elements of a ribbon-like structure in the presence of water waves was devised and implemented. Through an iterative process reliable information was recovered in a near-autonomous fashion. Over a series of tests, experimental setup was improved as was post-processing and data management techniques. It was shown that:

- Over a range of wave conditions a floating ribbon-like structure can successfully reside close enough to the water/air interface to be in a position to provide water wave information across length scales from one wavelength to multiple wavelengths.
- R^2 values for wave height tracking range from 0.92 to 0.98 with increasing agreement for increasing wavelength (across 16,600 wave events).
- R^2 values for wave period tracking range from 0.92 to 0.98 with increasing agreement for increasing wavelength (across 16,600 wave events).
- Wave troughs are tracked more accurately than wave crests due to increased spatial gradients on wave crests and the mechanical response of the sensor element.
- Typical relative mean errors in wave heights and wave periods are 6% and -0.1% respectively (depending on cut-off period).
- Typical standard deviations of relative mean errors in wave heights and wave periods are 7% - 9% and 2.5% respectively (depending on cut-off period).

Areas have been highlighted which would further improve the performance of the optical tracking method (see Chapter 7, Section "Further Work"). With these improvements successfully implemented, this technique could, at a reasonable time cost, be extended to cover multiple self-calibrating cameras to increase the field of vision to tens of wavelengths, potentially covering an entire wave flume from wave

paddle to beach. By incorporating experience from and recent advances in the use of cameras in dynamic and challenging situations such as image stitching, calibration and object tracking in the fields of mechatronics, autonomous vehicles and large area image aggregation the processing routines would be enhanced and made more efficient. With dedicated hardware (such as embedded digital signal processors (DSPs), Field Programmable Gate Arrays (FPGAs), array processing on Graphical Processing Units (GPUs) or through the use of cloud/parallel computing it is, in the authors opinion, feasible that entirely real-time (at the time scale of laboratory waves) two dimensional spatial wave maps could be provided for use in wave flumes. Where higher accuracy is required non-real time post processing which takes into account wave motions both upstream, downstream and prior and after in time could be incorporated into the algorithms.

Using an off-the-shelf camera, lighting and computer hardware, wave information at a high spatial resolution (mm-level accuracy across areas approximately of $1m^2$) and high temporal resolution (25 frames per second) was made available. Objects in this field of vision, whether moving or stationary, are also able to be tracked in parallel in two dimensions. This data could be used in a wide range of experiments including tests in the field of wave-structure interaction, wave-wave interaction and wave-current interaction - where the spatial information of wave dynamics could prove useful. Whilst the main purpose of these tests was to highlight the potential of ribbon-like sensor elements as wave measurement devices - which was achieved - the quality and quantity of data they provide could prove useful as a general measurement tool in hydraulic test facilities.

CHAPTER 5

Design, Construction and Testing of a Novel Sensor - Type I

5.1 Introduction

Two investigations were proposed in Chapter 1 in order to assess the feasibility of the floating ribbon-like wave measurement concept:

I Surface Tracking. To what extent can a floating array of sensors track the water-air interface?

II **Sensor Implementation**. What sensors are available or can be developed that can be integrated, powered, deployed and recovered in a floating sensor ribbon/array?

With confidence established in the ability of a ribbon to mechanically track the air/water interface over a range of sea states, *investigation I* as outlined in Chapter 4 has been addressed. *Investigation II*, on the incorporation of suitable sensors on to a floating ribbon structure, is the focus of this Chapter and Chapter 6 where two different sensor integration approaches are taken.

This chapter reports on preliminary tests and further secondary tests conducted in the Edinburgh Flume using a optical fibre based floating sensor array.

5.2 Design Criteria

When conceiving a new sensor system the following goals were identified:

- Spatial coverage far greater than a single point (as is available with a buoy for example) and greater than the single dominant wavelength.
- Wave period measurements of an accuracy comparable or surpassing those of the leading existing technology.
- Wave height measurements at a resolution and accuracy better than the leading existing remote, non-contact wide area wave measurements - such as bespoke camera configurations or X-Band Radar installations.
- Temporal resolution and data transfer suitable to allow on-the-fly processing, error correction and supply wave field data in near real time to the end-user.

In order that the development in time and space of an entire wave or collection of waves could be tracked the sensor was designed to have a length of two wavelengths (dominate wave period) or greater. The concept thus required a technology that offered multiple sensor points, mid-to-low cost, scalability and low size and weight so that it could be assembled into, or around, a floating ribbon. Figures 5.1a and 5.1b show sketches produced at the design conception stage.

Existing technologies were investigated, (see Chapter 3 for further details), and a summary of their various advantages and disadvantages can be seen in table 5.1 [25, 70, 72, 73, 74, 75, 76, 78, 79, 80, 109].

Following a review of existing technologies, other candidate (and in some cases novel) technologies were appraised. Fibre optics were investigated due to the fact that they do not require electrical conductors, are flexible and light and can be manufactured to any length. In terms of sensors (as opposed to their more common

Table 5.1. Summary of advantages and disadvantages of leading candidate technologies.

Wave Buoy	
Advantages	Established technology Calibration techniques well understood If correctly installed and calibrated provides good time-elevation data and statistical wave data. Above surface telemetry possible Can be deployed for long durations (years with servicing)
Disadvantages	Reduced reliability in steep waves Careful mooring consideration required Prone to storm damage, vessels, vandalism Not a fixed point (Lagrangian measurement). Buoy moves across and around waves as well us moving in heave. **Single point measurement - no spatial information** (steepness, shape, non-linearity), no wave evolution, difficult to infer directional information particularly in multi-modal sea states.
Bottom Mounted ADCP	
Advantages	Being located on the seabed can reduce likelihood of damage (in some cases) Array based measurement allows directionality of waves to be measured Good measurement of co-located currents which can be incorporated into wave measurement analysis Wide range of emitted frequencies to suit deep water to shallow water applications
Disadvantages	**Difficult to deploy for long duration** (at high frequencies required and as required for wave-field monitoring).(1 month is typical deployment) **Below surface telemetry required** (low bandwidth, increased expense) and frequent marine operations: retrievals and deployments **Depth attenuation** of pressure signal used in wave measurement algorithms Require heavy (up to 3000kg) seabed frames in energetic sites or being anchored to seabed in surf zone. Depth of deployment sets maximum resolvable wave lengths and directional resolution (beam spread angles at surface plus pressure gauge attenuation).
X-Band Radar	
Advantages	Not a single point measurement. Grid of data covering 100's metres to kms is possible at 10m-100m grid spacing. Good statistical wave properties achievable. Non-contact with the marine environment
Disadvantages	Emerging technology. Further trials required and are ongoing. Permit likely required for use (EM Spectrum, siting of radar tower etc.) **Individual wave-by-wave analysis more challenging**. Site specific filters required. **Complex calibration** and configuration at each site and when changing sampled region. **Poor temporal resolution** ($\approx$2.5s)

use as electromagnetic radiation conduits) they have been used to measure strain, temperature and pressure. Whilst searching the internet for novel uses of fibre optics, Measurand Inc., a Canadian technology company was found. Measurand offer fibre optic products to the motion capture industry via technology licensed from the Canadian Space Agency.

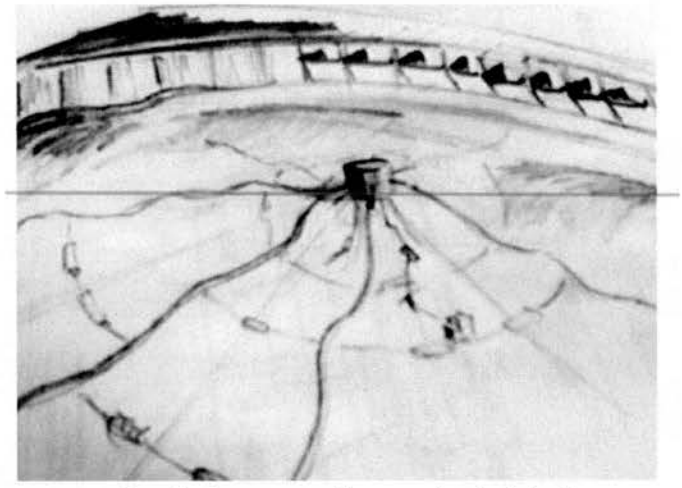

(a) Sketch shows central processing hub in the form of a floating enclosure (buoy) with radial and circular sensing elements. Rough sketch of wave basin (Edinburgh Curved Tank) shown for scale.

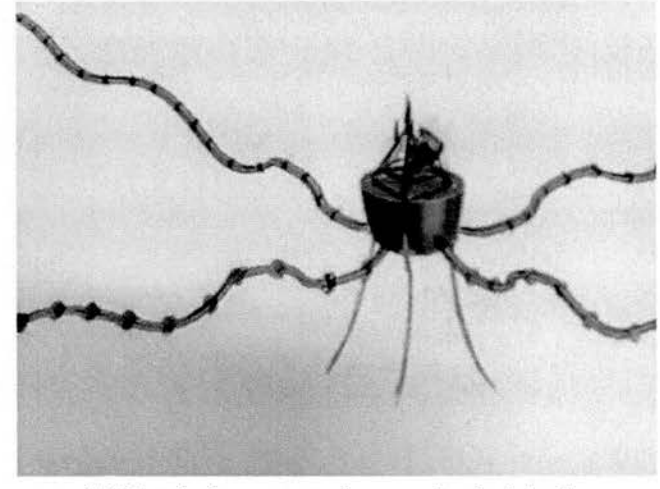

(b) Sketch shows central processing hub in the form of a marine buoy with radial sensing elements. Full Scale.

Figure 5.1. First hand-drawn concept sketches of floating ribbon sensor system prior to investigation and experiments.

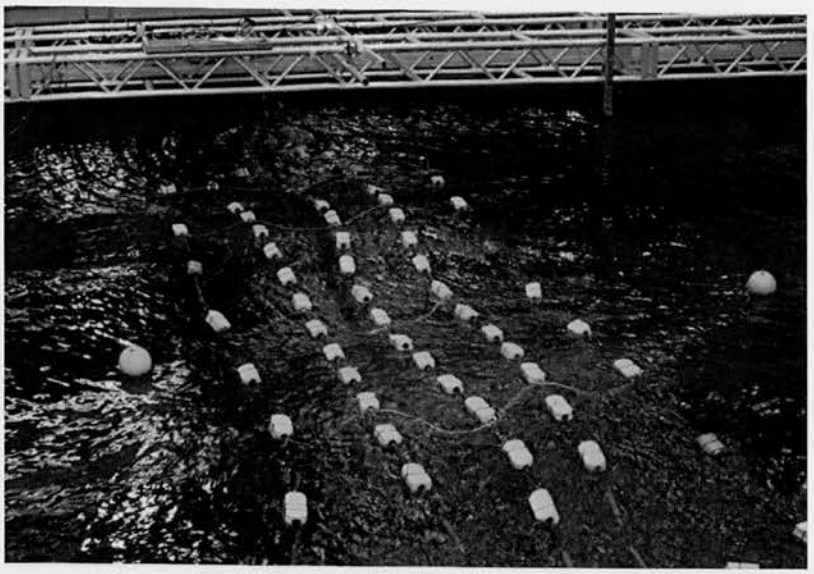

Figure 5.2. Photograph of realised sensor array based on the methodology of Chapter 6. Sensor exposed to irregular, mixed seas with moderate directional spreading in the Heriot-Watt wave basin.

5.3 Technology Selection: The Optical Fibre

A literature review of curvature sensing technology based on fibre optics led to a concept to integrate these sensors into a device capable of tracking water waves. An investigation followed on the feasibility of adapting this existing technology for use in wave flume environments by producing long, flexible floating sensor elements at a suitable scale and with sufficient robustness. It was conceived that these ribbon elements could go on to form the component part of an inter-connected ribbon "net" or lattice.

Shape Tape ™ is proprietary technology of Measurand Inc. and is based on optical fibres of lengths from 10cm to 10m (typically). The supplied fibre for use in this work was 7.1m long which offered a good trade off between length and spatial resolution (more details on the sensor follow in this Chapter). The fibres have had their interiors modified at positions along the fibre. These modifications serve to increase the amount of light that is lost at these zones. Fibres treated in this way offer 3000 times more sensitivity to bending than untreated fibres [110]. By measuring the amount of light lost at each zone, and through a factory calibration process, the degree of curvature can be measured surrounding these zones. This is due to the

linear relationship between curvature of the optical fibre and the degree of light lost [111, 112]. Sensor output is positive if the curvature is in one direction and negative when the curvature is in the opposite direction. By mounting sensors in multiple planes curvature across additional degrees of freedom can be measured.

Durability: The sensors have been tested by the manufacturer to over 200,000,000 bends without loss of performance. For comparison a linear wave field of period 8 seconds would subject a sensor to approximately 8,000,000 bends per year.

5.3.1 Principle of Operation

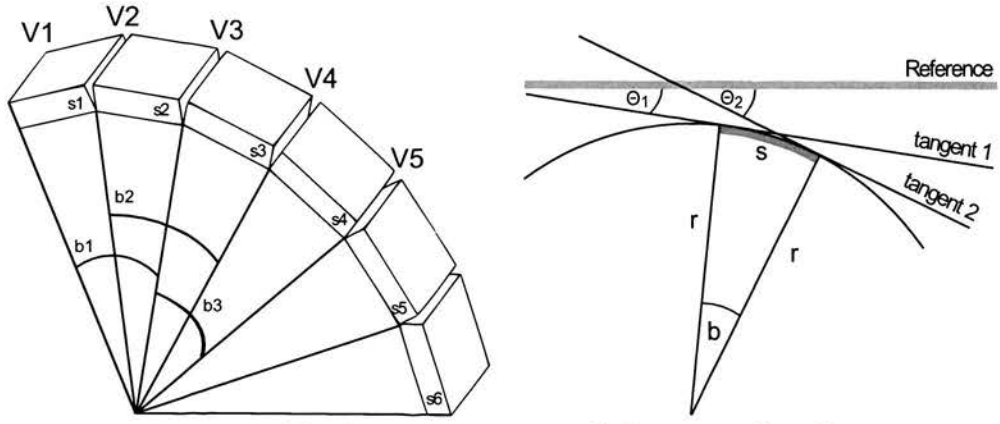

(a) Segmented bend

(b) Tangent angles with respect to reference plane

Figure 5.3. Curved object decomposed as segmented bends

The ribbon can be described as a series of rectangular sections connected by flexible joints as shown in figure 5.3a. Each segment along the length of the ribbon has a pair of sensors that provide an average bend for that segment - net angular change from each end of the segment is reported.

The bend is the difference between the two inclination angles $\boldsymbol{\theta}_1$ and $\boldsymbol{\theta}_2$, shown in figure 5.3b (formed by the arc's tangents) divided by the arc length, as the arc length approaches zero.

$$b = \frac{d\theta}{ds}$$

where $\boldsymbol{s}$ is the arc length in metres and $\boldsymbol{b}$ is bend in units of radians/length.

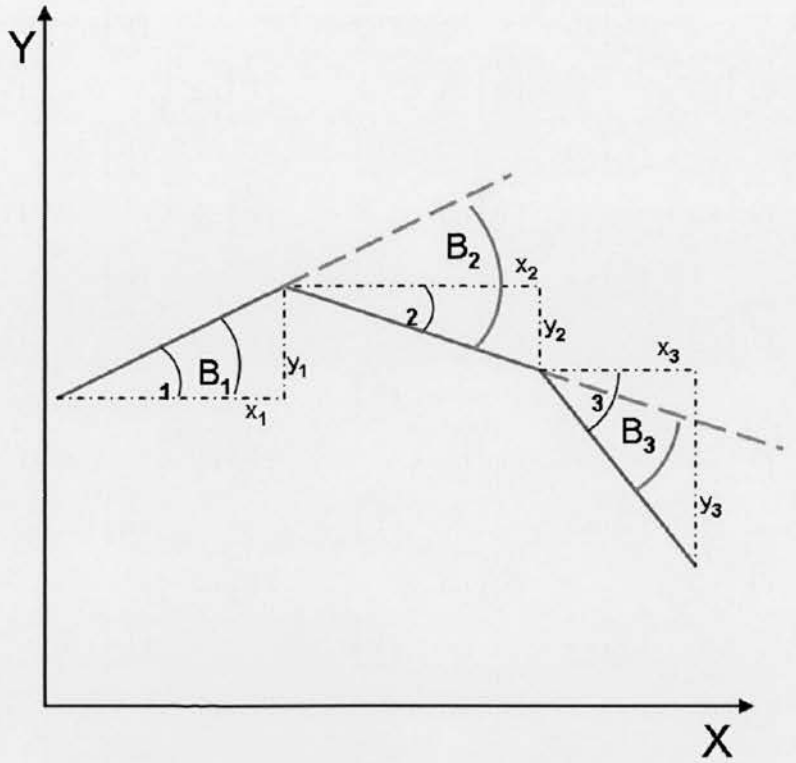

Figure 5.4. Angles and coordinates of segments in a ribbon

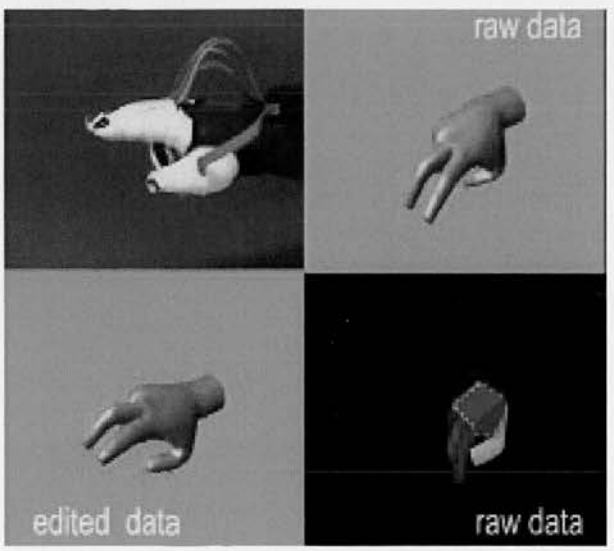

Figure 5.5. Screen grab from Measurand Inc. video showing fibre optic sensors attached to a human hand and the hand's motion being captured via a computer connected to the sensor glove. ©Measurand Inc.

The arc of the circle consists of a proportion of the overall circumference:

$$\frac{d\theta}{2 \cdot \pi} = \frac{s}{C}$$

where $\boldsymbol{C}$ is the circumference of the circle.

With $C = 2\pi r$, rearrangement leads to,

$$b = \frac{1}{r} \tag{5.1}$$

where b is bend and r is radius of curvature, with units of metres/radian.

Transforming bend information to position

Cartesian position is inferred by summing the individual bends at each vertex. The steps are as follows:

- Divide the curved ribbon in to flat segments (s1, s2, s3 etc.) separated by vertices (V1,V2,V3 etc.).
- Bend information at each vertex is known via the calibration coefficients applied to the received voltage from each location.
- Apply the associated bend angle to an initial point originating from flat-pose information.
- Through trigonometry derive the end position of the segment in x and y.
- Repeat for all segments, building up a chain of segments beginning at the previous segment end point co-ordinates with orientation given by the measured bend angle across that vertex.

A similar procedure is required for ShapeTapes containing both bend and twist sensing elements. The ShapeTape used in the study reported in this Chapter was a bend-only ribbon thus twist is not considered.

Spatial Sampling

As with time domain signals, if there is signal information varying within a single sampling region, this information will not be measured properly. High frequency (spatial domain) signals above the spatial sampling size will be lost and through aliasing also change the information gathered from sufficiently low frequency signals. The consequences of this is that bends should be gradual and smooth across the ribbon compared with sensor spacing. Finer sensor spacing allows higher spatial frequency components to be measured with the trade off being in manufacturability, cost and data processing complexity. A sensor density should be chosen to match the expected bends encountered in the application. The ribbon mechanical properties also play a role acting as a low-pass filter by resisting small length, large-angle bending. In the case of the ShapeTape used in this study a spring steel substrate onto which the optical fibres were glued was used. Testing of alternative mechanical spines/substrates was considered not necessary at this stage of proving feasibility. This decision was supported by qualitative results from experiments of the Shape Tape's wave tracking performance.

Expected sources of error

It was recognised that there would be a variety of sources of error when a flexible ribbon is used to try to capture wave surface elevations. Some of these are listed below and are discussed in detail later in the chapter.

- Spatial aliasing
  - Sensor density along the length of the ribbon must be chosen to match the intended curvature of the incident waves. Too few sensors will mean that bend information will be lost or the information associated with measured bends will be incorrectly integrated in to the resulting signal.
- Calibration
  - The sensors require calibration in the laboratory. These calibrations will have a precision-limited error and possibly systematic errors due to

the calibration procedure. In addition the calibrations could lose their relevancy over time due to the sensors becoming used, worn or distorted through mechanical use.

- Interpolation
  - Interpolation is carried out along the length of the ribbon to "smooth" the bend data. Reductions in over-applying the bend data to particular areas within an interpolated region are achieved by sharing the bend data across the region in a process labelled by Measurand as the 'double-ended approach'. The manufacturer's approach was used. In addition, the interpolation interval of "5" was chosen based upon manufacturer recommendations and a sensitivity study carried out to minimise interpolation error (where increasing the number effectively increasingly smooths the data but increases computation time). No benefits were seen by increasing this interval beyond "5".
- Integration
  - When the bend data is double-integrated integration drift occurs (as is experienced when using accelerometers). This is an unavoidable consequence of the integration. However, knowledge of the system can be used to reduce these effects (for example in inertial measurement systems sensor fusion processes impart information to the system that can correct for this drift via Kalman filters for example). High pass filters that are suitably tuned can reduce these errors.
- Sensor Accuracy
  - Each segment records bend with an inherent error of 1-2% (minimum). With the sensor segment length of the ribbons used in this work this implies an angular error of each segment of approximately 3°. As the orientations of each segment are summed along their length these errors will combine thus the ribbons position will, if no prior or real-time correcting information is supplied, fluctuate in overall, aggregate orientation. The

errors from the beginning of the ribbon will play more of a role as an error of a few degrees in the first portion of the ribbon will lead to a large displacement at the end over the full 7.1 metre length. Un-corrected errors on the end position of the ribbons of the order of tens of centimetres are therefore expected.

5.4 Preliminary Testing: Wave Flume Tests

A ShapeTape specification was conceived and subsequently manufactured by Measurand Inc. and delivered in January 2006 with testing commencing April 2006. Early tests focused on producing data that could readily be analysed using the supplied software before being used to create custom acquisition and processing routines. Initially 35 short duration regular wave tests were conducted followed by 3 irregular wave tests to assess the sensors' ability to track waves of varying frequency and amplitude.

5.4.1 Experimental Procedure

Integration with flume

To aid buoyancy of the ribbon, floats were installed along its length. A 3D computer controlled milling machine was programmed to machine cylinders (25mm diameter, 15mm length) with a slot to allow the ribbon to pass through. The material selected was Divynacell H100 supplied by DIAB. This closed cell material is used in the marine sector for buoyancy, insulation and sound proofing as it offers excellent strength and machinability with very low mass, having a density of 100kgm^{-3} with low water absorption.

The sensor supplied by Measurand comprised a 7.1m long (6.4m active length) ribbon with 32 sensorised zones positioned 201mm apart secured on a spring steel substrate.

Divynacell H100 floats were fitted along the length of the ribbon (see Figs. 5.6b and

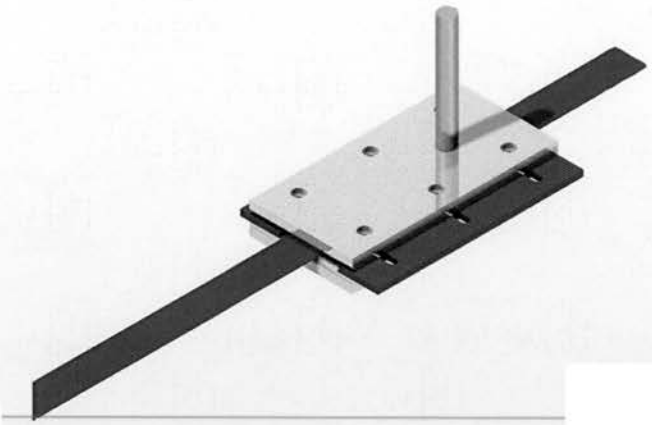

(a) Rendering of CAD flume bracket

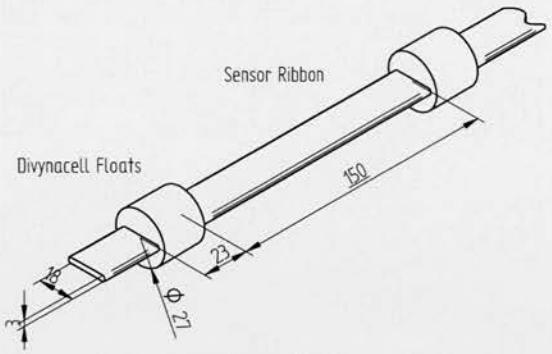

(b) CAD Drawing of ribbon with floats

Figure 5.6. The optical ribbon, bracket and floats - CAD

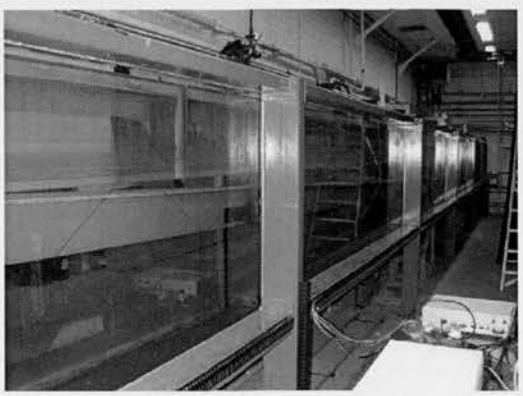

(a) The 20m Edinburgh Flume

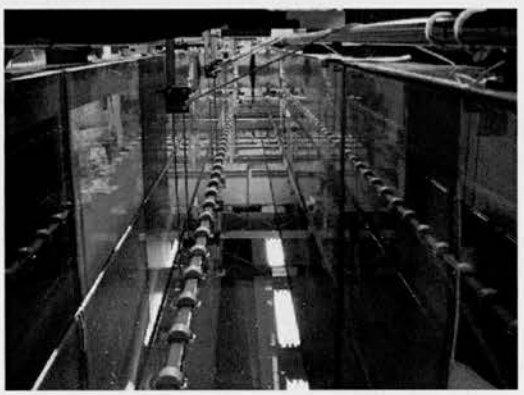

(b) The 7m ribbon in the Edinburgh Flume

Figure 5.7. The Edinburgh Flume

5.7b). The ribbon was waterproofed to a greater degree than the standard product by applying an extra layer of PVC tape and applying a small amount of plastic varnish.

An aluminium arm held with tension wires was suspended in the tank holding a bracket to locate the ribbon securely. Due to the nature of the ribbon, loading on the top surface could deform the optical fibres, leading to an increase in errors and potentially damaging the sensor. Mounting is thus important. The manufacturers suggest clamping via side pressure applied to the spring steel substrate. A custom bracket was designed and produced in-house to secure the ribbon at one end and to aid installation in wave tanks. Shown in figure 5.6a and constructed of stainless steel with grooved nylon inserts, this bracket grips the ribbon from each side with chamfered rear and front edges to prevent wear as the ribbon flexes upwards and downwards in response to waves.

It was conceived that for field use the ribbon would be attached to a moored buoy as opposed to the laboratory/flume walls. This buoy would require knowledge of its position coordinates in 6 degrees of freedom possibly using Real Time Kinematic GPS in combination with inertial sensors. These coordinates would be used to update the origin coordinates when computing the displacements from the ribbon's curvature - as discussed in Chapter 6 and Chapter 7.

For initial testing the origin was fixed in software at (0,0) (in X,Y coordinates where X is along the ribbon and Y is up) and in the laboratory at the mean water level approximately 5 metres downstream of the flume paddle.

5.4.2 Data Acquisition and Processing

Processing Raw Output Data

The procedures for translating vertex bend information in to position data are carried out in the Measurand proprietary program "ShapeWare II"™ and also in the supplied MATLAB Development Kit (MDK). The MDK was an essential tool, allowing creation and adaptation of post-processing algorithms.

Data was also post-processed in MATLAB's Simulink environment which provides a

more dynamic way to implement filtering of the data. An example Simulink routine that was used to provide the data in section 5.4.3 can be seen in figure 5.12.

Measurand-MATLAB MDK

The processing stages associated with each test using the MATLAB development kit are as follows:

- Connect to ShapeTape via RS232 Serial Channel (Com Port)
- Strip off header information and convert data to 16-bit double-precision values for use in MATLAB
- Subtract initial pose data from the data stream
- Internal script converts raw data from sensor to bend data - in radians per segment - using factory calibration data
- Bend data is interpolated into sub-segments to improve the distribution of curvature across a segment
- The X and Y components of the bend data are integrated along the length of the ribbon
- Scaling is applied to give positions in metres based on the ribbon length and number of segments and interpolated sub segments

5.4.3 Results and Discussion

Due to the spatial separation of the sensorised zones, Nyquist theorem implications lead to the ribbon being able to detect waves of wavelength greater than approximately 0.4 metres or approximately 0.5 seconds in period. Below this aliasing will occur. This frequency range limit has been used as one of the cut-off frequencies in subsequent post processing.

After initial set-up and many trial runs, 25 short tests (approx. 30 seconds) and 10 longer tests (approx. 60 seconds) of regular waves were conducted. In addition,

three 512 second JONSWAP (Joint North Sea Wave Project) tests were conducted. Wire-resistance wave gauges were present throughout all tests. In these tests the wave paddle software, wave gauges and Shape Tape were linked to three separate computers governed by their ability to operate the various hardware and software. This led to difficulties with synchronisation. The majority of analysis has however been conducted with a surface wave tracking study in mind as opposed to quasi-real time control where phase differences and latencies between signals would be important. In post-processing, cross-correlation [1] of signals was used to align the various sensor readings.

The supplied ShapeWare II software recorded ShapeTape deflections at approximately 100Hz on an Intel Pentium D (dual core), 2Gb RAM PC with visualisation frame rates of approximately 30fps. WaveLab 2 was used to sample the wave gauges and for frequency and time domain analysis of both the ShapeTape and wave gauge time elevation data.

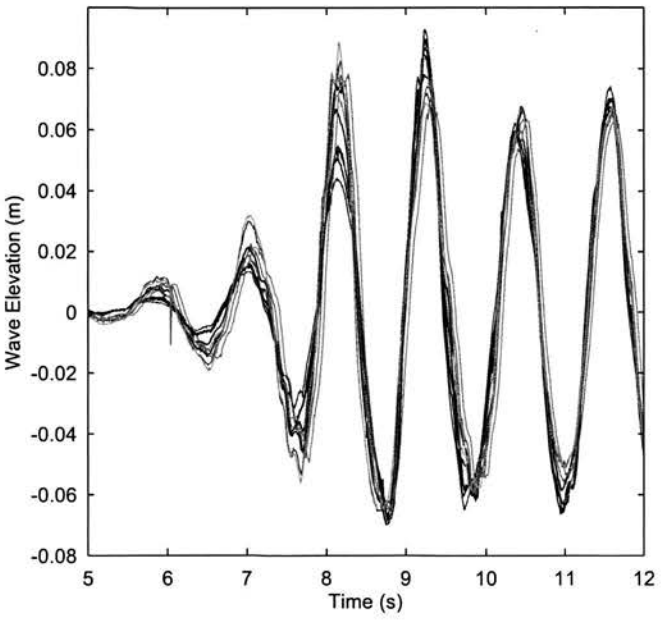

Figure 5.8. Regular wave data showing 7 seconds of waves from 5 seconds after start up. 11 repeat tests

[1] Through implementation of the MATLAB function $xcorr.m$ where two signals are compared for similarity across varying time lags. With sufficient care in setup the time lag associated with the point of maximum correlation corresponds to the time lag in signal acquisition.

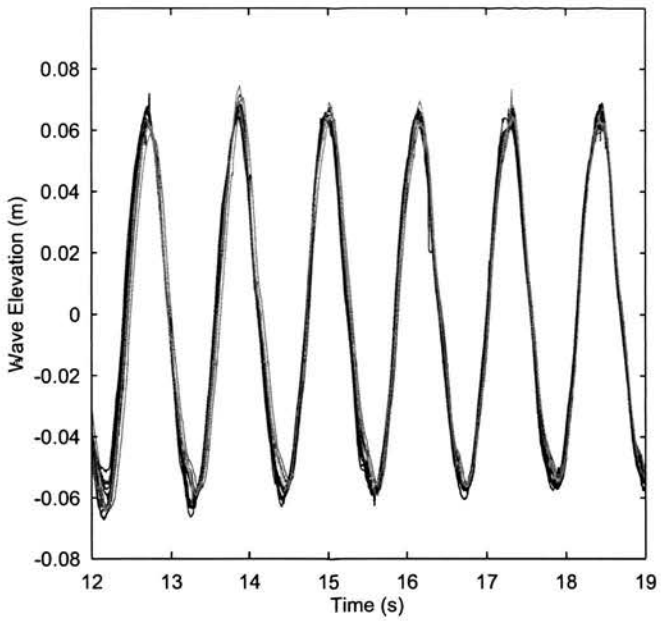

Figure 5.9. Regular wave data showing 6 seconds of waves from 12 seconds after start up. 11 repeat tests

Table 5.2. Repeatability tests. Regular waves excluding ramp up waves.

Wave Height			Wave Period		
Mean (m)	Std (m)	Std (%)	Mean (s)	Std (s)	Std (%)
0.1246	0.0021	1.7	1.1435	0.0028	0.24

Table 5.3. Repeatability tests. Regular waves including ramp up waves.

Wave Height			Wave Period		
Mean (m)	Std (m)	Std (%)	Mean (s)	Std (s)	Std (%)
0.1214	0.0033	2.8	1.1433	0.0043	0.38

Repeatability tests were conducted on regular wave trains and showed encouraging similarity in elevation-time traces (see Fig. 5.9). Greater deviation during the flume paddle ramp-up stage is evident, coinciding with greater actual deviation in tank wave heights but this does not fully account for the discrepancy. These plots were post-correlated (shifted in time) due to the lack of synchronisation during testing as previously discussed. Improved timing procedures will further remove uncertainty in gauging repeatability in terms of phase.

The process, internal to the proprietary software ShapeWare II, of interpolating and integrating curvature to produce XY coordinates for points along the ribbon leads to large-magnitude errors. This is to be expected due to the accumulation of integration error and the fact that small errors in angle near the base of the sensor result in large displacements 7.1 metres away. In addition to the unavoidable errors there seemed to be some regular artifacts and trends in the response of the sensor due to the experimental set-up. These errors (in addition to the inherent integration errors) were evident from initial laboratory dry-run trials where the derived data was observed to oscillate between positive and negative values (see Fig. 5.10). This is physically impossible due to the presence of the ground. High-amplitude, high-frequency spikes occasionally appear in the sampled ribbon data. These generally appear to be due to a memory buffering issue, occurring at similar stages in the acquisition. Also present in the raw bend data is a persistent anomaly occurring at the start of the ribbon where it is attached to the tank. Unwanted and/or periodically fluctuating pressure on the optical fibres may have been the cause. The raw bend data, however, appeared representative and robust and it was assumed that processing routines could be developed that could take into account the unique nature of the oscillation of the water waves and minimise the inherent errors and remove the software/hardware influenced artifacts.

Further data processing routines were implemented in MATLAB with the aim of isolating the large-magnitude oscillations from the time elevation series produced by the experimental set up and the integrations in ShapeWare II. Plotting elevation against horizontal position demonstrates the problem of the tail flipping (see Fig. 5.10). The surface waves are visible but are superimposed onto a curving error

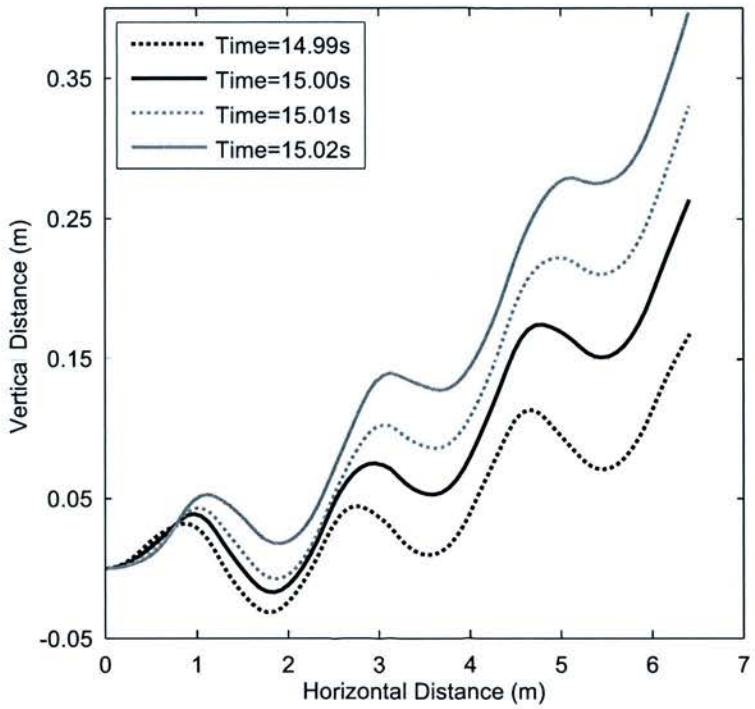

(a) Spatial ribbon data taken from four consecutive samples

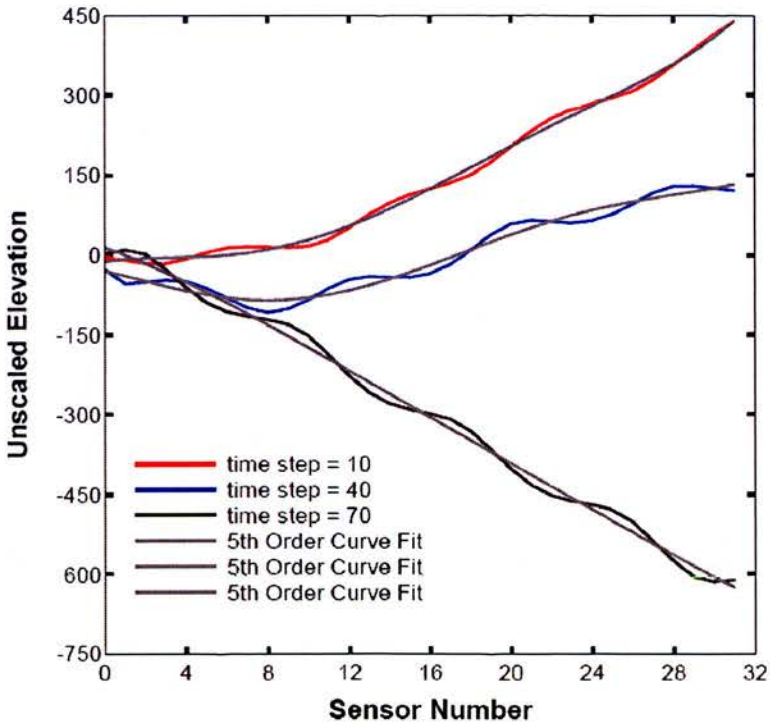

(b) Spatial ribbon data taken at three separate times with 5th order line fitting applied.

Figure 5.10. Examples showing spatial positioning errors (a) and (b) and preliminary method of assessing their impact (b).

line. In order to assess the degree to which the superimposed waves correlated with the actual waves, a preliminary scheme of processing was developed. By fitting a polynomial of order chosen to give the most consistent results and then subtracting it from the original data the ribbon's position is flattened. This basic method introduces errors in the final data and the "flattening" process was highlighted as requiring further development at this stage. Data from sensors on the ribbon nearest the beginning and end of the ribbon are most severely affected and for this reason, together with the origin anomaly, were generally discarded in further processing particularly in the wave-by-wave time series analysis.

After this initial processing, the gains of the individual sensor outputs are analysed. Any trends in sensor amplitude are removed by multiplying each sensor by an individual gain factor related to the average of the sensors selected for inclusion. This analysis suggested a requirement for an improved filtering algorithm that could take into account both sensor variation of response along the ribbon and in addition, a frequency dependent sensor response.

5.5 Improved Testing: Wave Flume Tests

Following the preliminary testing a new series of tests were conducted in parallel to the improved optical tracking method (4) across the same test matrix as listed in tables 5.4 and 5.5.

5.5.1 Experimental Procedure

Experiments were conducted in the Edinburgh 20m wave flume as described in Chapter 4. Figure 4.3 is repeated - for convenience - in figure 5.11.

It was expected that some mechanical modifications would be required to the ShapeTape to cope with immersion in water. However, experience in the preliminary tests gave confidence in the PVC tape and glue of the supplied instrument. After a day of testing the instrument was lifted up out to the tank rails and allowed to dry

Table 5.4. Regular wave test matrix

Test #	Wave Height (m)	Period (s)	Test #	Wave Height (m)	Period (s)
1	0.01	1.43	31	0.04	1.00
2	0.02	1.43	32	0.05	1.00
3	0.03	1.43	33	0.06	1.00
4	0.04	1.43	34	0.07	1.00
5	0.05	1.43	35	0.08	1.00
6	0.06	1.43	36	0.09	1.00
7	0.07	1.43	37	0.01	0.91
8	0.08	1.43	38	0.02	0.91
9	0.09	1.43	39	0.03	0.91
10	0.01	1.25	40	0.04	0.91
11	0.02	1.25	41	0.05	0.91
12	0.03	1.25	42	0.06	0.91
13	0.04	1.25	43	0.07	0.91
14	0.05	1.25	44	0.08	0.91
15	0.06	1.25	45	0.01	0.83
16	0.07	1.25	46	0.02	0.83
17	0.08	1.25	47	0.03	0.83
18	0.09	1.25	48	0.04	0.83
19	0.01	1.11	49	0.05	0.83
20	0.02	1.11	50	0.06	0.83
21	0.03	1.11	51	0.07	0.83
22	0.04	1.11	52	0.08	0.83
23	0.05	1.11	53	0.01	0.77
24	0.06	1.11	54	0.02	0.77
25	0.07	1.11	55	0.03	0.77
26	0.08	1.11	56	0.04	0.77
27	0.09	1.11	57	0.05	0.77
28	0.01	1.00	58	0.06	0.77
29	0.02	1.00	59	0.07	0.77
30	0.03	1.00	60	0.01	0.71

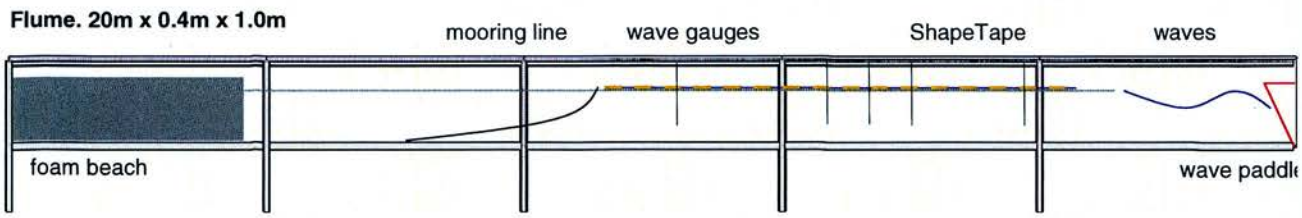

(a) Diagram of experimental configuration showing 20m Edinburgh flume and relative position of ShapeTape, wave gauges, mooring line and wave reflection-suppressing foam beach.

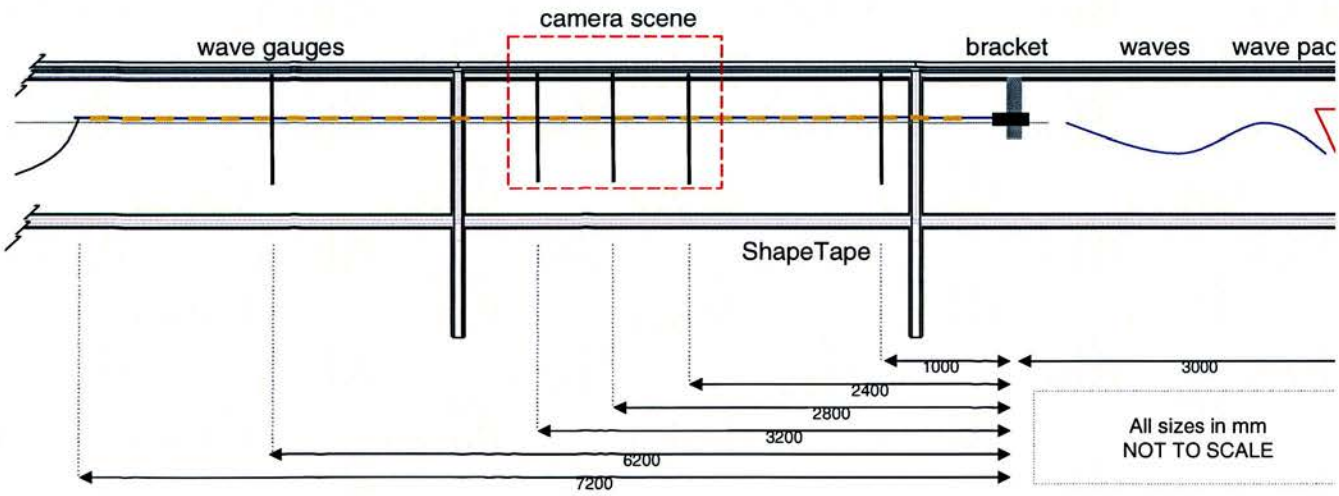

(b) Diagram of experimental configuration showing location of wave gauges, ShapeTape fixings and camera field of view.

Figure 5.11. Diagrams of experimental set-up showing (a) overall Flume layout and (b) locations of wave gauges and camera field of view.

Table 5.5. Irregular wave test matrix

Test Number	H_{m0} (m)	Peak Period, T_p (s)	Duration (s)
1	0.112	1.32	512
2	0.069	1.05	512
3	0.046	0.85	512
4	0.036	0.76	512
5	0.119	1.33	280 of 512
6	0.080	1.07	512

overnight. As testing progressed visual inspections were carried out for any signs of nicks or abrasion. Extra PVC tape was applied to the tail end of the unit to mitigate abrasion from attached moorings. A stiffer and easier to align mounting bracket was included in the test setup. An improved mooring system was implemented comprising 2m polymer string connected to a 1kg weight on the bottom of the flume.

5.5.2 Data Acquisition and Processing

Data was acquired and post processed under the following procedure:

Acquisition of data

MATLAB was used to acquire ShapeTape data over serial communications protocol using a customised version of the supplied ShapeTape MATLAB Development Kit. WaveLab 2 was used to acquire wire resistance wave gauge data with the wave gauges being calibrated daily using standard calibration procedure (based on moving wave gauges through a known displacement and measuring the voltage difference).

Post processing of bend data

Following acquisition the raw bend data was loaded using custom MATLAB scripts. Routines were implemented to convert the time-stamps comprising hh:mm:ss.ss to number of seconds elapsed. Spurious spikes were then removed via threshold value detection and corrected for via nearest neighbour interpolation. Data spikes due to system and/or memory buffer issues were removed in the same manner. A

low pass finite impulse response (FIR)* filter was imposed on the data following re-sampling from a non-deterministic sampling rate typical of Windows-type operating systems (usually between 30-32Hz) depending on processor activities to a fixed 25Hz sampling rate (to match camera frame rate). For comparison wave gauge data was loaded using MATLAB scripts and resampled from 64Hz to 25Hz to match bend data and the camera frame rate. Adjustments to the ShapeTape in terms of mean slope and flat-pose/initial position were then made.

*Finite impulse response filters were used throughout the processing procedure due to their ease of implementation in MATLAB and improved phase response with respect to infinite impulse response filters [113].

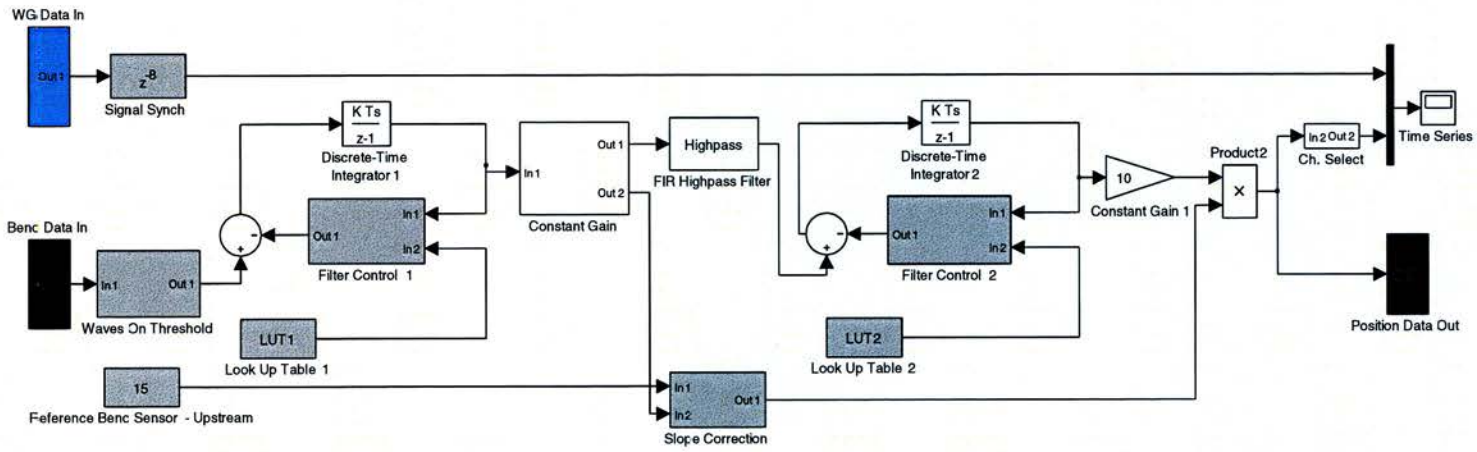

Figure 5.12. Example processing technique (Type-“RT2”). Simulink block diagram

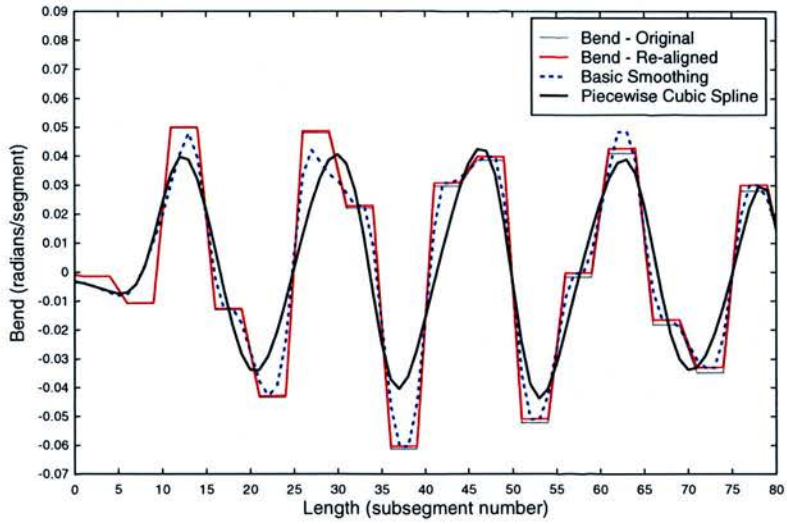

Figure 5.13. Various bend interpolation processing examples

Parameters investigated and used to provide threshold criteria for the data included filter cut-off frequencies and filter type, wave steepness, wave height and wave period. Figures 5.15 and 5.16 show the results of parameter space searching algorithms on regular wave tests. With no correction for these attributes large errors in wave height exist. Figure 5.13 shows pre-integration bend interpolation trials on raw bend data. No method during this processing stage was found that provided robust error reduction other than the method of small correction for initial pose position (shown in red). Throughout, sensed wave period is in good agreement with wire resistance wave gauge reported wave period regardless of post processing threshold levels as shown in figure 5.14.

5.5.3 Four Candidate Processing Techniques

A variety of post processing techniques were trialled based upon experience of analysing the preliminary irregular and regular wave tests and the revised regular wave tests (see previous section). Four of the most developed methods have been incorporated and are summarised under the relevant sections below. These four methods range from fully non-real-time, "post-processed", i.e., operations were

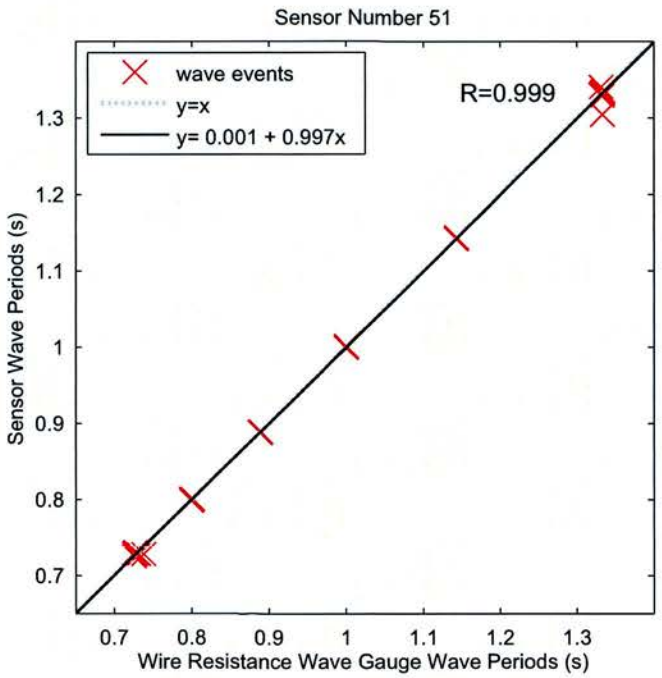

Figure 5.14. Preliminary regular wave tests.

carried out on the entire data set that could not be carried out on a section or sections of the data set on-the-fly, to real-time where operations were carried out on the data set as it entered the "system". All procedures were conducted in MATLAB or MATLAB Simulink on a mid-range Laptop.

Four processing techniques

The four processing techniques:

1. BF - **B**asic **F**iltering with look up table

2. AMF - **A**rbitrary **M**agnitude/Response **F**iltering

3. RT1 - **R**eal **T**ime filtering with on-the-fly adjustable filter weights

4. RT2 - **R**eal **T**ime filtering with look up table

Processing Technique 1. "BF". Basic Filtering

A zero-phase forward and reverse digital filter was applied to the entire data set at each of the integration stages. This was implemented via the MATLAB "filtfilt" function [114, 115]. This removed phase changes resulting from the application of the low and high pass filters but required that the entire data set (or a relatively large section of the data set) was present in advance and was thus non-real-time. The frequency dependence of the output, as experienced during regular wave tests, was incorporated using a "learned" look up table which is related to the peak period of the data set.

Processing Technique 2. "AMF". Arbitrary Magnitude/Response Filtering

As with the Basic Filtering approach a zero-phase forward and reverse digital filter was applied to the entire data set at the integration stage. Instead of a look-up-table the frequency dependency of the reported wave heights were incorporated into a single Arbitrary Magnitude Filter. This filter's magnitude response was determined from analysis of the regular wave tests and implemented as a high order (approximately 130) FIR filter. Due to the high order of the filter a group delay of approximately 2.5 seconds is introduced. Shorter order AMF filters were produced and trialled in semi-real-time simulations with group delays of approximately 0.6 seconds.

Processing Technique 3. "RT1". Real Time Processing - Method 1

In order to trial the ability of post-processing to be conducted in real-time or close to real-time post processing routines were developed in MATLAB Simulink with a fixed, discrete solver configuration. Zero-phase forward and reverse digital filters were replaced with FIR filters whose parameters could be changed by various control signals. These signals were derived from analysis of the regular wave tests and through basic optimisation routines. RT1 makes use of wave slope and wave period information derived from short-time FFT analysis and running mean procedures.

Processing Technique 4. "RT2". Real Time Processing - Method 2

An easier to implement method (in comparison to RT1) was developed that builds on the Basic Filtering (BF) technique but that resides inside of the Simulink time domain simulation. A look up table of filter parameters is used at the integration stages in order to choose a high-pass filter which has the minimum effect on the input signal. See figure 5.12 for more information.

5.5.4 Results - Regular Waves

Figures 5.17 and 5.18 show wave heights and wave periods reported by the sensor compared to those reported by wire resistance wave gauges. It can be seen that period again shows excellent agreement. Wave steepness can be seen to be influencing performance in figures 5.19 and 5.20. For figures 5.17 and 5.18 wave steepness has been used as a processing threshold whereby only waves below a steepness of 0.1 are included in analysis. This results in the exclusion of 8 of the steepest wave conditions from the test matrix of 60. As with the optical tracking tests, regular wave tests at the highest wave frequency (wave period of 0.71s) were excluded (with the exception of the test with the lowest wave amplitude at this frequency - test number 60).

Figure 5.19b and 5.20b shows the insensitivity of wave period error with changes in wave steepness (in the range of the utilised test matrix).

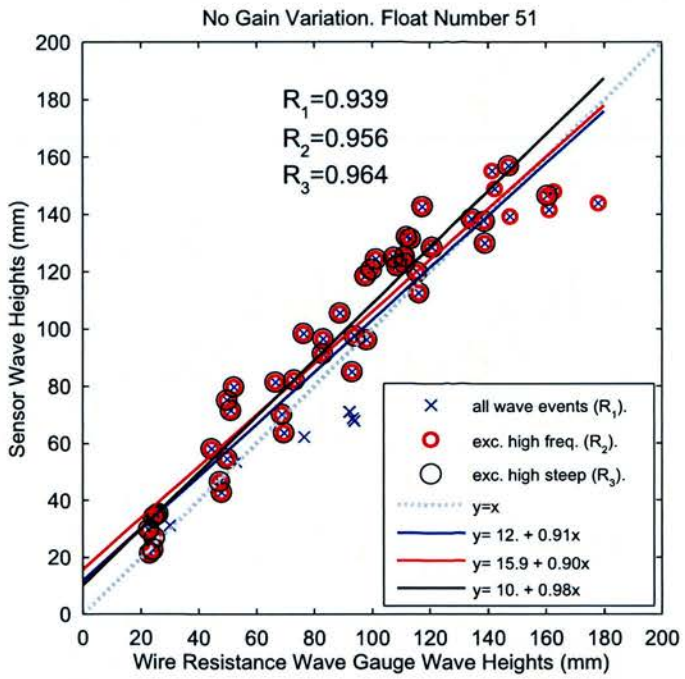

Figure 5.15. Preliminary regular wave tests. No frequency dependent adjustments made.

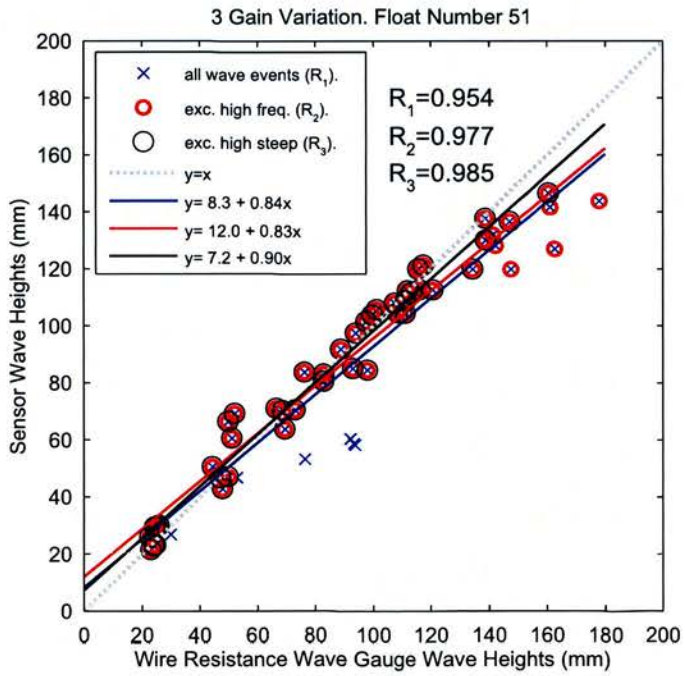

Figure 5.16. Preliminary regular wave tests. Three-zone frequency dependent adjustments made.

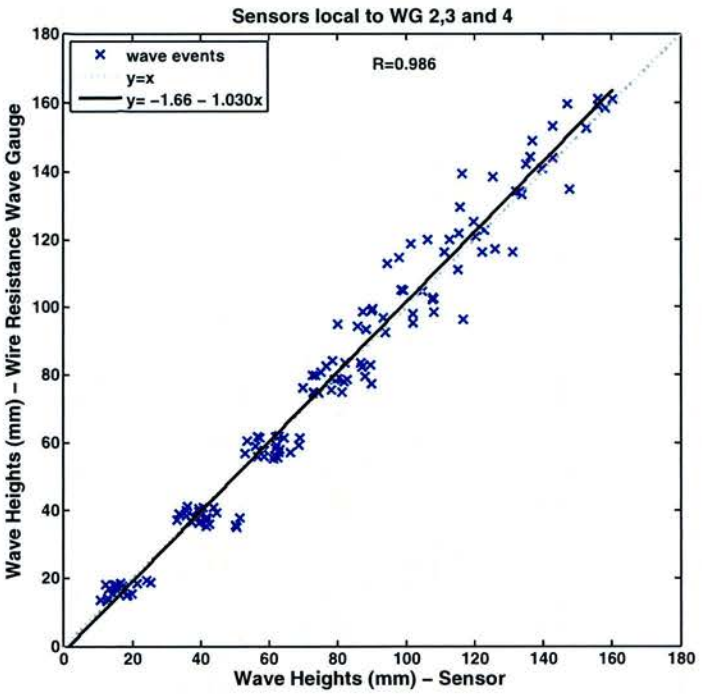

(a) Regular wave tests. Processed using the BF technique (see section 5.5.3).

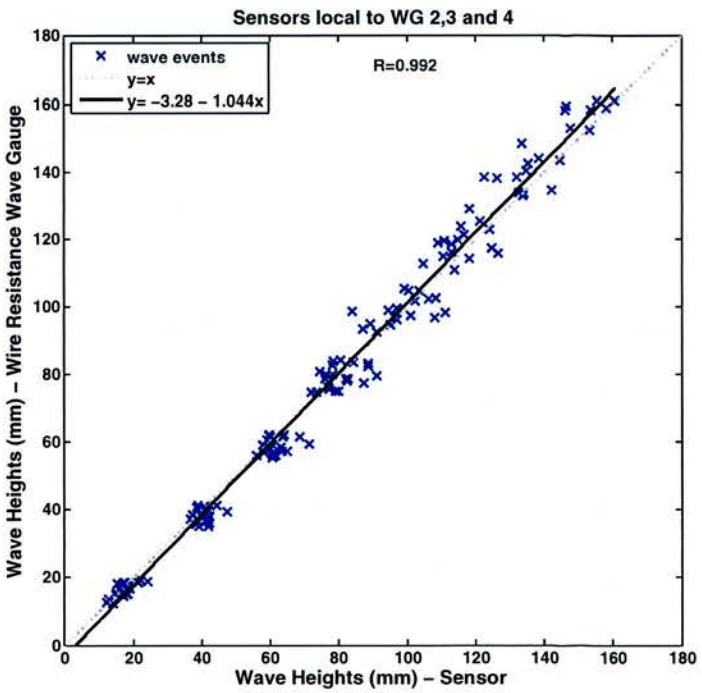

(b) Regular wave tests. Processed using the RT2 technique (see section 5.5.3).

Figure 5.17. Regular wave tests with steepness <0.1. Mean wave height recorded by wire resistance wave gauges versus sensor mean wave heights.

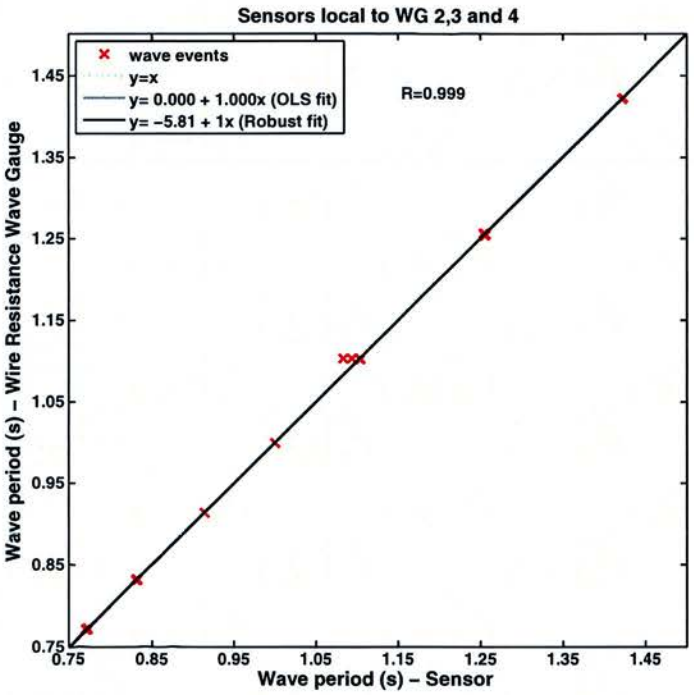

(a) Regular wave tests, processed using the BF technique (see section 5.5.3).

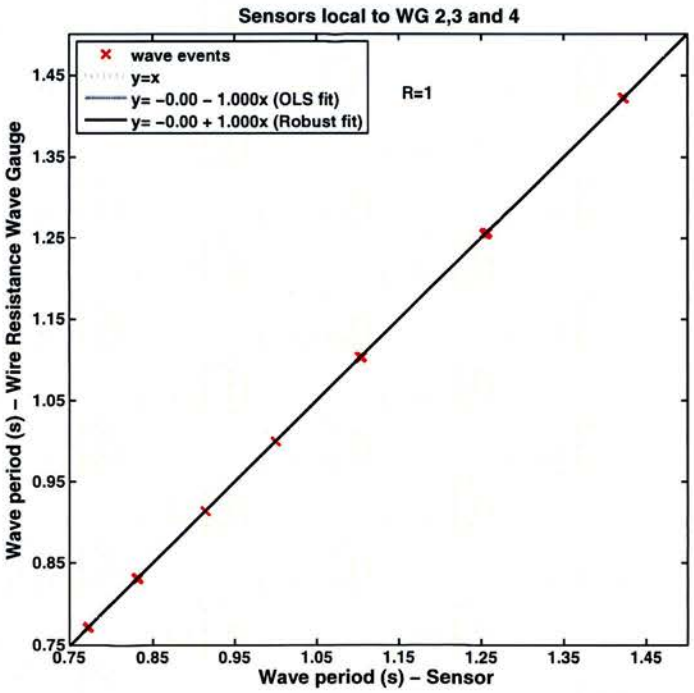

(b) Regular wave tests. Processed using the RT2 technique (see section 5.5.3).

Figure 5.18. Regular wave tests with steepness <0.1. Mean wave periods recorded by wire resistance wave gauges versus sensor mean wave periods.

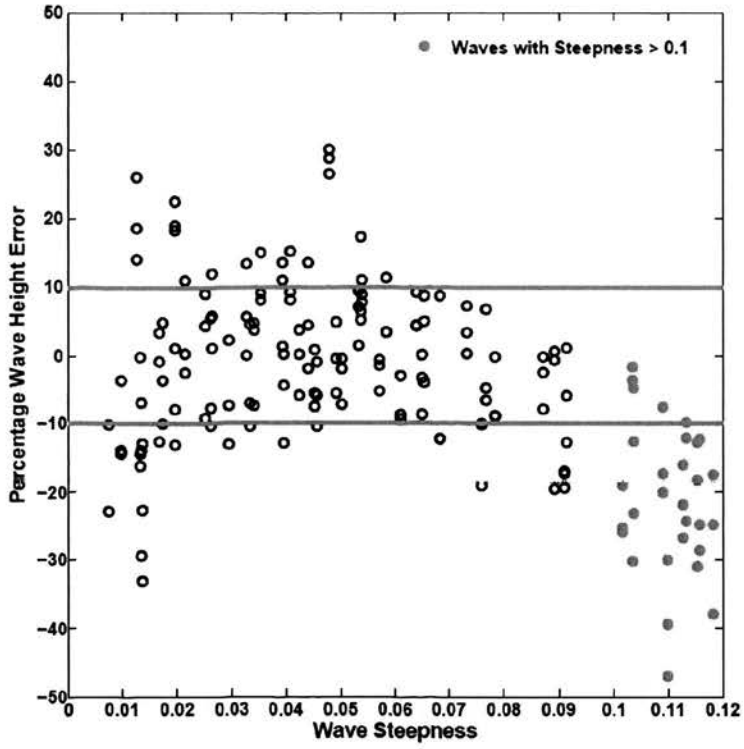

(a) Regular wave tests 1 to 60. Percentage error in wave heights for three sensors local to wire resistance wave gauges 2,3 and 4.

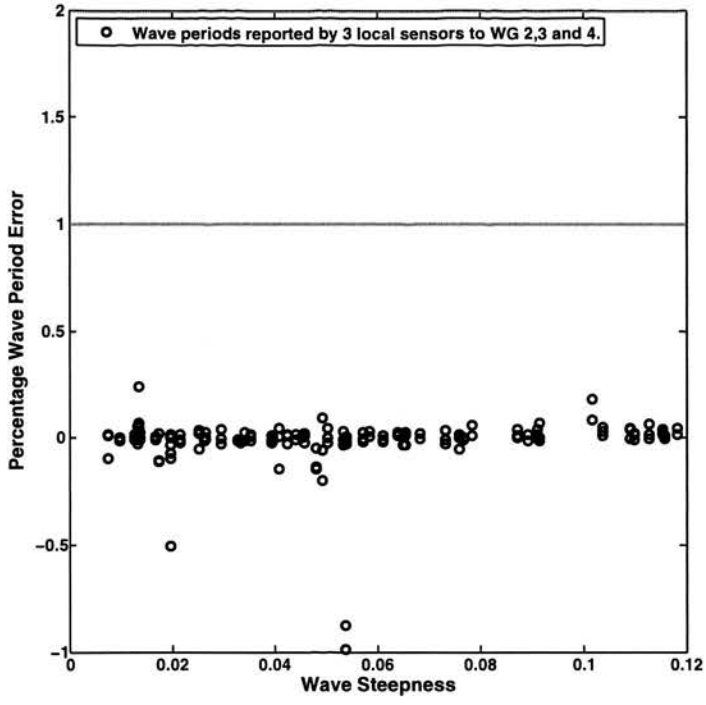

(b) Regular wave tests 1 to 60. Percentage error in wave periods for three sensors local to wire resistance wave gauges 2,3 and 4.

Figure 5.19. Regular wave tests 1 to 60. Percentage error in mean wave height and mean wave period (recorded by wire resistance wave gauges versus sensor mean wave heights) versus wave steepness. Percentage error greater than zero implies over-measurement by sensor. Processed using the BF technique.

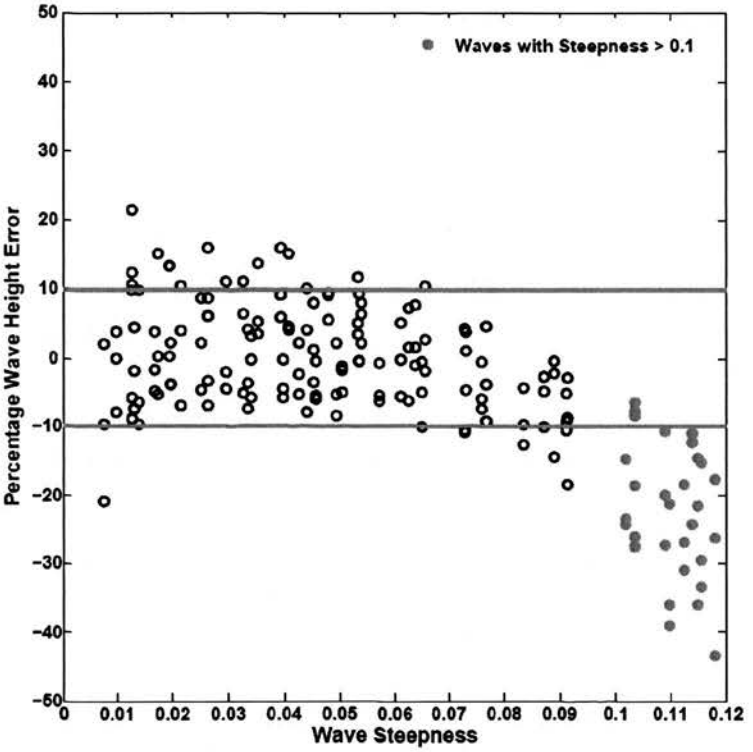

(a) Regular wave tests 1 to 60. Percentage error in wave heights for three sensors local to wire resistance wave gauges 2,3 and 4.

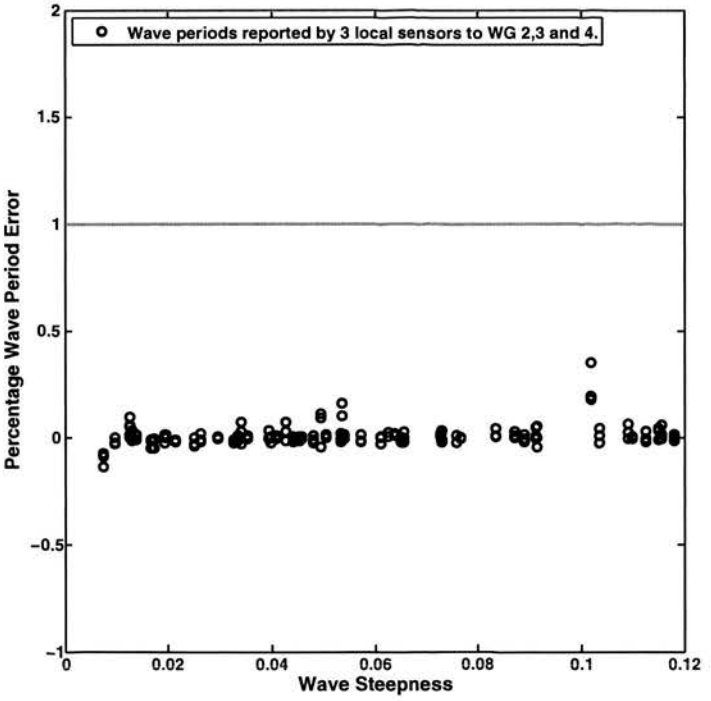

(b) Regular wave tests 1 to 60. Percentage error in wave periods for three sensors local to wire resistance wave gauges 2,3 and 4.

Figure 5.20. Regular wave tests 1 to 60. Percentage error in mean wave height and mean wave period (recorded by wire resistance wave gauges versus sensor mean wave heights) versus wave steepness. Percentage error greater than zero implies over-measurement by sensor. Processed using the RT2 technique.

5.5.5 Results - Irregular Waves

The following four subsections show wave-by-wave comparisons of wave height and wave period between wire resistance wave gauges and local sensor zones on the ShapeTape for the various candidate processing methods. Representative time-series surface elevation plots are also shown. Results from all four methods are summarised in section 5.5.6.

Processing Technique 1 - BF

Figures 5.21 to 5.26 show wave heights and wave periods reported from time series analysis of data reported by wire resistance wave gauges and the sensor in closest proximity to each wave gauge. Irregular tests 1 to 6 are plotted. All data points are plotted for this processing technique and the following three additional processing techniques. Reported summary statistics, however, incorporate varying degrees of data filtering such as limiting wave steepness or imposing minimum wave periods, as explained in the relevant sections. Varying degrees of correlation can be seen across the tests and across the sensor within each test. Generally the sensor furthest downstream shows the highest correlation with the wire resistance wave gauge, both in terms of wave height and wave period. In addition to the varying degrees of correlation there is large variation in bias between measurements, with significant over and under-prediction of waves between tests.

Figures 5.27 and 5.28 show time series of surface elevation for a centrally located sensor segment and its corresponding neighbouring wave gauge for irregular wave tests 1 to 6 processed under the BF technique.

Tables 5.6, 5.7, 5.8 and 5.9 show the number of waves that have been successfully matched in the time elevation time series between the sensor and the wire resistance wave gauges. "Matched" implies that the wave matching routine found a pair of waves in the two time series. Waves whose values fell outside of minimum/maximum steepness, size or period were excluded with the balance included and labelled "In Range".

Table 5.6. Irregular wave tests - time domain processed using BF technique. Number of waves in processed samples.

Test	Number of waves BF processed			% Waves excluded during each processing stage		
	Wave gauge	Matched	In range	Matched	In range	Total
1	391	353	343	9.7	2.8	12.3
2	483	447	440	7.5	1.6	8.9
3	537	509	498	5.2	2.2	7.3
4	584	543	532	7.0	2.0	8.9
5	209	189	180	9.6	4.8	13.9
6	437	408	402	6.6	1.5	8.0

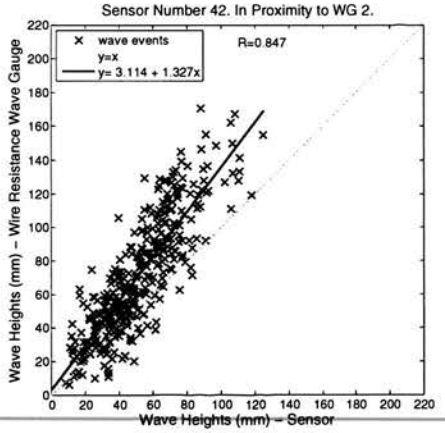

(a) Sensor vs WG no.2. Wave heights

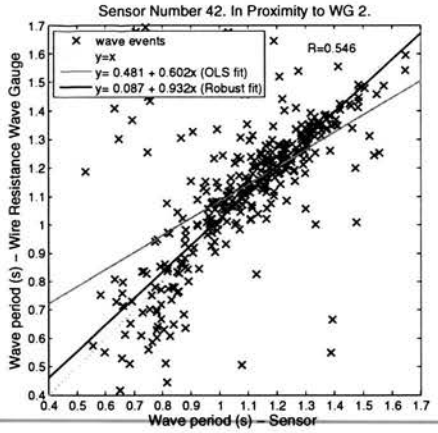

(b) Sensor vs WG no.2. Wave periods

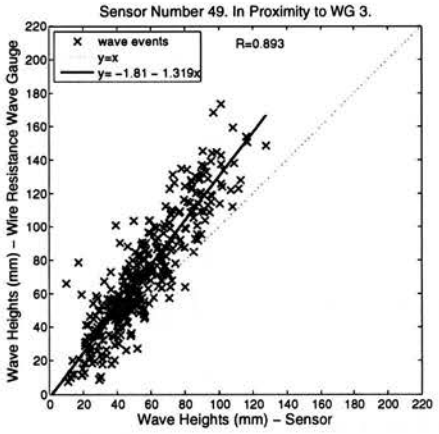

(c) Sensor vs WG no.3. Wave heights

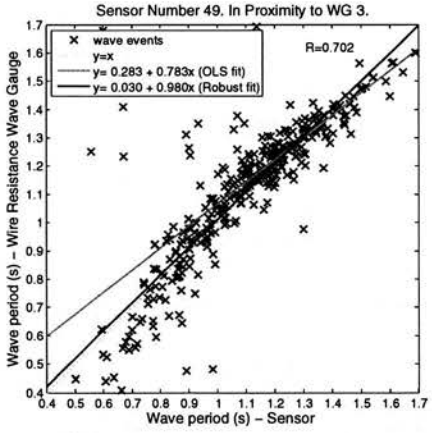

(d) sensor vs WG no.3. Wave periods

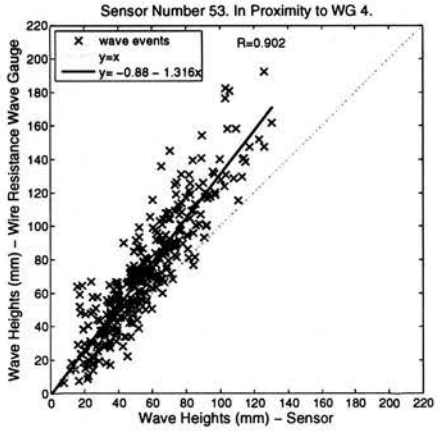

(e) Sensor vs WG no.4. Wave heights

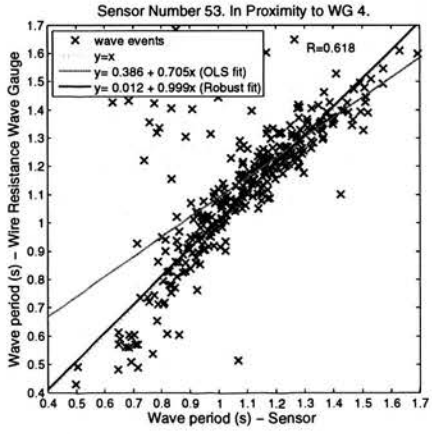

(f) Sensor vs WG no.4. Wave periods

Figure 5.21. Test 1 - Wave-by-wave matching. Heights and periods. Processing: "BF" implemented.

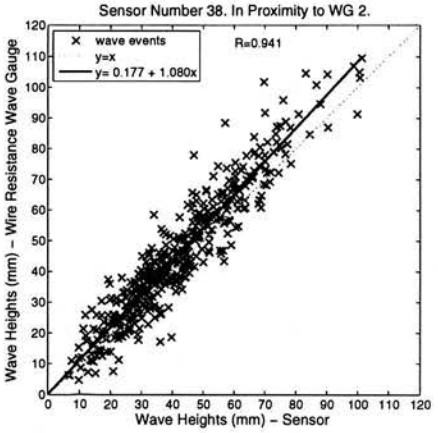

(a) Sensor vs WG no.2. Wave heights

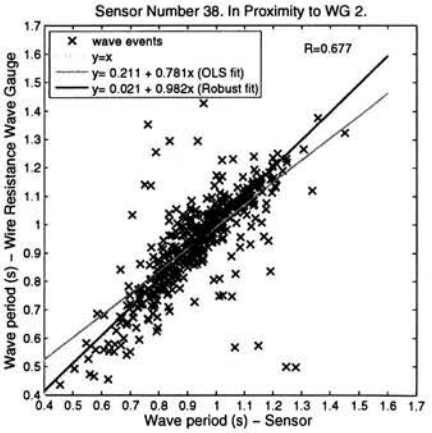

(b) Sensor vs WG no.2. Wave periods

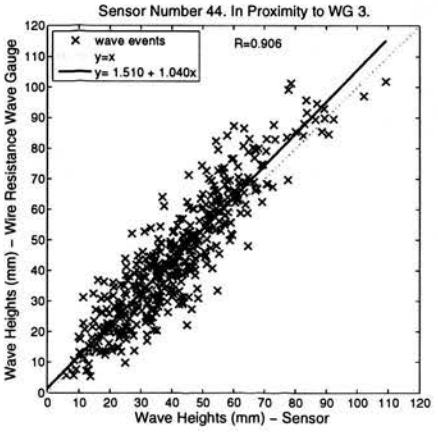

(c) Sensor vs WG no.3. Wave heights

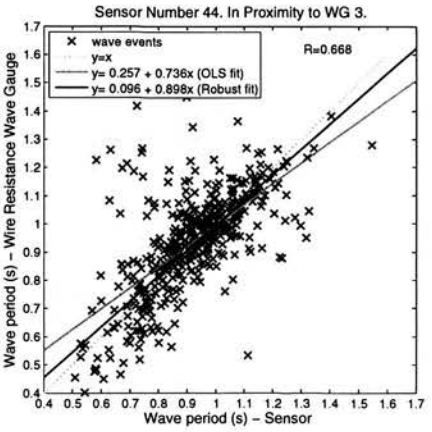

(d) Sensor vs WG no.3. Wave periods

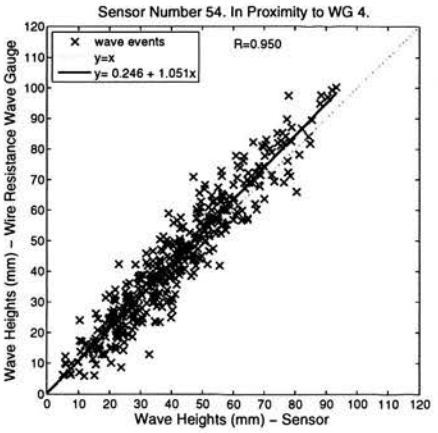

(e) Sensor vs WG no.4. Wave heights

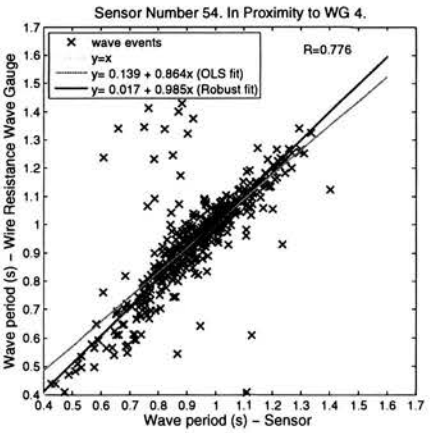

(f) Sensor vs WG no.4. Wave periods

Figure 5.22. Test 2 - Wave-by-wave matching. Heights and periods. Processing: "BF" implemented.

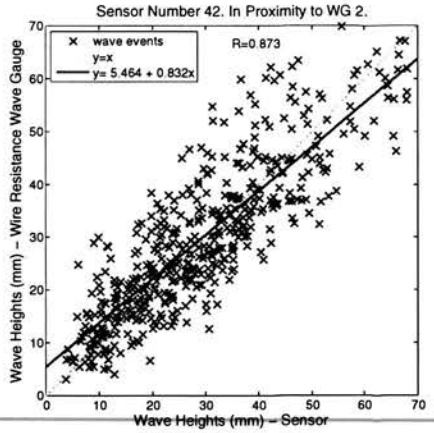

(a) Sensor vs WG no.2. Wave heights

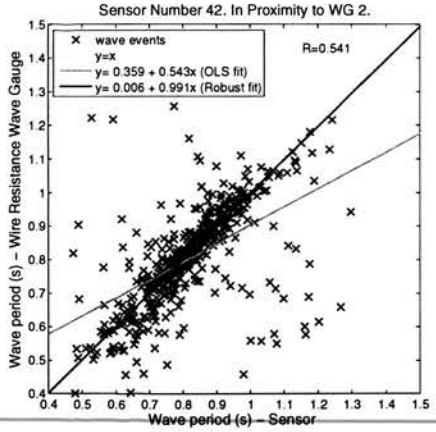

(b) Sensor vs WG no.2. Wave periods

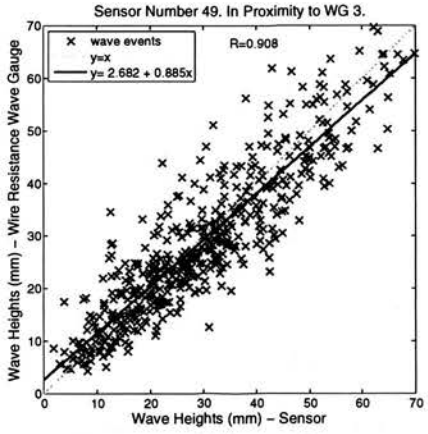

(c) Sensor vs WG no.3. Wave heights

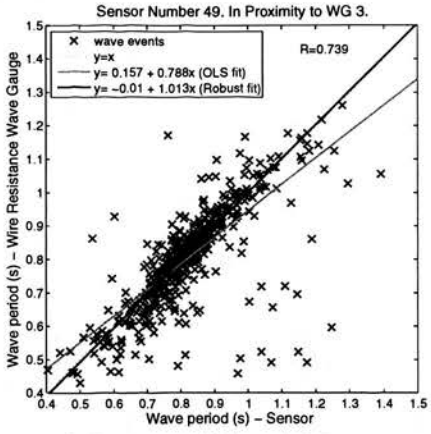

(d) Sensor vs WG no.3. Wave periods

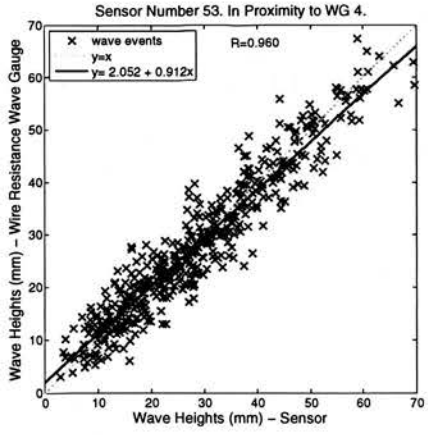

(e) Sensor vs WG no.4. Wave heights

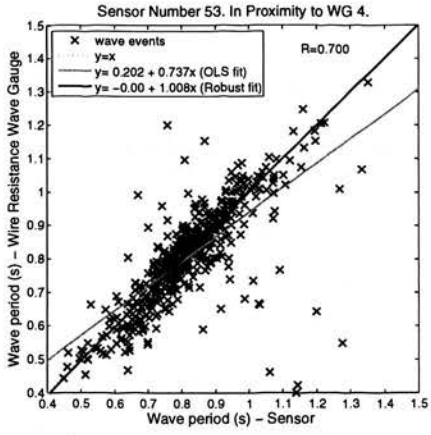

(f) Sensor vs WG no.4. Wave periods

Figure 5.23. Test 3 - Wave-by-wave matching. Heights and periods. Processing: "BF" implemented.

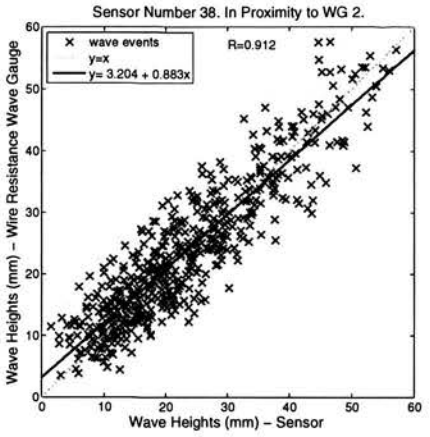

(a) Sensor vs WG no.2. Wave heights

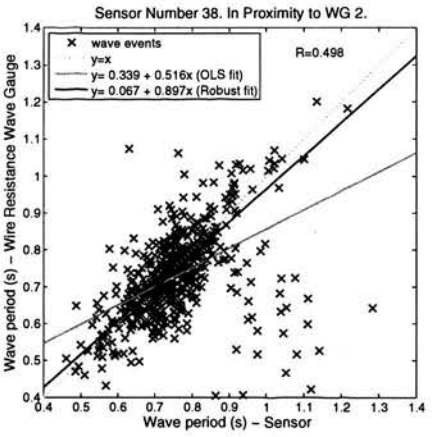

(b) Sensor vs WG no.2. Wave periods

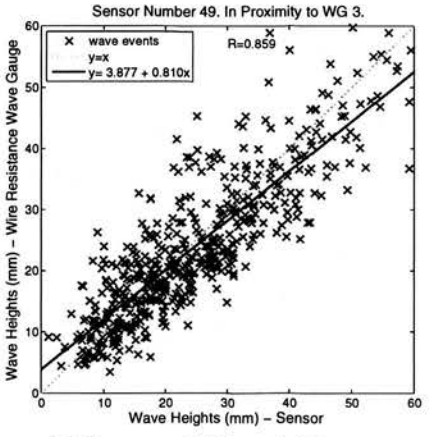

(c) Sensor vs WG no.3. Wave heights

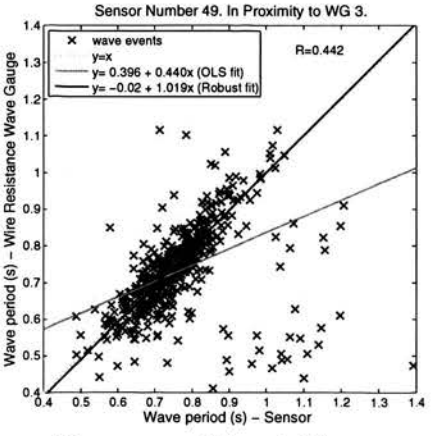

(d) sensor vs WG no.3. Wave periods

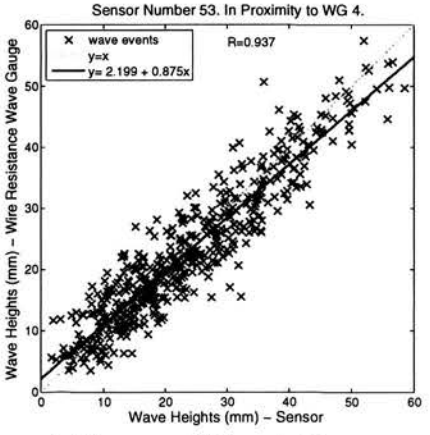

(e) Sensor vs WG no.4. Wave heights

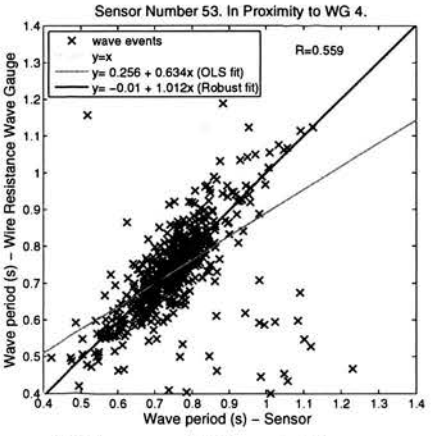

(f) Sensor vs WG no.4. Wave periods

Figure 5.24. Test 4 - Wave-by-wave matching. Heights and periods. Processing: "BF" implemented.

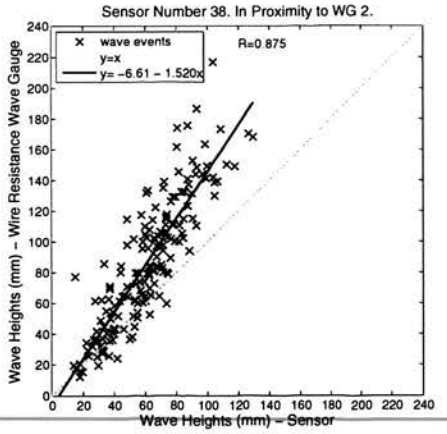

(a) Sensor vs WG no.2. Wave heights

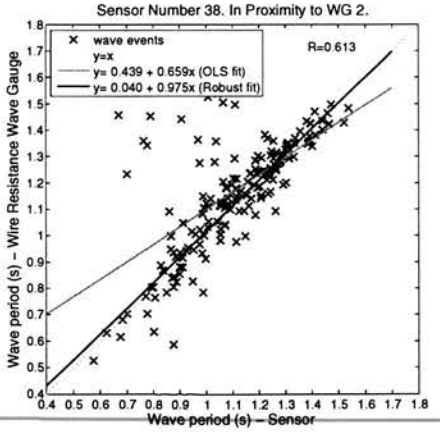

(b) Sensor vs WG no.2. Wave periods

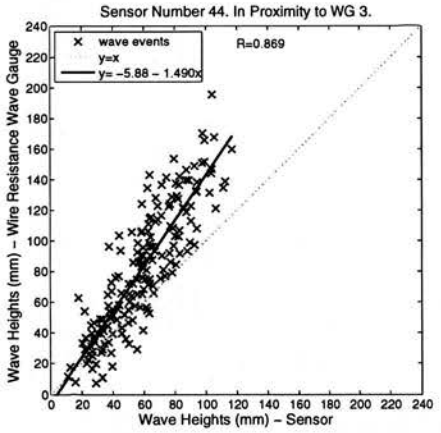

(c) Sensor vs WG no.3. Wave heights

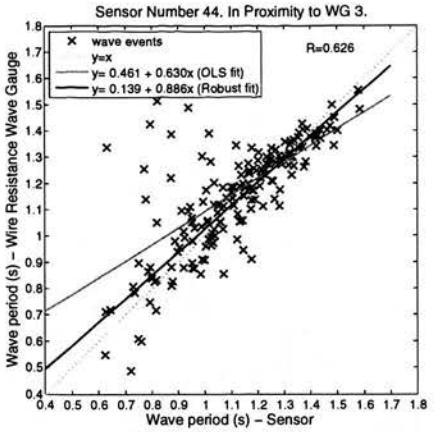

(d) Sensor vs WG no.3. Wave periods

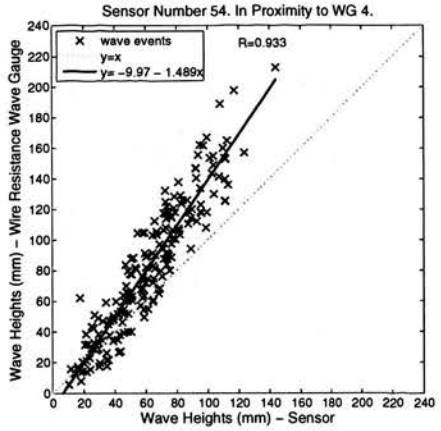

(e) Sensor vs WG no.4. Wave heights

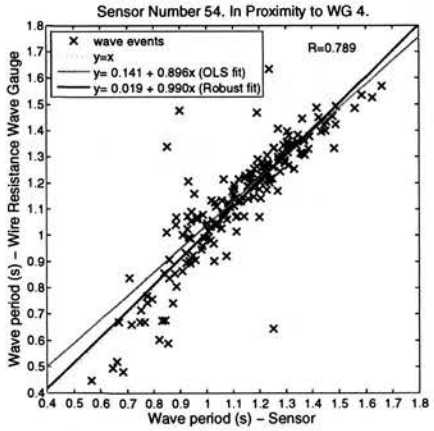

(f) Sensor vs WG no.4. Wave periods

Figure 5.25. Test 5 - Wave-by-wave matching. Heights and periods. Processing: "BF" implemented.

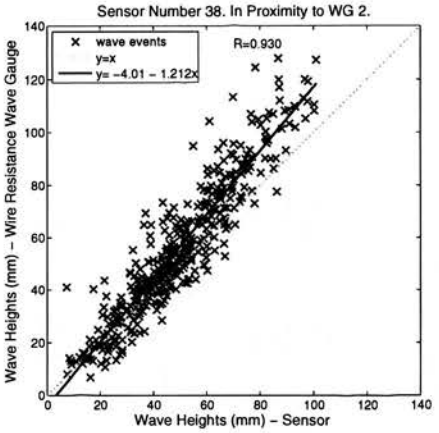

(a) Sensor vs WG no.2. Wave heights

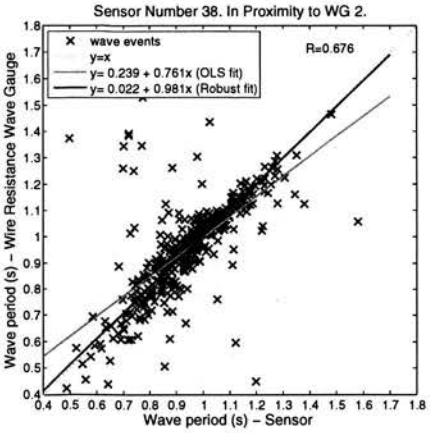

(b) Sensor vs WG no.2. Wave periods

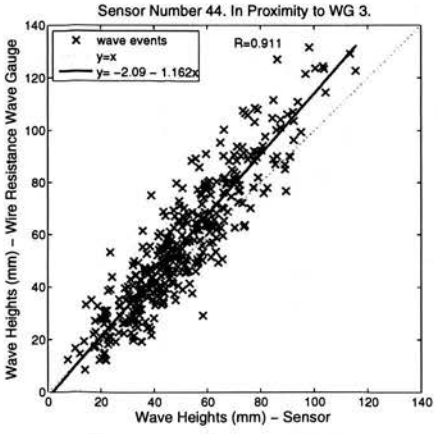

(c) Sensor vs WG no.3. Wave heights

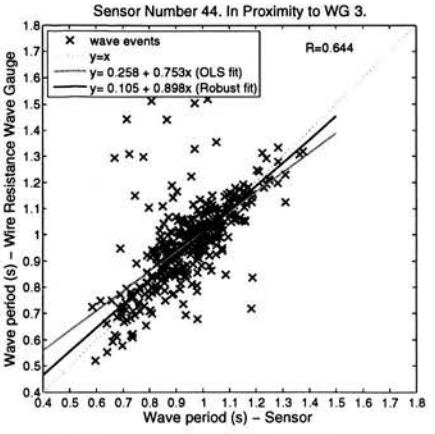

(d) Sensor vs WG no.3. Wave periods

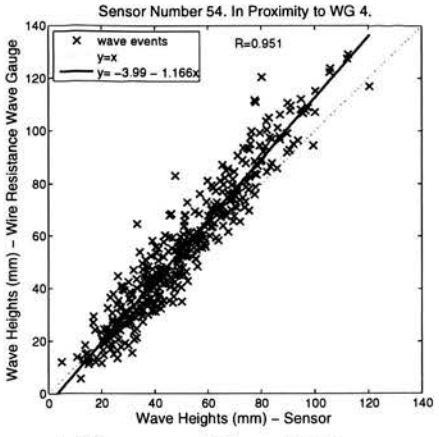

(e) Sensor vs WG no.4. Wave heights

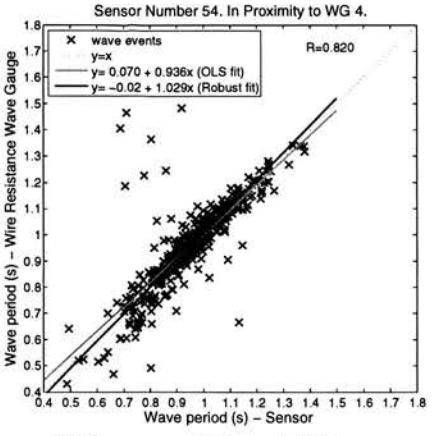

(f) Sensor vs WG no.4. Wave periods

Figure 5.26. Test 6 - Wave-by-wave matching. Heights and periods. Processing: "BF" implemented.

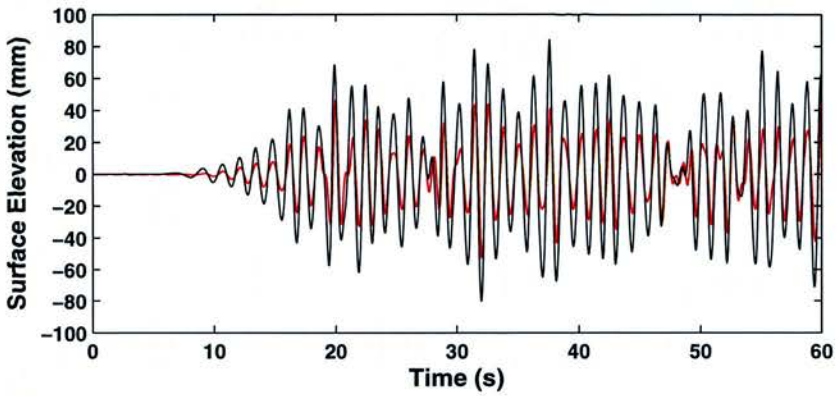

(a) Surface elevation time series. Wire resistance wave gauge and Sensor, Test 1

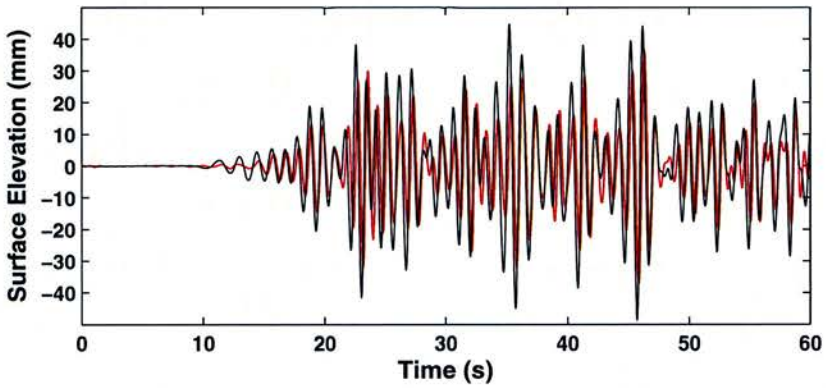

(b) Surface elevation time series. Wire resistance wave gauge and Sensor, Test 2

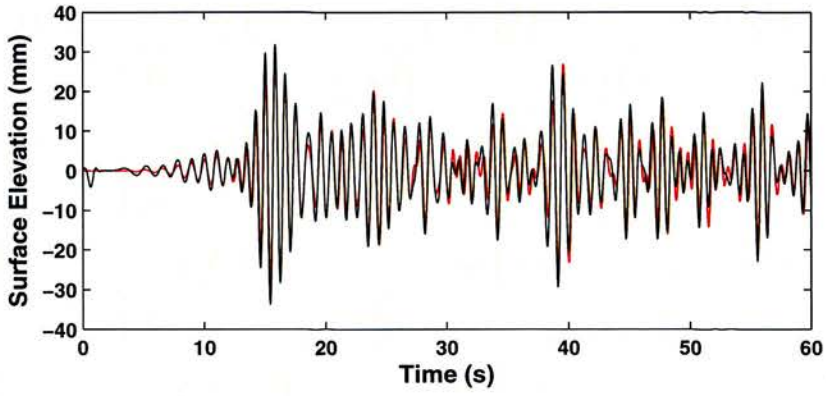

(c) Surface elevation time series. Wire resistance wave gauge and Sensor, Test 3

Figure 5.27. Irregular wave tests - wave elevation versus time. "BF" Processed. Solid red line is sensor, solid black line is wave gauge.

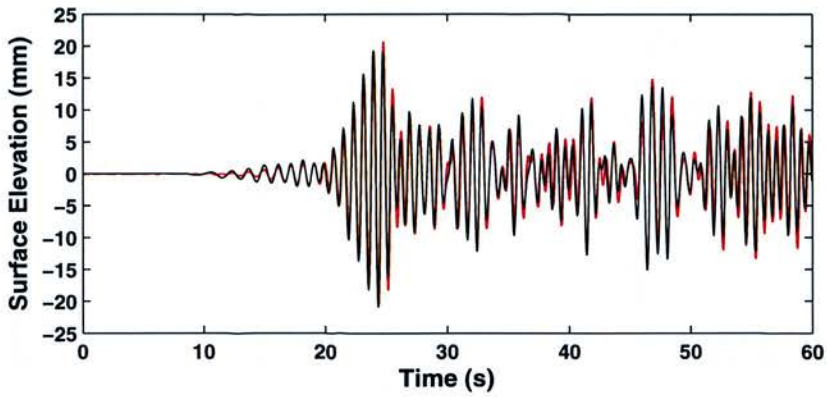

(a) Surface elevation time series. Wire resistance wave gauge and Sensor, Test 4

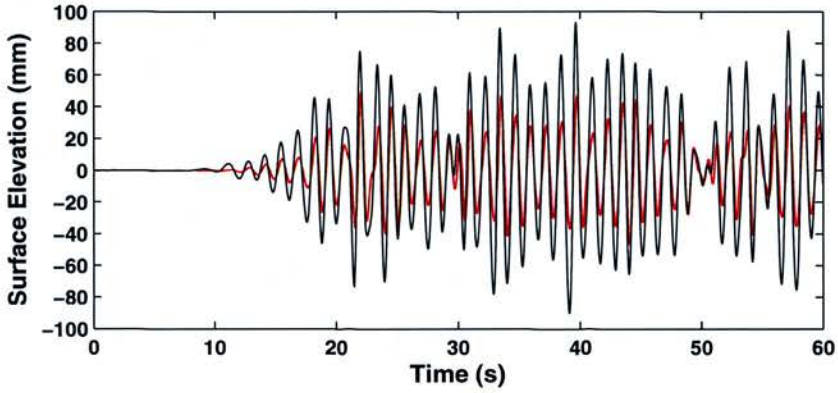

(b) Surface elevation time series. Wire resistance wave gauge and Sensor, Test 5

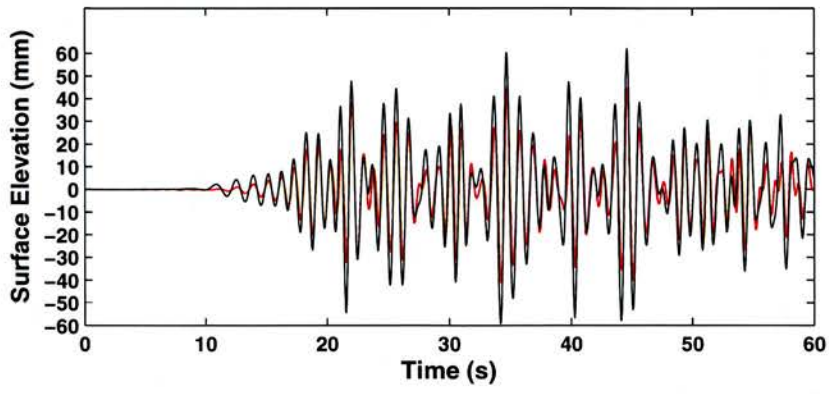

(c) Surface elevation time series. Wire resistance wave gauge and Sensor, Test 6

Figure 5.28. Irregular wave tests - wave elevation versus time. "BF" Processed. Solid red line is sensor, solid black line is wave gauge.

Processing Technique 2 - AMF

Figures 5.29 to 5.34 show wave heights and wave periods reported from time series analysis of data reported by wire resistance wave gauges and the sensor in closest proximity to each wave gauge. Irregular tests 1 to 6 are plotted. Varying degrees of correlation can be seen across the tests. However, compared to the "BF" method variation across the sensors within each test has reduced along with sensor bias.

Figures 5.35 and 5.36 show time series of surface elevation for a centrally located sensor segment and its corresponding neighbouring wave gauge for irregular wave tests one to six processed under the AMF technique.

Table 5.7. Irregular wave tests - time domain processed using arbitrary magnitude (AM) filtering. Number of waves in processed samples.

Test	Number of waves AMF processed			% Waves excluded during each processing stage		
	Wave gauge	Matched	In range	Matched	In range	Total
1	379	354	347	6.6	2.0	8.4
2	462	429	426	7.1	0.7	7.8
3	502	477	465	5.0	2.5	7.4
4	582	554	534	4.8	3.6	8.2
5	200	191	186	4.5	2.6	7.0
6	456	426	424	6.6	0.5	7.0

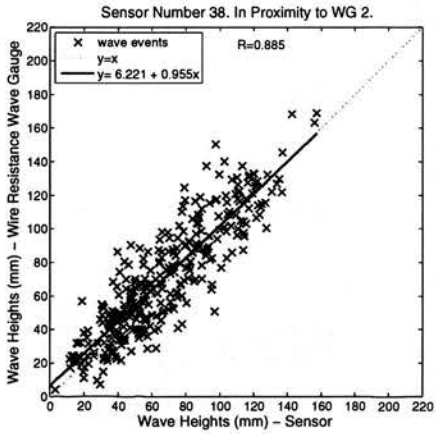

(a) Sensor vs WG no.2. Wave heights

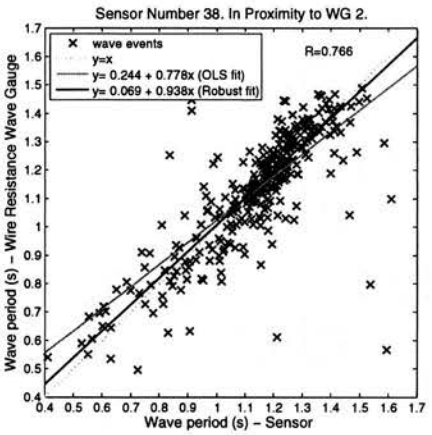

(b) Sensor vs WG no.2. Wave periods

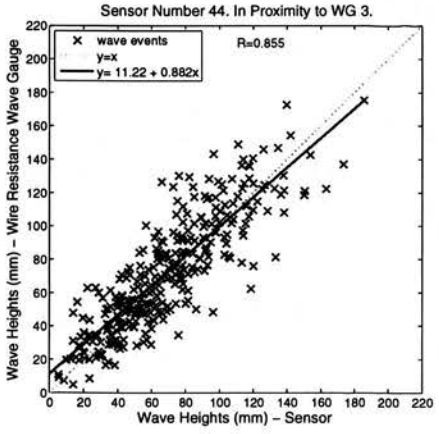

(c) Sensor vs WG no.3. Wave heights

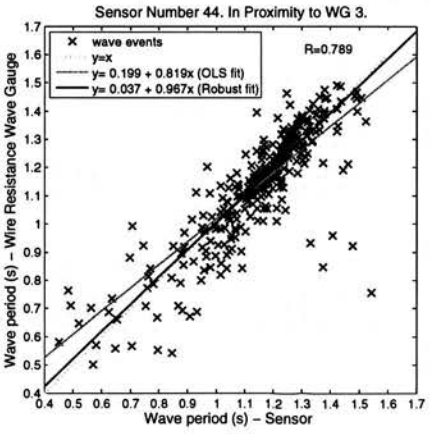

(d) sensor vs WG no.3. Wave periods

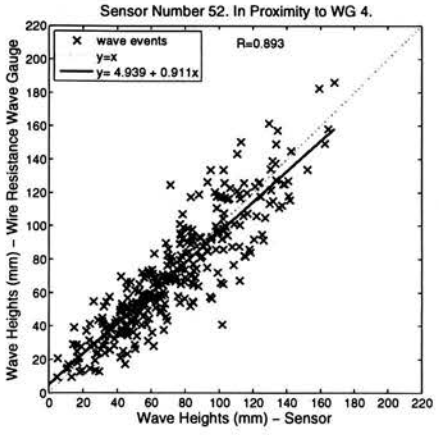

(e) Sensor vs WG no.4. Wave heights

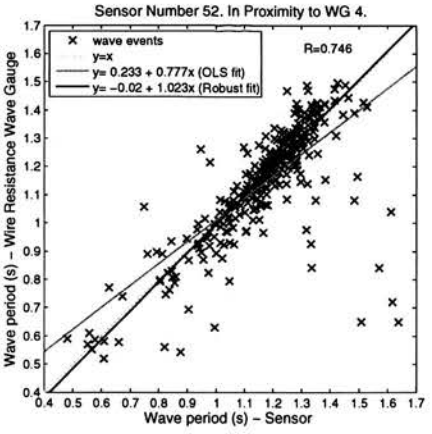

(f) Sensor vs WG no.4. Wave periods

Figure 5.29. Test 1 - Wave-by-wave matching. Heights and periods. Processing: "AMF" implemented.

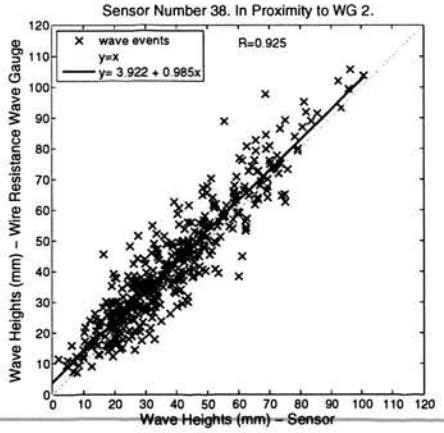

(a) Sensor vs WG no.2. Wave heights

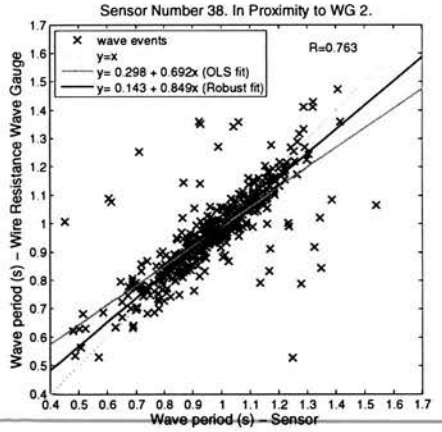

(b) Sensor vs WG no.2. Wave periods

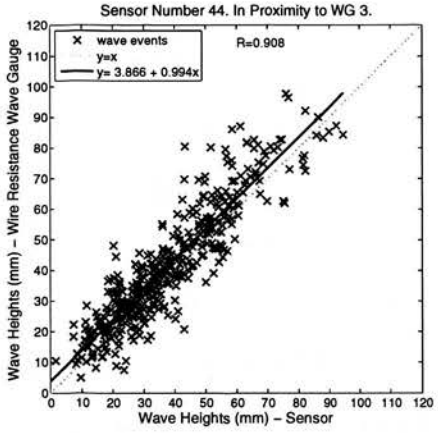

(c) Sensor vs WG no.3. Wave heights

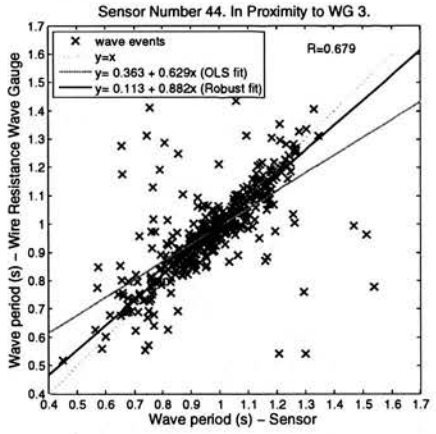

(d) Sensor vs WG no.3. Wave periods

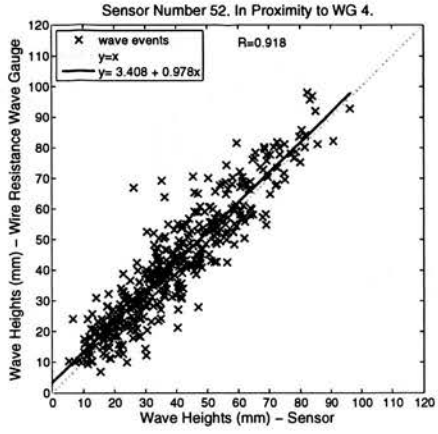

(e) Sensor vs WG no.4. Wave heights

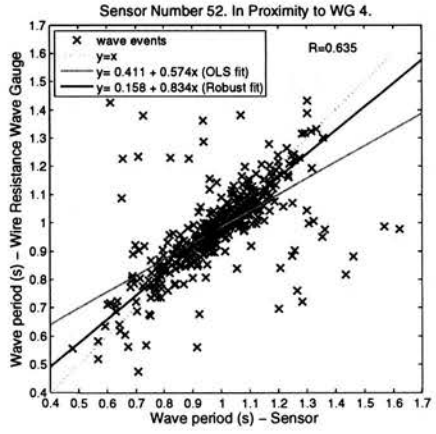

(f) Sensor vs WG no.4. Wave periods

Figure 5.30. Test 2 - Wave-by-wave matching. Heights and periods. Processing: "AMF" implemented.

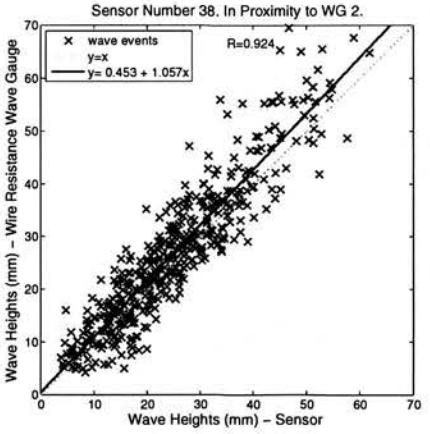

(a) Sensor vs WG no.2. Wave heights

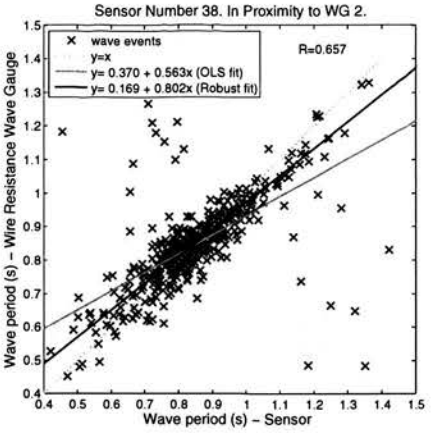

(b) Sensor vs WG no.2. Wave periods

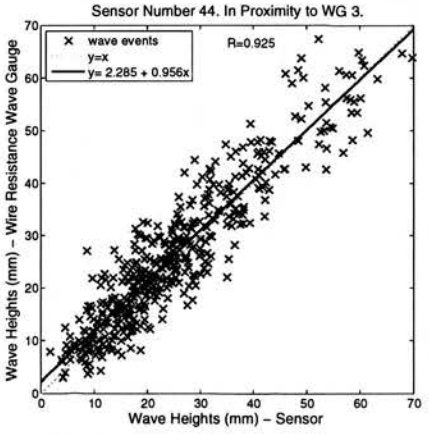

(c) Sensor vs WG no.3. Wave heights

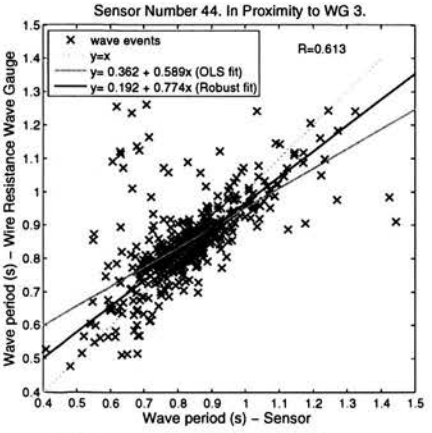

(d) Sensor vs WG no.3. Wave periods

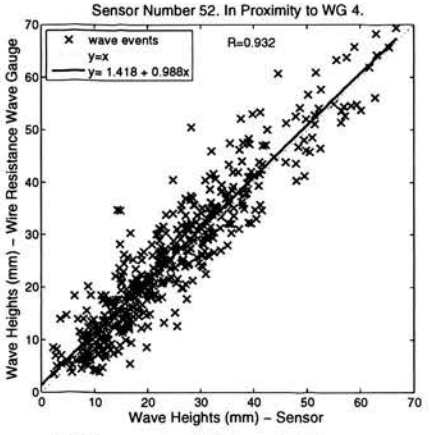

(e) Sensor vs WG no.4. Wave heights

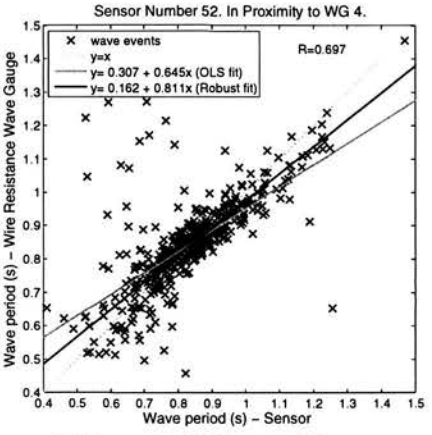

(f) Sensor vs WG no.4. Wave periods

Figure 5.31. Test 3 - Wave-by-wave matching. Heights and periods. Processing: "AMF" implemented.

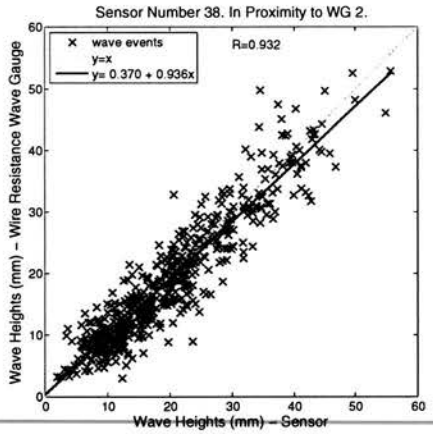

(a) Sensor vs WG no.2. Wave heights

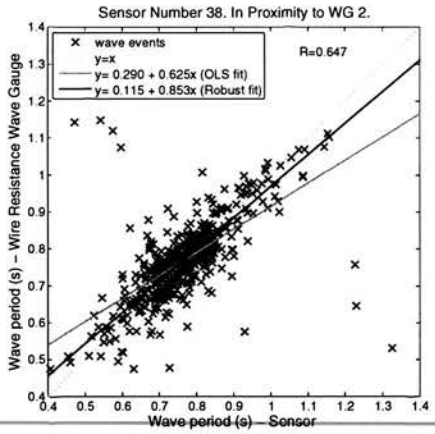

(b) Sensor vs WG no.2. Wave periods

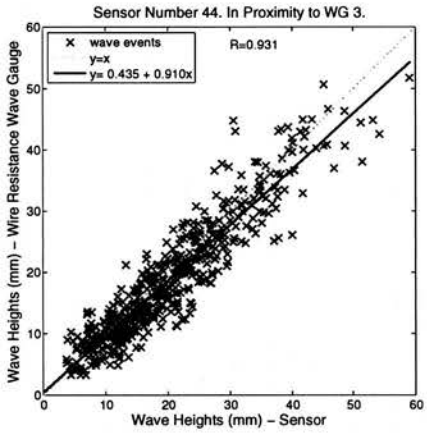

(c) Sensor vs WG no.3. Wave heights

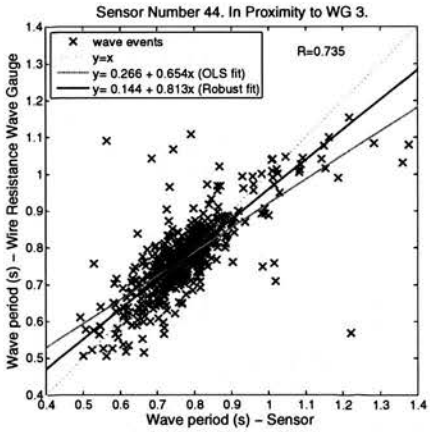

(d) sensor vs WG no.3. Wave periods

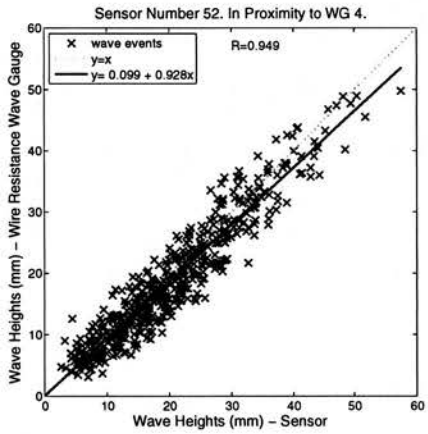

(e) Sensor vs WG no.4. Wave heights

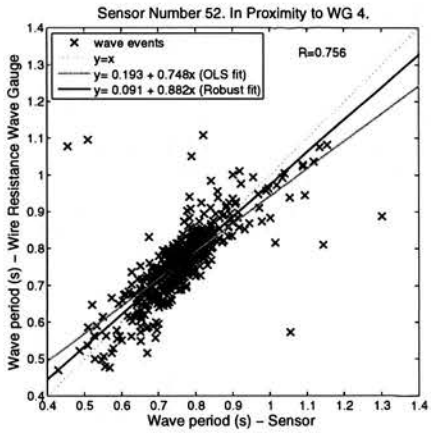

(f) Sensor vs WG no.4. Wave periods

Figure 5.32. Test 4 - Wave-by-wave matching. Heights and periods. Processing: "AMF" implemented.

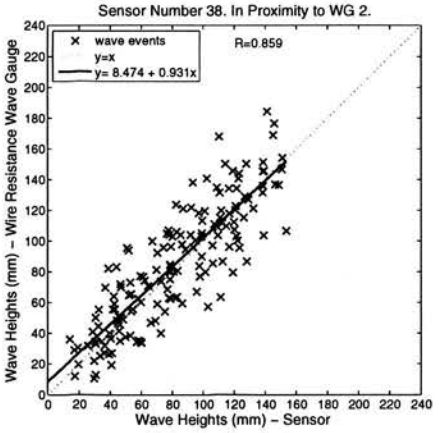

(a) Sensor vs WG no.2. Wave heights

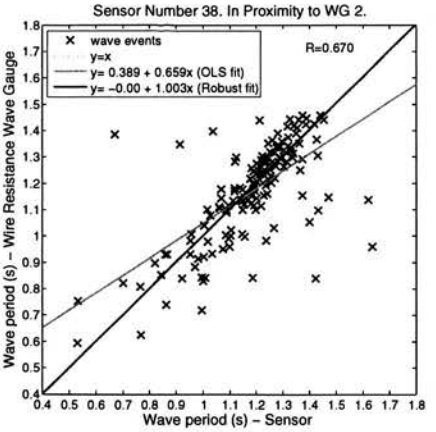

(b) Sensor vs WG no.2. Wave periods

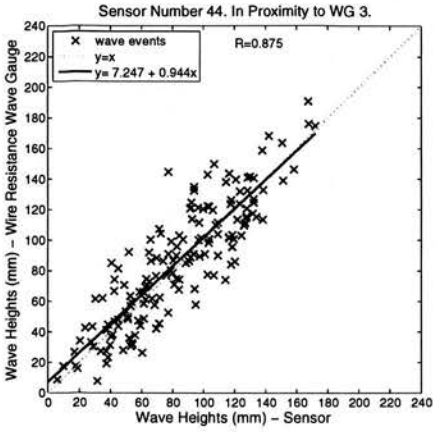

(c) Sensor vs WG no.3. Wave heights

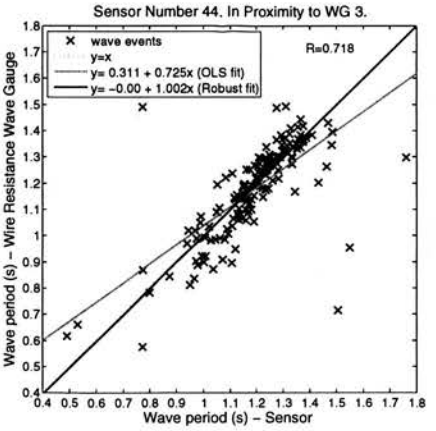

(d) Sensor vs WG no.3. Wave periods

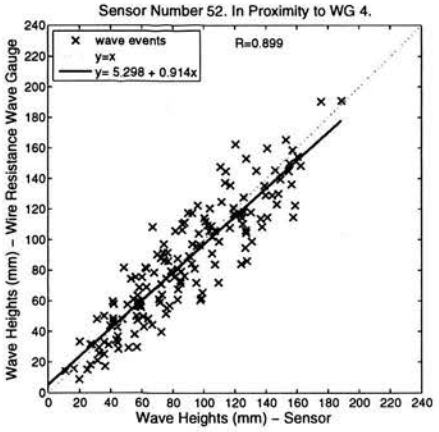

(e) Sensor vs WG no.4. Wave heights

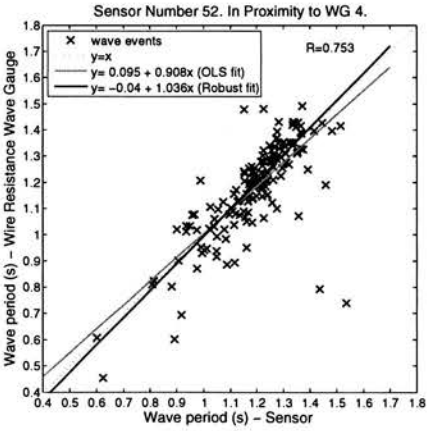

(f) Sensor vs WG no.4. Wave periods

Figure 5.33. Test 5 - Wave-by-wave matching. Heights and periods. Processing: "AMF" implemented.

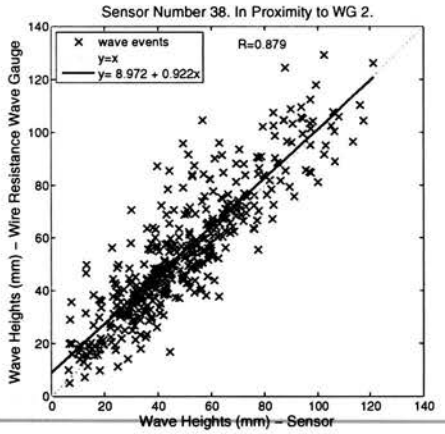

(a) Sensor vs WG no.2. Wave heights

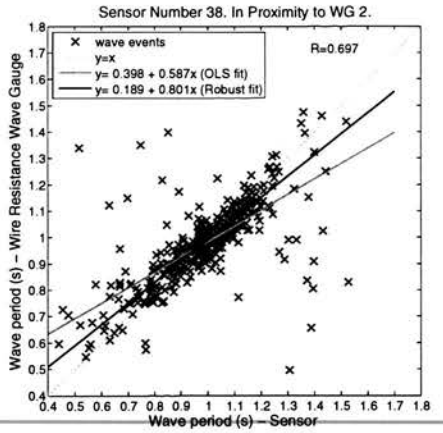

(b) Sensor vs WG no.2. Wave periods

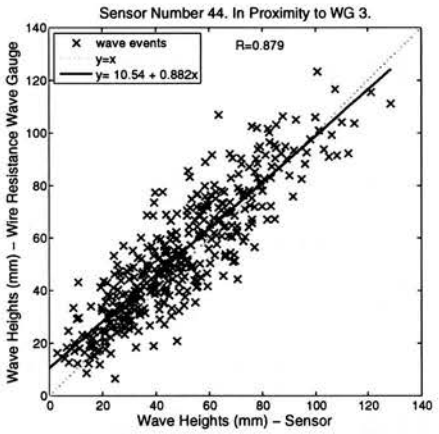

(c) Sensor vs WG no.3. Wave heights

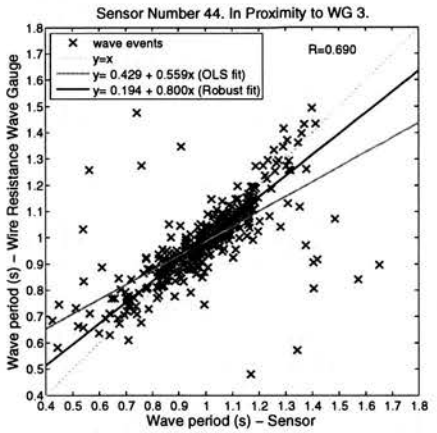

(d) Sensor vs WG no.3. Wave periods

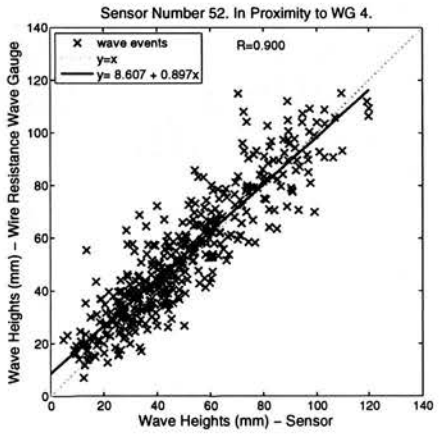

(e) Sensor vs WG no.4. Wave heights

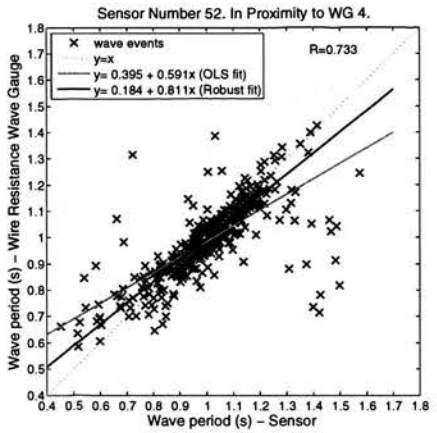

(f) Sensor vs WG no.4. Wave periods

Figure 5.34. Test 6 - Wave-by-wave matching. Heights and periods. Processing: "AMF" implemented.

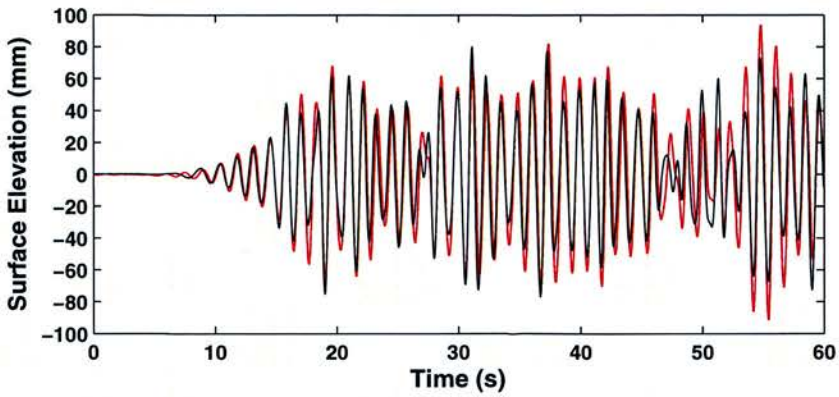

(a) Surface elevation time series. Wire resistance wave gauge and Sensor, Test 1

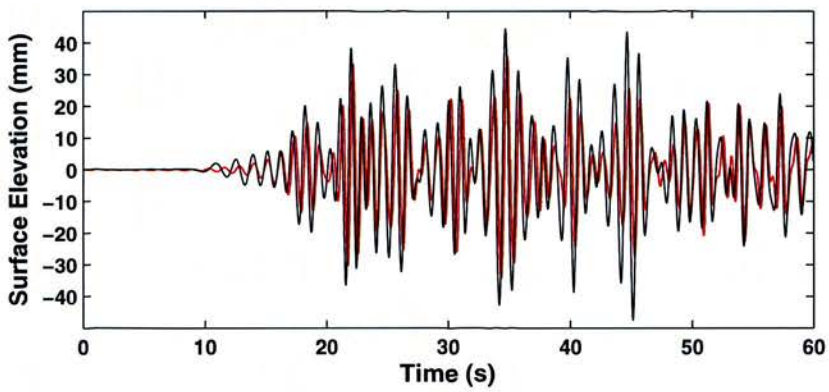

(b) Surface elevation time series. Wire resistance wave gauge and Sensor, Test 2

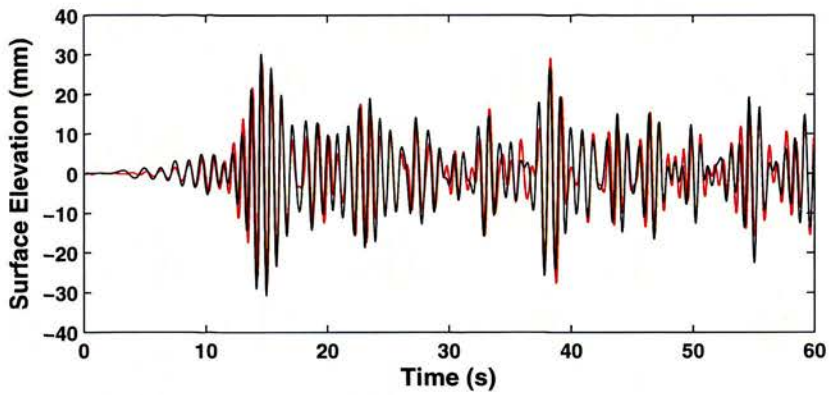

(c) Surface elevation time series. Wire resistance wave gauge and Sensor, Test 3

Figure 5.35. Irregular wave tests - wave elevation versus time. AMF Processed

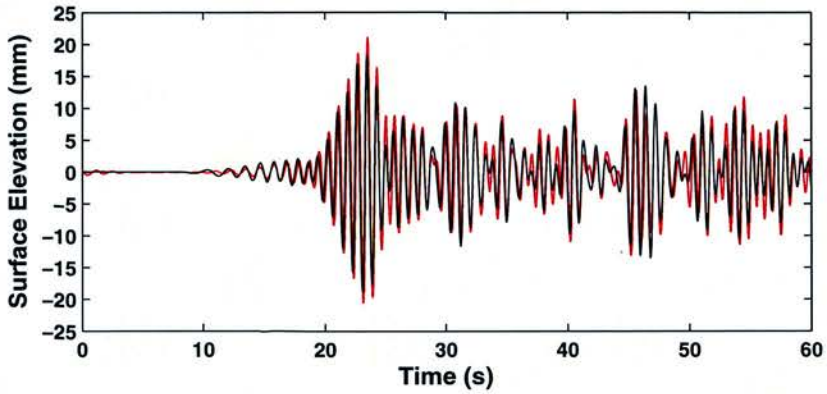

(a) Surface elevation time series. Wire resistance wave gauge and Sensor, Test 4

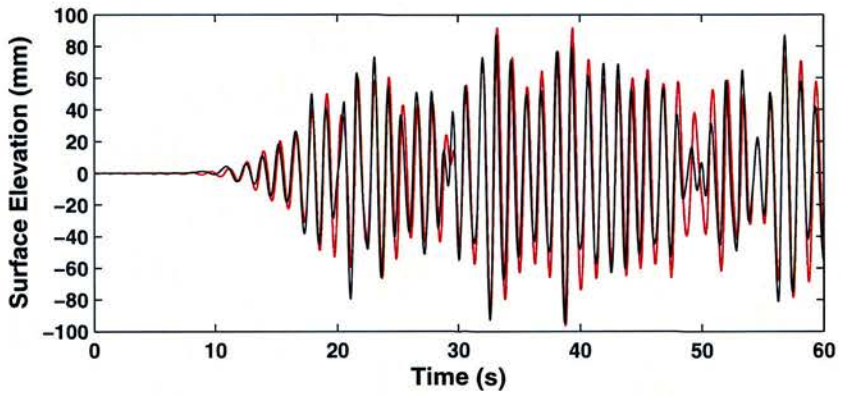

(b) Surface elevation time series. Wire resistance wave gauge and Sensor, Test 5

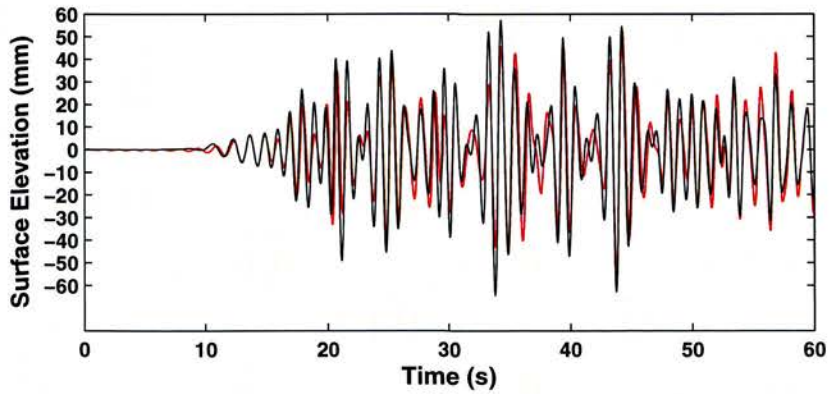

(c) Surface elevation time series. Wire resistance wave gauge and Sensor, Test 6

Figure 5.36. Irregular wave tests - wave elevation versus time. AMF Processed

Processing Technique 3 - RT1

Figures 5.37 to 5.42 show wave heights and wave periods reported from time series analysis of data reported by wire resistance wave gauges and the sensor in closest proximity to each wave gauge. Irregular tests 1 to 6 are plotted. Varying degrees of correlation can be seen across the tests. However, compared to the "BF" method variation across the sensors within each test has reduced along with sensor bias. Correlation in wave height and wave period is highest for the most downstream sensor. Whilst visually correlation in wave period has improved over the previous methods the presence of multiple potential "outliers" significantly reduces the correlation values.

Figures 5.43 and 5.44 show time series of surface elevation for a centrally located sensor segment and its corresponding neighbouring wave gauge for irregular wave tests one to six processed under the RT1 technique.

Table 5.8. Irregular wave tests - time domain processed using the RT1 procedure. Number of waves in processed samples.

Test	Number of waves RT1 processed			% Waves excluded during each processing stage		
	Wave gauge	Matched	In range	Matched	In range	Total
1	383	342	334	10.7	2.3	12.8
2	436	393	388	9.9	1.3	11.0
3	504	480	469	4.8	2.3	6.9
4	543	502	481	7.6	4.2	11.4
5	207	189	185	8.7	2.1	10.6
6	431	400	396	7.2	1.0	8.1

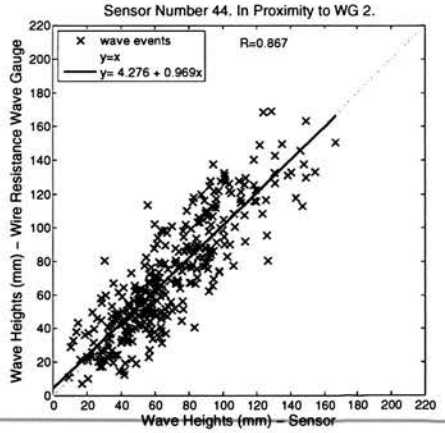

(a) Sensor vs WG no.2. Wave heights

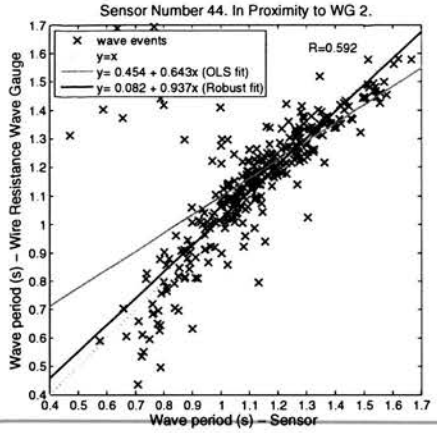

(b) Sensor vs WG no.2. Wave periods

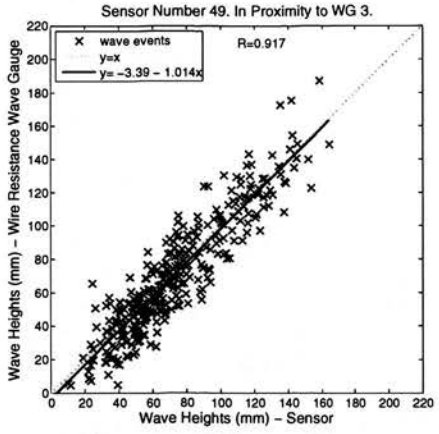

(c) Sensor vs WG no.3. Wave heights

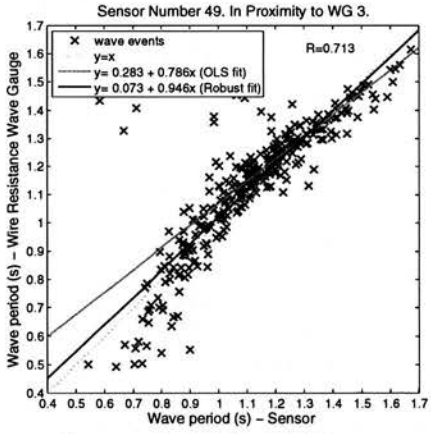

(d) sensor vs WG no.3. Wave periods

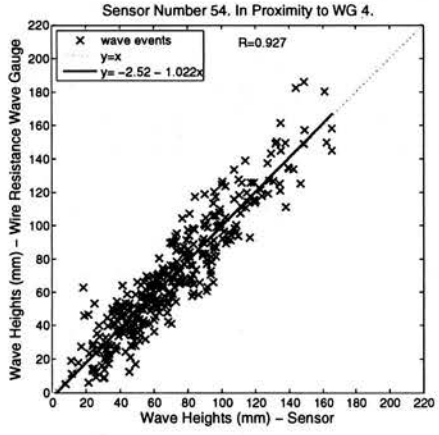

(e) Sensor vs WG no.4. Wave heights

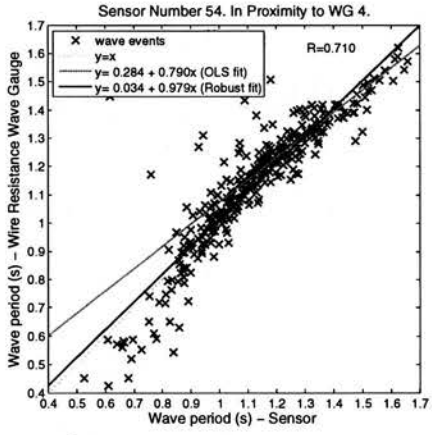

(f) Sensor vs WG no.4. Wave periods

Figure 5.37. Test 1 - Wave-by-wave matching. Heights and periods. Processing: "RT1" implemented.

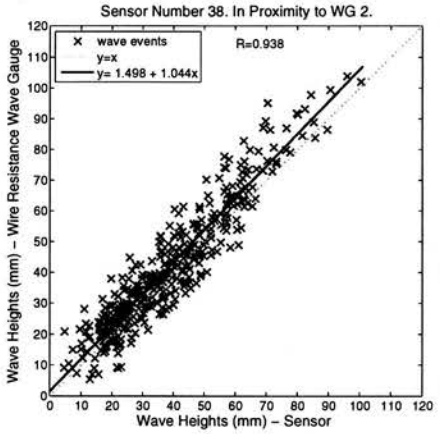

(a) Sensor vs WG no.2. Wave heights

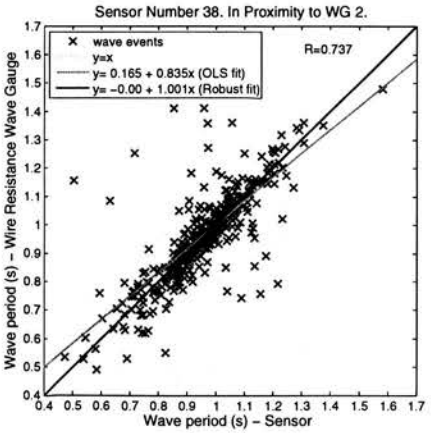

(b) Sensor vs WG no.2. Wave periods

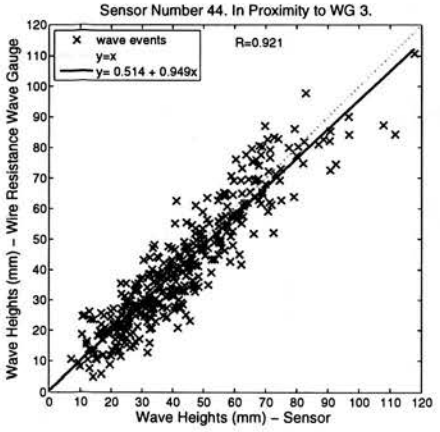

(c) Sensor vs WG no.3. Wave heights

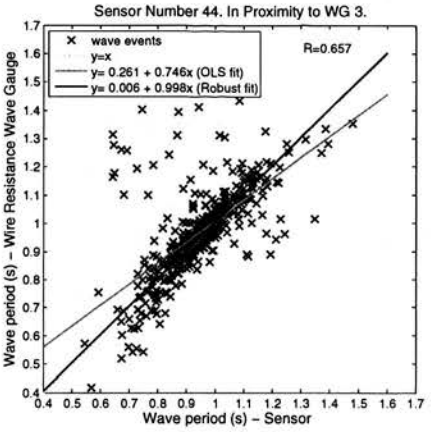

(d) Sensor vs WG no.3. Wave periods

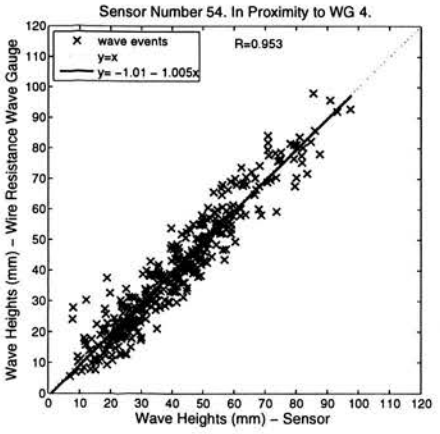

(e) Sensor vs WG no.4. Wave heights

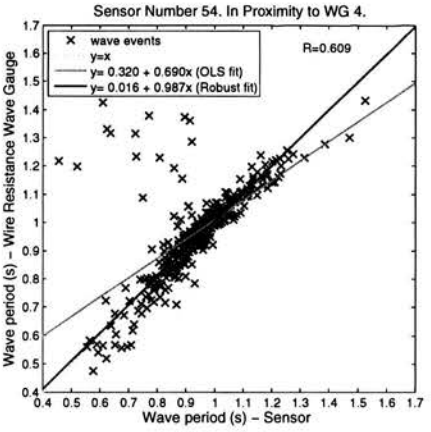

(f) Sensor vs WG no.4. Wave periods

Figure 5.38. Test 2 - Wave-by-wave matching. Heights and periods. Processing: "RT1" implemented.

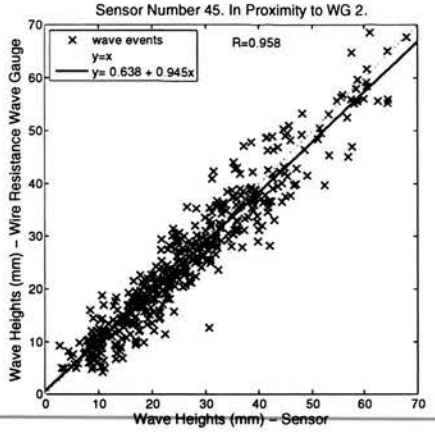

(a) Sensor vs WG no.2. Wave heights

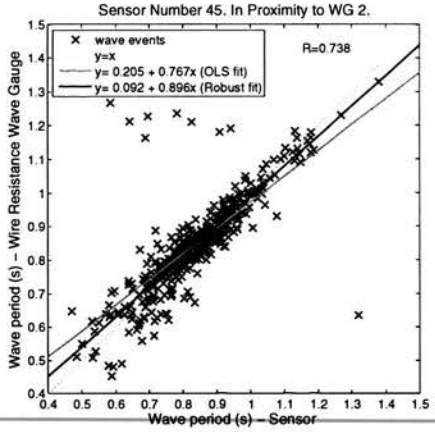

(b) Sensor vs WG no.2. Wave periods

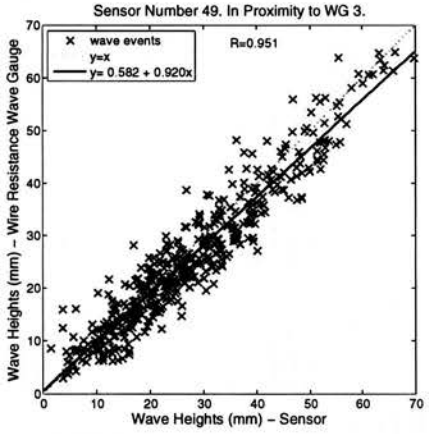

(c) Sensor vs WG no.3. Wave heights

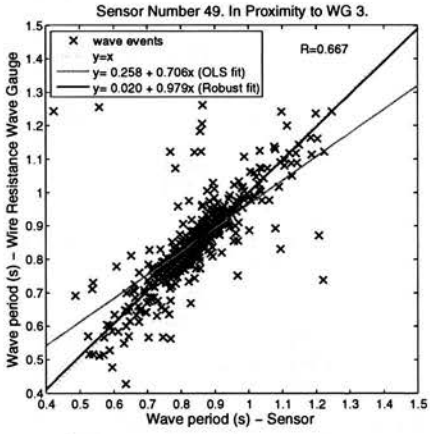

(d) Sensor vs WG no.3. Wave periods

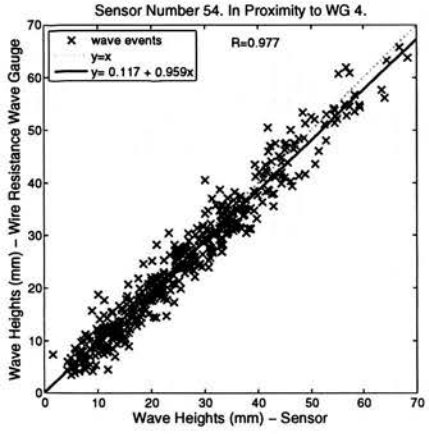

(e) Sensor vs WG no.4. Wave heights

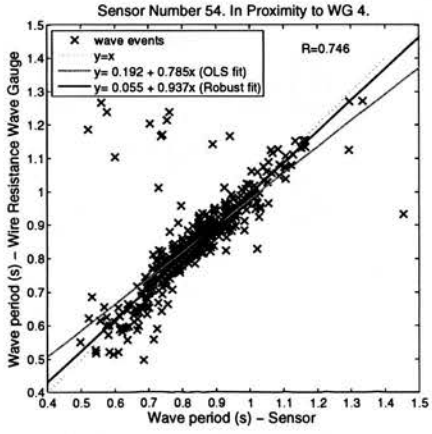

(f) Sensor vs WG no.4. Wave periods

Figure 5.39. Test 3 - Wave-by-wave matching. Heights and periods. Processing: "RT1" implemented.

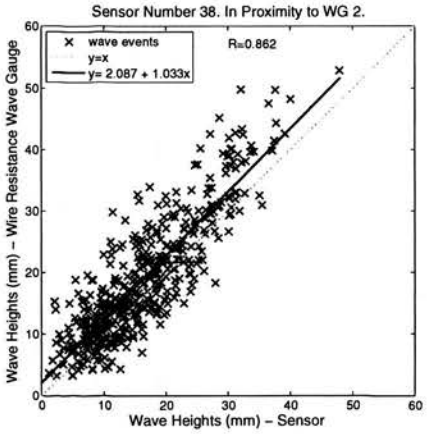

(a) Sensor vs WG no.2. Wave heights

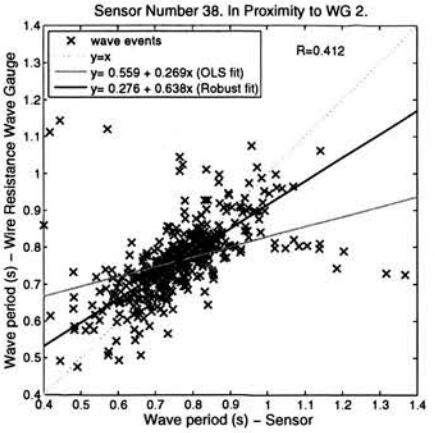

(b) Sensor vs WG no.2. Wave periods

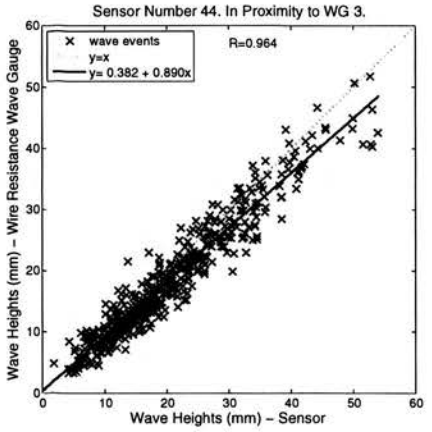

(c) Sensor vs WG no.3. Wave heights

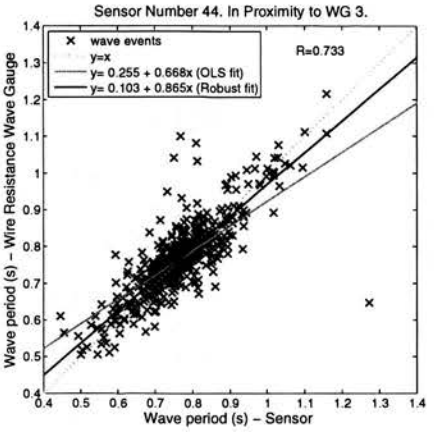

(d) sensor vs WG no.3. Wave periods

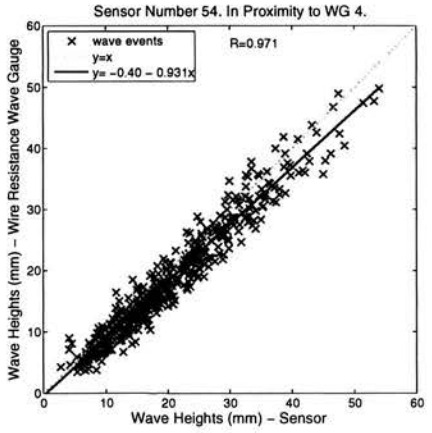

(e) Sensor vs WG no.4. Wave heights

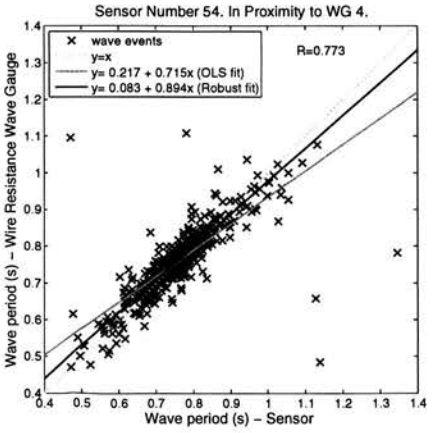

(f) Sensor vs WG no.4. Wave periods

Figure 5.40. Test 4 - Wave-by-wave matching. Heights and periods. Processing: "RT1" implemented.

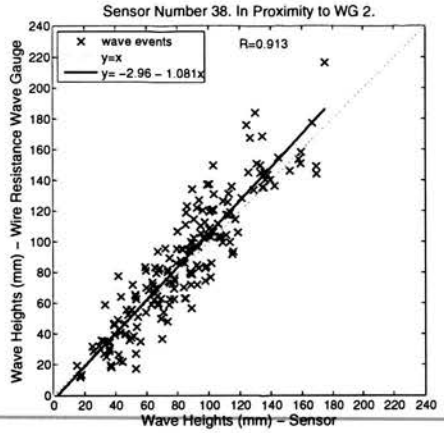

(a) Sensor vs WG no.2. Wave heights

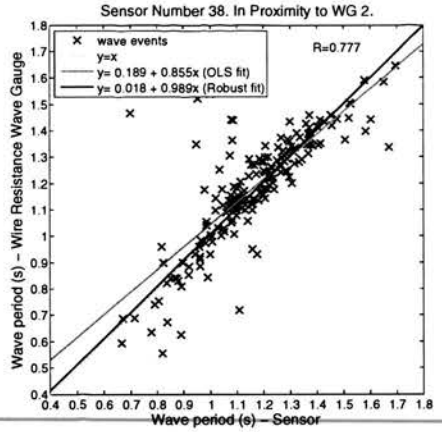

(b) Sensor vs WG no.2. Wave periods

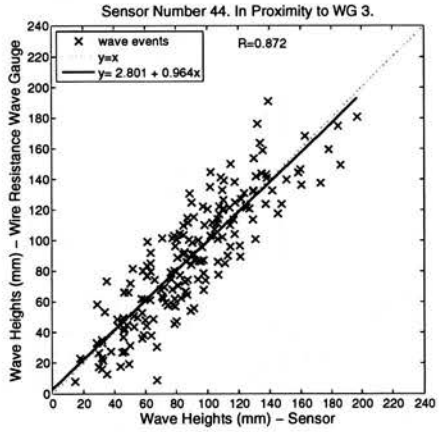

(c) Sensor vs WG no.3. Wave heights

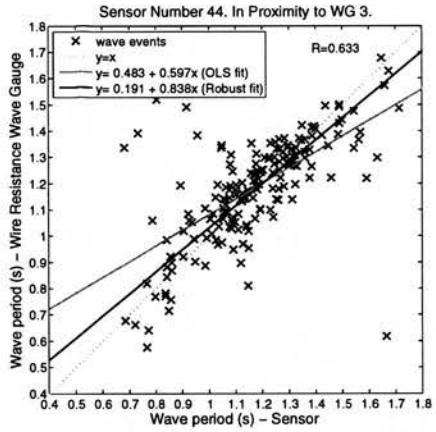

(d) Sensor vs WG no.3. Wave periods

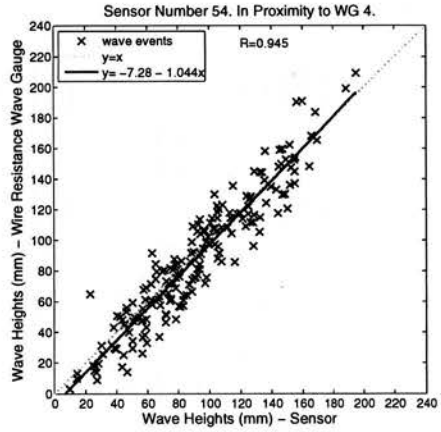

(e) Sensor vs WG no.4. Wave heights

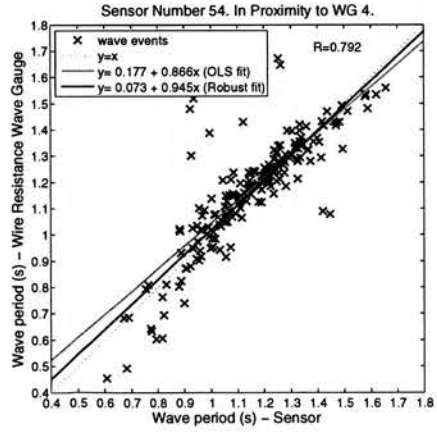

(f) Sensor vs WG no.4. Wave periods

Figure 5.41. Test 5 - Wave-by-wave matching. Heights and periods. Processing: "RT1" implemented.

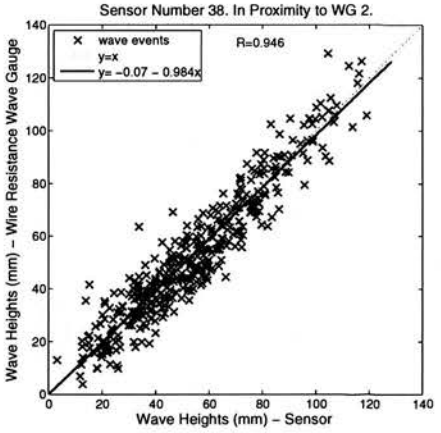

(a) Sensor vs WG no.2. Wave heights

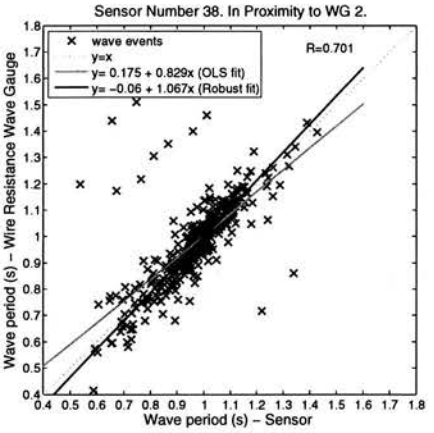

(b) Sensor vs WG no.2. Wave periods

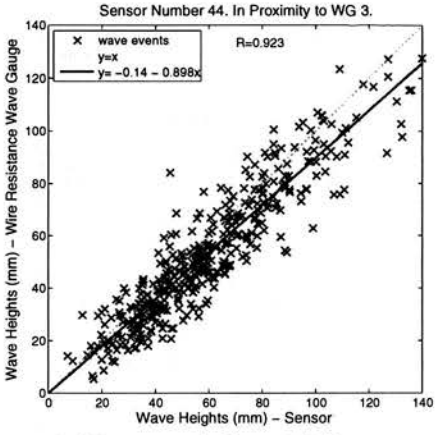

(c) Sensor vs WG no.3. Wave heights

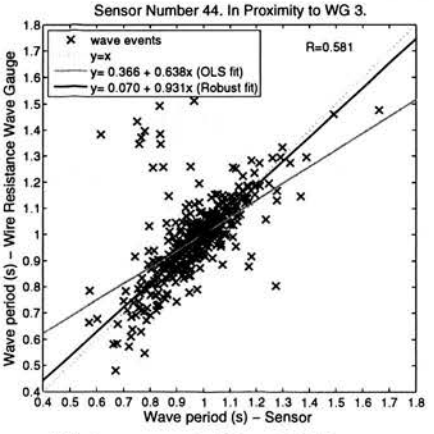

(d) Sensor vs WG no.3. Wave periods

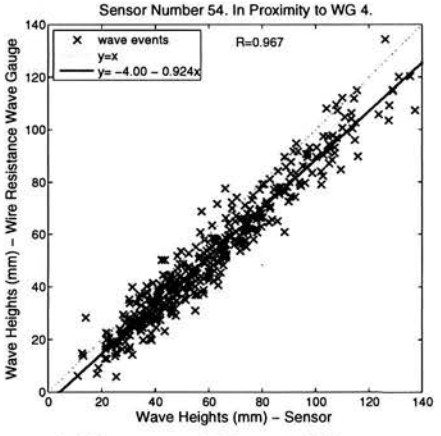

(e) Sensor vs WG no.4. Wave heights

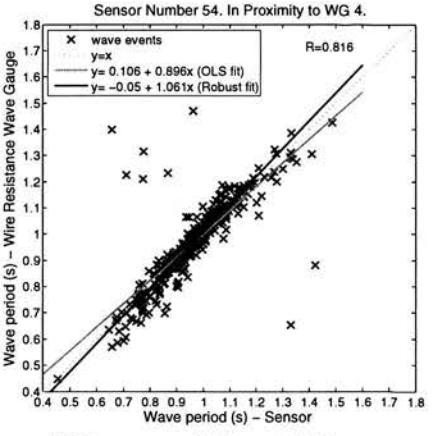

(f) Sensor vs WG no.4. Wave periods

Figure 5.42. Test 6 - Wave-by-wave matching. Heights and periods. Processing: "RT1" implemented.

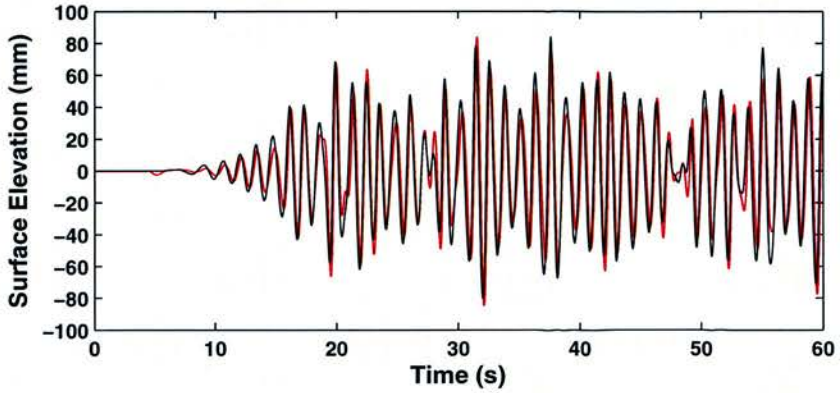

(a) Surface elevation time series. Wire resistance wave gauge and Sensor, Test 1

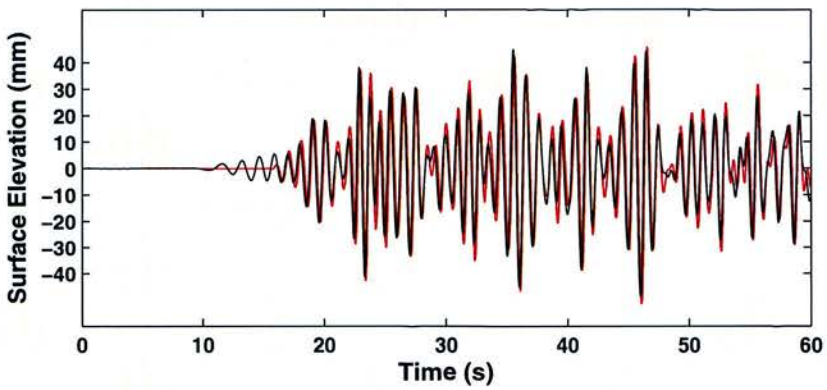

(b) Surface elevation time series. Wire resistance wave gauge and Sensor, Test 2

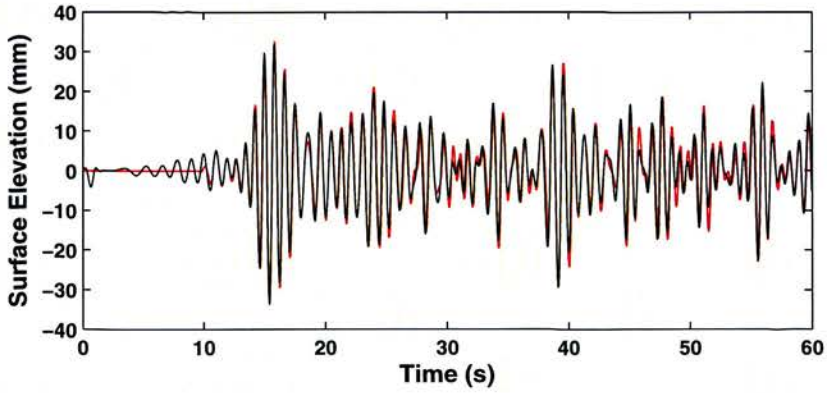

(c) Surface elevation time series. Wire resistance wave gauge and Sensor, Test 3

Figure 5.43. Irregular wave tests - wave elevation versus time. RT1 Processed

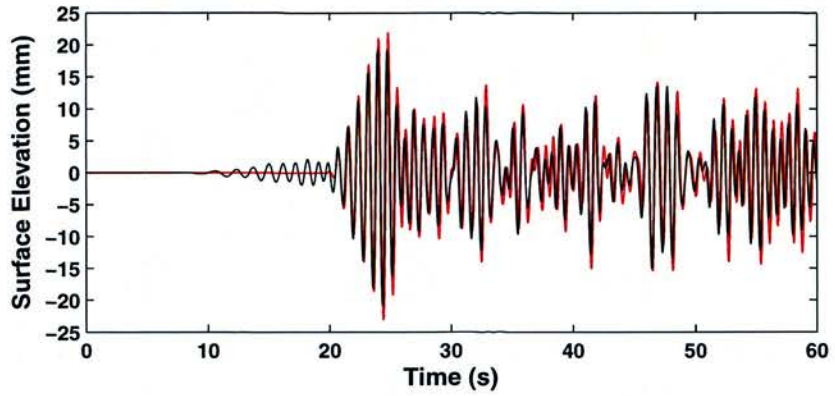

(a) Surface elevation time series. Wire resistance wave gauge and Sensor, Test 4

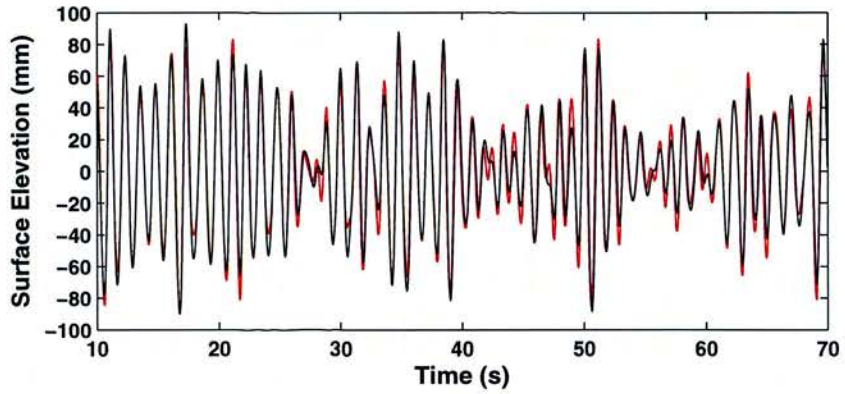

(b) Surface elevation time series. Wire resistance wave gauge and Sensor, Test 5

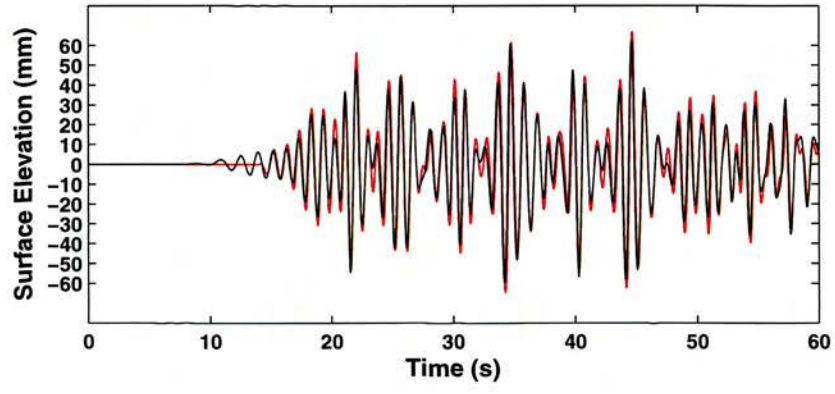

(c) Surface elevation time series. Wire resistance wave gauge and Sensor, Test 6

Figure 5.44. Irregular wave tests - wave elevation versus time. RT1 Processed

Processing Technique 4 - RT2

Figures 5.45 to 5.50 show wave heights and wave periods reported from time series analysis of data reported by wire resistance wave gauges and the sensor in closest proximity to each wave gauge. Irregular tests 1 to 6 are plotted. Varying degrees of correlation can be seen across the tests. However, compared to the "BF" method variation across the sensors within each test has reduced along with sensor bias. Correlation in wave height and wave period remains highest for the most downstream sensor but the variation has reduced from previous methods. Visually, wave period correlation has improved over the previous methods with a reduced number of potential "outliers". Sensitivity to the method of data fitting ("Ordinary Least Squares" compared to "Robust Fitting") is particularly evident in the wave period plots.

Figures 5.51 and 5.52 show time series of surface elevation for a centrally located sensor segment and its corresponding neighbouring wave gauge for irregular wave tests one to six processed under the RT2 technique.

Table 5.9. Irregular wave tests - time domain processed using the RT2 procedure. Number of waves in processed samples.

Test	Number of waves RT2 processed			% Waves excluded during each processing stage		
	Wave gauge	Matched	In range	Matched	In range	Total
1	391	346	336	11.5	2.9	14.1
2	447	405	397	9.4	2.0	11.2
3	542	495	483	8.7	2.4	10.9
4	584	542	537	7.2	0.9	8.0
5	200	188	182	6.0	3.2	9.0
6	437	401	396	8.2	1.2	9.4

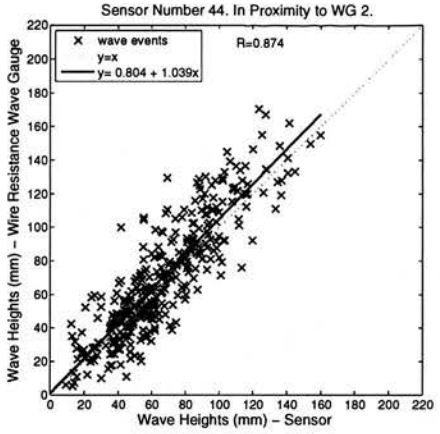

(a) Sensor vs WG no.2. Wave heights

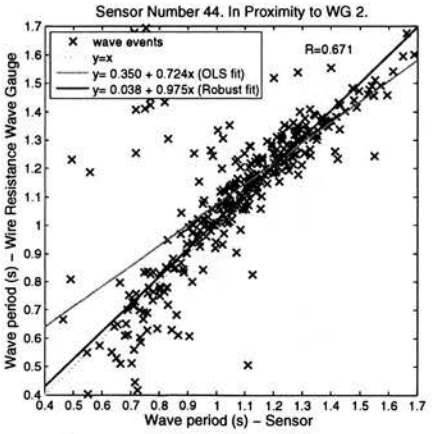

(b) Sensor vs WG no.2. Wave periods

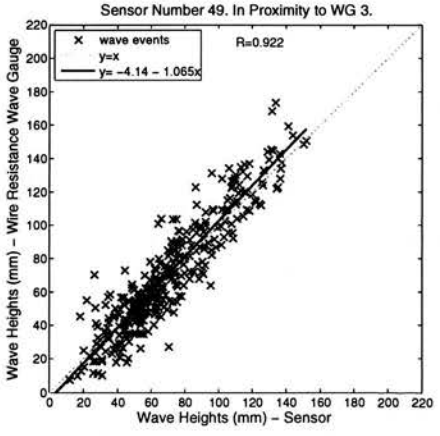

(c) Sensor vs WG no.3. Wave heights

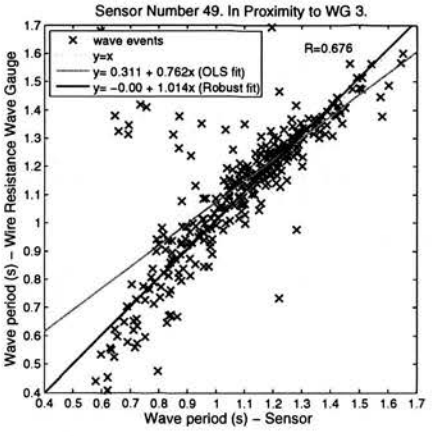

(d) sensor vs WG no.3. Wave periods

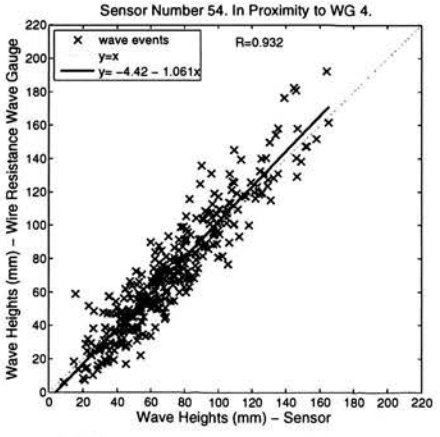

(e) Sensor vs WG no.4. Wave heights

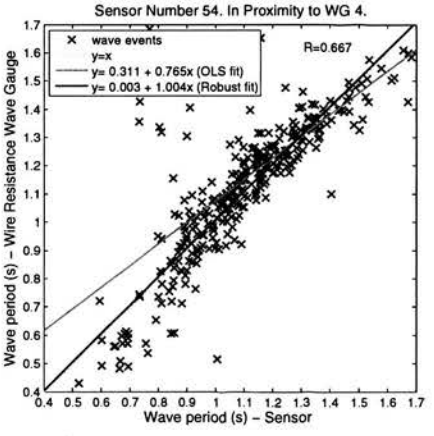

(f) Sensor vs WG no.4. Wave periods

Figure 5.45. Test 1 - Wave-by-wave matching. Heights and periods. Processing: "RT2" implemented.

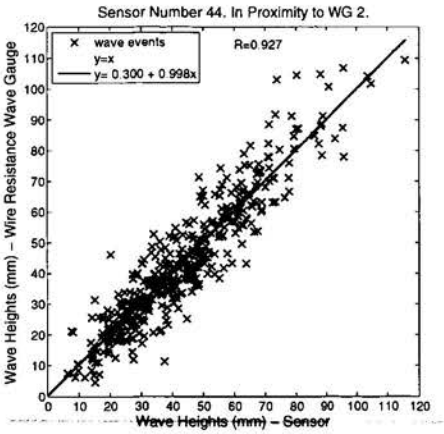

(a) Sensor vs WG no.2. Wave heights

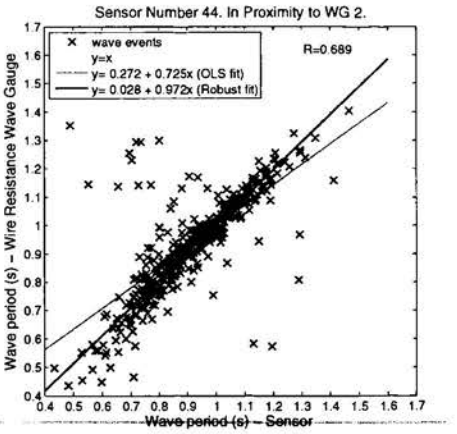

(b) Sensor vs WG no.2. Wave periods

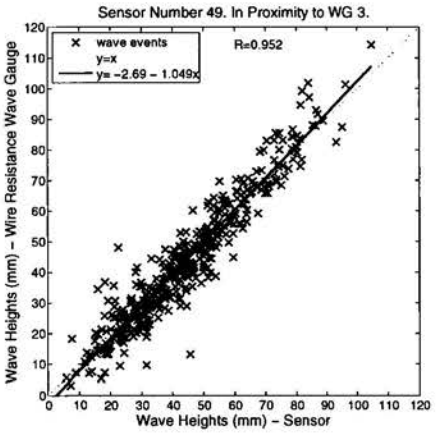

(c) Sensor vs WG no.3. Wave heights

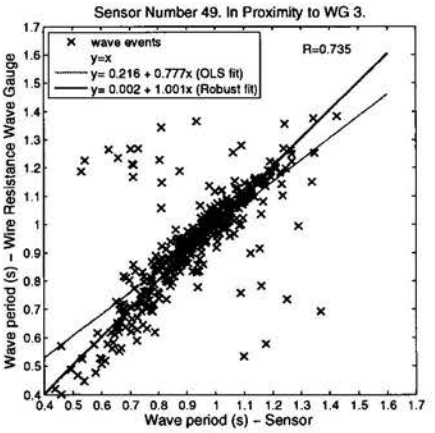

(d) Sensor vs WG no.3. Wave periods

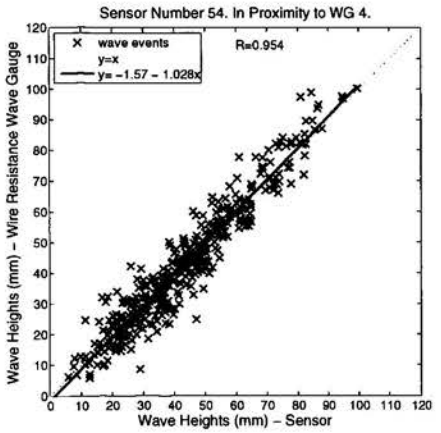

(e) Sensor vs WG no.4. Wave heights

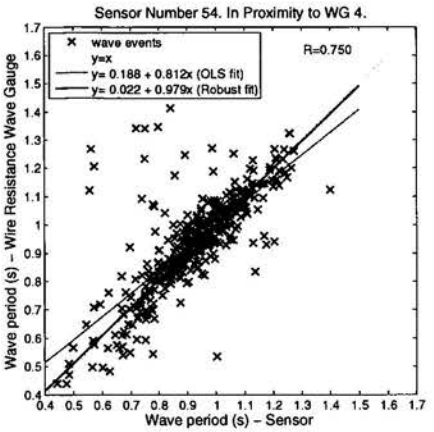

(f) Sensor vs WG no.4. Wave periods

Figure 5.46. Test 2 - Wave-by-wave matching. Heights and periods. Processing: "RT2" implemented.

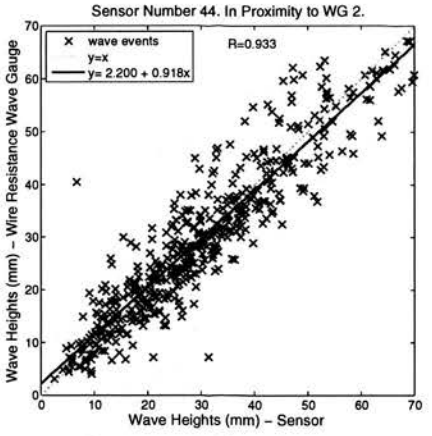

(a) Sensor vs WG no.2. Wave heights

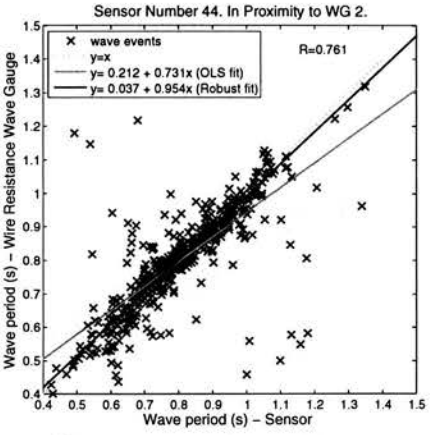

(b) Sensor vs WG no.2. Wave periods

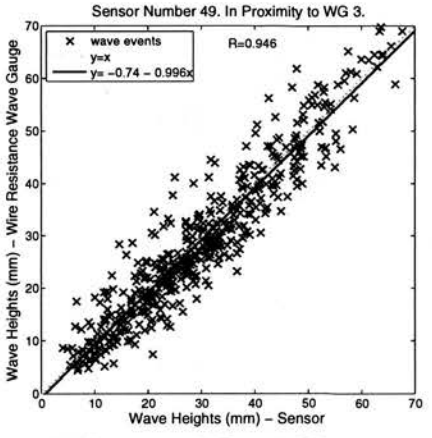

(c) Sensor vs WG no.3. Wave heights

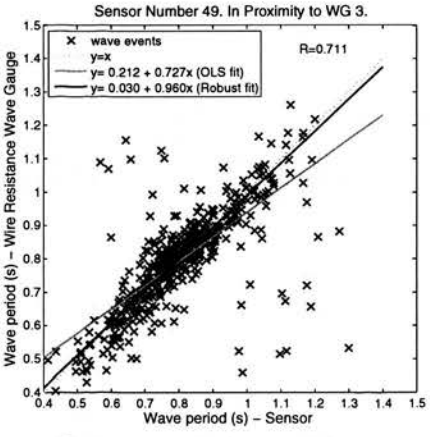

(d) Sensor vs WG no.3. Wave periods

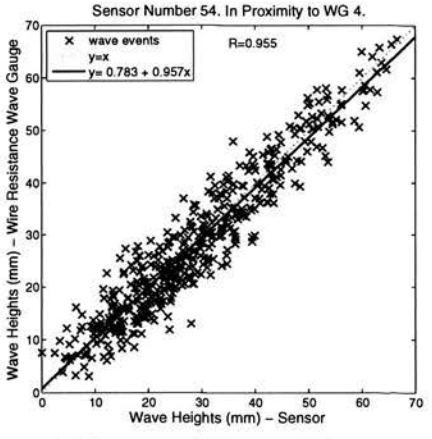

(e) Sensor vs WG no.4. Wave heights

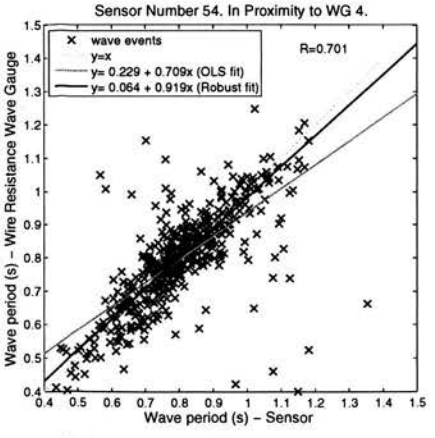

(f) Sensor vs WG no.4. Wave periods

Figure 5.47. Test 3 - Wave-by-wave matching. Heights and periods. Processing: "RT2" implemented.

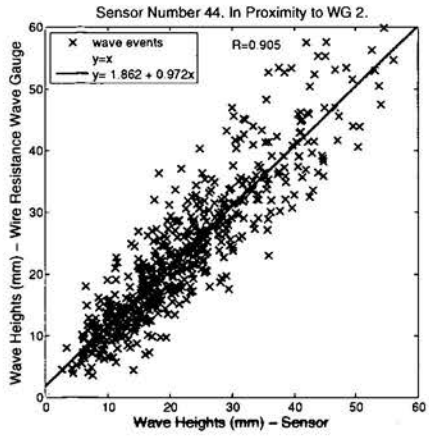

(a) Sensor vs WG no.2. Wave heights

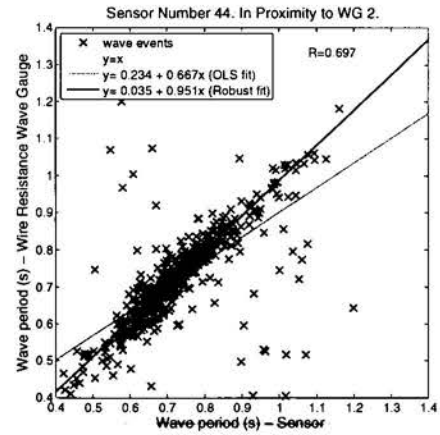

(b) Sensor vs WG no.2. Wave periods

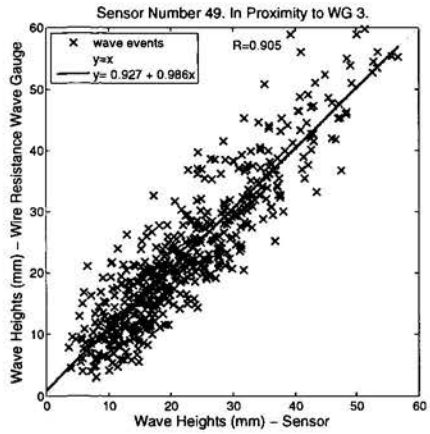

(c) Sensor vs WG no.3. Wave heights

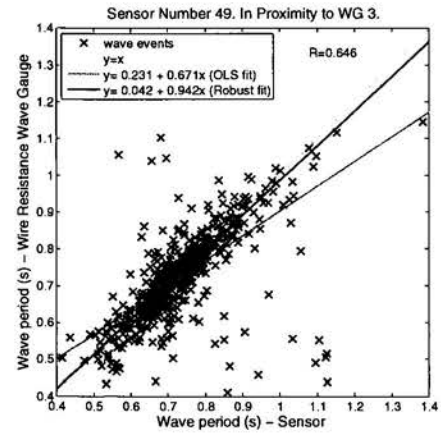

(d) sensor vs WG no.3. Wave periods

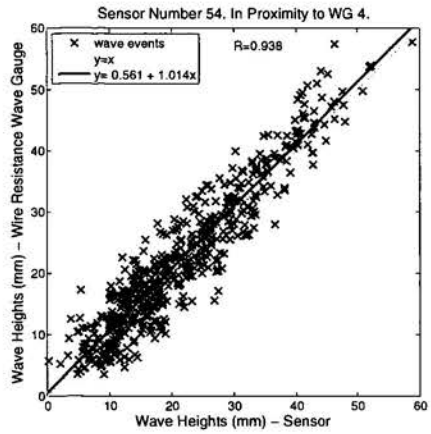

(e) Sensor vs WG no.4. Wave heights

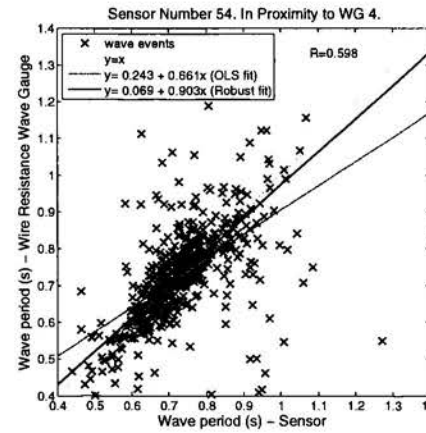

(f) Sensor vs WG no.4. Wave periods

Figure 5.48. Test 4 - Wave-by-wave matching. Heights and periods. Processing: "RT2" implemented.

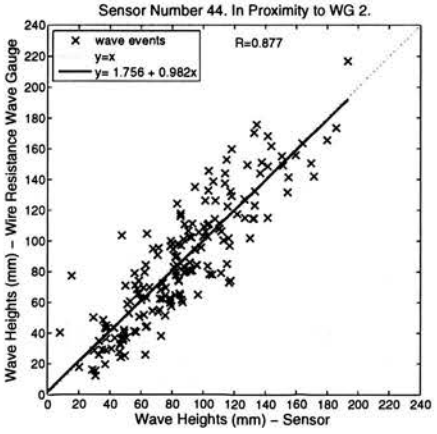

(a) Sensor vs WG no.2. Wave heights

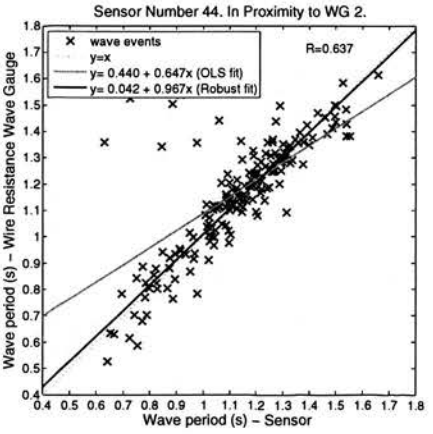

(b) Sensor vs WG no.2. Wave periods

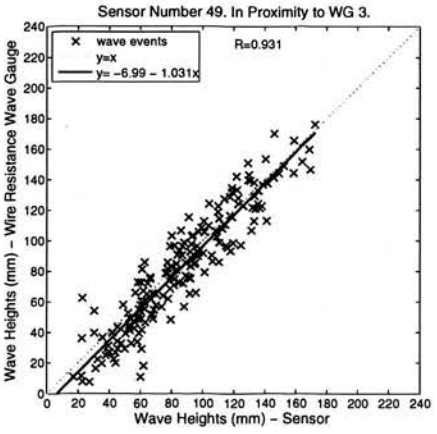

(c) Sensor vs WG no.3. Wave heights

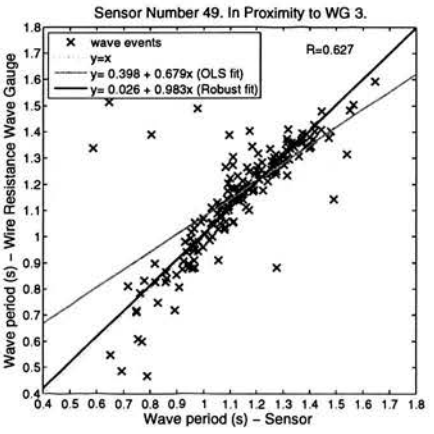

(d) Sensor vs WG no.3. Wave periods

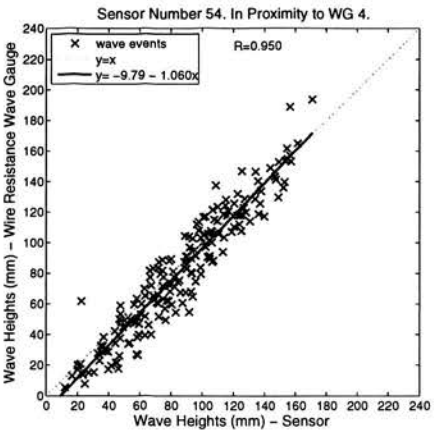

(e) Sensor vs WG no.4. Wave heights

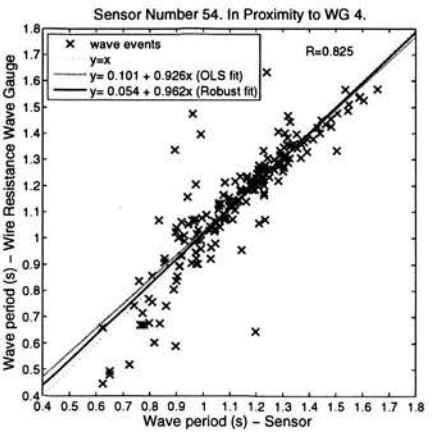

(f) Sensor vs WG no.4. Wave periods

Figure 5.49. Test 5 - Wave-by-wave matching. Heights and periods. Processing: "RT2" implemented.

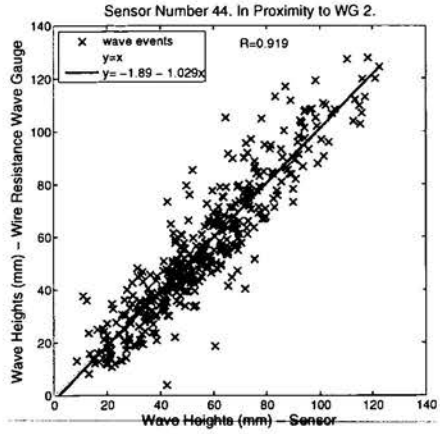

(a) Sensor vs WG no.2. Wave heights

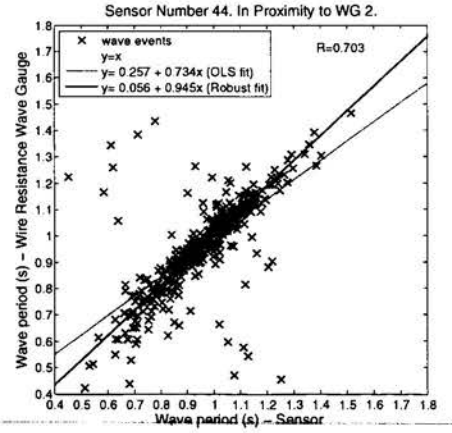

(b) Sensor vs WG no.2. Wave periods

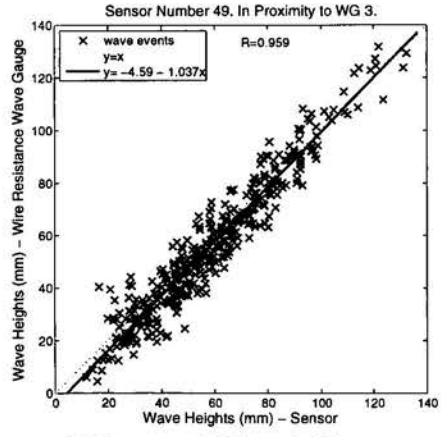

(c) Sensor vs WG no.3. Wave heights

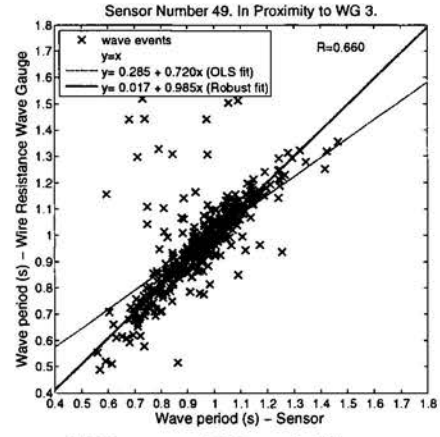

(d) Sensor vs WG no.3. Wave periods

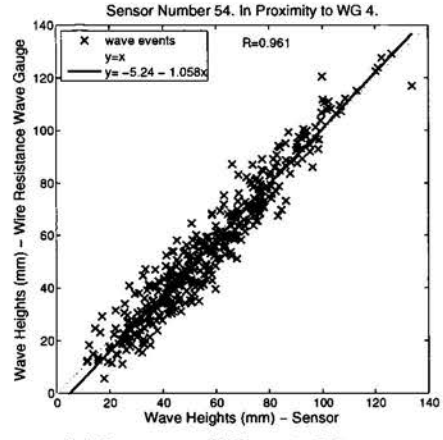

(e) Sensor vs WG no.4. Wave heights

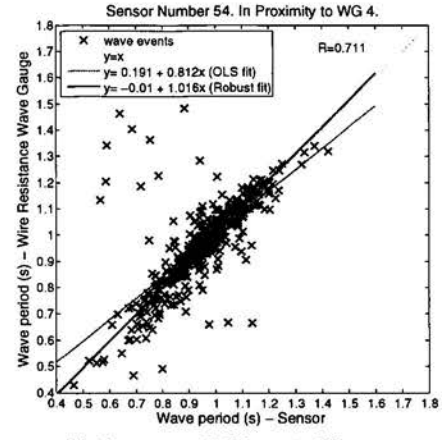

(f) Sensor vs WG no.4. Wave periods

Figure 5.50. Test 6 - Wave-by-wave matching. Heights and periods. Processing: "RT2" implemented.

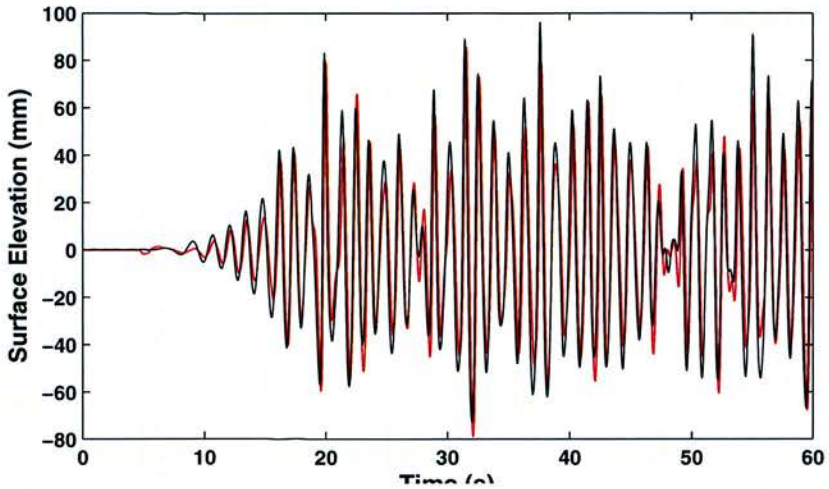

(a) Surface elevation time series. Wire resistance wave gauge and Sensor, Test 1

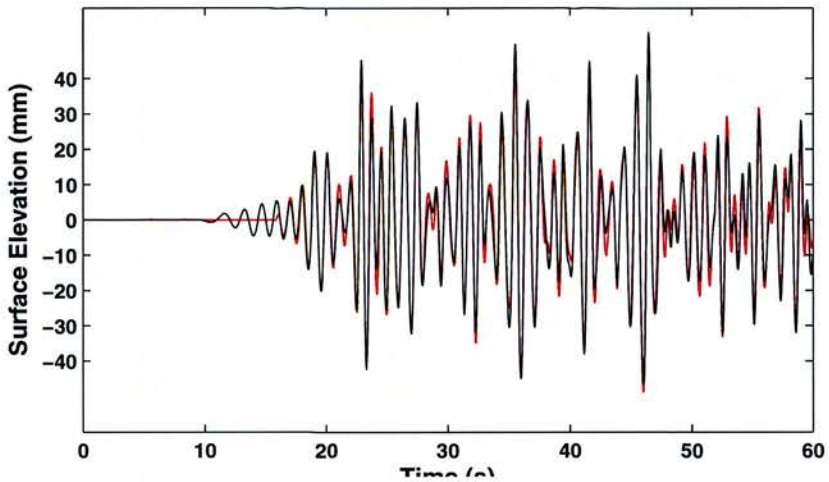

(b) Surface elevation time series. Wire resistance wave gauge and Sensor, Test 2

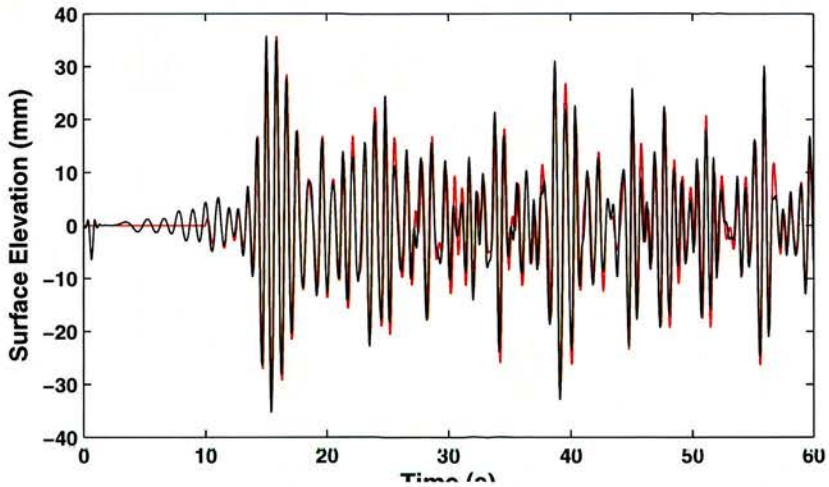

(c) Surface elevation time series. Wire resistance wave gauge and Sensor, Test 3

Figure 5.51. Irregular wave tests - wave elevation versus time. RT2 Processed

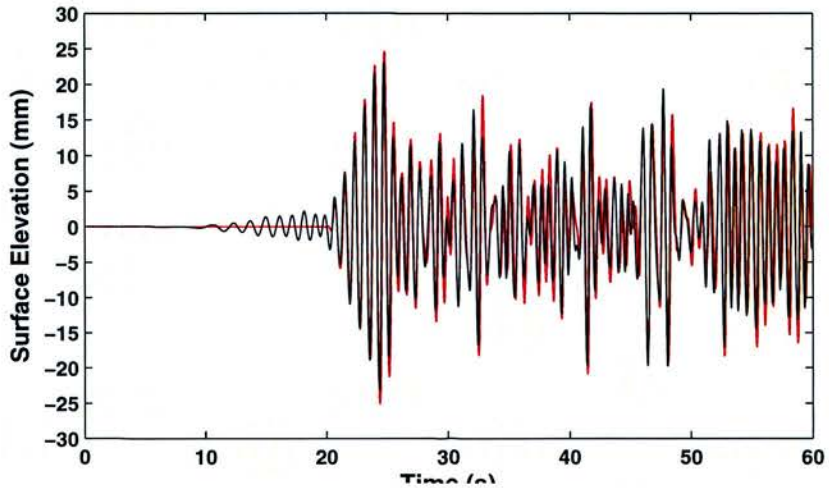

(a) Surface elevation time series. Wire resistance wave gauge and Sensor, Test 4

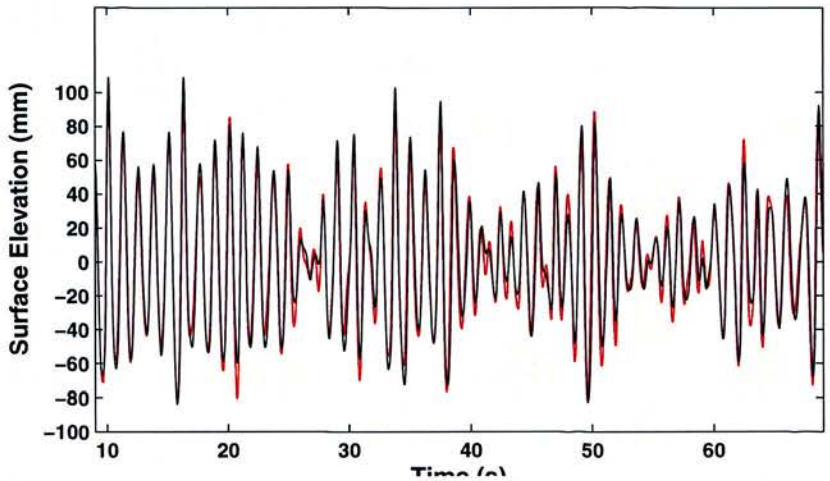

(b) Surface elevation time series. Wire resistance wave gauge and Sensor, Test 5

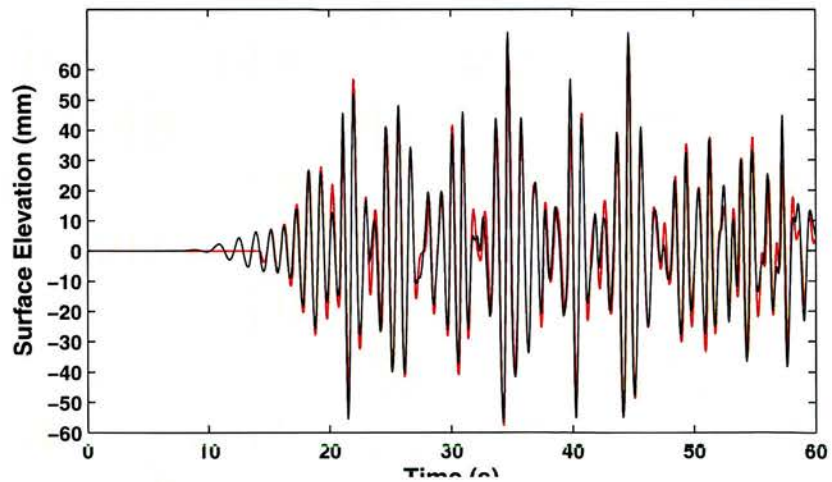

(c) Surface elevation time series. Wire resistance wave gauge and Sensor, Test 6

Figure 5.52. Irregular wave tests - wave elevation versus time. RT2 Processed

5.5.6 Results - Summary

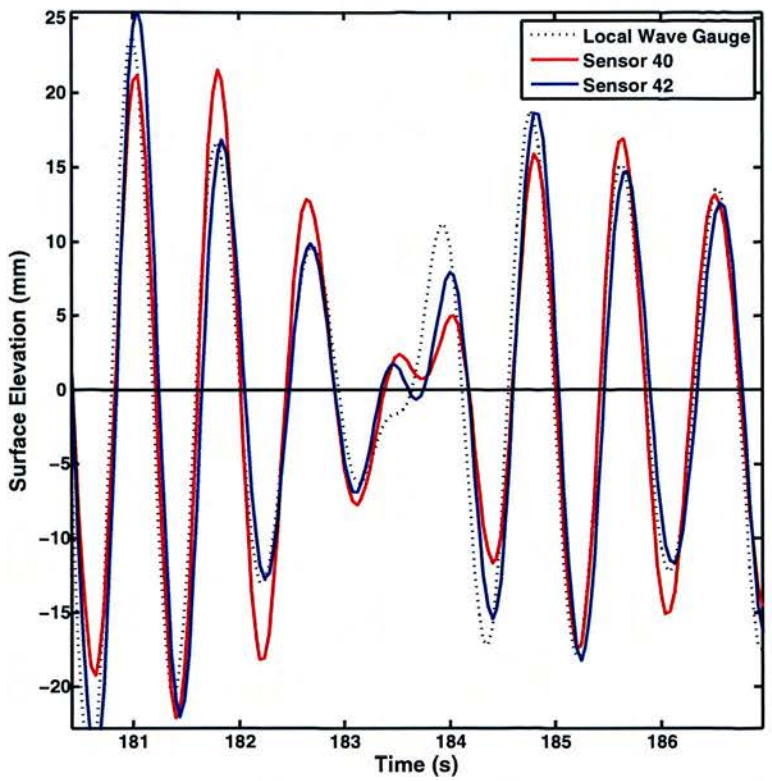

Figure 5.53. Snapshot of time series showing zero-crossing analysis issues.

Table 5.10. Irregular waves. Time domain results. H_m

Test	$H_m(mm)$					Error %				Error Reduction %		
	WG	BF	AMF	RT1	RT2	BF	AMF	RT1	RT2	AMF	RT1	RT2
1	70	54	68	70	69	-22.9	-2.9	0.0	-1.4	87.5	100.0	93.8
2	42	41	39	41	44	-2.4	-7.1	-2.4	4.8	-200.0	0.0	-100.0
3	26	30	25	27	28	15.4	-3.8	3.8	7.7	75.0	75.0	50.0
4	19	24	20	19	21	26.3	5.3	0.0	10.5	80.0	100.0	60.0
5	84	61	83	87	91	-27.4	-1.2	3.6	8.3	95.7	87.0	69.6
6	54	50	50	57	57	-7.4	-7.4	5.6	5.6	0.0	25.0	25.0

The differences in column one (the maximum number of waves detected by the wire resistance wave gauges) between tables 5.6, 5.7, 5.8 and 5.9 are due to the wave matching routines whereby the start and end points of the tests are adjusted automatically if errors occur during processing which would otherwise cause the routine

to fail and require manual processing. These slight shifts of the time series lead to slightly longer or shorter test samples that are made available for post processing and statistical analysis. This could be eliminated by implementing a further stage to the processing that re-aligned the two sets of signals and clipped the test runs to a fixed number of waves and as such has been added to the further work section.

Table 5.11. Irregular waves. Time domain results. T_m

Test	T_m (s)					Error %				Error reduction %		
	WG	BF	AMF	RT1	RT2	BF	AMF	RT1	RT2	AMF	RT1	RT2
1	1.16	1.07	1.16	1.12	1.14	-8.1	-0.6	-3.9	-2.3	93	51	72
2	0.97	0.93	0.97	0.95	0.94	-4.4	0.2	-2.5	-3.8	96	42	13
3	0.85	0.83	0.83	0.84	0.80	-2.4	-1.5	-1.4	-5.6	37	42	-138
4	0.77	0.76	0.77	0.77	0.73	-0.8	-0.1	-0.1	-4.6	83	88	-504
5	1.18	1.10	1.19	1.16	1.16	-6.5	1.2	-1.8	-1.2	82	73	82
6	0.98	0.96	1.00	0.97	0.97	-2.7	1.2	-1.5	-1.8	55	44	34

Table 5.12. Irregular waves. Time domain results. $H_{1/3}$

Test	$H_{1/3}$ (s)					Error %				Error reduction %		
	WG	BF	AMF	RT1	RT2	BF	AMF	RT1	RT2	AMF	RT1	RT2
1	111	81	103	103	104	-27.2	-6.6	-6.7	-5.5	75.7	75.2	79.7
2	65	61	60	61	63	-5.7	-7.8	-5.9	-3.5	-38.2	-3.5	37.6
3	42	46	38	40	43	11.6	-9.6	-3.5	3.7	17.6	70.0	67.9
4	30	37	31	30	31	23.1	1.8	-1.7	3.9	92.2	92.7	83.1
5	133	93	124	133	131	-30.1	-7.2	-0.1	-1.6	76.0	99.6	94.6
6	83	74	76	87	82	-10.5	-8.9	4.2	-1.6	15.2	59.6	85.0

Table 5.13. Irregular waves. Time domain results. $T_{H1/3}$

Test	$T_{H1/3}$ (s)					Error %				Error reduction %		
	WG	BF	AMF	RT1	RT2	BF	AMF	RT1	RT2	AMF	RT1	RT2
1	1.22	1.13	1.20	1.15	1.14	-7.5	-1.4	-5.8	-6.4	81.5	22.7	13.7
2	1.00	0.95	1.01	0.97	0.96	-4.2	1.7	-2.1	-3.8	58.4	49.1	9.5
3	0.85	0.83	0.85	0.85	0.83	-2.5	0.1	-0.4	-2.4	95.2	83.7	1.8
4	0.78	0.77	0.78	0.78	0.75	-0.7	-0.4	0.4	-3.4	40.1	47.5	-370.7
5	1.24	1.15	1.22	1.27	1.27	-7.4	-1.9	2.3	2.6	73.8	68.8	64.6
6	1.01	0.98	1.04	1.00	0.97	-2.9	3.3	-1.1	-3.6	-14.2	61.5	-23.8

Table 5.14. Percentage of waves excluded prior to performing Kernel Density Estimate (KDE) error analysis for the four processing techniques. Stricter wave property criteria, such as reducing the maximum allowable wave steepness allowable, were enforced from "low" to "high".

Threshold Label	Waves excluded % (by process type)			
	BF	AMF	RT1	RT2
"Low"	2.0	1.2	1.3	2.0
"Medium"	9.0	7.0	8.1	7.5
"High"	15.4	12.9	14.9	14.8

Table 5.15. Percentage errors in wave period for all irregular wave tests across 3 sensor locations

Threshold	Percentage Error in Wave Period (all waves)				
	Parameter	BF	AMF	RT1	RT2
low	mean	0.6	-0.3	1.5	1.2
	std	11.6	13.0	9.1	11.3
med	mean	1.3	0.2	1.6	1.6
	std	10.3	11.4	9.0	9.9
high	mean	1.2	0.5	1.4	1.2
	std	10.1	9.8	9.6	10.1

Tables 5.10, 5.11, 5.12 and 5.13 show, respectively, time domain statistical results for H_m, T_m, $H_{1/3}$ and $T_{H1/3}$ and the associated relative errors and reduction/increase in the magnitude of percentage error of the various processing techniques compared to the errors of the Basic Filtering technique.

Figures 5.57 to 5.64 show the likelihood of the magnitude of the relative error in wave heights and wave periods plotted against wave steepness. It can be seen that removing very small waves (below 3mm), very short waves (below 0.45 seconds) and steep waves (above 1/10) reduces the maximum spread of relative errors. Table 5.14 gives the percentage of waves that are required to be excluded in order to improve confidence in keeping measurements below a given error level.

Frequency-Domain Analysis

Spectral analysis was conducted using WaveLab 2 under the standard configuration: low-pass filters with cut-offs at three times the peak frequency and Hanning windows

Table 5.16. Percentage errors in wave height for all irregular wave tests across 3 sensor locations

Threshold	Percentage Error in Wave Height (all waves)				
	Parameter	BF	AMF	RT1	RT2
low	mean	4.3	-0.2	-6.4	-2.3
	std	22.1	24.5	19.6	18.7
med	mean	5.2	0.9	-5.3	-1.3
	std	20.7	23.1	17.6	16.6
high	mean	6.6	2.2	-0.1	-0.2
	std	19.2	20.9	14.7	15.2

used in FFTs configured with 20% taper width and 20% overlap [103]. The results of the spectral analysis can be seen in tables 5.17 and 5.18 which show comparison statistics for T_p and H_{m0} respectively.

Table 5.17. Spectral analysis of irregular wave tests. T_p in seconds.

	T_p (s)								Error %			
Test	WG	BF	WG	AMF	WG	RT1	WG	RT2	BF	AMF	RT1	RT2
1	1.28	1.28	1.28	1.28	1.28	1.28	1.28	1.28	<0.1	<0.1	<0.1	<0.1
2	1.00	1.00	1.00	1.08	1.00	1.00	1.00	1.00	<0.1	7.9	<0.1	<0.1
3	0.85	0.85	0.85	0.85	0.85	0.85	0.85	0.85	<0.1	<0.1	<0.1	<0.1
4	0.76	0.76	0.76	0.76	0.76	0.76	0.76	0.76	<0.1	<0.1	<0.1	<0.1
5	1.28	1.28	1.28	1.28	1.28	1.28	1.24	1.17	<0.1	<0.1	<0.1	-5.7
6	0.98	0.98	1.02	1.11	0.98	0.98	0.98	0.98	<0.1	8.1	<0.1	<0.1

Table 5.18. Spectral analysis of irregular wave tests. H_{m0} in mm.

	H_{m0} (mm)								Error %			
Test	WG	BF	WG	AMF	WG	RT1	WG	RT2	BF	AMF	RT1	RT2
1	111	82	110	103	111	103	111	106	-26.7	-6.0	-7.3	-4.7
2	67	62	65	60	66	65	66	66	-6.8	-7.6	-2.5	-1.1
3	43	45	40	37	43	43	43	44	3.8	-7.8	-0.3	2.2
4	34	36	34	34	34	35	34	33	6.5	1.2	2.0	-3.2
5	116	87	114	106	120	118	119	117	-24.6	-7.3	-1.6	-1.3
6	89	76	88	81	89	86	92	90	-15.2	-8.2	-3.3	-1.5

5.6 Discussion

Processing Techniques

During analysis of the preliminary regular wave tests it became apparent that choosing suitable filtering parameters would play an important role in being able to improve the wave height matching ability of the sensor. Whilst the wave-by-wave period reported from the sensor agrees very well with wire resistance wave gauges, if no correction for wave period is considered, wave height correlation is considerably smaller than wave period correlation (see Fig. 5.15). Taking wave period in to account in post-processing improves wave height correlation significantly, as shown in figure 5.16. Various filtering processes were trialled with the goal of finding a solution that could be implemented on standard computing hardware in real-time. In comparing the filtering techniques listed in this work, it should be noted that further work is required in assessing their performance, reliability and stability across the multitude of parameters that exist in this dynamic (both spatially and temporally) system. It should also be noted that comparing the filtering techniques is complex. Whilst the AMF filtering technique provides broadly the largest improvement in wave height and wave period relative error magnitude, it is conducted once all the data is collected and is not suitable for a real-time or near-real-time implementation. Also, its effect on the rest of the data set outwith the 3 sensor segments near the centre of the ribbon has not been fully investigated.

The RT1 process tends to produce fewer outlier events than the AMF procedure with the benefit of being able to be conducted in near-real-time. Given that this method relies on changing filters, based on incoming wave parameters, more work is required to test its validity across a wider range of wave conditions. The RT1 process shows the most consistent improvement over the basic method (BF) in terms of wave heights but tends to under-predict mean wave period when compared to the AMF method. Despite this under-prediction of mean wave period (which remains small in absolute terms and when compared to wave height errors) the RT1 method and its simplified successor, the RT2 process, show the most promise. In some tests

RT2 performs better in terms of correlation of measurements and given that it is significantly simpler than RT1 would be the recommended filtering technique to benchmark against.

Further testing and analysis would be required to further test the validity of the generated look-up tables. In addition, look-up tables could incorporate further wave slope information as trials have shown promising results. Input from researchers in the signal processing field would be very useful as would having access to people with machine learning expertise. Incorporating look-back, look-forward and spatially aggregated data into the measurements would likely be required to achieve an optimal solution. This should also include capturing known wave physics along with implementing the processing algorithms in a manner conducive to incorporating augmentative sensors by way of sensor fusion. This is particularly required when moving from two dimensional spatial arrays to fully three dimensional arrays.

Wave Period and Wave Height Error

With such high cross-correlation values of the wave elevation time series between wave gauges and sensors in addition to the regular wave period results it is surprising to see the magnitude of the standard deviations in wave period matching for some tests. This is also evident in the wave-by-wave matching process of the optical tracking processes described in Chapter 4. With improved wave matching algorithms, many of the large wave period errors (see Fig. 5.53 for an example of wave matching "near-misses") could be significantly reduced which would reduce the frequency of very large relative wave height errors where small waves existing around the MWL play a role. It is recognised however that the large increases in error when moving from regular to irregular waves cannot all be attributed to sub-optimal matching routines. The combination of increased non-linearity in the wave field, building up of reflections, steeper waves and wave combinations are likely to play key roles in the measurements obtained. Optimising the mechanical matching of the system with the waves was necessarily outside of the scope of this work but properties such as ribbon stiffness, resistance to twist, spring, buoyancy and inertia will play a role in the ribbon's ability to both track waves and cause interactions with both

the waves (through diffracted and reflected waves from floatation jackets) and with neighbouring sensor segments.

For wave period analysis, in addition to Ordinary Least Square (OLS) line fitting of the instrument comparison graphs, linear regression was introduced to assist processing optimisation by giving a more reliable indication of parameters that can indicate relative improvements in wave period matching. The presence of outliers in the data made OLS fitting an over sensitive tuning parameter for this stage of development. Robust fitting was implemented with the MATLAB robustfit.m algorithm. Ideas for improving a wave-by-wave matching algorithm are included in the Further Work section and include making use of prior knowledge of wave physics, i.e., the dispersion equation, taking advantage of the zero-crossing and curvature information available from surrounding sensor nodes and sensor nodes both in the past and through feedback loops, future knowledge.

Wave steepness has been identified as a source of large wave height underestimation. This is particularly evident with waves above a steepness of 0.1. Further work is needed to investigate whether the sensors provide "flags" for these high steepness events which could be used to give improved confidence bounds on measurements. For example there may be information about these events such as high amplitude slope data or large magnitude derivative information which is contained in measurements taken before, after or adjacent (spatially) to the wave event. An investigation of this sort would also be useful in tackling very small waves on and around the zero-crossing threshold and long, shallow waves where neighbouring information and knowledge of the dispersion equation could likely lead to improved wave filtering.

It is interesting that the ribbon sensor performs asymmetrically in terms of wave crest and wave trough tracking. Wave trough measurements show reduced errors compared to wave crest and given that the ribbon measures curvature and can provide wave shape taking advantage of the shape of parts of each wave could play a role in improving sensor performance.

A note on the Aalborg tests

Following testing in the Edinburgh flume the ribbon was tested in the wave basin of Aalborg University through a travel grant awarded through the EU Coordinated Action fund. The purpose of these tests was to investigate how the ribbon would physically behave in both larger, longer waves and in mixed and directional sea states. A large amount of video footage was taken which was used (along with the measured data) in consultation with Measurand Inc. in the planning of possible improvements or alternative solutions to measuring wave fields with floating ribbon-like elements. The data from Aalborg is not included in this thesis as where the tests were conducted in a similar manner (Aalborg flume with regular and irregular tests), no new information is provided and where the tests were conducted in mixed, directional seas, the "bend-only" Sensor cannot be expected to have properly captured three dimensional data. The value in these fully mixed, three dimensional tests comes from observing how a floating ribbon mechanically behaves. Example images from the Aalborg test footage are shown in figures 5.54a and 5.54b.

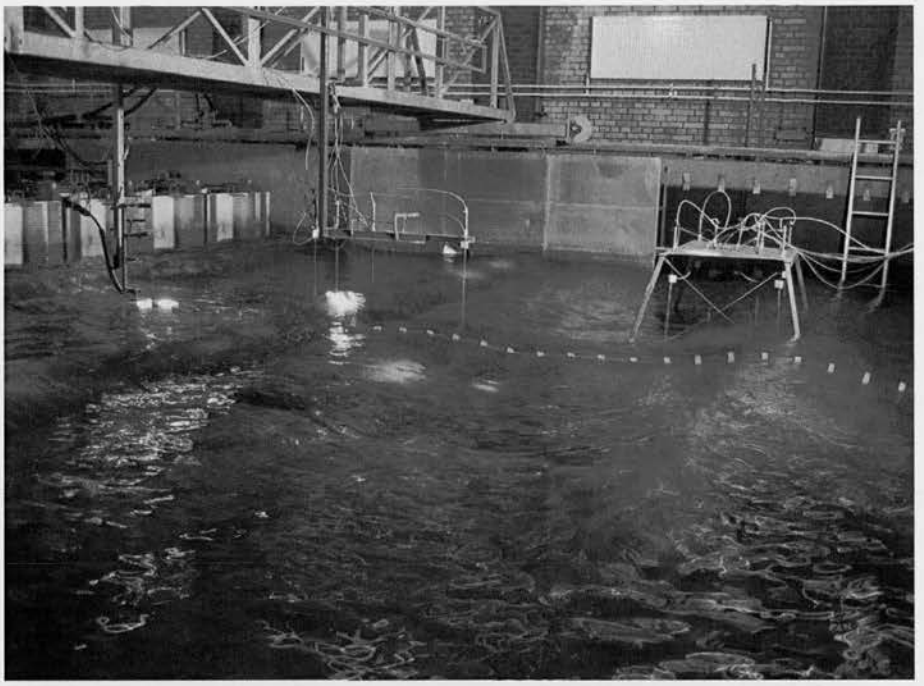

(a) Long crested, medium height irregular waves.

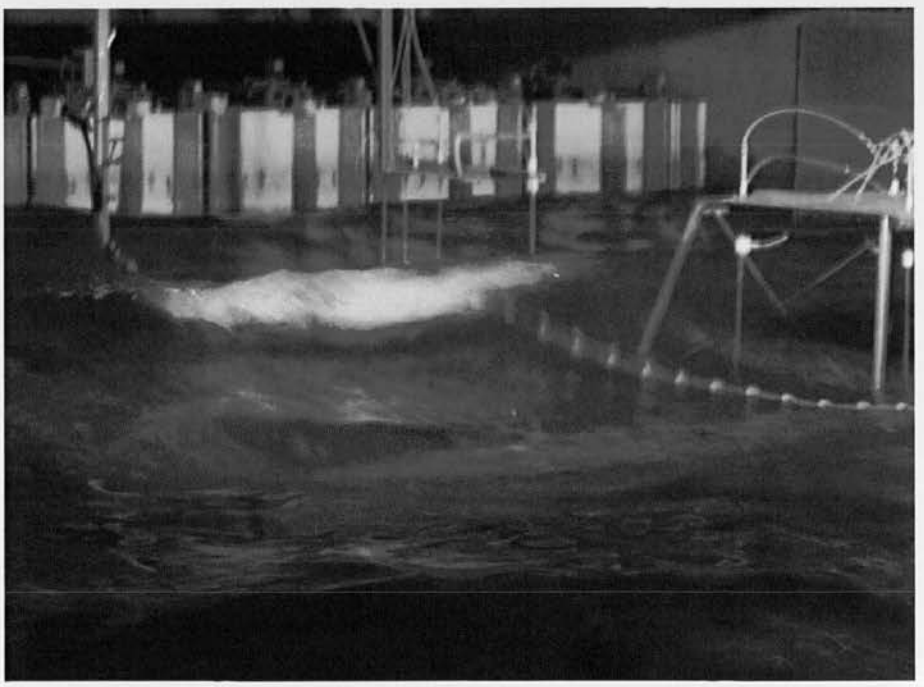

(b) Short crested, steep irregular waves including wave breaking.

Figure 5.54. Frame-grabs of Aalborg basin tank tests.

5.7 Conclusion

A summary of the sensor's performance is listed below:

Regular Waves

- Mean wave height error at the zones closest to the wire resistance wave gauges across all regular wave tests (excluding those above steepness of 0.1) were -2.1% with standard deviation of 7.9% (where negative percentages represent an under-measurement).

- Mean wave period error at the zones closest to the wire resistance wave gauges across all regular wave tests (excluding those above steepness of 0.1) were -0.01% with standard deviation of 0.05%.

- In terms of errors and variation along the sensor ribbon the mean error across all regular wave tests (excluding those above steepness of 0.1) from sensor number 10 to 70 (out of a total of 81) was -8.3% with standard deviation of 6.8%. The mean standard deviation in the wave gauge readings from WG2 to WG 4 (central position of the ribbon) was 1.3%.

Irregular Waves

- Mean wave height error at the zones closest to the wire resistance wave gauges across all irregular wave tests (excluding those above steepness of 0.1) ranged between -6.4% and 4% across the processing methods. Standard deviation of wave height errors ranged between 18.7% and 24.5% across the processing methods.

- Mean wave period error at the zones closest to the wire resistance wave gauges across all irregular wave tests (excluding those above steepness of 0.1) ranged between were -0.2% and 1.2%. Standard deviation of wave period errors ranged between 9.1% and 13%.

- With tighter threshold ("medium"), which is mainly achieved by removing shallow-sloped waves, mean wave height error reduces to between -1.3% and 5.2% with associated standard deviation in the range 16.6% and 23.1%.

- Under "medium" threshold mean wave period error is between 0.2% and 1.6% with associated standard deviation reduces to between 9% and 11.4%.

Tables 5.15 and 5.16 give summary statistics from the combined irregular wave tests on a wave-by-wave basis comprising approximately 6500 individual waves.

Errors and Uncertainties

In order to transform the measured bend data to position data integrations are required, resulting in integration drift on to the data. These affects are in addition other sources of error which are listed in section 5.3.1. A variety of processes have been explored during this work to deliver surface elevation data whilst minimising local-solution finding and over-restrictive techniques. The concept of this sensor stemmed from the goal of having online real-time data "upstream" of marine equipment. With this is mind there is a large amount of additional work required in optimising, assessing and implementing processing techniques to allow access to useful and timely data. Further work is also required to investigate the effects of filtering, smoothing and processing techniques on the data reported from sensors, particularly in an along-ribbon sense. Section 8.5 in Chapter 8 contains a collation of the further work highlighted in each of the three research report sections: the optical method of measuring surface-tracking ability; the optical fibre-based sensor concept outlined in this chapter and the outcomes of the MEM-based sensor concept in Chapter 6

Conclusion

It has been shown that a floating ribbon-like device can be constructed, installed and operated to track the free surface at the scales available in the Edinburgh flume. The *raw* bend data recorded by the fibre-optic system is high quality and does not require extensive post processing or filtering. In order to provide reliable *position*

data post processing and filtering is required. The ribbon itself survived the limited test schedules in both the Edinburgh Flume and the test tanks of Aalborg University which included breaking waves and mixed and directional sea states.

Wave period is accurately tracked across all periods tested during regular wave tests from 0.77 seconds to 1.43 seconds. Wave period error is consistently below 1% for regular waves and 10% for waves in irregular wave fields. Reported wave heights show dependence on wave slope. For relatively steep waves (in this case greater than 1/10) the wave height error is large with wave height significantly below the actual wave height. Errors of a factor of 2 are typical in these waves. Wave period measurement error is not affected by wave slope.

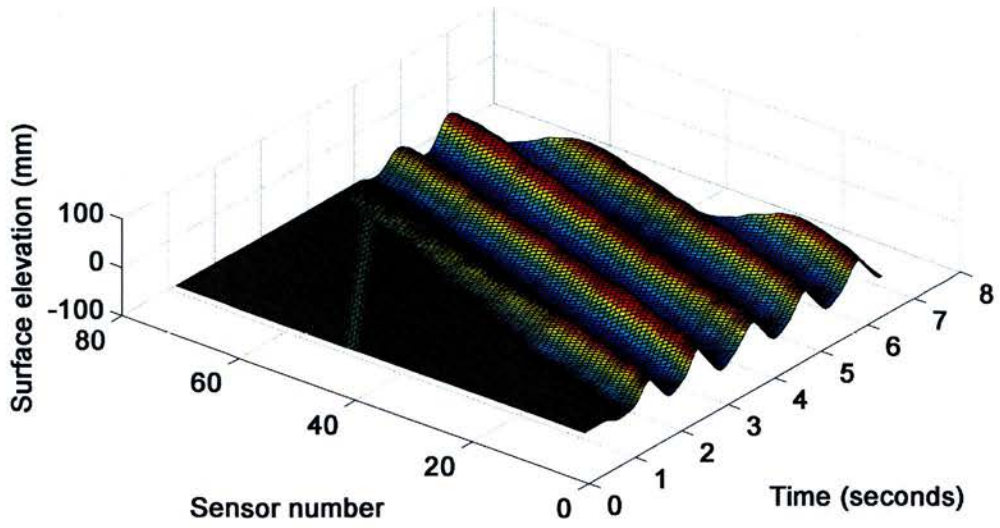

(a) Regular test 2. $T_m = 1.42(s)$. $H_m = 61(mm)$

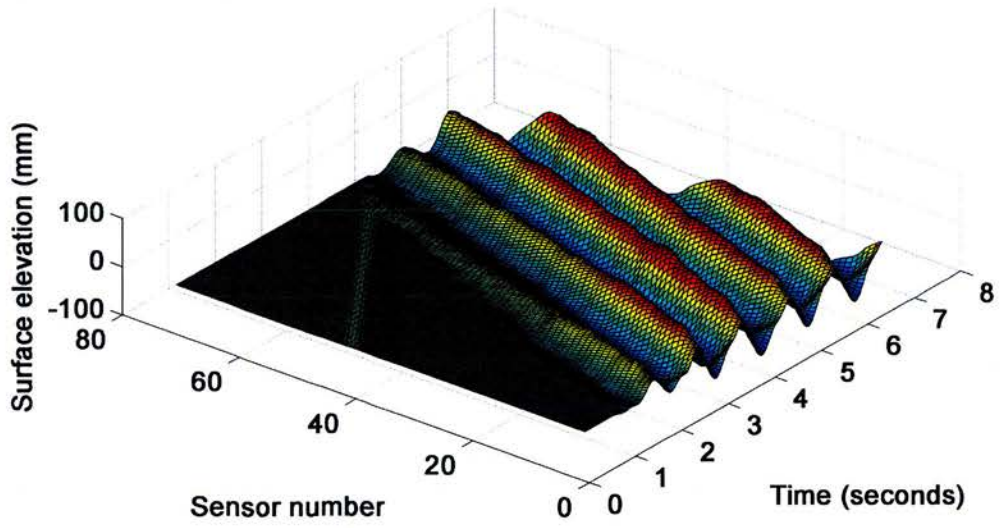

(b) Regular test 13. $T_m = 1.25(s)$. $H_m = 105(mm)$

Figure 5.55. Surface elevation across ribbon for 8 seconds of regular tests 2 and 13.

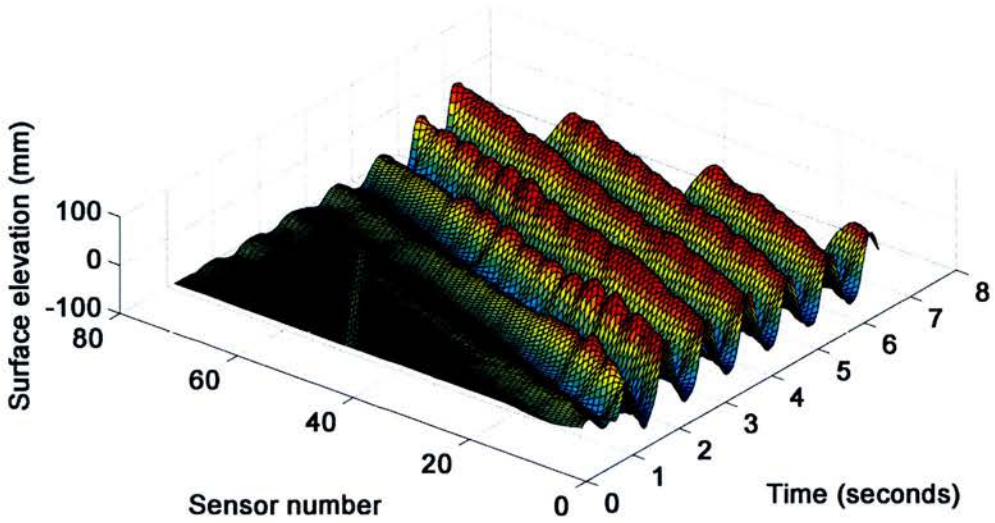

(a) Regular test 26. $T_m = 1.1$(s). $H_m = 166$(mm)

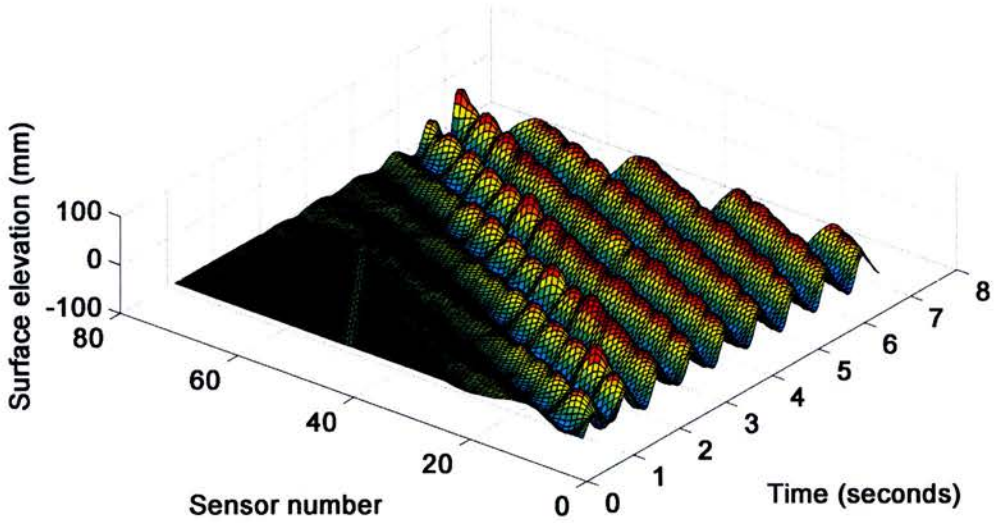

(b) Regular test 40. $T_m = 0.91$(s). $H_m = 95$(mm)

Figure 5.56. Surface elevation across ribbon for 8 seconds of regular tests 26 and 40.

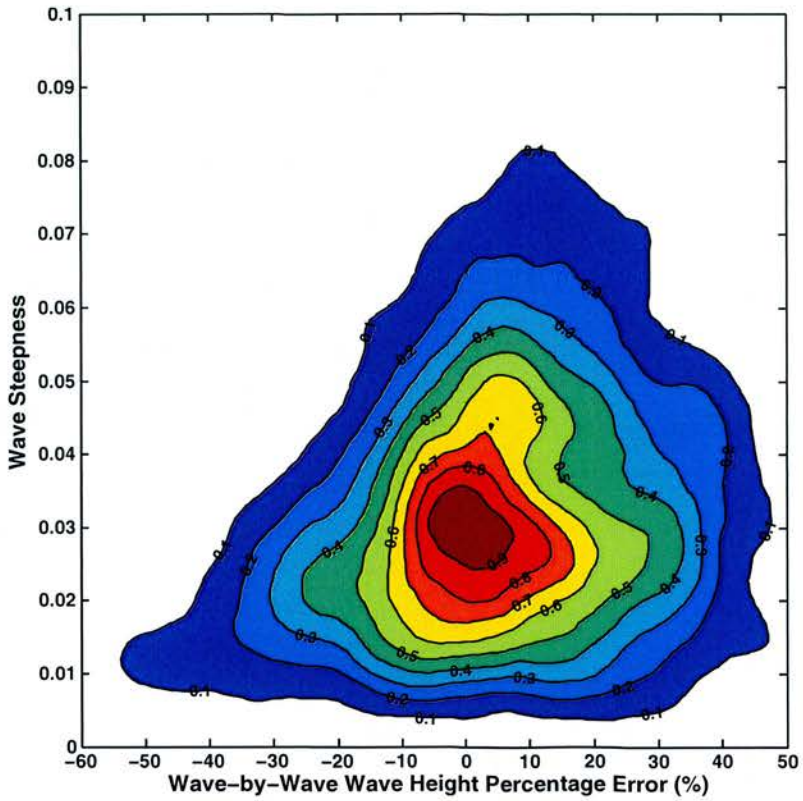

(a) All irregular waves. BF Low. Wave height error

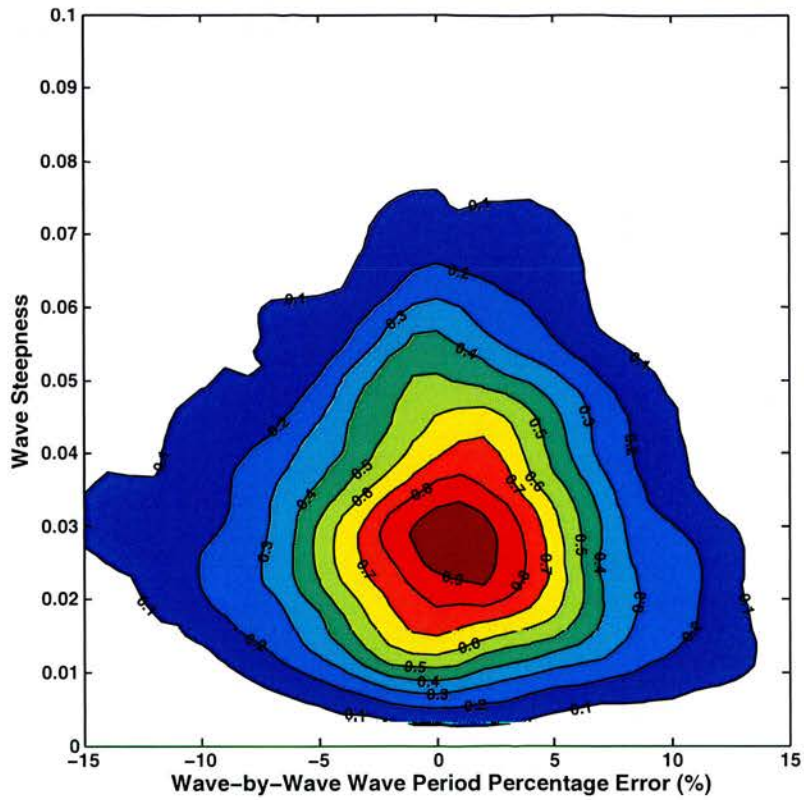

(b) All irregular waves. BF Low. Wave period error

Figure 5.57. All waves from all irregular wave tests passing "Low" threshold. BF Processed. Positive error implies over-measurement by sensor.

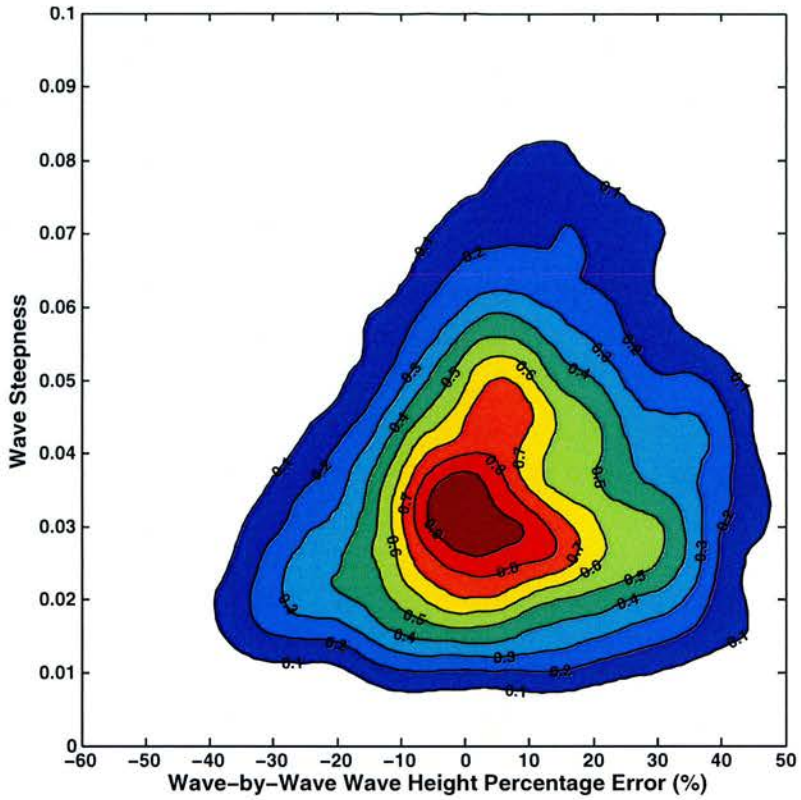

(a) All irregular waves. BF High. Wave height error

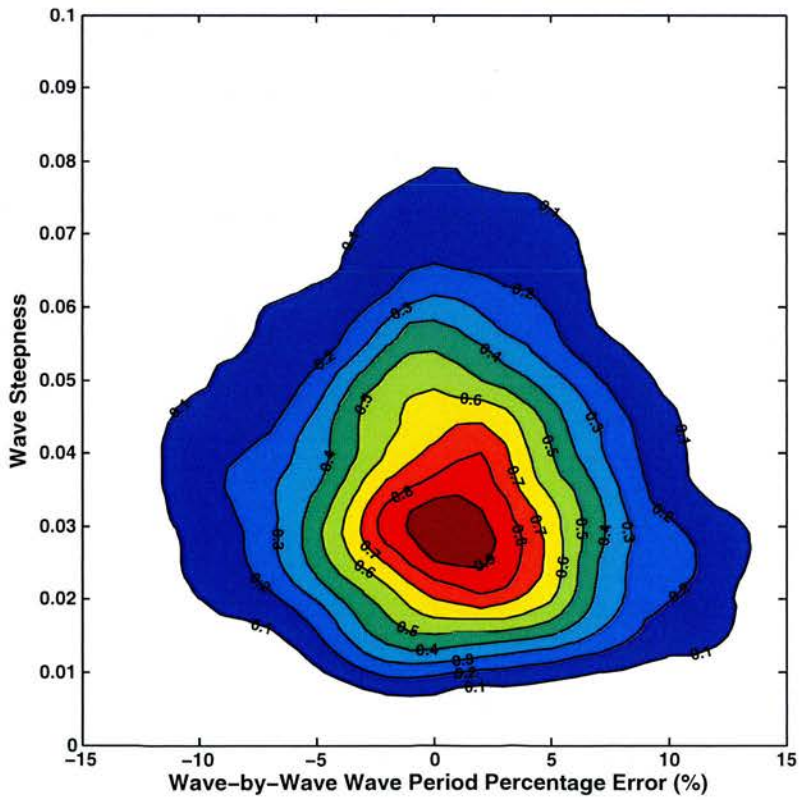

(b) All irregular waves. BF High. Wave period error

Figure 5.58. All waves from all irregular wave tests passing "High" threshold. BF Processed. Positive error implies over-measurement by sensor.

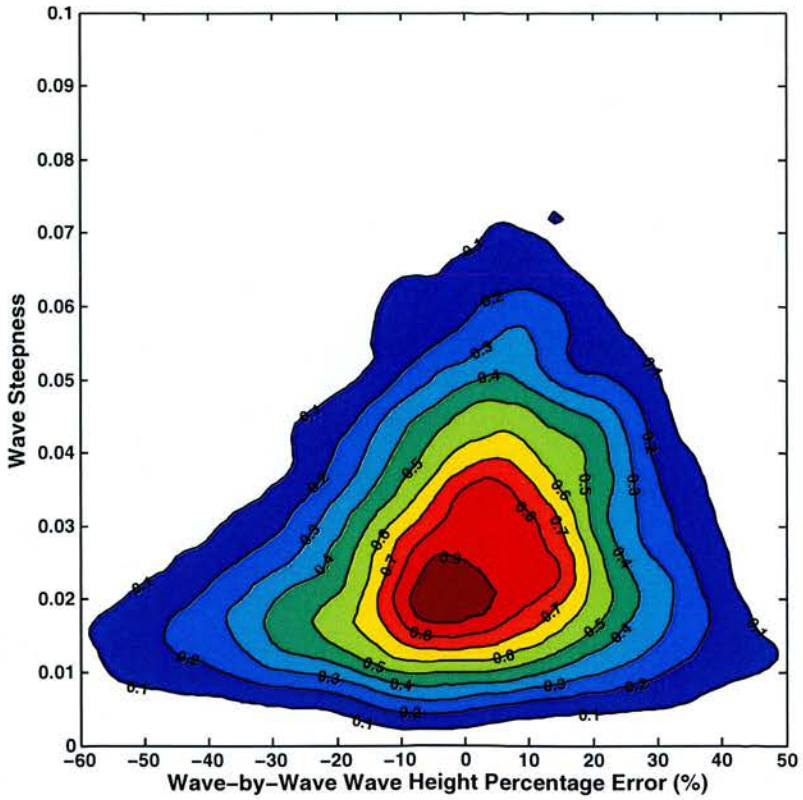

(a) All irregular waves. AMF Low. Wave height error

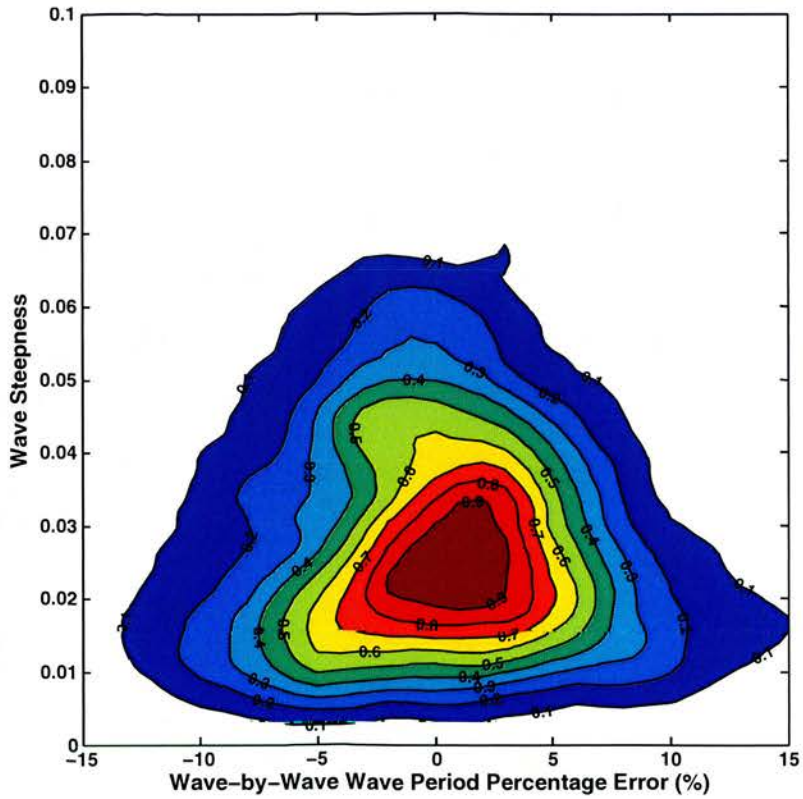

(b) All irregular waves. AMF Low. Wave period error

Figure 5.59. All waves from all irregular wave tests passing "Low" threshold. AMF Processed. Positive error implies over-measurement by sensor.

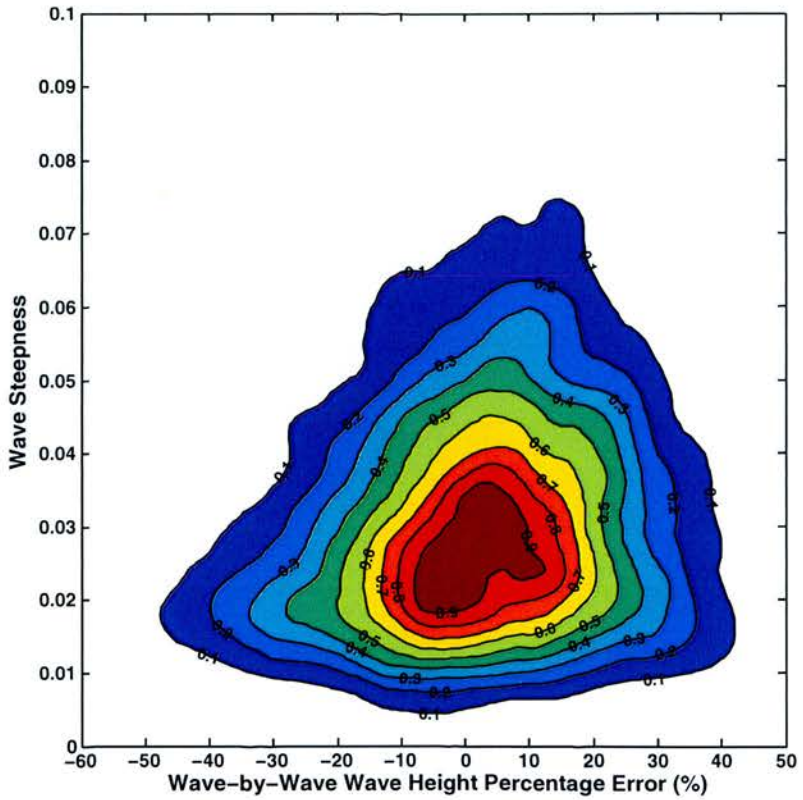

(a) All irregular waves. AMF High. Wave height error

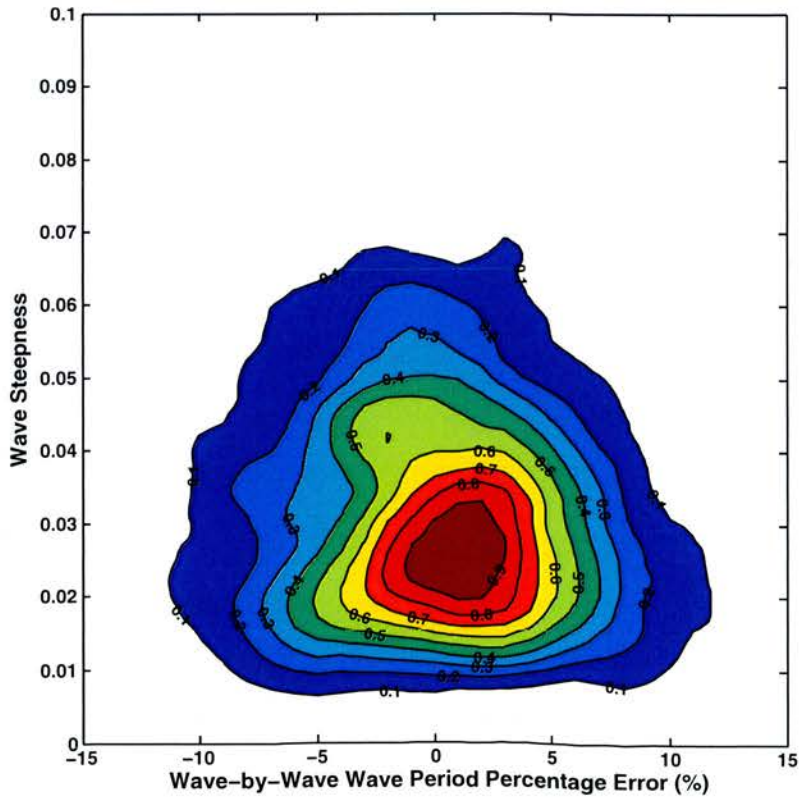

(b) All irregular waves. AMF High. Wave period error

Figure 5.60. All waves from all irregular wave tests passing "High" threshold. AMF Processed. Positive error implies over-measurement by sensor.

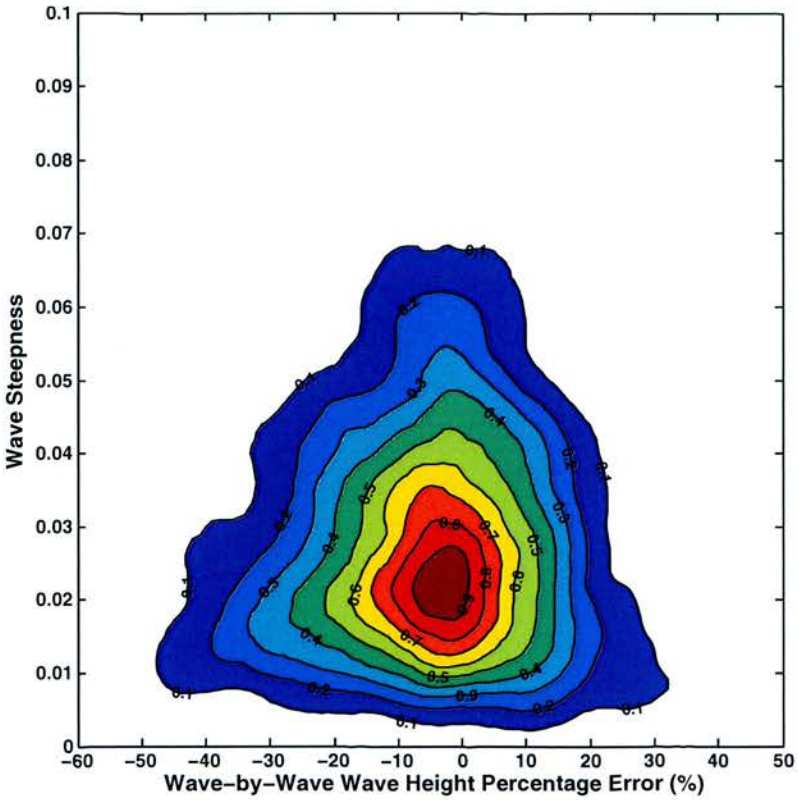

(a) All irregular waves. Real Time Low. Wave height error

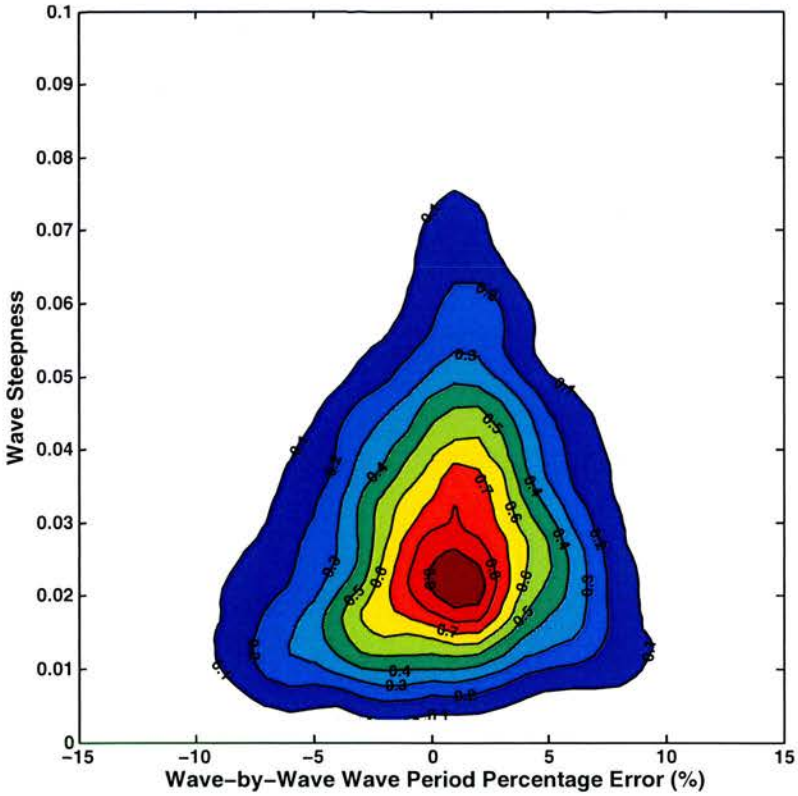

(b) All irregular waves. Real Time Low. Wave period error

Figure 5.61. All waves from all irregular wave tests passing "Low" threshold. Real Time (RT1) Processed. Positive error implies over-measurement by sensor.

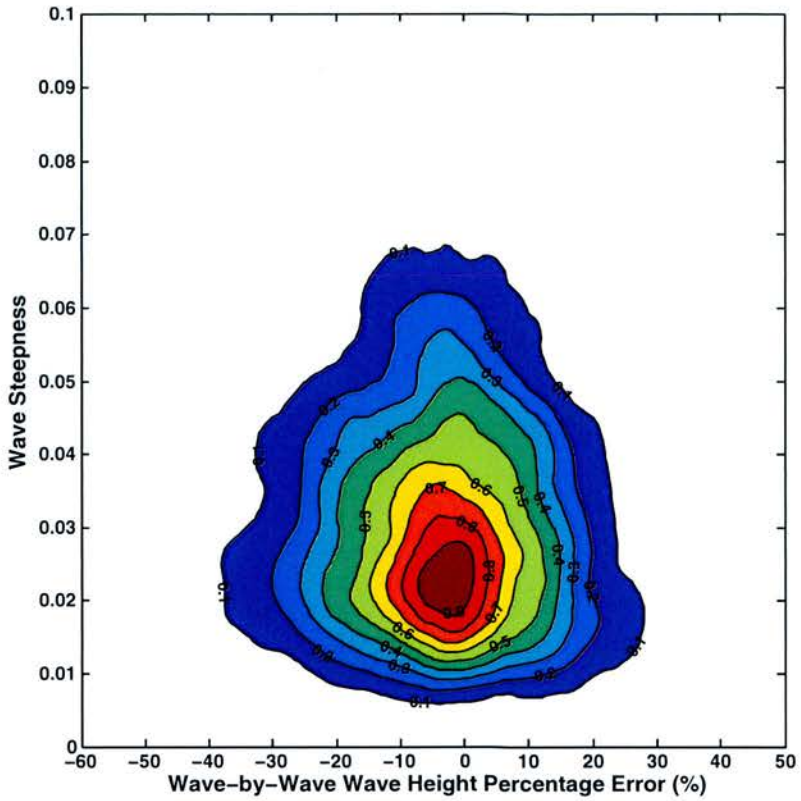

(a) All irregular waves. Real Time High. Wave height error

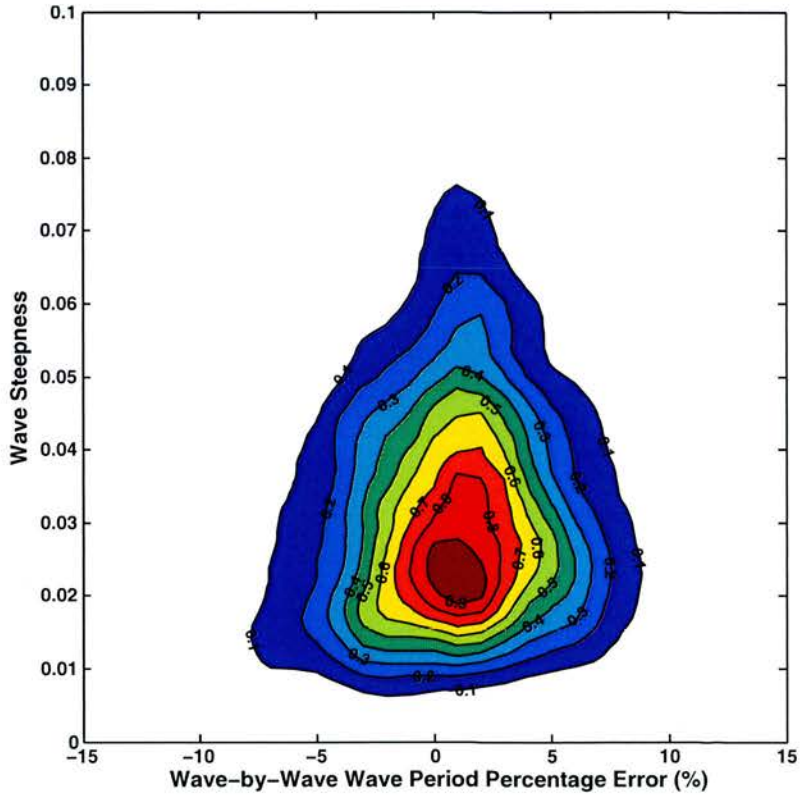

(b) All irregular waves. Real Time High. Wave period error

Figure 5.62. All waves from all irregular wave tests passing "High" threshold. Real Time (RT1) Processed. Positive error implies over-measurement by sensor.

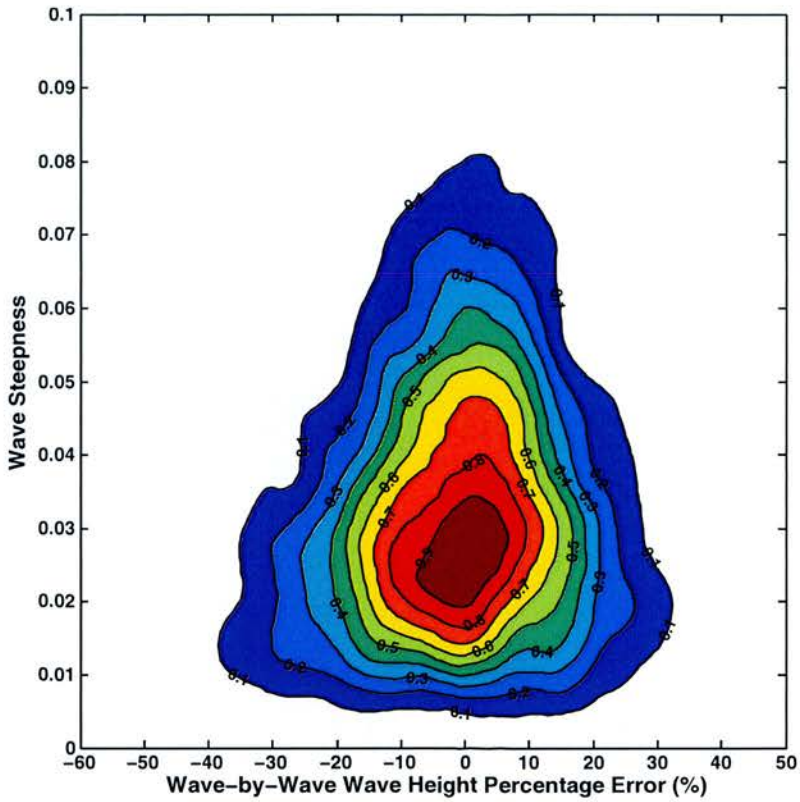

(a) All irregular waves. Real Time Low. Wave height error

All irregular waves. Real Time Low. Wave period error]

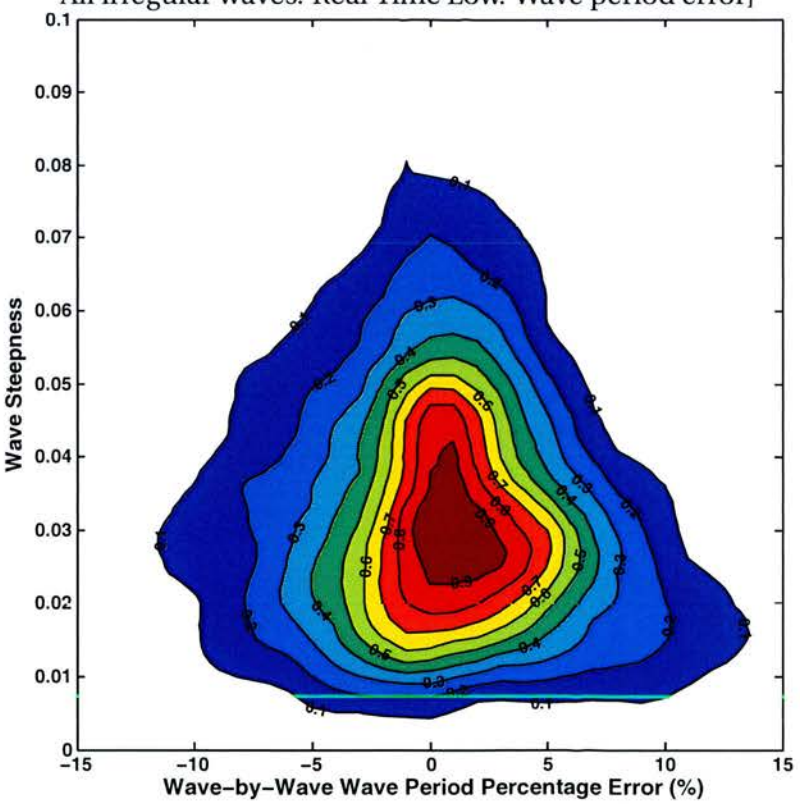

Figure 5.63. All waves from all irregular wave tests passing "Low" threshold. Real Time (RT2) Processed. Positive error implies over-measurement by sensor.

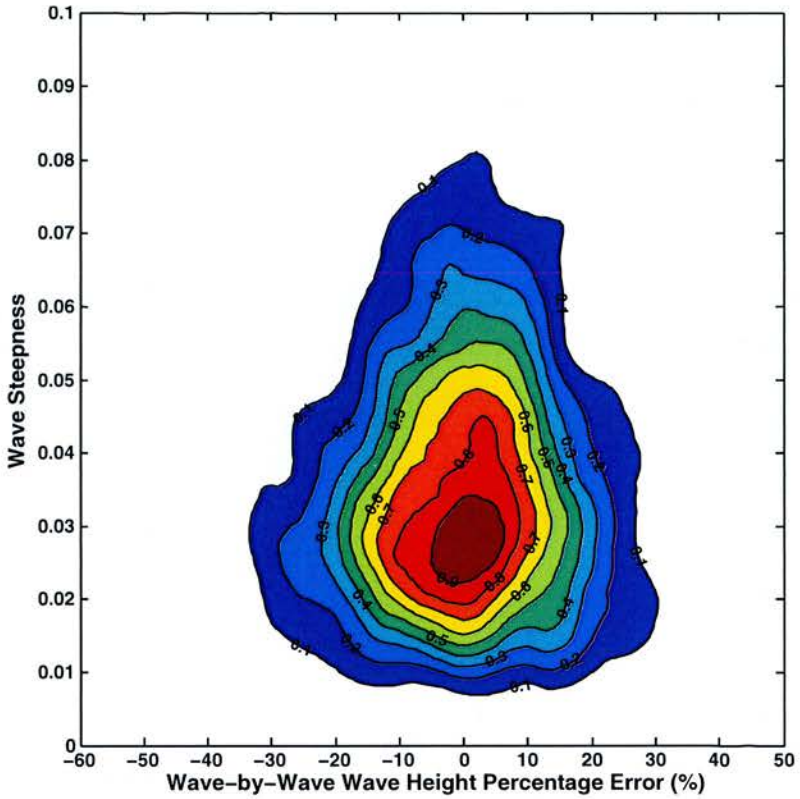

(a) All irregular waves. Real Time High. Wave height error

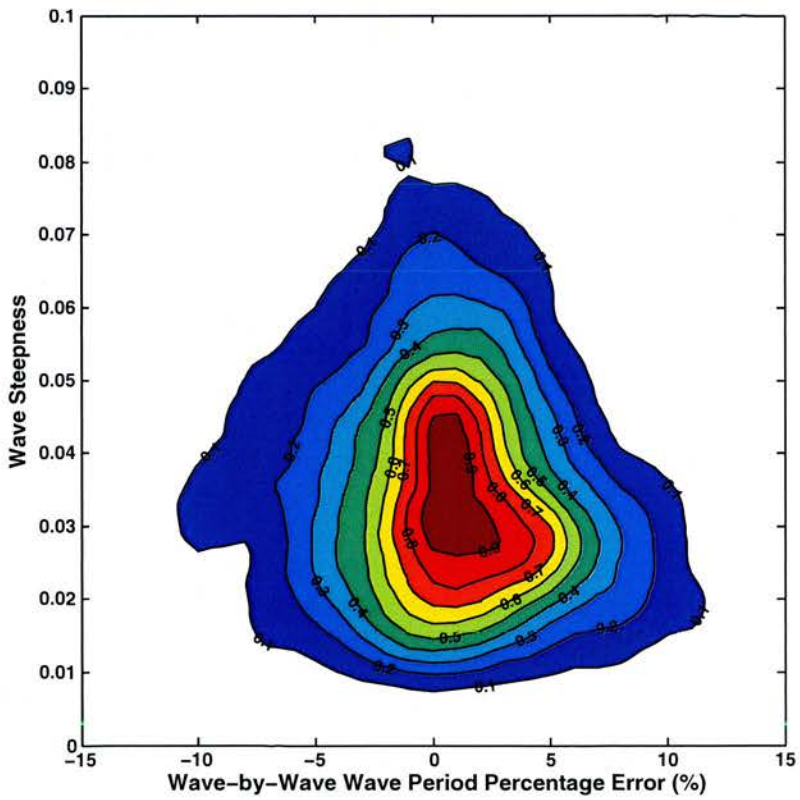

(b) All irregular waves. Real Time High. Wave period error

Figure 5.64. All waves from all irregular wave tests passing "High" threshold. Real Time (RT2) Processed. Positive error implies over-measurement by sensor.

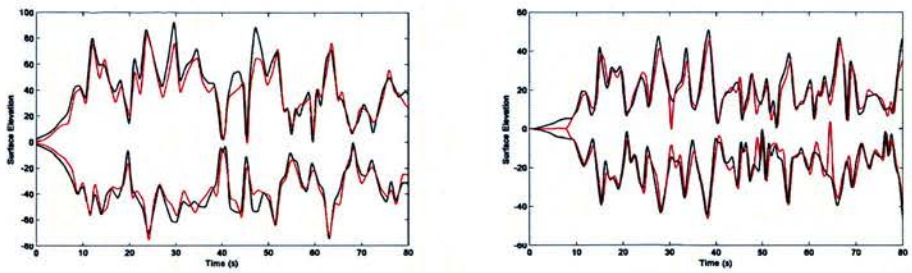

(a) Irregular Test 1

(b) Irregular Test 2

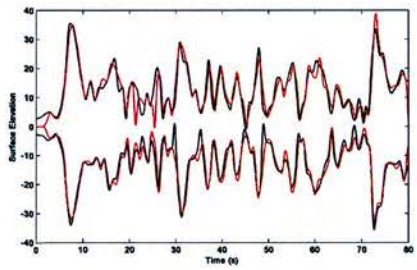

(c) Irregular Test 3

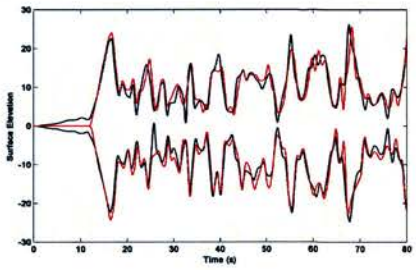

(d) Irregular Test 4

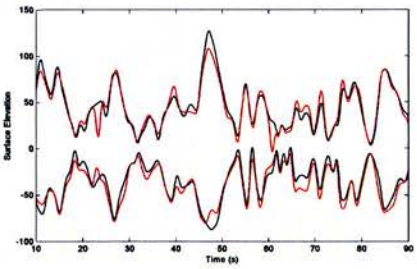

(e) Irregular Test 5

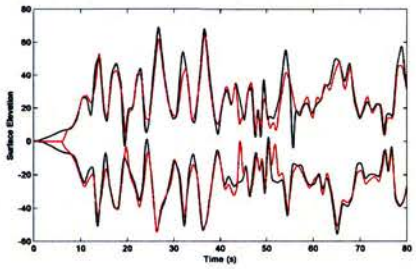

(f) Irregular Test 6

Figure 5.65. Wave envelope example with possible use in wave group tracking. Irregular wave tests 1 to 6. Solid red line shows sensor data, solid black line shows wave gauge data.

CHAPTER 6

Design, Construction and Testing of Multiple Novel Sensors - Type II

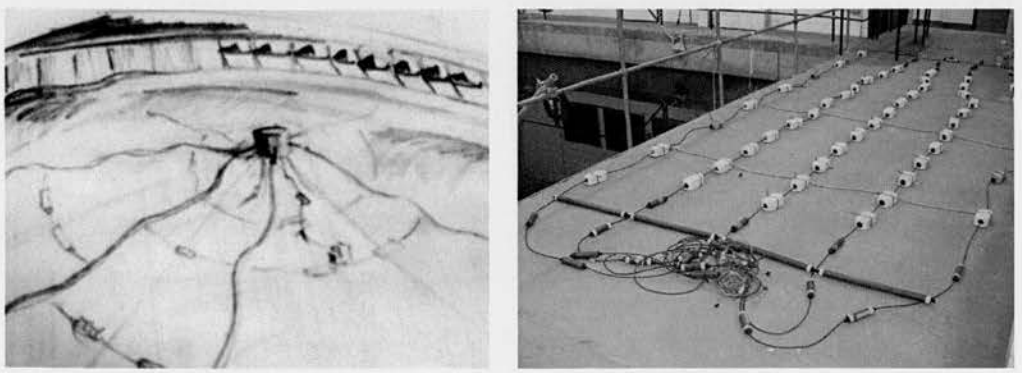

(a) Original conceptual sketch of floating sensor array

(b) First configuration of the MEM-based sensor array.'

Figure 6.1. Concept (a), and Mark I MEMs-based array during testing in Heriot-Watt Deep Basin (b).

Following the trial of a two dimensional floating wave sensor, discussed in Chapter 5, funding was secured to develop the concept towards a three dimensional array of floating sensors. In developing a 3D sensor array, alternative technologies that could overcome some of the issues and limitations (see Section 5.6, Chapter 5) of the optical fibre-based technology were explored. In summary, these limitations were: the non-modular nature of the ribbons which have to be pre-specified and fabricated in a time consuming process; susceptibility of the flat ribbon substrate

to buckling and fatigue and expected limitation in maximum length of a fabricated ribbon. A key consideration was the ability to have a reconfigurable sensor system - primarily in order to allow tests at various scales - hence modularity and flexibility were important features.

This chapter briefly outlines three alternative technology types to the optical fibre based technology of Chapter 5. Sections 6.3.1 to 6.3.3 provide brief overview of the three types of sensor technology used. The sensor package developed in this work is then outlined in 6.3.4 and its construction and design reported in section 6.4.

Survivability tests conducted at the GWK facility in Hannover and preliminary array tests conducted at the Heriot-Watt University wave basin are reported , respectively, in sections 6.5 and 6.6.

Figure 6.1b shows the first array configuration during preparations to test sensor performance in the Heriot-Watt University wave basin. In the image, from left to right, the five longitudinal-running elements are subsequently referred to as "Ribbon 4", "Ribbon 1", "Ribbon 2", "Ribbon 3" and "Ribbon 4". Ribbon 4 has wrapped back on itself around the array with only the left-hand "ribbon" utilised in analysis.

6.1 Technology Selection: Sensor Component Types

Advances in fabrication methods in the semiconductor industry have led to the development of a whole category of miniature and increasingly affordable sensor platforms termed micro-electro-mechanical systems (MEMs). These systems are designed to either measure an environmental parameter or to act as an actuator with common MEMs systems being accelerometers and pressure sensors where annually billions of units are manufactured. MEMs advantages lie in their low power consumption requirements, reliability, robustness in exposure to vibration and shock etc., lack of moving parts along with fundamental advantages (fast response time, low inertia etc.) gained due to their miniature scale [116, 117].

6.1.1 Angular Rate Sensors

Angular rate sensors (ARS) measure rotational speed. To realise angle or orientation, the angular rate is integrated over time, providing angle as a function of time.

$$\theta(t) = \int_0^t \omega(t')\mathrm{d}t'$$

where ω = angular rate, t = time and θ = angle

The MEMs angular rate sensor takes advantage of the Coriolis force. When an observer present in a rotating frame views an object moving in this rotating frame they see an apparent acceleration of the object. By setting up a known vibration on a platform inside the sensor unit any rotation around the plane of this vibrating platform causes a vibration in a detection transducer on another axis. The measured Coriolis accelerations are converted to angular rate using the known mass and velocity of the vibrating platform.

6.1.2 Magnetometers

Magnetometers are sensors for magnetic field detection which are used throughout the fields of oceanography, geophysics, archaeology and more recently consumer electronics. There are two basic types: scalar magnetometers measure the total strength of the magnetic field they are exposed to and vector magnetometers, as the name suggests, can measure the component of the magnetic field in a particular direction relative to their orientation. Packaging three vector magnetometers orthogonally together creates a "tri-axis" magnetometer capable of providing the x,y,z components of magnetic field strength.

6.1.3 Accelerometers

Accelerometers measure acceleration relative to a local inertial frame. They are found throughout the fields of transport, navigation, consumer electronics and in the motion monitoring of people, goods, vehicles and structures. The accelerometers used

in this thesis are of the MEMs type arranged orthogonally to provide the components of acceleration in the x,y,z directions. They consist of a proof mass which when forced to move by acceleration changes the capacitance of circuits connected to surrounding structures. Processing the signal (the varying capacitances) from the structures surrounding the mass leads to acceleration in one, two or three directions.

6.1.4 The Measurand / UoE Sensor Package

Two types of sensor package were specified then designed, fabricated and supplied by Measurand Inc. The first consisted of a combination of tri-axis magnetometers, tri-axis accelerometers and tri-axis angular rate sensors making a full inertial measurement unit (IMU). The second comprised tri-axis angular rate sensors only and are labelled throughout as Angular Rate Sensors (ARS). Figure 6.4a and 6.4b show, respectively, a technical drawing and photograph of the printed circuit board (PCB) of an IMU-type sensor.

In order to get hands-on experience with these types of sensors in a hydraulic laboratory setting, Measurand Inc.'s existing sensor packages used in their geophysical monitoring systems were used. These were used to commission both Measurand's custom software and our own in house software using MATLAB via the Measurand Software Development Kit (SDK). During this time a design specification was worked on that would lead to smaller and more effective sensors. Reductions of 60% in size and 75% in weight were achieved over two iterations in transition from the "off-the-shelf" Measurand geotechnical sensor package to the custom Measurand/UoE design (see Fig. 6.4).

Design considerations included size, weight, cost, lead time, sensitivity and resolution, power consumption and, importantly, data communication.

In order to give design guidance to Measurand Inc., in terms of which angular rate sensors to procure and what adjustment circuitry to incorporate, a series of tests were conducted in the Edinburgh Basin (see Fig. 6.3). A dummy array of sensor ribbons was constructed using spring steel substrate with outer covering of PVC made buoyant via evenly spaced Divynacell floats. Co-aligned 10mm diameter infra-

red marker buoys were attached to each float via 100mm long, 1mm diameter light weight rods. A pair of Qualysis system tracking cameras and associated software were used to estimate the angular rates of each individual float. This data was passed on to Measurand Inc.

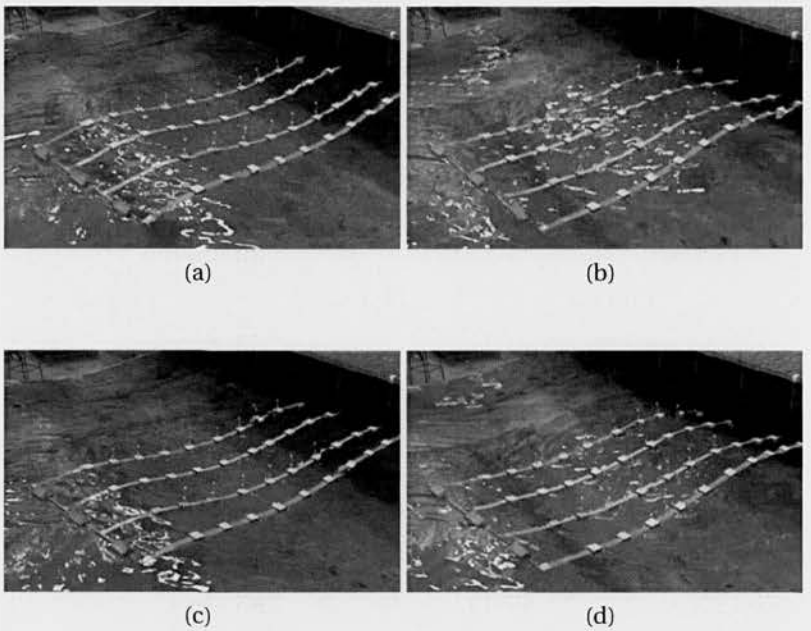

Figure 6.2. Sensor specification trials. Video footage of dummy array in Edinburgh curved tank. Frames $\approx$ 2 seconds apart.

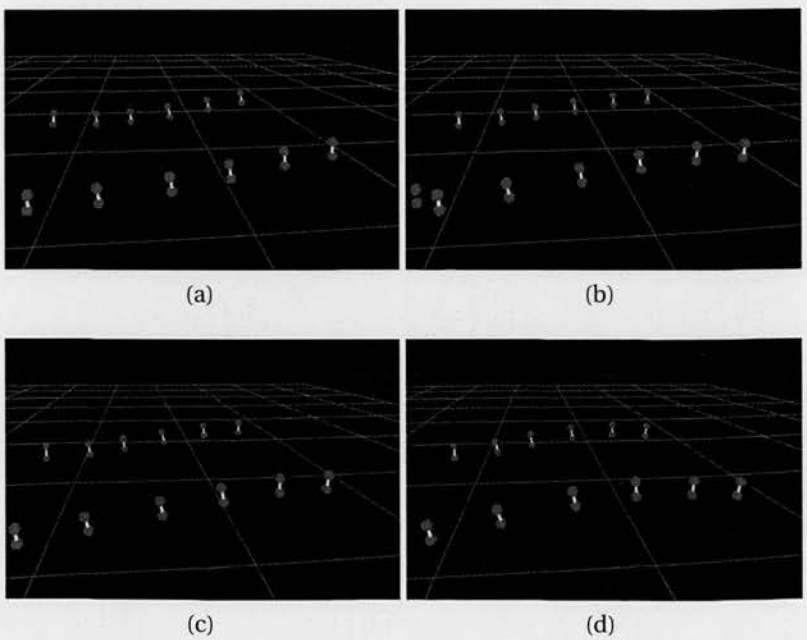

Figure 6.3. Sensor specification trials. Outputs from Qualysis-tracked dummy array tests. Frames ≈ 2 seconds apart.

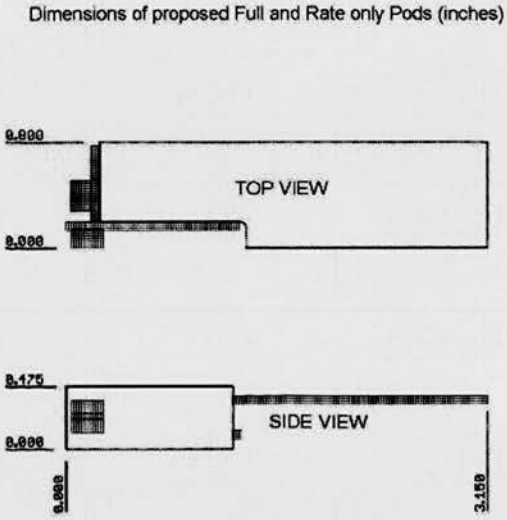

(a) Custom sensor dimensions

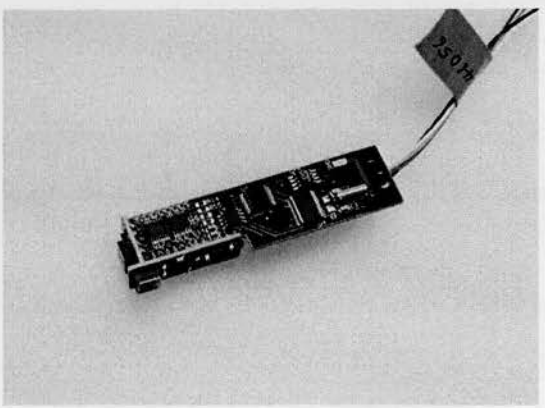

(b) Custom sensor. Type Inertial Measurement Unit (IMU) comprising 3-axis accelerometer, 3-axis angular rate, 3-axis magnetometer.

Figure 6.4. Custom sensor bare board dimensions and photograph.

6.2 Sensor Design and Construction

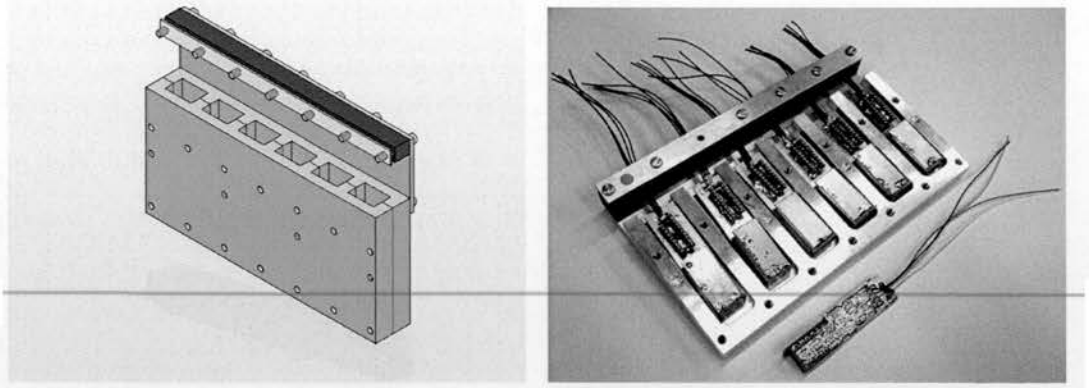

(a) CAD concept and design of mould

(b) Original mould, mounting method and a manufacturer-supplied PCB (with no MEM sensors on board)

Figure 6.5. Original mould, mounting method and a Measurand supplied dummy chip (with no sensors on board)

6.2.1 Cable selection

The move away from fibre optic-based ribbons as a means to increase robustness and modularity (as discussed earlier) led to a requirement to find a suitable alternative. Several options where explored including loose/flexible cabling inside flexible hose/tubing, multiple cables bound together laterally, solid tubing with flexible hose joints and single cables. Single cables were chosen for simplicity and to allow testing of the surface tracking ability and incorporation of sensor nodes. Subsequently, a test programme was conducted using an extensive range of single-cable types.

Standard laboratory cables held in University stores were trialled in the flume by connecting up to the original mark I sensor pods (mechanically not electrically, i.e., through housings to ensure waterproofing and tensioning but not terminated). It became evident that density, stiffness, diameter, material, spring, torsion resistance and cable lay were all important factors in surface tracking performance.

Thus, the choice of cable involved balancing three interconnected considerations:

1. electrical compatibility with a given sensor configuration
2. mechanical robustness and integration with waterproofing system
3. interference with surface tracking ability of floating sensor pods

Weight and dimensions

High density cables tended to be more robust with a greater choice of materials but conflicted with consideration 3 and also caused problems interfacing with miniaturised waterproofing solutions. At the sensor/enclosure interface cable glands having a specification exceeding IP68 and o-rings protect the sensors against water ingress [118]. The scale of the enclosures and contained sensors led to a cable gland with a maximum allowable cable of no greater than 6.5mm. Cable glands with a greater aperture are commercially available but these were not constructed from plastic, being brass or stainless steel, and therefore unsuitable in terms of weight and, to a lesser degree, cost.

Material

Cable outer materials that provide good protection against water ingress and resistance to chemicals found in sea-water (such as organic surfactants) have various trade offs in terms of availability, physical flexibility and cost. Three candidates were identified: polyurethane, thermoplastic elastomer (TPE) and rubber. The latter has a tradition of use in challenging marine environments but could not be found to match other requirements, particularly in terms of conductor sizing and conductor sheathing properties which in general were too heavy and stiff for this scale of system. TPE and Polyurethane were selected as possible choices and compared against further parameters.

Conductors

To allow greater flexibility of sensor configuration multiple cores are advantageous. This increases the diameter and weight of the cable however, and limits the choice

of cable construction. Sensor configurations were chosen that would not lead to too complex a cable choice but would allow some flexibility in testing, for instance, allowing single ribbons to be tested in the Edinburgh Flumes whilst varying sensor spacing and importantly reconfiguration into an array for testing in the Heriot-Watt basin. After a large amount of cable samples were trialled, an unshielded eight core, 0.25sqmm (approximately 23AWG) cable was selected with a twisted layout around a central polymer tensile cord with a flexible TPE outer sheath.

This cable provided flexibility in array configuration due to its combination of dimensions, physical properties, price and availability and its conductor number which allowed two separate instrument circuits to exist on one cable.

Voltage Drop

Voltage drop along the cable/sensor length is calculated as follows:

$$V_D = IR$$

where V_D=voltage drop, I = current draw of sensors and R = total resistance of cable.

$$R = 2L_C K_C$$

where L_C= length of cable and K_C= resistance of cable per metre. K_C=70Ω/km for the selected "Chainflex CF9" cable (see Fig. 6.9).

Figure 6.6 shows the voltage drop calculated over a variety of cable lengths and sensor densities. The design of the sensor packages leads to a maximum permissible voltage drop of $1.5V$ ($12V$ supply minus minimum operating voltage of $10.5V$). Any sensor configuration must be selected to be under the $1.5V$ voltage drop curve.

Sensor Communication

These sensor configuration choices coincided with Measurand's parallel efforts to design a communication bus system that would meet our agreed goals of minimal power consumption and highest possible sample rate. This component of the initial

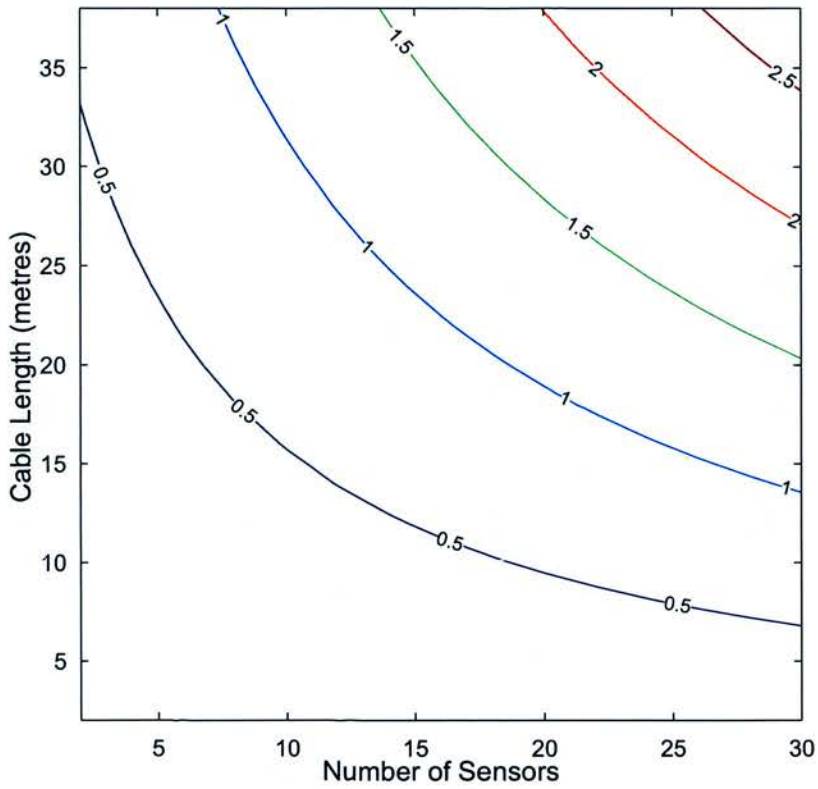

Figure 6.6. Cable and Sensor configuration based on maximum permissible voltage drop.

design process took up more time than anticipated with consequences on the amount of testing that could be subsequently achieved.

The final configuration of communication-bus system comprised sensor unit and microprocessor connected in parallel, communicating via the RS485 protocol. With each unit having a dedicated microprocessor any combination of sensors can be integrated in to a ribbon. Figure 6.7 shows the wiring of each pod.

Cable Supplier

Igus Ltd. [1] was chosen after searching many cable companies and trialling their products. Unlike many other companies Igus offer a large selection of cable types, short lead times and no minimum order quantity which allowed an extensive range of cable types and configurations to be tested in the flume.

[1] "Chainflex" and image in figure 6.9 ©IGUS Ltd.

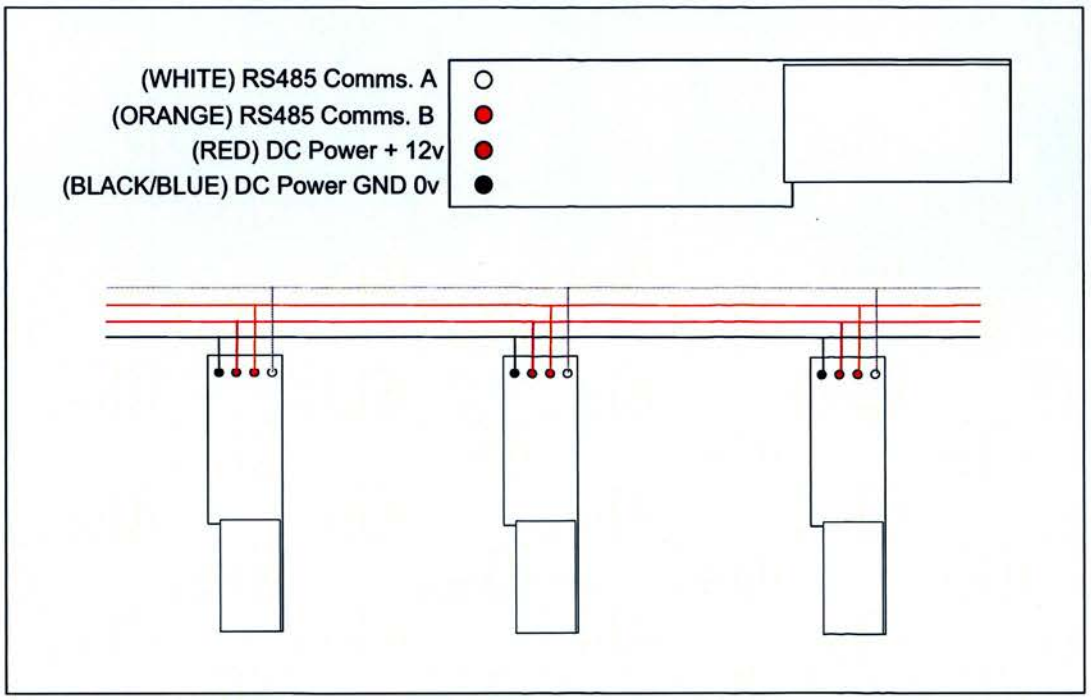

Figure 6.7. Sensor wiring diagram

Table 6.1. Summary of laboratory cable specifications.

Outer Material	Cores	Core Diameter	Construction	Tensile Member	Outer Diameter	Density	Price
flex.TPE	8	0.25sqmm	twisted	polymer	6.5mm	40kg/km	Ĩ.30GBP/m

(a) Rendering of PVC pods based on the CAD designs and model.

(b) Photograph of constructed PVC pods and surrounding floats (coloured tapes used for identification purposes).

Figure 6.8. Sensor packages as supplied by Measurand Inc.

Figure 6.9. Selected cable for laboratory sensor ribbons and arrays.

Summary of cable properties:

- Designed for harsh environment moving robotic assemblies
- TPE Outer - Flexible, High resistance to UV, bio-oils and oils
- Flexible Conductors
- Central element for high tensile stress

6.2.2 Floatation

Along-cable buoyancy was provided by Divynacell floats cut into 150mm x 100mm x 100mm blocks from a 1000mm x 1000mm x100mm pre-laminated board. A 25mm diameter hole was bored into which the PVC canisters could be inserted. The corners

of the cuboids were chamfered and the floats were then cut in half along a plane parallel to the water surface on which they would float.

The floats were designed to be quick and easy to manufacture and to allow fast assembly and disassembly (hence being constructed in two halves rather than being threaded on from one end of the sensor ribbon to the other). The final floatation jackets can be seen in figure 6.8b.

6.2.3 Waterproofing

The bare-board printed circuit boards (PCBs) supplied by Measurand required integration into a waterproof housing. After several design iterations it was decided to encapsulate the PCBs in a suitable resin and then to insert this encapsulated board inside a waterproof canister. There are two major methods of making waterproof bare PCBs: potting and encapsulation. Both involve surrounding the bare PCB with a liquid which will set when exposed to air, a hardening agent, heat, UV light or a combination of these. Various factors affect the choice of resin to use including the tolerance of the electronic components to heat (during exothermic setting), the required level of waterproofing, thermal resistance, electrical resistance and tolerance to electro-magnetic interference. Weight, hardness, flexibility, pricing, tooling and the possibility of re-entry/access for repair work are other important factors.

Potting differs from encapsulation as a container is used to mount the PCB within and once filled with the resin this container becomes physically attached to the board. A common example of this is in joining cables together in the field where a cigar shaped plastic tube with two holes for resin filling becomes part of the overall assembly.

Encapsulation involves moulds and, when set, the resin-surrounded PCB is removed from the mould. Encapsulation was chosen since a primary consideration in this work is weight minimisation and to allow interfacing with the power/data cable and the PVC outer canisters. There is a science and technique to creating well finished encapsulations. Many factors effect the final product including:

- The design of the mould: clearances, finish, construction material, pitting

- The release agents used: silicon, wax, liquid, aerosol etc.
- The method of applying release agents, coverage and thickness
- Temperature: mixing consistency, usability window and setting time/finish
- Bubbles - a major source of encapsulation problems
  - formed during mixing of chemicals and pouring
  - bubble escape and reformation during setting affected by temperature, viscosity and mould design
  - applying vacuum to mix before pouring can be essential

After advice from epoxy coating companies and extensive and time consuming trials a product supplied from Robnor Resins was selected. This polyurethane based mixture comes as two separate liquids (pre-weighed) and was mixed in a large container before being put in a vacuum jar for approximately 1 minute. It was then poured using piping bags into the mould apertures in one corner (minimising air entrainment and allowing any air build-up to escape up the other side of the PCB. Once set after 24 hours, the encapsulated sensor feels like tough rubber, being slightly flexible but extremely resistant to abrasion. With the vacuum stage included, the failure rate (excessive bubble density and/or distribution) reduced from 1 in 12 encapsulated sensors to 1 in 48 compared to moulding without vacuum. Alignment of the PCBs inside the mould chambers was a fiddly process, requiring the boards to be free from all of the faces of the mould with a gap of only a few mm. Thick solder wire was used to suspend the PCBs into the cavities due to its ability to be bent and then maintain its shape. Figure 6.10 shows the aluminium moulds produced on a 3D computer controlled milling machine and the PCBs pre-encapsulation. Ejector bolts were used to push apart the two halves of the mould once the resin had cured completely. A special plastic tool was machined to help release the PCBs from the mould whilst minimising bending of the sensors and hence minimising the risk of sensor board damage.

When trialling various resins, actual sensor PCBs could not be used for cost reasons. Dummy PCB's were constructed from PCB base boards and various ubiquitous chips

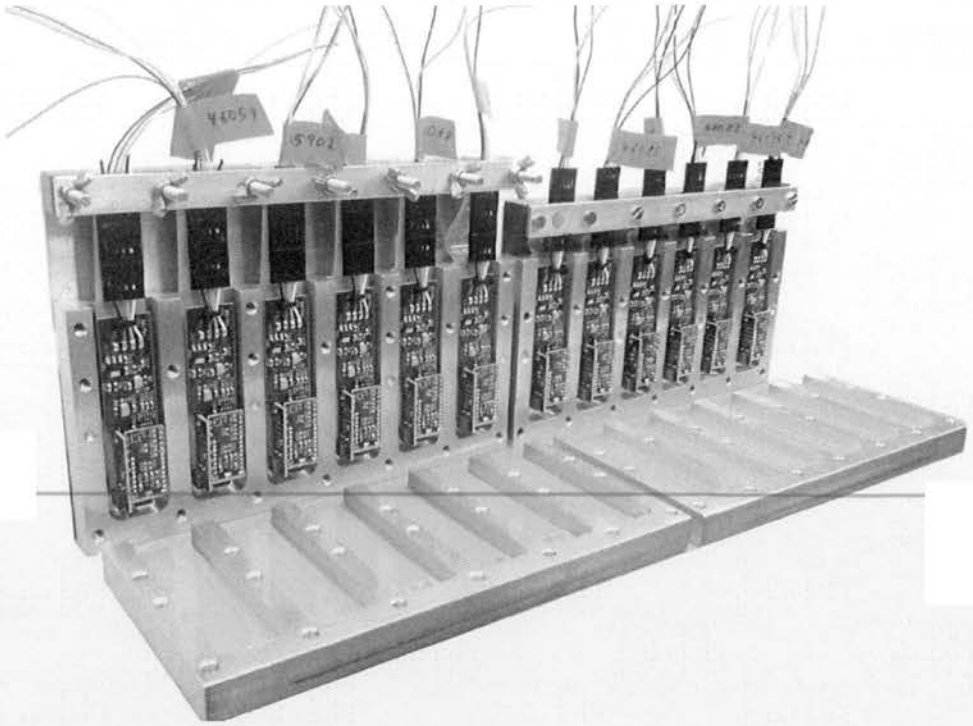

Figure 6.10. Aluminium moulds for sensor encapsulation. First trial plastic mounts (as shown in black) later replaced with solder wire pegs

were glued on to simulate the roughness and void density of the actual sensors. These dummy chips proved useful for assessing the performance of the resins and also the design of the aluminium moulds. As a result of this testing the moulds and mounting methods were changed. The original test mould and dummy PCBs can be seen in figure 6.5.

6.2.4 Termination, Power Supply and Data Communication

Measurand use small (approximately 150mm x 100mm x 25mm) "Windows CE" ™machines to interface with their sensors. These machines can send data to software applications via ethernet or wireless. A customised version of these was produced named DL16 for this project which accepts up to 16 different sensor ribbons. The DL16 communicates with the sensors using RS232 protocol, therefore converter boxes are required between the RS485 operating sensors and the DL16. These were also designed and supplied by Measurand. Fuses of an appropriate rating (dependent on sensor configuration) were added in line with the power line during testing.

Power was delivered to the sensors via the DL16 RS232 connections and continued through the RS485 converters.

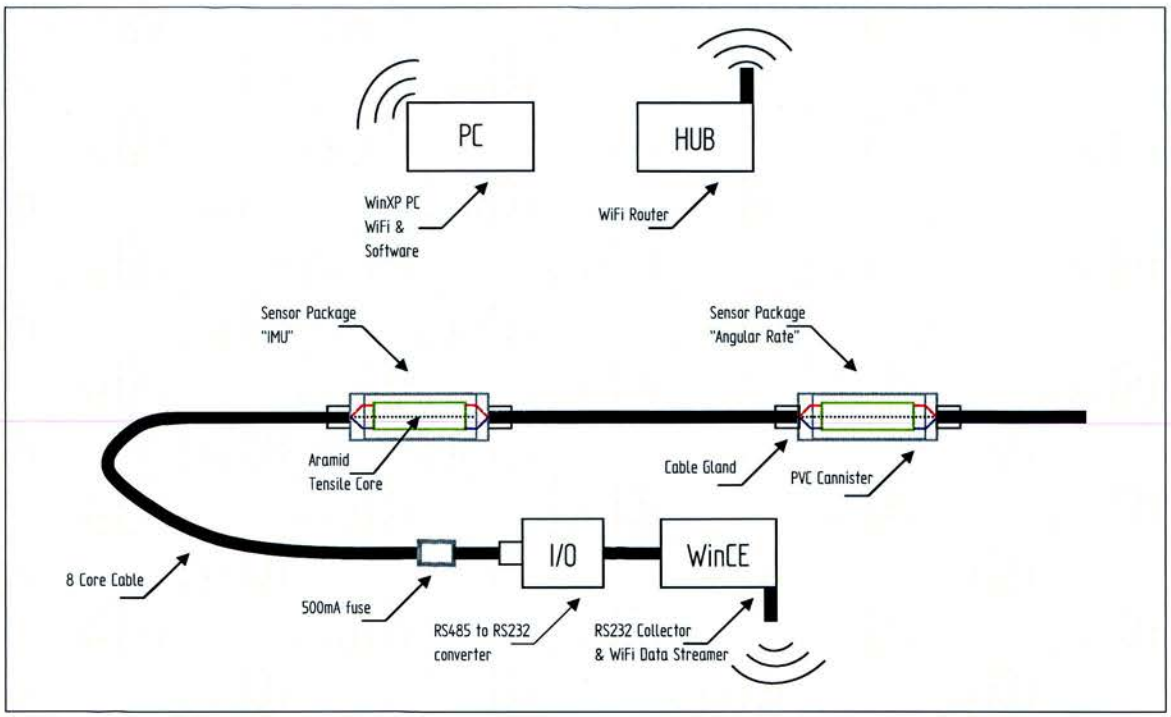

Figure 6.11. Schematic showing WaveTape configuration and communication process.

6.3 Testing at the GWK, Hannover

The following section outlines tests conducted at the Grosse Wellenkanal (GWK) hydraulic laboratory at Hannover Germany, one of the largest wave flumes in the world at 300m long, 7m deep and 5m wide. Figures 6.14, 6.15 and 6.16 show photographs of the ribbon sensor installed in the test facility.

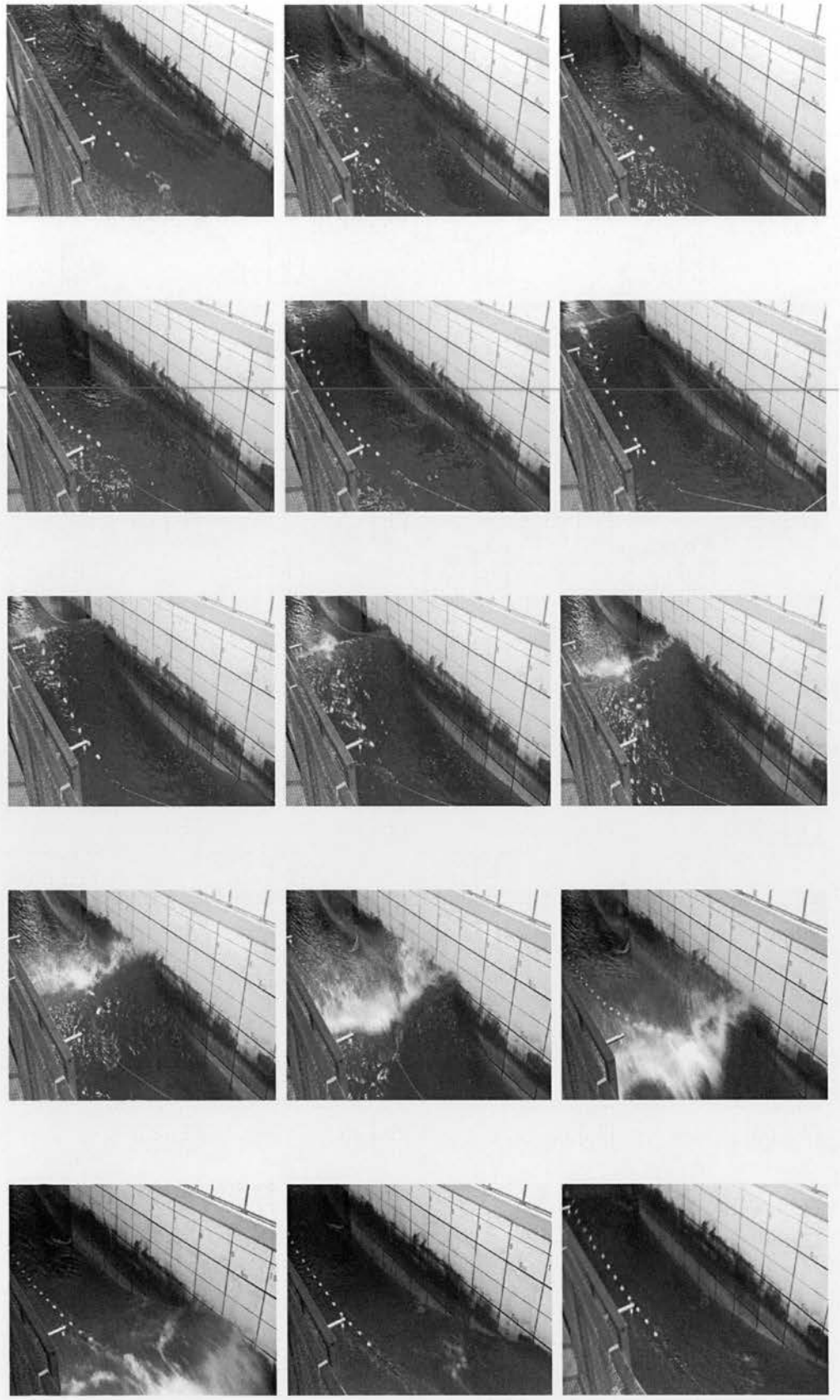

Figure 6.12. Frame grabs of GWK test footage. 1.5m (approx.) breaking wave. Flume wall grid shows 0.5m divisions.

6.3.1 Motivation

During 2009 the opportunity arose to assist in a European Union HydraLab III Project being conducted at the Grosse Wellenkanal (GWK), Hannover Germany [119]. Capable of producing regular, irregular and focused waves at scales of one quarter and above this facility provided an environment well suited for testing the robustness of the new cable-based design. Priority was given to programme's central research area, investigating the impact forces experienced by a model bridge element. Testing of the sensor ribbon was undertaken on an opportunity basis around this main investigation thus ribbon sensor tests were not extensive.

6.3.2 Experimental Procedure

A suitably scaled ribbon configuration was designed and constructed to meet the testing window at GWK [2]. The ribbon comprised two full IMU type sensor packages at the head and tail ends with 21 ARS in between, spaced 0.75m apart, totalling a sensing length of 18m. A 7m flying lead was included to allow for power and communications connection. Sensor assembly is shown in figure 6.13.

Unlike the laboratory scale and array sensor units, testing at this scale and under these forces required a new approach to construction. The tensile member of the "Chainflex CF9" cable needed to be continuous throughout the sensor ribbon, with each sensor package wired into the cable with the surrounding PVC enclosures pre-threaded on to the cable. This ensured that the cable glands and internal electrical connections do not experience excessive axial and perpendicular forces. The roles of the components in the pods for this deployment were thus separated: the central tensile member of the cable took the strain; the gable gland rubber maintained the sealing between cable and pods; and the end caps of the pods - which were unthreaded - maintained the watertight compartment.

Due to the nature of assisting in the testing programme at GWK, the test matrix or testing schedule could not be influenced. This meant conducting trials on-the-

[2] At short notice and with the assistance of Terry Patterson, Murray Simpson and Gordon Sellar

(a) Preparing the 18m GWK sensor - insertion and wiring of moulded sensors

(b) Preparing the 18m GWK sensor - closing of end-caps, electrical dry-tests and labelling

Figure 6.13. Sensor construction prior to testing at GWK, Hannover.

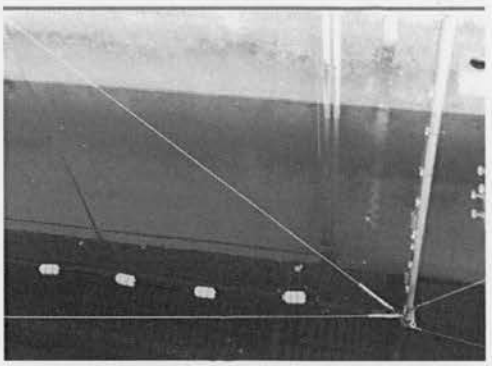

(a) Sensor mounting technique in GWK. Steel scaffold bar with tensioning wires secured to flume rails.

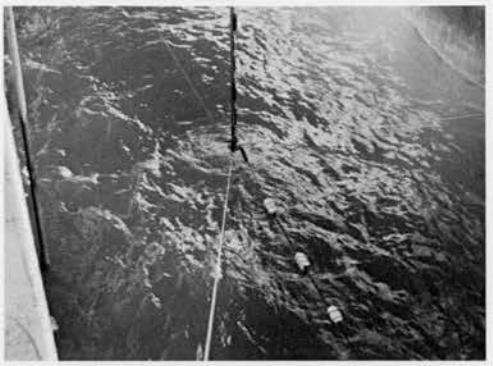

(b) Sensor mounting during wave flume operation

Figure 6.14. 1/4 scale sensor during testing at GWK, Hannover.

fly as opportunities arose and in parallel to the other tasks required in the main project. This lead to the ribbon being exposed to some very extreme waves early in the experiment.

6.3.3 Results

All of the results from the GWK facility are qualitative and come from observing the sensor's behaviour during testing, analysing the video footage and inspecting the sensor after testing. In addition, valuable knowledge was gained relating to the

Table 6.2. Test matrix of waves used at GWK facility with sensor ribbon installed.

Wave Type	Peak wave period (s)	Significant wave height (m)	Expected max wave height (m)
Focused	3.4		1.51
Focused	3.4		1.51
Focused	3.4		1.51
Regular	3.4	0.9	
Regular	6.7	0.9	
Regular	3.4	1.1	
Regular	5.6	1.1	
Regular	3.4	1.1	
JONSWAP	4.5	0.9	1.48
JONSWAP	5.6	0.9	1.45
JONSWAP	6.7	0.9	1.43

logistics of sensor transport, installation and commissioning.

Survivability

Given the lack of previous trials in these conditions, care had to be taken to reduce the risk of damaging the sensor on any given test run. Initially the mooring tension on the sensor was deliberately set at a minimum. Consisting of approximately 0.2kg on a 10mm diameter polymer rope which was hung over another plastic rope connected across the width of the flume. This small amount of tension held the sensor ribbon longitudinally down the tank in still water but provided little resistance to the ribbon when exposed to wave crests and troughs. As confidence increased, a test was conducted with more substantial mooring tension of approximately several kilograms. This one hour long irregular wave condition had a peak period of 4.5 seconds and significant wave height of 0.9m.

6.3.4 Discussion

Having been in the water for 3 days and exposed to the wave attacks summarised in table 6.2 the cable was then retrieved and inspected. Of the 184 pre-encapsulation soldered connections none failed. Of the 184 (individually ferruled) screw terminal

Figure 6.15. Ribbon testing at GWK, Hannover

connections, none failed. During the first test the wireless connection between the DL16 and a data acquisition PC failed. Investigation revealed that the most likely cause was that the control equipment had overheated and rebooted. The GWK facility reached temperatures of over 40 $^{\circ}$ C during testing in the hottest weather for a decade. With the lid of the control box (which protected the DL16 from splashing) opened no further interruptions were experienced.

Having reviewed the video footage the extent of cable "snatching" at the point of sensor attachment to the vertical pole (as seen in Figs. 6.14a and 6.14b) was concerning. This not only puts unwanted forces on the cable but since the first sensorised pod lies in close proximity to this point the motion it records is not indicative of the passing wave. A much longer (of order several metres) of flying lead would be an improvement but was not possible in-situ due to the design of the sensor and the selected water depth which left a large distance to the DL16 housing. At the concept stage of the project it was conceived that in any large hydraulic test facility or in the open sea the sensor would be attached to a floating platform, e.g., a buoy which would greatly reduce the fixed point attachment snatching dynamics. The

(a) Frame grab number 1

(b) Frame grab number 2

(c) Frame grab number 3

(d) Frame grab number 4

Figure 6.16. Frame grabs of video footage of sensor responding to waves at GWK, Hannover.

development of an attachment buoy is briefly outlined in Appendix B.

Whilst the addition of a buoy adds expense, presents the same challenges in deployment and operation as a standard measurement buoy and incorporates their limitations, a working system would provide tens to hundreds of measurement points compared with the standard single "point" measurement provided by an off-the-shelf wave measurement buoy.

With the limited control of the testing environment and the limited time to deploy and operate the sensor it is difficult to conclude on the importance of the poor data recovered. The tests did highlight how critical mooring is to the ability of a single ribbon to track the water surface. Certain long waves had a wavelength more than double than the length of the sensor. In these cases the sensor would either fall down the rear of a passing crest, collapsing like a concertina or be pulled taught down the front face of a crest. More rigorous and controlled testing would be required to conclude on the feasibility of finding correct mooring configurations for wavelengths greater than the sensor length.

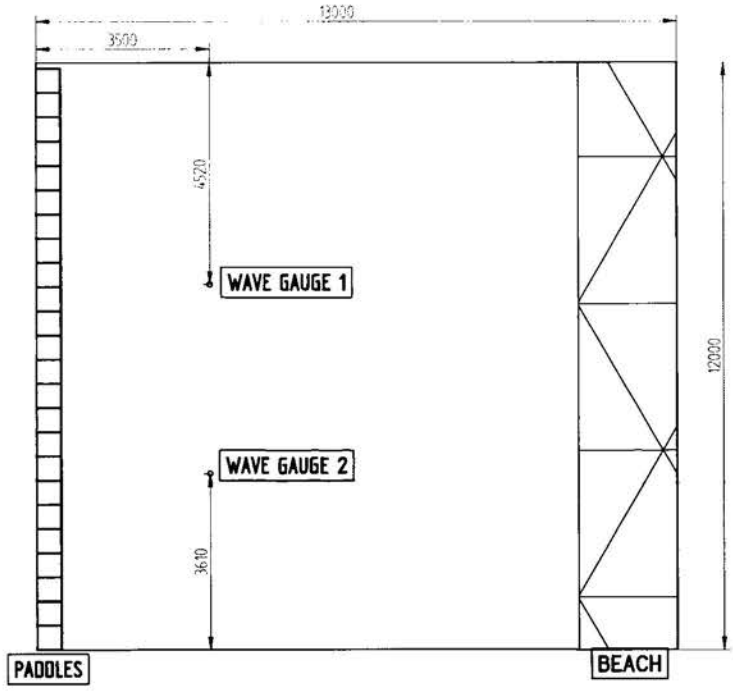

Figure 6.17. Schematic showing dimensions of Heriot-Watt Deep Basin. Dimensions in mm.

6.4 Sensor Array Testing at Heriot-Watt Deep Water Basin

6.4.1 Motivation

In December 2010 the opportunity arose to access Heriot-Watt University's deep water wave basin. At 15m by 15m and 3m deep, unlike Edinburgh's own demonstration curved tank, this basin can accommodate a reasonably sized sensor array and attached moorings. Having access to this facility allowed a first investigation in to 3D array effects such as array rotations and twists and mooring designs which could not be carried out in wave flumes or the smaller Edinburgh curved tank. Whilst exposed to short-crested irregular seas the dynamics of a modular array were monitored and component sensor outputs measured.

Throughout one week of testing the time and assistance of Heriot-Watt's Dr. Vladimir Krivstof was generously given. [3]

[3] In particular his knowledge of knot-tying (and un-tying) and dingy control proved essential.

6.4.2 Experimental Set Up

Tests were conducted in the Heriot-Watt basin which features hinged-flap type wave-maker paddles controlled via Edinburgh Designs software. Wave gauges were sampled through a custom Heriot-Watt acquisition system and the unprocessed (non-calibrated) voltage signals saved to text files. Calibration of the wave gauges was conducted at the beginning of each day after running set-up wave fields to aid mixing of conductive particles in the basin.

Array Configuration

From the available encapsulated sensor pods, connectors and peripherals a suitably sized sensor array was designed and constructed. The array comprised three identical ribbon types with sensor pod spacing of 0.35m with 10 ARS pods terminated at both sides by a full IMU pod. As IMUs are an order of magnitude more expensive than ARS units, it was not possible to fit an IMU to each sensing position. These ribbons are shown as the three central ribbons in figure 6.18. A fourth ribbon, comprising the 18m long ribbon used in the GWK tests was used to surround the central three ribbons and provide an extra two ribbon elements at the array edges. This had a sensor pod spacing of 0.75m and can be shown on the left and right edges of figure 6.19. Ribbon lateral separation was 0.7m.

Lateral Bracing and Mooring

Through a process of trial and error a cable was chosen to cross-brace the array to prevent each ribbon either narrowing or widening towards/away from the their neighbouring ribbon. The cable chosen offered a good compromise of weight and stiffness and was selected following trials in the basin of a variety of cross-bracing cabling. This process was carried out by visual inspection.

At the attachment end of the array a semi-flexible boom arrangement was implemented. This comprised four lengths of PVC tubing of the same type as used in the sensor pod canisters. The tube end-connectors were also of the same type as used

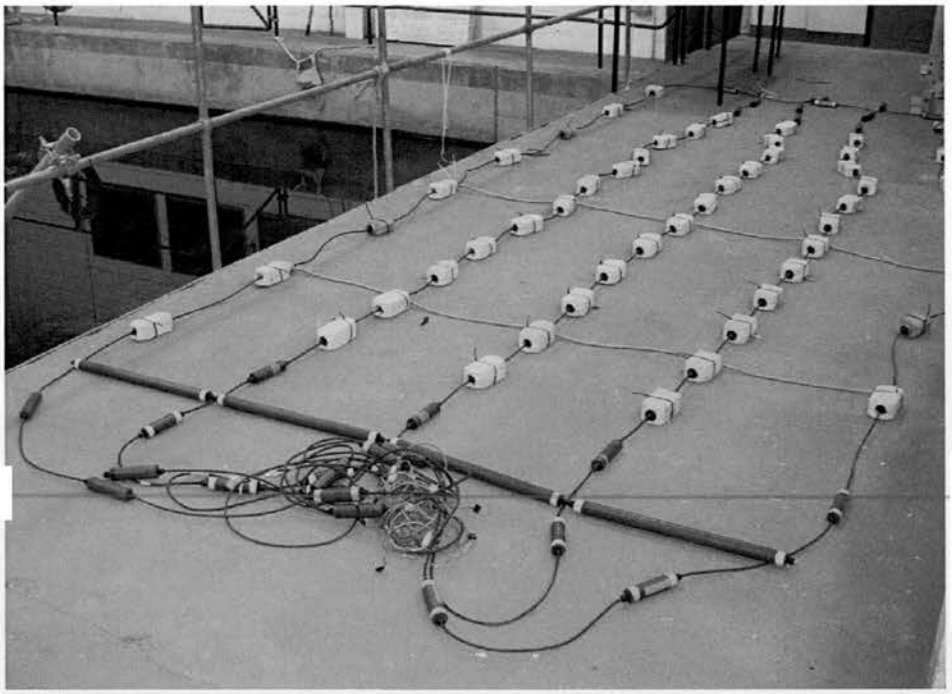

Figure 6.18. The first configuration of the MEM-based sensor array. Pre-deployment "dry tests"

in the sensor pod canisters, which made the tubing buoyant and enabled a central "spine" of cable through the tubes to act as fasteners and attachment points for the power and communication flying leads. The four beam boom was connected via two mooring lines to a central buoy approximately 1m rearward of the booms which provided the ability of the array to move in yaw.

At the downstream end of the array mooring lines were attached to the array corners and secured to the beach.

Table 6.3. Regular wave test matrix

Test #	Wave Period (s)	Wave Height (m)	Angle (deg)
1	1.00	0.08	0
2	1.00	0.14	0
3	1.25	0.08	0
4	1.25	0.14	0
5	1.00	0.08	10
6	1.00	0.08	20
7	1.25	0.08	10
8	1.25	0.08	20

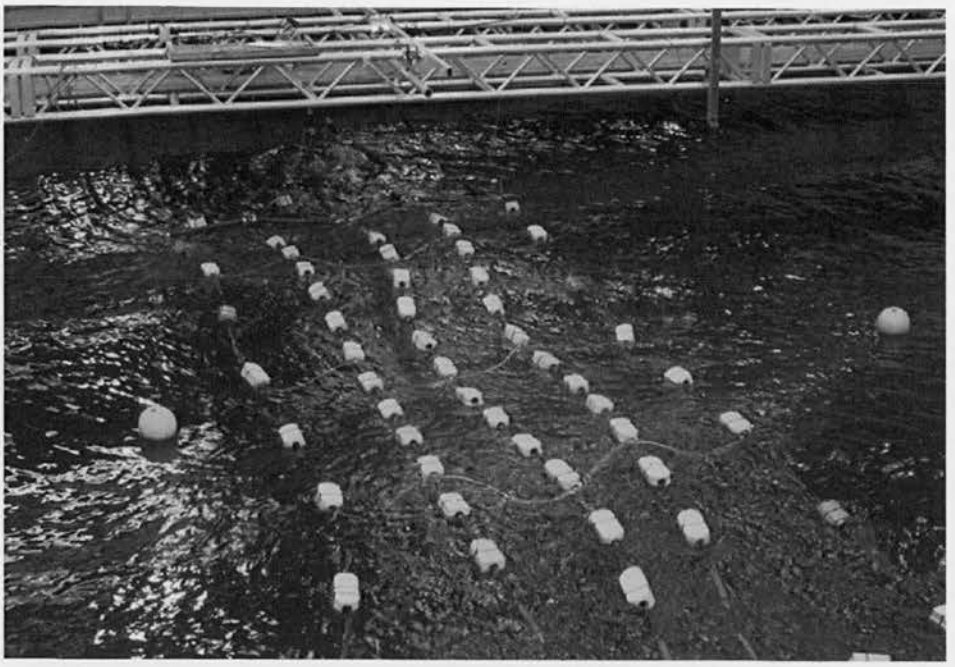

Figure 6.19. The first configuration of sensor array. Deployed "wet tests" in irregular waves.

Table 6.4. Irregular wave test matrix - Bretschneider spectra

Test #	H_m0 (m)	T_p (S)	Spreading
1	0.2	1.6	None
2	0.2	1.6	cos(72)
3	0.2	1.6	cos(48)
4	0.2	1.6	cos(24)
5	0.2	1.6	cos(12)

6.4.3 Data Processing

Data is recorded via a customised version of Measurand's software. A large amount of time was spent by Measurand on adding features to the software, that during testing, became apparent that they were required. These features included the ability to set the initial starting position of a deployed array, to automatically adjust for sensor pod misalignment (within the waterproof housings) and to programmatically update the look-up-tables for array configuration. As is typical with new software and hardware development, bugs were common.

As with the ShapeTape system, separate processing software was developed in MATLAB in parallel to the updates to the proprietary software. This was done to allow

customised post-processing and filtering of data and to enable future integration with other systems, such as WEC control strategies. Array data, exported from Measurand software as ascii "text" files, are imported into MATLAB via a custom script. For full orientation sensor pods the following parameters are imported: vertex positions x,y,z, vertex angles in x,y,z, accelerations in x,y,z, magnetic outputs in Gauss in x,y,z, angular rates in x,y,z and temperature. Angular rate-only sensor pods output no acceleration or magnetic measurements.

Alternative approaches (similar in structure to those outlined in Chapter 5) based on MATLAB Simulink and incorporating dynamic filters were trialled but are incomplete. As such, a processing routine based on the internal process of the Measurand software, implemented in MATLAB, has been reported here.

Further work is required to compare and extend various processing techniques.

Roll Calibration

Once raw data has been imported a routine uses an upsampled and smoothed portion of the angular rate data and searches the x,y,z angular rate triplets for signals that are in and out of phase with respect to each other. This stage of processing can reveal if a particular sensor pod was installed, or has become, upside down relative to its neighbours. If the phase-finder routine suspects upside down sensors, the user is alerted and the data can be manually inspected and assigned an orientation value. The next stage involves taking the rms values of the angular rate triplets and applying a rotation to the data around the longitudinal axis (wave direction). Previous knowledge of the upside-down or upright nature of the pods is used in the calculation to ensure the proper rotation matrix is used. A list of correction angles is thus created for each pod in each ribbon element of the array. Once a first estimate of each pods initial orientation in roll is made the impact of these roll corrections are tested on the dataset via cross-correlation on the angular rate data in the pitching mode. Figure 6.20 shows the results of this stage of roll calibration on irregular wave test 1, ribbon number 1. Each line shows the results of an iterative stage of testing the pods for self-alignment. A higher correlation coefficient is searched for by rotating each pod

around the longitudinal axis and comparing the output data to the previous pod. In figure 6.20 the final output data is shown by the solid black line which shows the least pod-by-pod deviation and highest level of correlation.

The final array of correction angles, found by the method above, are applied to the angular rate data for the entire test run. Whilst this method can align each pod relative to each other a reference to the global reference frame is required. Work is incomplete on making this element automatic and robust but an intermediate routine of animating the position vectors in time against neighbouring ribbons for long-crested waves quickly reveals any requirement to "flip" the entire array. Figure 6.21 shows this scenario where a ribbon has passed the self-alignment process but is clearly misaligned with its neighbouring ribbon.

Referencing to a global/laboratory frame can be achieved with the ribbon configurations used in these tests but due to insufficient time this has not been incorporated. This would be achieved, however, by using the full positioning information available from the orientation sensor pods at each end of the ribbons due to the presence of 3-axis magnetometers. These would give a dynamic "origin" whose position could be tracked in time and applied to the subsequent downstream angular-rate-only sensor pods.

Initially, the orientation of each pod, at $t = 0$, is represented by $R_{n(t=0)}$ as shown in equation 6.1.

$$R_{n(t=0)} = \begin{bmatrix} 0 & 1 & 0 \\ 0 & 0 & 1 \\ 1 & 0 & 0 \end{bmatrix} \tag{6.1}$$

Angular rate data is then transformed (via the transformation matrices in equations 6.4 to 6.6) to a matrix A, describing the change in angle from the previous time step. A is found by matrix multiplication of the changes in each direction e.g., by $A = A_x * A_y * A_z$. Due to the order of matrix multiplication being important the matrix multiplication order is periodically swapped to minimise errors. R, the orientation of the pods, is updated at each time step by matrix multiplication with the change

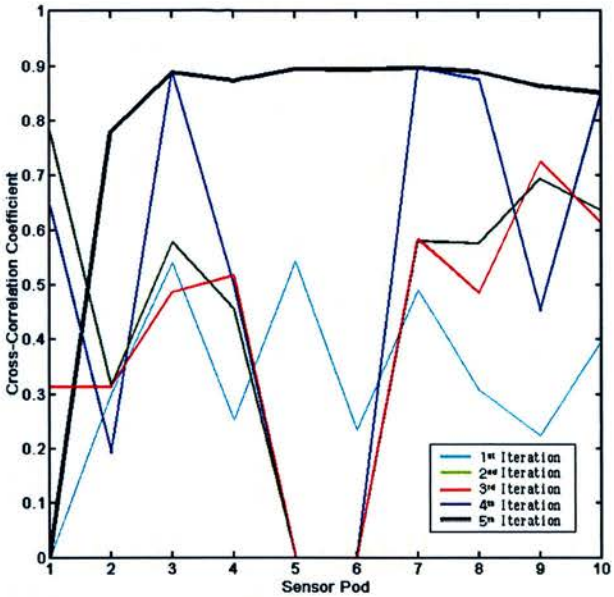

Figure 6.20. Sensor pod roll calibration. Sensor cross-correlation reveals and iteratively corrects pre-test roll offsets.

in angles in 3D space as shown in equation 6.2. The position of a sensor pod, (n), is found by the sum of the position of the upstream pod, (n-1), and the change in position over the last time step (see equation 6.3), where L is the separation of each pod. A high pass filter was then applied to the vertical and horizontal position data.

$$R_{nt} = R_{(t-1)} * A_{n(t-1,t)} \tag{6.2}$$

$$\begin{bmatrix} X \\ Y \\ Z \end{bmatrix}_{nt} = \begin{bmatrix} X \\ Y \\ Z \end{bmatrix}_{(n-1)t} + R_{nt} \begin{bmatrix} 0 \\ 0 \\ L \end{bmatrix} \tag{6.3}$$

$$A_x = \begin{bmatrix} 1 & 0 & 0 \\ 0 & \cos(\omega_x \Delta t) & -\sin(\omega_x \Delta t) \\ 0 & \sin(\omega_x \Delta t) & \cos(\omega_x \Delta t) \end{bmatrix} \tag{6.4}$$

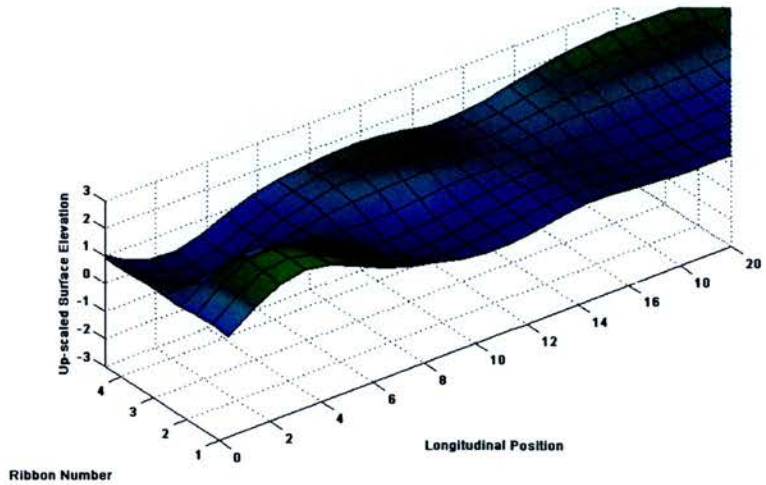

(a) Ribbon 4 is misaligned with its neighbours.

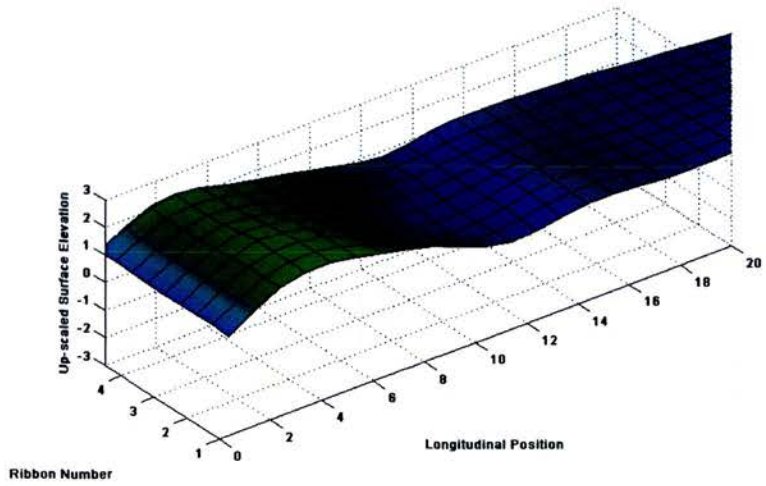

(b) Ribbon 4 rotated through 180 around the longitudinal centre line.

Figure 6.21. Manual post-processing of ribbon data. Irregular wave test number 1.

Table 6.5. WaveTape - Regular waves. Wave height error.

Mean Wave Height (m)		Error		
Wave Gauge	Wave Tape	Absolute (m)	Relative (%)	Standard Deviation of Error Across WT (%)
0.105	0.088	0.017	-15.7	6.5
0.177	0.180	-0.003	1.5	9.2
0.109	0.103	0.006	-5.9	4.9
0.172	0.186	-0.014	8.2	5.6
0.105	0.096	0.009	-8.8	5.4
0.095	0.095	0.000	-0.2	11.7
0.095	0.096	-0.001	1.4	6.0
0.090	0.097	-0.008	8.8	8.7

$$A_y = \begin{bmatrix} \cos(\omega_y \Delta t) & 0 & -\sin(\omega_y \Delta t) \\ 0 & 1 & 0 \\ -\sin(\omega_y \Delta t) & 0 & \cos(\omega_y \Delta t) \end{bmatrix} \tag{6.5}$$

$$A_z = \begin{bmatrix} \cos(\omega_z \Delta t) & -\sin(\omega_z \Delta t) & 0 \\ \sin(\omega_z \Delta t) & \cos(\omega_z \Delta t) & 0 \\ 0 & 0 & 1 \end{bmatrix} \tag{6.6}$$

6.4.4 Results

6.4.5 Regular Waves

Tables 6.5 and 6.6 show respectively wave height and wave period errors from 8 regular waves tests. Absolute and relative error is reported along with the standard deviation of the relative error across the each of the four ribbons in the array. Figure 6.22 shows surface elevation against time reported by ribbons 1 to 4 for 8 central, angular-rate only, sensor pods for the first 6 seconds of a regular wave test.

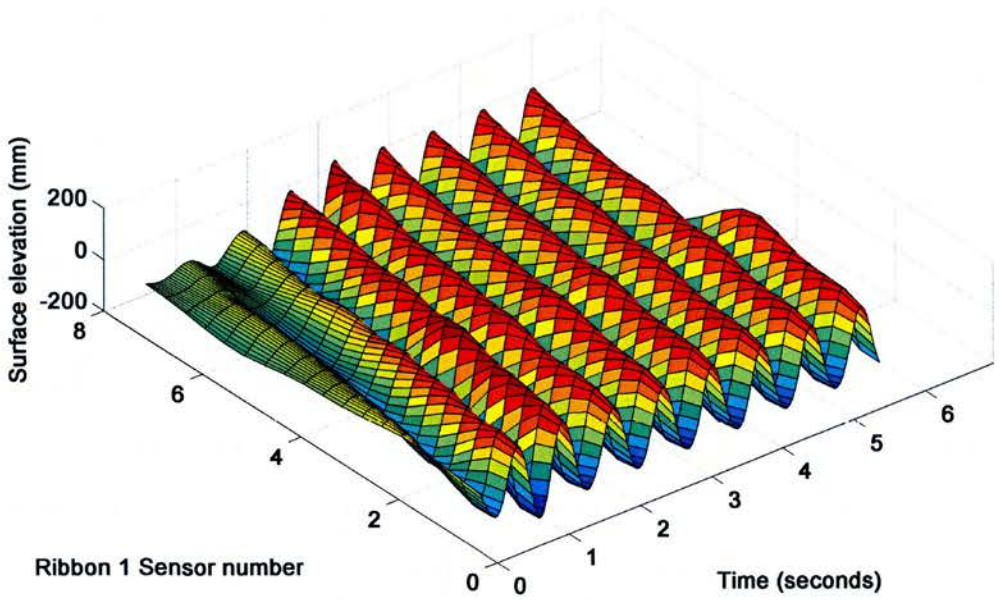

(a) Surface elevation. Ribbon 1

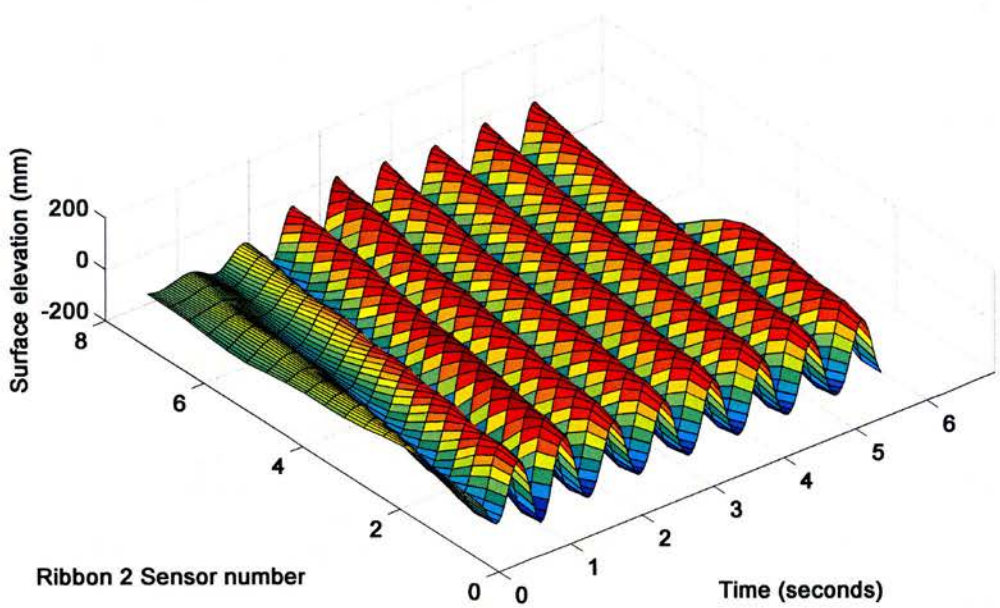

(b) Surface elevation. Ribbon 2

Figure 6.22. Surface elevation across ribbons 1 and 2 for 8 seconds of regular wave test 1.

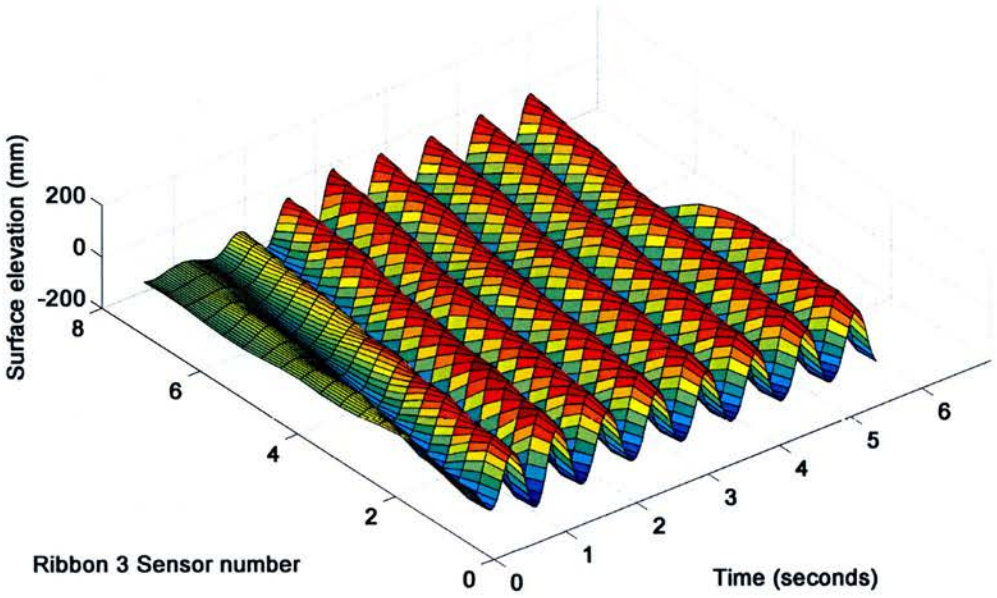

(c) Surface elevation. Ribbon 3

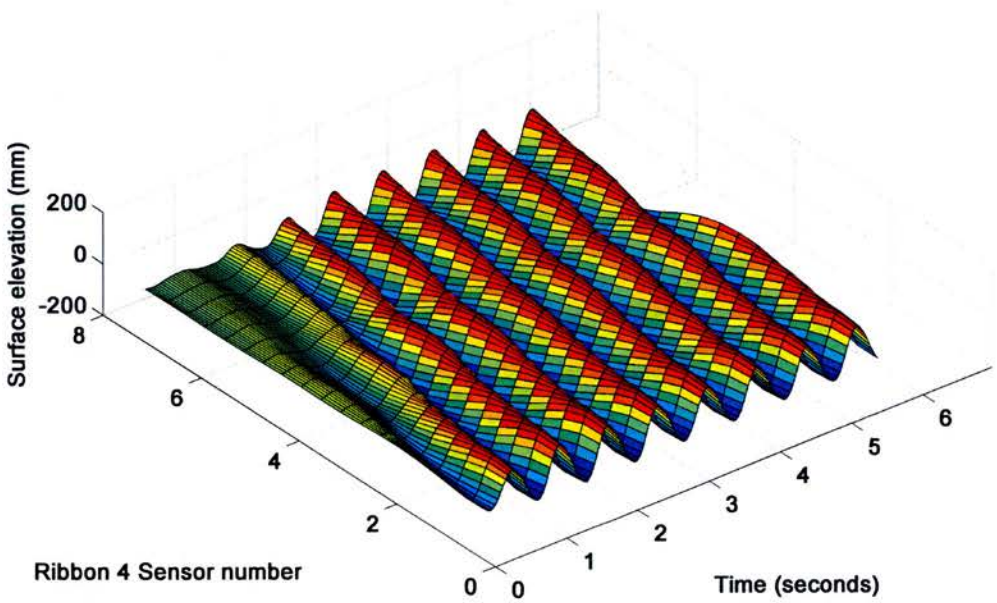

(d) Surface elevation. Ribbon 4

Figure 6.22. Surface elevation across ribbons 3 and 4 for 8 seconds of regular wave test 1.

Table 6.6. WaveTape - Regular waves. Wave period error.

Mean Wave Period (s)		Error		
Wave Gauge	WaveTape (WT)	Absolute (s)	Relative (%)	Standard Deviation of Error Across WT (%)
1.00	1.00	0.00	0.13	0.11
1.01	1.00	0.00	-0.32	0.22
1.25	1.25	0.00	0.11	0.13
1.25	1.25	0.00	0.17	0.16
1.01	1.00	0.00	-0.16	0.19
1.00	1.00	0.00	0.04	0.20
1.25	1.25	0.00	-0.31	0.10
1.25	1.25	0.00	0.01	0.08

Irregular Waves

Tables 6.7 and 6.8 show results from frequency domain analysis of the irregular wave tests. Brett-Schneider wave spectra were used with H_{m0}, T_p and spreading parameters shown in table 6.4. Table 6.7 reports T_p as measured by a local wave gauge and T_p found by taking the average peak period result from four evenly distributed pod positions along each ribbon of the sensor array. Table 6.8 reports H_{m0} as measured by a local wave gauge and H_{m0} found by taking the average significant wave height result from four evenly distributed pod positions along each ribbon of the sensor array.

Figure 6.23a shows H_{m0} found by the array compared to H_{m0} reported by wire resistance wave gauges across all five irregular wave tests and all four ribbon elements of the array. Each value of H_{m0} is the average of all pods in a ribbon. There appears to be a trend of increased H_{m0} for ribbon 4. This should be investigated further.

Figure 6.23b shows T_p found by the array (averaged as above) compared to T_p reported by wire resistance wave gauges across all five irregular wave tests and all four ribbon elements of the array. There is possibly a trend of central ribbon elements reporting longer wave periods. Again, this should be investigated through further testing.

Figure 6.24 shows surface elevation against time reported by ribbons 1 to 4 for six central, angular-rate only, sensor pods for the first eight seconds of a irregular wave

test number 1.

Figure 6.25 shows twelve frames of a MATLAB animation showing the spatial evolution of the measured wave field in time in 0.2 second intervals. Surface position data in the vertical direction has been multiplied by a gain of approximately ten to enhance the visibility of the waves.

Whilst time domain methods of analysing the 3D wave field were trialled they are not complete and due to time constraints only frequency domain analysis can be reported.

Figure 6.26 shows directional wave spectra produced using the MATLAB Directional Wave Spectra Toolbox Version 1.4 (DIWASP) toolbox for all five irregular wave tests. These spectra were produced using the extended maximum entropy principle (EMEP) having first been produced using the more basic direct Fourier transform method (DFTM) having taking guidance from the DIWASP user manual and relevant literature (see [59, 60, 120, 25]).

Frequency resolution was set to 0.025Hz and directional resolution to 3°. Generally, these figures show directional spreading to be increasing with test number as expected with the exception of figure B.4b.

6.4.6 Discussion

Two issues were encountered in the Heriot-Watt tests - during dry-testing of the array and wet testing on the penultimate day - which impacted on the test programme. The first involved a persistent software crash which meant no data acquisition could be conducted. After extensive troubleshooting the fault could not be found and Measurand Inc. were contacted. Within a day their software engineer, Murray Simpson, had isolated the problem and uploaded a fix. The problem was due to the unprecedented number of sensors that had been attempting to communicate with the Measurand software. The second issue was less difficult to troubleshoot; a central wave-maker paddle failed. The powerful springs which counter the hydrostatic force of the water on the paddle returned home suddenly when the wire cable snapped. Testing was abandoned and the tank would remain out of action until February

Table 6.7. Summary of error in T_p. Irregular wave tests 1 to 5.

Test #	Sensor Element	T_p (s)		Error	
		Wave Gauge	Wave Tape	Absolute (s)	Relative (%)
1	Ribbon 1	1.60	1.53	0.07	-4.1
	Ribbon 2	1.60	1.59	0.01	-0.6
	Ribbon 3	1.60	1.58	0.02	-1.2
	Ribbon 4	1.60	1.56	0.04	-2.3
2	Ribbon 1	1.60	1.52	0.08	-5.1
	Ribbon 2	1.60	1.60	0.00	0.0
	Ribbon 3	1.60	1.60	0.00	0.2
	Ribbon 4	1.60	1.55	0.05	-3.0
3	Ribbon 1	1.58	1.51	0.07	-4.3
	Ribbon 2	1.58	1.61	-0.04	2.5
	Ribbon 3	1.58	1.61	-0.04	2.4
	Ribbon 4	1.58	1.55	0.02	-1.6
4	Ribbon 1	1.60	1.56	0.04	-2.4
	Ribbon 2	1.60	1.62	-0.02	1.3
	Ribbon 3	1.60	1.62	-0.02	1.3
	Ribbon 4	1.60	1.54	0.06	-3.6
5	Ribbon 1	1.58	1.55	0.03	-1.9
	Ribbon 2	1.58	1.57	0.00	-0.3
	Ribbon 3	1.58	1.55	0.02	-1.5
	Ribbon 4	1.58	1.53	0.05	-3.0

Table 6.8. Summary of error in H_{m0}. Irregular wave tests 1 to 5.

Test #	Sensor Element	H_{m0} (m)		Error	
		Wave Gauge	Wave Tape	Absolute (s)	Relative (%)
1	Ribbon 1	0.21	0.20	0.01	-5.5
	Ribbon 2	0.21	0.20	0.01	-6.4
	Ribbon 3	0.21	0.19	0.02	-8.1
	Ribbon 4	0.21	0.20	0.01	-3.6
2	Ribbon 1	0.21	0.20	0.01	-4.7
	Ribbon 2	0.21	0.20	0.01	-6.7
	Ribbon 3	0.21	0.20	0.01	-7.0
	Ribbon 4	0.21	0.21	0.00	-2.3
3	Ribbon 1	0.21	0.21	-0.00	1.1
	Ribbon 2	0.21	0.22	-0.01	3.3
	Ribbon 3	0.21	0.22	-0.01	6.5
	Ribbon 4	0.21	0.24	-0.03	15.3
4	Ribbon 1	0.21	0.20	0.01	-6.2
	Ribbon 2	0.21	0.20	0.01	-4.6
	Ribbon 3	0.21	0.21	0.00	-0.9
	Ribbon 4	0.21	0.23	-0.02	8.3
5	Ribbon 1	0.22	0.19	0.03	-13.6
	Ribbon 2	0.22	0.18	0.04	-17.4
	Ribbon 3	0.22	0.20	0.02	-10.5
	Ribbon 4	0.22	0.23	-0.01	2.6

2010. Figure 6.27 shows the missing paddle which without the restoring force of the stretched spring has given in to the pressure of the basin's water.

Despite these experimental issues, testing at Heriot-Watt was very informative as were tests carried out at other facilities which offered test features not available within the University of Edinburgh. Additional tests, carried out on individual components of the array would prove useful along with designing and assessing processing routines which would benefit from testing in highly controllable small-scale wave flumes. A large proportion of the test programme was allocated to system design, equipment procurement and to the integration of all of the various sub-systems.

In terms of mechanical performance, visually, the sensors constructed of cable-joined-elements, as opposed to flat ribbons, track the water surface well. Tests should be conducted on the MEM based system in the flume with the optical tracking system in place to quantify the surface tracking ability. As with the optical fibre-based system, the effects on sensor performance of floatation-jacket design, levels of buoyancy, cable construction and array configuration, whilst incorporated, were not fully-optimised. It was expected and observed that mooring design plays a significant role in array response. A variety of simple solutions were found to work in the laboratory but further work is needed to find suitable mooring solutions as array scale increases.

The limited testing at the GWK facility gives confidence in the robustness of long, thin floating sensor arrays. Encouragingly, subsequent design and fabrication of a fully-marinised 1/4 scale ribbon and the relative ease with which it was constructed using standard offshore cable industry practices gives further confidence in the concept.

Sensor ribbon number 4[4], whose spatial separation differs from ribbons 1 to 3, appears to require more care when post-processing, particularly if interpolation methods are used to transform the dynamic sensor pod positions to a fixed laboratory reference frame. In addition, the greater separation of the sensor pods likely introduces increased errors. More work is required on testing the ability to operate mixed-sensor density systems and to incorporate data interpolation within any

[4]In order to increase the footprint of the array the sensor ribbon designed for testing at the GWK facility was used to "surround" the identical three central ribbon arrays. This involved ribbon 4 being placed alongside ribbon 1, turned 90 degrees at the foot of the array, turned a further 90 degrees at ribbon 3 and then following back to the head of the array, parallel to ribbon 3.

configuration.

6.4.7 Conclusions

A summary of the sensor's performance during preliminary tests is listed below:

Regular Waves

Preliminary testing of the MEM-based sensor ribbons (in array form capable of measuring position in three dimensions) show mean wave height error across all regular wave tests of -1.3% with standard deviation of 8.4%. Across the length of the ribbons themselves, the mean standard deviation in relative error was 7.25%. Wave period errors were small at less than 0.1% relative error with a relative standard deviation of less than 0.2% and mean standard deviation along the length of the ribbon of less than 0.2%.

Irregular Waves

In irregular waves, mean significant wave height is under-predicted, across a range of directional seas, by 3% with standard deviation, across the tests and individual ribbons forming the array, of 7.5%. Peak wave period is under-predicted by 1.3% with standard deviation of 2.2%.

Preliminary direction wave analysis shows promise with the trend of increasing wave spreading highlighted by the directional spectra. More work is needed to assess the sensitivity of directional wave analysis to the configuration of instrument array used as an input since the floating array offers the ability to input over forty wave slope and wave elevations and for computational reasons with the methods used here this must be reduced to a sub-set of the available data.

It has been shown that MEM-based sensors can be incorporated onto thin, long and flexible, cable-based elements and made sufficiently waterproof and robust to allow laboratory based experimentation on their ability to track water waves. Whilst testing on these systems has been limited, the results of a basic data processing technique

suggest that further work in assessing their performance as a wave-measuring sensor system is merited.

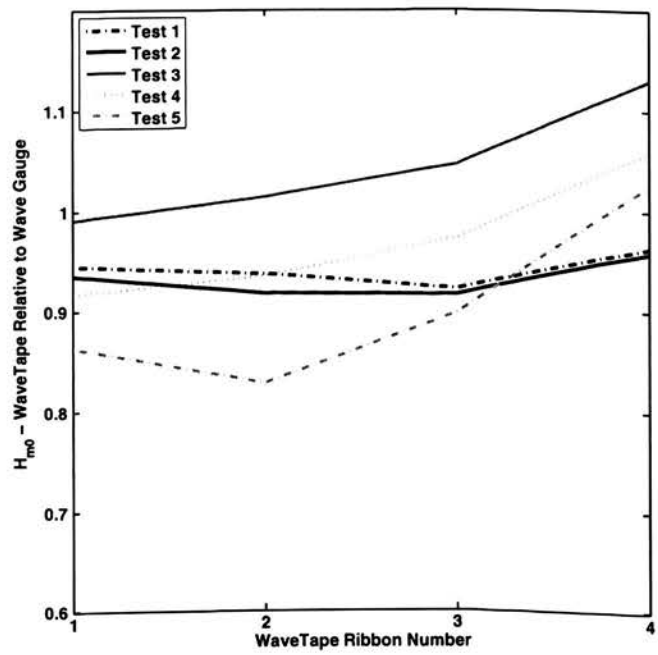

(a) Variation of H_{m0} across WaveTape array for irregular tests 1 to 5

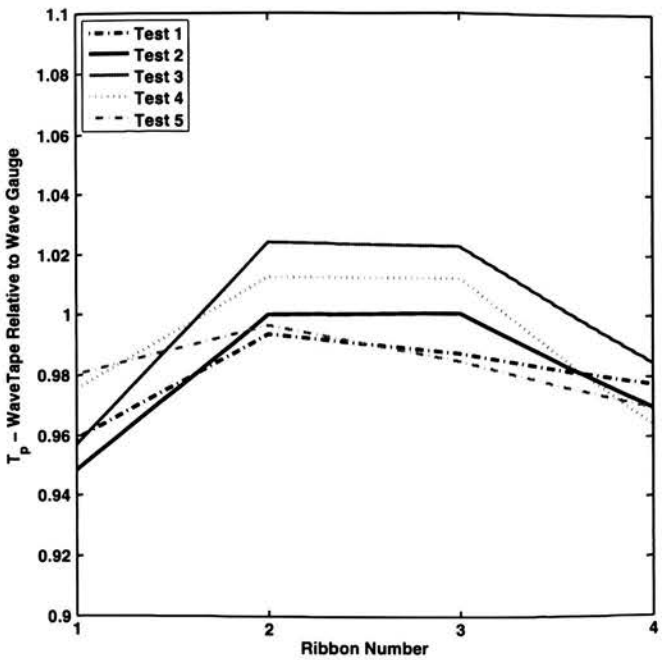

(b) Variation of T_p across WaveTape array for irregular tests 1 to 5

Figure 6.23. Variation of H_{m0} and T_p across WaveTape array for irregular tests 1 to 5

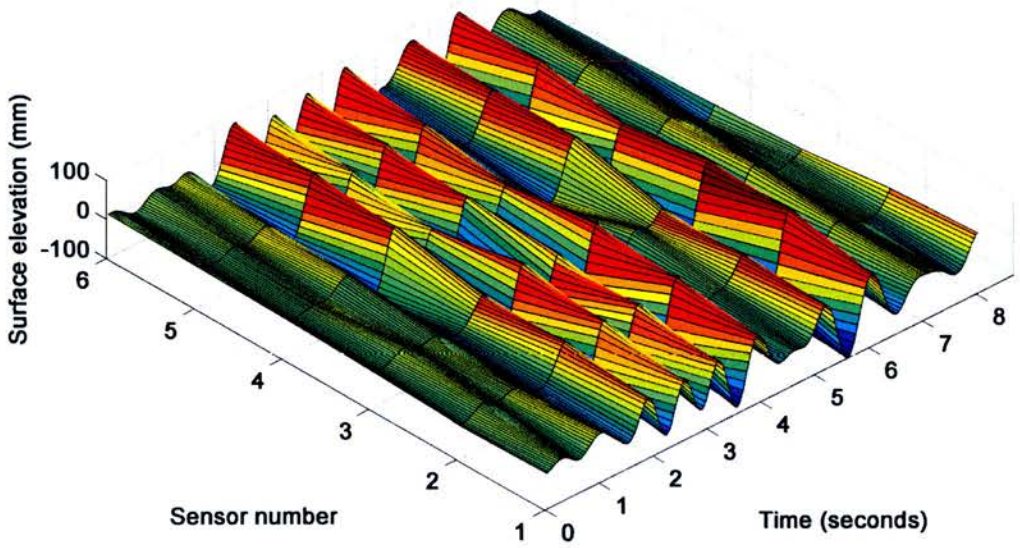

(a) Surface elevation. Ribbon 1.

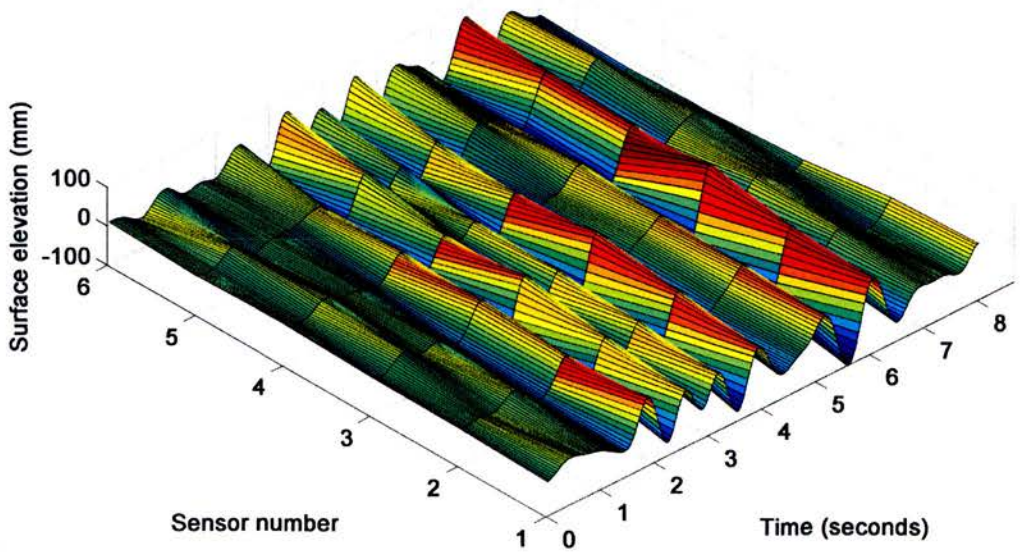

(b) Surface elevation. Ribbon 2.

Figure 6.24. Surface elevation across ribbons 1 and 2 for 8 seconds of irregular wave test number 1

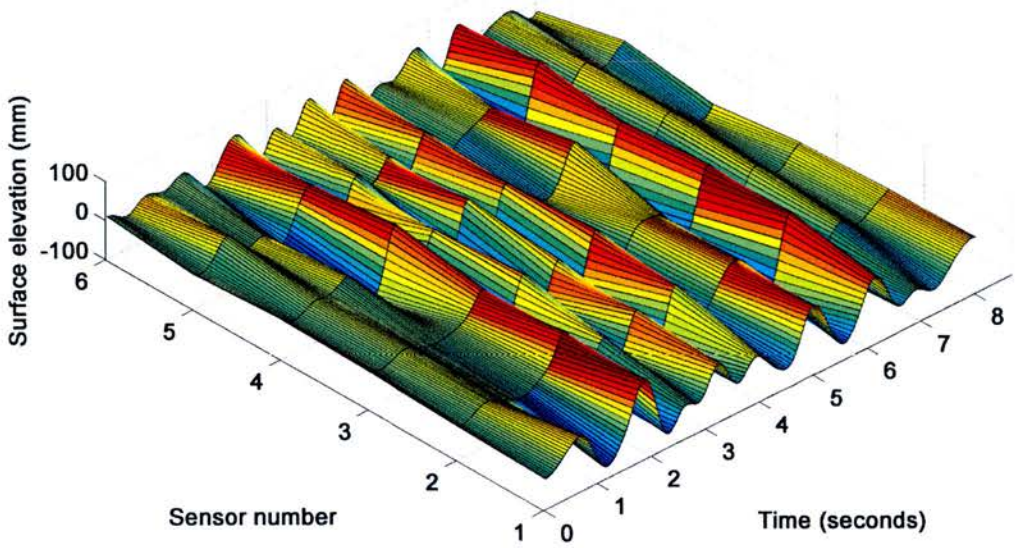

(c) Surface elevation. Ribbon 3.

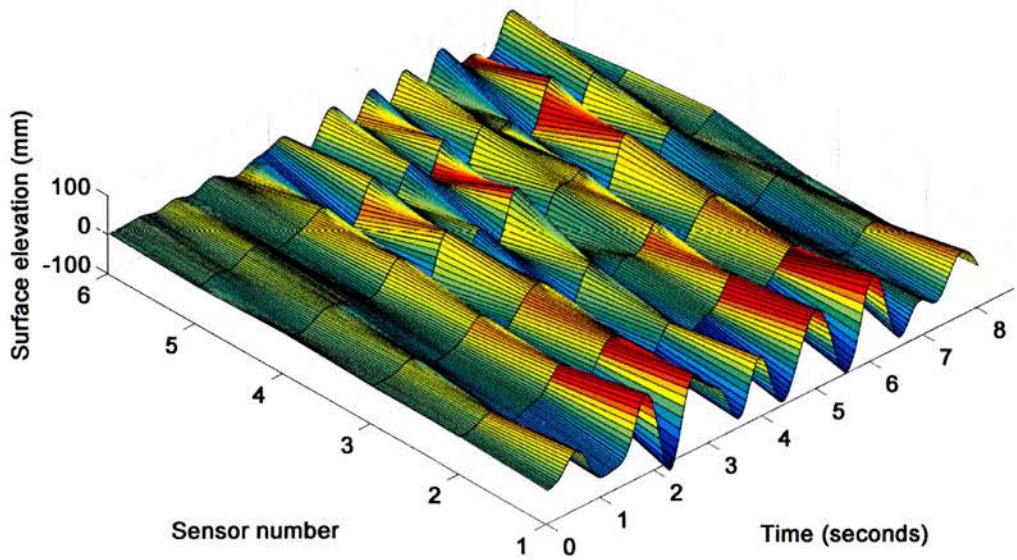

(d) Surface elevation. Ribbon 4.

Figure 6.24. Surface elevation across ribbons 3 and 4 for 8 seconds of irregular wave test number 1

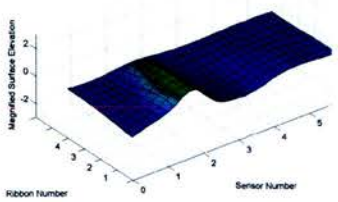

(a) time=4.72s

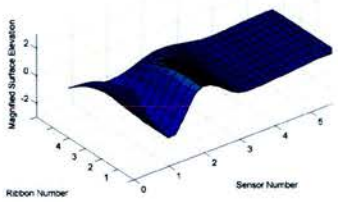

(b) time=4.88s

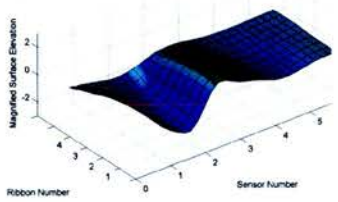

(c) time=5.04s

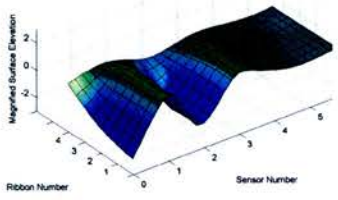

(d) time=5.20s

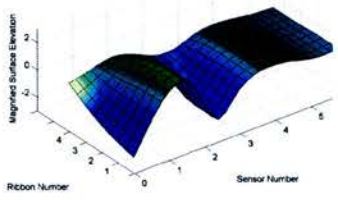

(e) time=5.36s

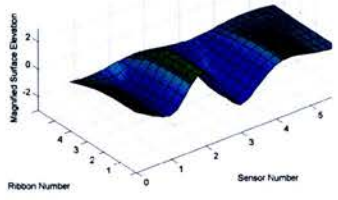

(f) time=5.52s

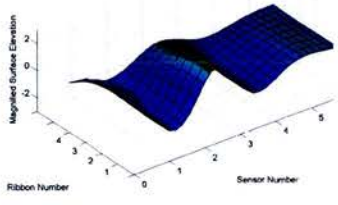

(g) time=5.68s

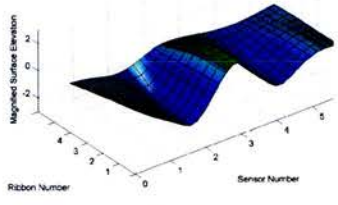

(h) time=5.84s

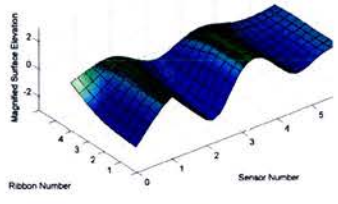

(i) time=6.00s

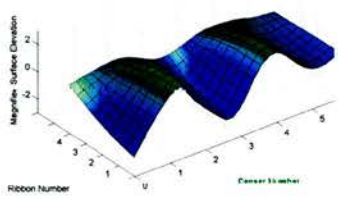

(j) time=6.16s

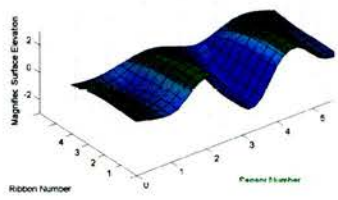

(k) time=6.32s

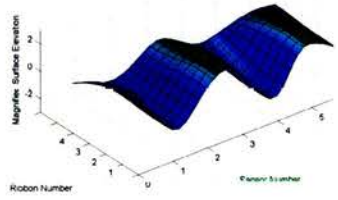

(l) time=6.48s

Figure 6.25. Surface elevation across sensor array for irregular wave test number 1. Frame grabs showing time evolution of wave field.

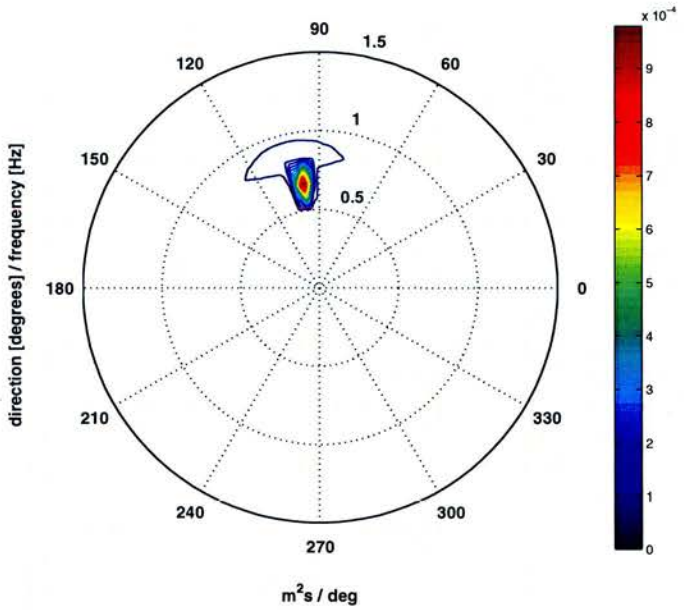

(a) Directional spectra for irregular wave test 1

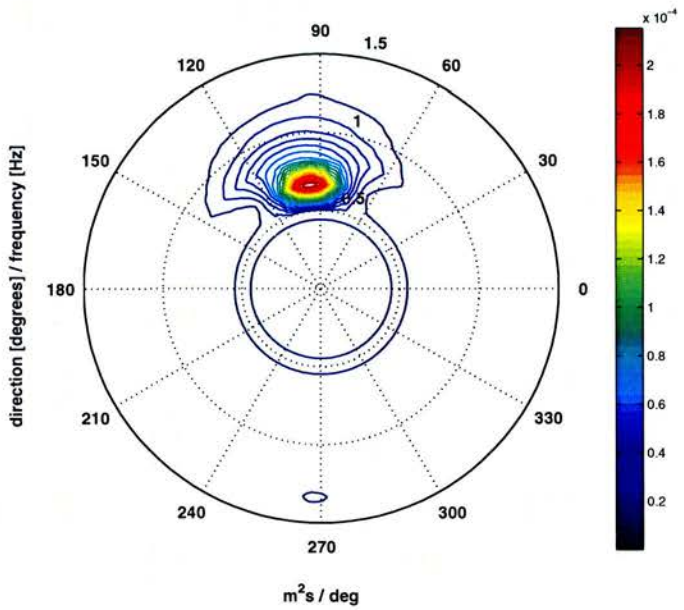

(b) Directional spectra for irregular wave test 2

Figure 6.26. Directional wave spectra produced using the EMEP method. Tests 1 and 2

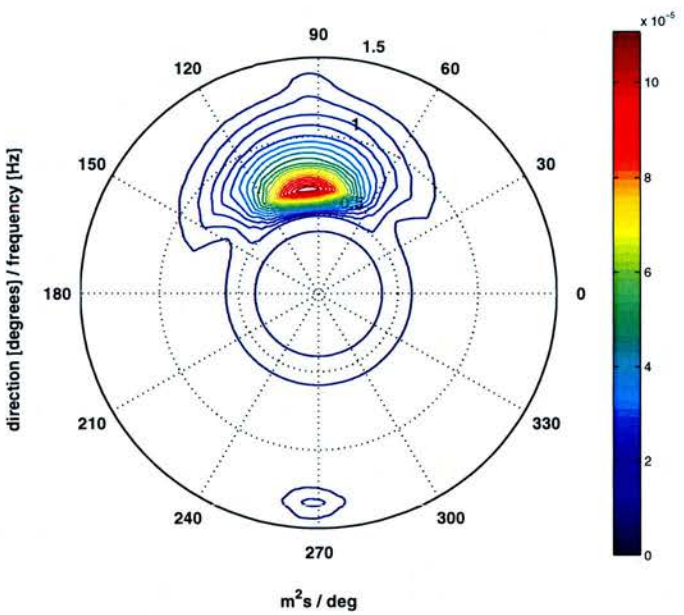

(c) Directional spectra for irregular wave test 3

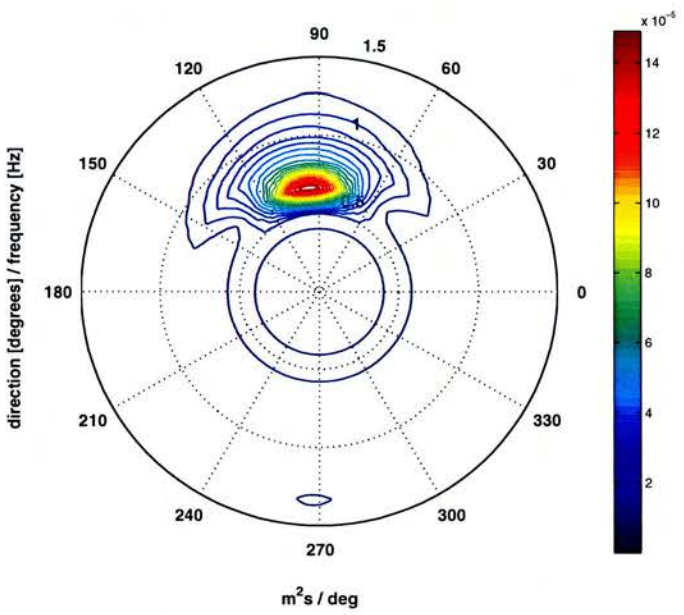

(d) Directional spectra for irregular wave test 4

Figure 6.26. Directional wave spectra produced using the EMEP method. Tests 3 and 4

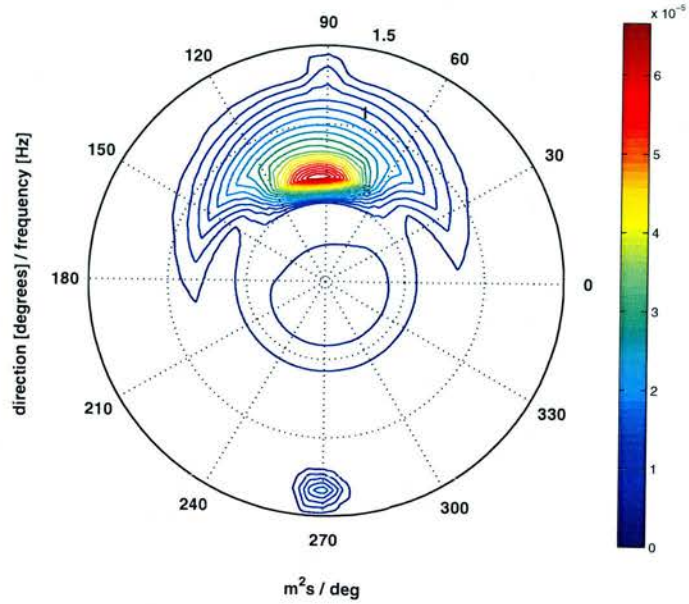

(e) Directional spectra for irregular wave test 5

Figure 6.26. Directional wave spectra produced using the EMEP method. Test 5

Figure 6.27. Paddle failure ends testing. Spring failure on paddle number 7 (4 from left in image).

CHAPTER 7

Summary Discussion on the Three Reports

This Chapter provides a short review of the motivation for this work and moreover, an overview of the three experimental reports which formed Chapters 4 to 6 and a summary of discussion points raised.

7.1 Review of Motivation

Marine renewable energy can potentially play a significant role in energy, wealth and job creation in the United Kingdom. In Scotland in particular, machines designed to extract wave and tidal power have access to a large resource with 10% and 25% shares of the estimated European resource. Parallel to the wave and tidal sectors, the more established field of offshore wind energy extraction is gathering pace in UK coastal waters, as is the increase in aquacultural activities. As demand grows for hydrocarbons, minerals and food, an increasing amount of technology and infrastructure will likely be applied in the marine environment. Improved knowledge of wave fields in these coastal and deep waters could assist marine industries by enabling:

- Improved initial machine/structure design to suit environmental conditions

- Improved numerical modelling of wave dynamics
- Improved ability of marine equipment to react to the dynamic wave field
  - Avoidance of extreme loads
  - Additional extraction of energy
  - Mitigation of fatigue-inducing loads
- Reduced risk in marine operations for deployment, recovery and maintenance of offshore infrastructure
  - Vessel-to-WEC/TEC operations
  - Vessel-to-structure/moorings/foundations operations
  - Vessel-to-vessel operations

This work was an investigation of a novel sensor concept that could lead to improved knowledge of wave fields through capturing surface elevation data across a wide area and making this data available to users in a timely manner. It was foreseen that if the sensor concept proved infeasible in terms of marine survivability or mass production due to cost, but otherwise functioned well, that it could have a use in the benchmarking and calibration of existing wave measurement techniques or new designs of sensors.

In order to develop the sensor concept and to assess the various resulting designs, multiple experiments were devised and implemented. These experiments are summarised in section 7.2.

The main conclusions from these three components of the investigation are outlined in Chapter 8 where the wide range of further work is also collated.

7.2 Experimental Techniques and Discussion Summary

This work can be divided into three sections: the first deals with the physical ability of a floating ribbon-like element to track the water/air interface due to buoyancy;

the second involves one implementation of sensors onto such a floating ribbon and focuses on two dimensional wave tracking ability; and the third involves a different implementation of sensors to form a floating and modular sensor array which can extend measurement capability into three dimensions.

7.2.1 Surface Tracking Assessment using an Optical Technique

In order to assess the ability of floating like elements to track the water/air interface a series of experiments were conducted in the University of Edinburgh 20m wave flume. These involved using an off-the-shelf video camera to film regular and irregular wave tests whilst a buoyant and flexible ribbon-like structure experienced the incident waves. A variety of materials and floating elements were trialled. With qualitative evidence of tracking ability for early implementations the ShapeTape technology of Measurand Inc. was then trialled - firstly as a demonstrator ribbon and latterly as a fully active measuring instrument. Wire resistance wave gauges were used throughout to provide reference surface elevation data against which the outputs of the optical tracking (camera) technique and the ShapeTape instrument could be compared. Effort was required in both the initial setup of the experiments in terms of lighting and camera arrangement. Through extensive testing a methodology was devised that could obtain high quality data without requiring rigorous, complex or unstable configuration. Image processing and analysis techniques were implemented. Time was required in both gaining experience of their use and in the subsequent processing of a quarter of a million images. Data analysis was primarily based upon time series analysis using zero-crossing methods.

Summary of Discussions on the Optical Tracking Method

- Wave steepness plays a significant role in the performance of the image tracking system.

- Further tests are required at and beyond the low and high wave frequencies used during these experiments.

- More sophisticated image calibration and processing techniques from other fields could be employed. However, the techniques used did provide robust insight into the surface tracking ability of the sensor ribbons.
- Performance varies between wave-crest tracking and wave-trough tracking with the latter exhibiting lower error.
- There is a lot of scope to optimise routines to reduce processing time.
- KDEs may be an appropriate tool in the analysis of relationships between measured parameters and their errors.
- Implementing multiple-camera techniques to increase the field of view to beyond several wavelengths would be relatively straight forward and should be investigated.

7.2.2 Testing of a Two Dimensional Wave Sensor Array

A 7.1m ShapeTape was adapted to allow it to be used on the surface of the wave flumes. A variable height attachment rig located the instrument at a fixed position inside the Edinburgh 20m wave flume. In parallel to the optical tracking technique regular and irregular waves were generated with the ShapeTape recording resulting bend along its length by means of monitoring the light intensity at specific measurement zones along the internal optical fibres. This bend data was used to construct ribbon displacement information along the ribbon length. These displacements were compared to reference surface elevation data.

Summary of Discussions on the Two Dimensional Wave Sensor Array

- Results of the optical tracking method and preliminary 2D sensor tests suggest that the floating sensor concept is not suitable for laboratory based measurements where accuracy and repeatability in the mm range are required.
- Signal processing plays an important role in improving (and reducing) sensor performance.

- More wire resistance wave gauges (reference measurements) would enable improved spatial analysis of the sensor.
- Design features such as floatation jacket shape, buoyancy and varying stiffness of materials, whilst incorporated, were not fully optimised and will likely play a role in sensor performance.
- Wave steepness plays a role in data quality.
- Large magnitude errors are evident for a relatively small proportion of individually (time-domain) analysed waves, particularly in wave period. Given that regular wave tests show excellent period agreement more analysis of these individual events is required.
- Wave groups appear, after preliminary analysis, to be tracked well.
- Care is required when undertaking wave-by-wave, zero-upcrossing / zero-downcrossing analysis, particularly around the inclusion or exclusion of very small perturbations around the mean water level.
- Since the floating sensor exhibits inherent complex dynamics whilst attempting to measure a moving and complex system it is likely that a sophisticated processing technique is required to achieve optimal sensor performance or to expand the range of waves over which the sensor can provide reliable results.
- Existing knowledge of the dynamics of water waves could play a role in these advanced processing techniques.

7.2.3 Testing of a Three Dimensional Wave Sensor Array

Following experiments on a two dimensional wave sensor the next phase of experiments involved different types of sensor incorporated into long flexible elements. Instead of optical fibres measuring bend, angular rate sensors, measuring the rate of tilt in three directions, and full inertial measurement units, measuring angular rate, acceleration and heading in three directions were used. These sensors were of the micro-electro-mechanical (MEM) sensor type. This approach offered the ability

to build custom wave arrays in two and three dimensions with any desired sensor spacing and with a variety of linking elements (the mechanical component between sensor zones). A large amount of time was taken in the conception, design and fabrication of suitable array elements. This included selecting the correct MEM sensors, cables (which serve the triple role of electrical, communication and mechanical back-bone), waterproof housings, floatation jackets, mooring arrangements and sensor distribution. Being novel, these instrument arrays required a large degree of troubleshooting. Iterative improvements were required in device hardware and software. Once constructed and commissioned partial survivability testing was conducted at the GWK facility in Hannover, Germany and array testing was conducted, in a limited time window, at the Heriot-Watt University wave basin. As with the two dimensional tests, surface elevation reported by the instrument array was compared against surface elevation measured by wire resistance wave gauges. As wave array sensor coverage increases (both in scale and density/resolution) there are relatively fewer points to compare against due to the availability of reference wave gauges. In moving to three dimensions the ability of the array to measure wave directionality and wave spreading was assessed in preliminary tests.

Summary of Discussions on the Three Dimensional Wave Sensor Array

- Design, procurement and sub-system integration of the sensor array was challenging and complex and therefore time consuming.

- As with most new equipment, development issues occurred with cumulative consequences.

- It was shown that carefully selected cables (in addition to the ribbons used in the ShapeTape 2D tests) can track the water surface.

- The design concept of lightweight and waterproof housings were shown to be suitable for use in laboratory settings and with the incorporation of strain relief are suitable up to 1/4 scale for limited periods (days). Thus the system is suitable to allow further, more rigorous testing.

- The design concept lends itself to simple fabrication techniques to enable scaling up - as shown by the fully-"marinised" 1/4 scale sensor which was designed and fabricated in parallel to these tests (Appendix B).

- Mooring plays an important role and further testing is required. Several working solutions, however, were implemented in the laboratory.

- Automatic and robust initial-positioning/calibration of the arrays is critical to allow subsequent analysis of obtained data. A semi-automatic process was successfully developed.

- Analysis of the data reported by a wave-array is complex and analysis of the data in near-real time is non-trivial. Progress was made in this area and some of the successful techniques developed in the 2D array tests (e.g., look-up-tables and online adaptive filtering) can be integrated in to the 3D array analysis.

- Improvements in computational power and efficiency and reductions in cost and power consumption of MEM systems would assist any further development of remote, array-based systems.

- Analysis of preliminary regular and irregular wave tests suggests that the system could meet the design objectives.

CHAPTER 8

Conclusions and Further Work

8.1 Feasibility Study on the Surface Tracking Ability of Floating Ribbons using an Optical Technique

The optical tracking technique described in Chapter 4 and summarised in section 7.2.1 has been used to quantify the ability of the floating ribbon used in this work to physically track water waves. These waves were both regular and irregular in nature with the later conforming to the JONSWAP spectra. Under these conditions the flexible ribbon tracks the surface well. The presence of a bias to over estimation of wave height requires further investigation but from wave-by-wave analysis it was found that the ribbon followed the surface with a mean error of approximately 6% and a standard deviation in wave tracking relative errors of approximately 7% to 9%. Wave period tracking was excellent with mean errors below 0.5% and standard deviation in wave tracking relative errors of 2.5%. From analysis of the data it is evident that large outlier events in the wave-by-wave analysis could be further reduced with improved post-processing routines.

Whilst surface tracking ability is encouraging this method is certainly far removed from a non-contact measurement technique. The sensor itself does interfere with the water surface and due to non-linear dynamics and inherent mechanical limitations

can not fully adhere to the surface at all times. The more dynamic the wave field is and the steeper the waves become the more time the sensor ribbon spends partially submerged below wave crests. Selecting a suitable mechanical structure and sensor density mitigates this to an extent but for precision laboratory work, where mm and below levels of accuracy are required, using a floating element is unsuitable.

The optical tracking technique itself could prove useful in a variety of wave flume physical tests with little modification and is currently being used by a PhD student at the University to investigate the flexing of non-rigid vertical structures in addition to being used in undergraduate wave run-up experiments. The method developed could have particular utility in terms of wave measurement (as opposed to the wave-object interactions mentioned) where spatial information of the waves is important - such as reflection analysis and wave spectra and wave group evolution.

8.2 Design, Construction and Testing of a Two Dimensional Wave Sensor Array

A sensor was conceived and developed that is able to report wave elevation in near real-time across a distance of up to several wavelengths in two dimensions. The instrument was exposed to both regular and irregular waves of varying heights, periods and steepness. Whilst a large amount of further development of both the post-processing and data analysis would prove useful the instrument and its associated software can provide useful estimates of wave period and wave elevation in addition to other wave parameters such as wave slope.

The sensor reported waves with a mean error in wave height of approximately -6% to 4% and a standard deviation in relative errors of approximately 18.7% and 24.5%. Wave period tracking was good with mean errors between 0% and 1% and standard deviation in relative errors of 9.1% and 13%.

With tighter restrictions on data threshold levels, i.e., by restricting reported waves to within smaller ranges of a given parameter, such as wave steepness or minimum wave height, the standard deviations of relative error in reported waves falls to

approximately 15% for wave height and 10% for wave period. Under this process waves with a steepness greater than 0.1 are excluded in addition to waves below 0.6 second period and 4mm wave height. With this level of data exclusion, typically a further 15% of wave events are excluded from the statistical analysis in addition to the 7% to 14% of wave events that are unable to be suitably matched by the wave-by-wave analysis routines in their current form.

Due to the level of inaccuracy reported at these scales and the interaction with the media being measured this method of wave measurement is not suitable for laboratory testing at this scale where mm levels of accuracy are required. However, at larger scales where near real-time spatial information (as opposed to a point measurement) is required this technology could provide useable surface elevation data. Additionally, the ability of a marine based machine or device to use this instrument's provided data on wave curvature, wave period, wave slope - or other wave parameters such as those describing wave "groupiness" - could prove as useful in a decision making process as surface elevation. For example, a WEC may not be capable of responding to wave height changes on a wave-by-wave basis and may instead be tuned to a different parameter that suitably characterises the wave-field.

8.3 Design, Construction and Preliminary Testing of a Three Dimensional Wave Sensor Array

A sensor was developed following the same concept as outlined in the previous section. MEM-based sensors were used as opposed to optical fibres. A cable-based mechanical linkage was also used as opposed to a ribbon-like linkage. The majority of available time was spent on system design and construction. Testing was conducted in three separate facilities. Work was carried out on processing routines that could assess the ability to make the system "real-time" and to integrate some of the "lessons-learned" from the 2D experiments on the optical-fibre based system (e.g., dynamic filters) but these are incomplete thus are unreported. Whilst no time-domain analysis is reported, each pod of each ribbon is coherent with its neighbours, qualitatively

tracks the surface well and has reported data reliably during all tests. In order to provide some quantitative measurements spectral analysis was conducted on 8 regular wave tests and 5 irregular waves with varying (increasing) degrees of wave spreading.

Preliminary testing of the MEM-based sensor ribbons (in array form capable of measuring position in three dimensions) show mean wave height error across all regular wave tests of -1.3% with standard deviation of 8.4%. Mean along-ribbon standard deviation in relative error was 7.25%. Wave period errors were small at less than 0.1% relative error with a relative standard deviation of less than 0.2% and mean standard deviation, along-ribbon, of less than 0.2%.

In irregular waves, error in mean H_{m0} is -3% with standard deviation, across the tests and individual ribbons forming the array, of 7.5%. Peak wave period is under-predicted by 1.3% with standard deviation of 2.2%. Early directional wave analysis give confidence since they capture both the mean direction and the increased wave spreading of the irregular wave tests conducted.

8.4 A Note on Scale

Sensor arrays having a variety of physical sizes, sensor densities, masses and "stiffnesses" were fabricated and tested in the wave flumes and wave basins of the University of Edinburgh, Heriot-Watt University, Aalborg University and the GWK, Hannover. It was established that the properties of an array which inhibit wave tracking include high inertia, low buoyancy and overly stiff interconnections between each sensing element. The effects on performance of these properties are relative to the properties of the wave field they are exposed to (in particular, wave height, wave length and local wave curvature). Whilst none of the fabricated arrays were light, flexible and mechanically responsive enough to track small wave heights of single-digit centimetres to the accuracy of a wire resistance wave gauge, it has been shown that as wave heights and wavelength increase above approximately 100mm and 1 second period (representing the upper range capability of a small wave flume) the sensors' physical characteristics become more suited to surface tracking. Considerable effort was

focused on minimising the mass and bulkiness of the sensor elements and floatation aids. Given, however, that the arrays are individually assembled prototypes consisting of developmental components (which tend to be larger than mass production items) there is a limitation to the degree of miniaturisation possible.

Considering the non-optical-fibre array, with reductions in mass and volume of approximately 50% certainly achievable by utilising lighter epoxy, connectors and enclosures the array could be suitable for use in hydraulic test facilities offering testing at approximately 1:30 scales and above. The new All-Waters Combined Current and Wave Test Facility due to open in Edinburgh in 2013 offers a wave-field that would be ideally suited for the further development of an updated array. This facility is capable of wave heights of 0.7m at a period of 2 seconds which offers a good match for the dimensions of the sensor array developed as part of this thesis. Testing in this facility would expose the array to waves 150% longer and double the height of those that were possible in all tests previously conducted (other than survivability tests conducted at GWK).

The sensor arrays, as tested, were designed for laboratory testing but the concept calls for a larger, more robust, version to be deployed at sea. Before assessing an array's ability to survive the rigours of use in the field, testing at large scale facilities should be carried out. It is expected, however, that as scale increases the development focus would be less on miniaturisation and more on strength, material selection and component attachment methods.

The original concept of the array centred on providing WEC (and other ocean equipment) with real-time wide-area wave measurement in order that the machines could adapt their behaviour to improve performance. Given that designing fully-representative WEC systems including power take-off is extremely difficult at small scales (below 1:30) the arrays' inability to compete with small-scale laboratory measurement set-ups may not limit its potential utility.

8.5 Further Work

Since beginning this thesis the offshore renewable industries have progressed significantly. Arrays of devices are not yet generating to the grid but prototypes have become full-scale devices and full-scale devices have relinquished their berths to second generation machines. The need for improved wave field information remains. And, in the case of the offshore wind industry, has increased. Whilst some steps have been taken to either rule-out or rule-in the sensor concepts outlined in this thesis, further work is needed in particular areas. An upside to the broad approach taken, however, is in the large and expanding amount of *further work* identified, which is outlined in the following sections, largely in bulleted format for compactness.

8.5.1 Optical Tracking Technique

With further enhancement of processing algorithms and using experience of image processing gained during the analysis of these tests, it is believed that image processing by a camera or camera array, could lead to the ability to readily investigate hydraulic test flume / tank problems where wave spatial information is required. The following list summarises opportunities for improvement and further work:

- Camera calibration.
  - Improved calibration at test start-up should be implemented through the use of calibration grids and other standard procedures as used in the fields of robotics and computer vision.
- Camera configuration.
  - Settings such as lighting level, focusing and resolution should be optimised.
- Further tests
  - More tests should be conducted at the limits of the techniques abilities, i.e., very steep and breaking waves and very long waves.

  - Tests should be conducted without the presence of the flexible ribbon sensors and floats to provide baseline information.

- Multiple cameras should be used to increase the field of vision and to increase resolution.
- High frequency diffracted waves need to be better imaged and processed.
- Optimisation should be carried out on wave and object tracking routines to reduce analysis-time.
- Post-processing, once improved, should be embedded onto dedicated hardware or designed to be run in a parallel way.
- Wave-by-wave tracking could be enhanced (as with sensor analysis), particularly in the area of programmatic decision making where suspected erroneous waves are identified.

8.5.2 Two Dimensional Wave Sensor Array

To a large extent, having designed and implemented an experimental procedure, efforts then turned to data processing. A major improvement to testing would be to integrate proposed data-processing and end-user requirements into the experimental design so that targeted tests, including calibration procedures, are identified earlier. There is additional scope for further work in the following areas:

- Signal processing. Collaboration from the signal processing field would aid analysis.
- Collaboration with array-based signal processors. Even in two dimensions, the sensor ribbon provides information as an array.
- Improved experimental set-up featuring more wire resistance wave gauges and better test-matrix selection.
- Investigation into the hydrodynamic response of the sensor.

  - Construction of a numerical model/s to assess the effects of varying sensor mechanical properties and sensor response to waves.
  - Experimental tests to assess the effects of varying parameters such as floatation configuration.

- Mooring design, implementation and scalability.
- Wave-by-wave analysis routines including appropriate treatment of errors propagated due to zero up-crossing analysis finding erroneous waves in one of the compared time series.
- Collaboration with researchers involved in wave modelling.

8.5.3 Three Dimensional Wave Sensor Array

In addition to the items listed in the further work section above, which are also required in the development of a 3D sensor array, the following list of activities have been identified:

- Further targeted laboratory testing.
- Collaboration with the fields of array processing, informatics and machine-learning to produce improved data processing algorithms.
- Investigation into alternative representations of 3D systems (e.g., quaternion) and utilise established techniques and tools in other fields (e.g., computer 3D graphics).
- 3D mooring solutions
- Sensor integration with other systems such as GPS, acoustics and existing wide-area wave measurement techniques such as multiple camera configurations and radar systems.
- Investigation into features of an array configuration that would inhibit increasing scale and "deployability" such as power consumption, reliability, safety. Many issues were considered and some are briefly outlined in Appendix B.

Bibliography

[1] DTI. Energy white paper. our energy future - creating a low carbon economy. Tech. Rep., Department of Trade and Industry, The Crown (2003).

[2] Parliamentary Office of Science and Technology. The future of UK gas supplies. Short Report, Parliamentary Office of Science and Technology (2004).

[3] Scottish Executive. Scotland's renewable energy potential - beyond 2010. Consultation Paper, The Scottish Executive (2004).

[4] DTI. Atlas of UK marine renewable energy resources. Tech. Rep., Department of Trade and Industry, UK Government (2004).

[5] ABPmer. Potential nature conservation and landscape impacts of marine renewable energy developments in welsh territorial waters. Tech. Rep., CCW Policy Research Report 04/8 (2005).

[6] AEA Technology Future Energy Solutions. Status and research development priorities: Wave and marine current energy. Tech. Rep. FES-R-132, Department for Trade and Industry, UK Government. (2002).

[7] Garrad Hassan. Scotland's renewable resource. Tech. Rep., Garrad Hassan and Partners Limited (2001).

[8] Allan, G., McGregor, P. G., Swales, J. K. & Turner, K. Impact of alternative electricity generation technologies on the Scottish economy: an illustrative input-output analysis.
Proceedings of the Institution of Mechanical Engineers, Part A Journal of Power and Energy **221**, 243–254 (2007).

[9] The Carbon Trust. Future marine energy. Tech. Rep., The Carbon Trust (2006).

[10] The Offshore Valuation Group. The offshore valuation: a valuation of the UK's offshore renewable energy resource. Tech. Rep., The Offshore Valuation Group (2010).

[11] Scottish Executive. Lewis wind farm inquiry report. Tech. Rep., Scottish Executive (2008). URL http://www.scotland.gov.uk/Topics/Business-Industry/Energy/Infrastructure/Energy-Consents/Applications-Database/Wind/Lewis-Decision-Index.

[12] Scottish Executive. Beauly-Denny transmission line. Inquiry Report, Scottish Executive (2010). URL http://www.scotland.gov.uk/Topics/Business-Industry/Energy/Infrastructure/Energy-Consents/Beauly-Denny-Index.

[13] Boehlert, G. W. & Gill, A. B. Environmental and Ecological Effects of Ocean Renewable Energy Development: A Current Synthesis. In Oceanography, vol. 23 (2010).

[14] Thorpe, T.W. A brief review of wave energy. Tech. Rep., Thorpe TW (1999).

[15] Parker, R. P. M., Harrison, G. P. & Chick, J. P. Energy and carbon audit of an offshore wave energy converter.
Proceedings of the Institution of Mechanical Engineers, Part A: Journal of Power and Energy **221**, 1119–1130 (2007).

[16] Clement, A. et al. Wave energy in europe: current status and perspectives.
Renewable and Sustainable Energy Reviews **6**, 405 – 431 (2002).

[17] Dalton, G., Alcorn, R. & Lewis, T. Case study feasibility analysis of the pelamis wave energy convertor in ireland, portugal and north america. Renewable Energy **35**, 443 – 455 (2010).

[18] University of Edinburgh. Matching renewable electricity generation with demand. Tech. Rep., The Scottish Executive (2006).

[19] DTI. The transmissions issues working group - final report. Tech. Rep., Department of Trade and Industry, The Crown (2003).

[20] Harris, A. Smart grid thinking - power super grid. Engineering Technology **4**, 46 –49 (2009).

[21] The Royal Academy of Engineering. Making green growth real: UK offshore wind supply chain. The Royal Academy of Engineering (2011).

[22] BVG Associates. UK content analysis of Robin Rigg offshore wind farm. A report commissioned by E.ON Climate & Renewables (2011).

[23] SuperGen Marine Consortium. Supergen marine energy research. Monograph, SuperGen Marine (2007).

[24] UK Energy Research Centre, U. UKERC marine (wave and tidal current) renewable energy technology roadmap. Summary Report, UKERC (2007).

[25] Ingram, D. EQUIMAR, Equitable Testing and Evaluation of Marine Energy Extraction Devices in terms of Performance, Cost and Environmental Impact: D2.7 Protocols for wave and tidal resource assessment. Tech. Rep., The Equimar Consortium (2011).

[26] Harrison, G. & Wallace, A.R. Sensitivity of wave energy to climate change. Energy Conversion, IEEE Transactions on **20**, 870–877 (2005).

[27] WaveNet. Wavenet. final report from european wave energy thematic network on wave energy. Tech. Rep., Wavenet (2003). URL http://www.wave-energy.net/.

[28] Falnes, J. Optimum control of oscillation of wave-energy converters. Tech. Rep., NTNU, Norway (1993). URL http://folk.ntnu.no/falnes/web_arkiv/InstFysikk/optcontrl.pdf.

[29] Salter, S. H., Taylor, J. & Caldwell, N. Power conversion mechanisms for wave energy. IMechE Proc. part M - Engineering for the Maritime Environment **M**, 1–27 (2002).

[30] Korde, U. Control system applications in wave energy conversion. In Proceedings of OCEANS, 2000. MTS/IEEE., vol. 3, 1817 –1824 (2000).

[31] Hals, J., Falnes, J. & Moan, T. A comparison of selected strategies for adaptive control of wave energy converters. Journal of Offshore Mechanics and Arctic Engineering **133** (2011).

[32] Budal, K. & Falnes, J. Wave-power conversion by point absorbers. Norwegian Maritime Research **6**, 2–11 (1978).

[33] Skyner, D. Solo duck linear analysis. Tech. Rep., The University of Edinburgh (1987).

[34] Pizer, D. Numerical prediction of the performance of a solo duck. Tech. Rep., The Edinburgh Wave Group, The University of Edinburgh (1992).

[35] Nebel, P. Synthesis of Optimal Control of a Wave Energy Converter. Ph.D. thesis, The University of Edinburgh (1994).

[36] Falnes, J. & Budal, K. Wave-power absorption by parallel rows of interacting oscillating bodies. Applied Ocean Research **4**, 194 – 207 (1982).

[37] Budal, K. & Falnes, J. Wave power conversion by point absorbers: A Norwegian Project. International Journal of Ambient Energy **3**, 59 – 67 (1982).

[38] Budal, K. & Falnes, J. Optimum operation of improved wave-power converter. Marine Science Communications **3**, 133 – 150 (1977).

[39] Falnes, J. Optimum control of oscillation of wave-energy converters. International Journal of Offshore and Polar Engineering **12**, 147 – 155 (2002).

[40] Babarit, A., Guglielmi, M. & Clement, A. H. Declutching control of a wave energy converter. Ocean Engineering **36**, 1015 – 1024 (2009).

[41] Korde, U. A. Performance of a wave energy device in shallow-water nonlinear waves: part ii. Applied Ocean Research **19**, 13 – 20 (1997).

[42] Price, A. New perspectives on wave energy converter control. PhD Thesis (2009). URL http://www.era.lib.ed.ac.uk/bitstream/1842/3109/1/PriceAAE%20PhD%20Thesis%2009.pdf.

[43] Falnes, J. Ocean Waves and Oscillating Systems (Cambridge University Press, 2002).

[44] Falnes, J. On non-causal impulse response functions related to propagating water waves. Applied Ocean Research **17**, 379 – 389 (1995).

[45] Whitakker, T. & Foley, M. Optimisation of wave power devices towards economic wave power systems. In Proc. of World Renewable Energy Conference VIII, Aberdeen, UK. (2005).

[46] Yemm R., T. C., Henderson R. The OPD Pelamis WEC: current status and onward programme. In Proc. 4th European Wave Energy Conference, Alborg, Denmark. (2000).

[47] Pugh, D. T. Tides, Surges and Mean Sea-Level (John Wiley & Sons, 1996).

[48] Airy, G. On tides and waves. Encylopaedia Metropolitana (mixed sciences) **5**, 241–396 (1845).

[49] Goda, Y. Random Seas and Design of Maritime Structures (World Scientific, 2000).

[50] Smith, G. Preliminary wave energy device performance protocol, Annex II Report. Tech. Rep., International Energy Agency (2007).

[51] U.S. Army Corps of Engineers. Coastal engineering manual. engineer manual 1110-2-1100. Tech. Rep., U.S. Army Corps of Engineers, Washington, D.C. (2002).

[52] European Marine Energy Centre. Tank testing of wave energy conversion systems: Marine renewable energy guides. Tech. Rep., European Marine Energy Centre Ltd., Orkney, UK (2009).

[53] Hashimoto, N. Analysis of the directional wave spectra from field data. In Liu, P.-F. (ed.) Advances in Coastal and Ocean Engineering, vol. 3, 103–143 (World Scientific, Singapore, 1997).

[54] Davidson, M. A., Huntley, D. A. & Bird, P. A. D. A practical method for the estimation of directional wave spectra in reflective wave fields. Coastal Engineering **33**, 91 – 116 (1998).

[55] Kahma, K., Hauser, D., Krogstad, H., Lehner, S., Monbaliu, J. & Wyatt, L. Measuring and analysing directional spectra of ocean waves - COST action 714, eur 21367. Tech. Rep., European Union (2005).

[56] Longuet-Higgins, M., Cartwright, D. & Smith, N. Observations of the directional spectrum of sea waves using the motions of a floating buoy. In Ocean Wave Spectra, 111 – 136 (Prentice-Hall, Englewood Cliffs, NJ, USA, 1963).

[57] Pedersen, T., Goldberg, J., Lohrmann, A. & Siegel, E. Resolving transformed wave directions near coastalstructures. In International Conference on Coastal Engineering (ICCE) (2006).

[58] Benoit, M. & Goasguen, G. Comparative evaluation of directional wave analysis techniques applied to field measurements. In

Proceedings of the 9th International Offshore and Polar Engineering Conference (ISOPE), vol. 3 (1999).

[59] Johnson, D. Directional wave spectra toolbox (diwasp) user manual. Tech. Rep., MetOcean Solutions Ltd. (2010).

[60] Cruz, J., Mackay, E. & Martins, T. Advances in wave resource estimation measurements and data processing. In Proc. 7th European Wave and Tidal Energy Conference (Oporto). (2007).

[61] Earle, M. D., Steele, K. E. & Wang, D. W. C. Use of advanced directional wave spectra analysis methods. Ocean Engineering **26**, 1421 – 1434 (1999).

[62] Benoit, M., Frigaard, P. & Schaffer, H. Analysing multidirectional wave spectra : A tentative classification of available methods. In Proc. 27th IAHR Seminar. Multidirectional Waves and their Interaction with Structures, 131 – 158 (1997).

[63] Nielsen, P. Analysis of natural waves by local approximations. Journal of Waterway, Port, Coastal, and Ocean Engineering **115**, 384 – 396 (1989).

[64] Johannessen, T. B. & Swan, C. On the nonlinear dynamics of wave groups produced by the focusing of surface-water waves. In Proceedings of the Royal Society of London, Series A, vol. 459, 1021–1052 (2003).

[65] Longuet-Higgins, M. S. Eulerian and lagrangian aspects of surface waves. Journal of Fluid Mechanics **173**, 683–707 (1986).

[66] AXYS Technologies Inc. TRIAXYS Directional Wave Buoy: Datasheet. Tech. Rep., AXYS Technologies Inc., Canada (2010).

[67] Teledyne RD Instruments. Workhorse waves array: Datasheet. Tech. Rep., Teledyne RD Instruments, CA, USA (2009).

[68] Nortek AS. AWAC Platform: Datasheet. Tech. Rep., Nortek AS, Norway (2010).

[69] Ocean Waves GMBH. Wamos II Summary Specifications: Data Sheet. Tech. Rep., Ocean Waves GMBH, Germany (2012).

[70] Chung-Chu Teng et al. National data buoy center 1.8-meter discus buoy, directional wave system. In Proceedings of OCEANS, 2007. MTS/IEEE., 1 –9 (2007).

[71] Steele, K. E., Wang, D. W., Earle, M. D., Michelena, E. D. & Dagnall, R. J. Buoy pitch and roll computed using three angular rate sensors. Coastal Engineering **35**, 123 – 139 (1998).

[72] Rorbaek, K. & Andersen, H. Evaluation of wave measurements with an acoustic doppler current profiler. In Proceedings of OCEANS, 2000. MTS/IEEE., vol. vol.2, 1181 – 1187 (2000).

[73] Boake, C. Nortek User Symposium (Presentation), France. (2008).

[74] Energy Technology Institute, ETI. http://www.energytechnologies.co.uk (2011).

[75] Teledyne RDI. ADCP Deployment Planning Software (2011).

[76] SonTek. Sonwave-pro: Directional wave data collection. Tech. Rep., SonTek, San Diego, CA, USA (2001).

[77] Nortek AS. Datasheet: AWAC / Real Time Systems. Tech. Rep., Nortek AS, Oslo, Norway (2011).

[78] Eshbaugh, J. & Frasier, S. Measurement of sea surface displacement with interferometric radar. J. Atmos. Ocean. Technol. (USA) **19**, 1087 – 95 (2002).

[79] Hessner, K., Reichert, K., Dittmer, J. & Borge, J. C. N. Ocean wave measurements by x-band radar - from spectral wave parameters to single wave detection. Tech. Rep., OceanWaveS GmbH (2003).

[80] Ocean Waves GMBH. Wamos II data comparison and error statistics (2007). URL http://www.oceanwaves.org/download/PDF/E_STAT2007.pdf.

[81] Reichert, K., Hessner, K., Trankmann, I. & Lund, B. X-band radar as a tool to determine spectral and single wave properties. Tech. Rep., OceanWaveS GmbH, Luneburg, Germany (2004).

[82] Reichert, K. Correspondance and letter of support (2008).

[83] Wyatt, L., Green, J. & Middleditch, A. Wave, current and wind monitoring using HF radar. In Proceedings of the IEEE/OES 8th Working Conference on Current Measurement Technology, 53 – 57 (2005).

[84] Wyatt, L. R., Green, J. J., Middleditch, A., Moorhead, M. D., Howarth, J., Holt, M. & Keogh, S. Operational wave, current, and wind measurements with the pisces hf radar. Journal of Oceanic Engineering. IEEE **31**, 819 –834 (2006).

[85] Belmont, M., Horwood, J., Thurley, R. & Baker, J. Shallow angle wave profiling lidar. Journal of Atmospheric and Oceanic Technologly **24**, 1150 – 1156 (2007).

[86] van Unen, R., van Beuzekom, A., Forristall, G., Mathisen, J. & Starke, J. WACSIS-wave crest sensor intercomparison study at the Meetpost Noordwijk measurement platform. In Proceedings of OCEANS, 1998. MTS/IEEE., vol. 3, 1757 –1761 vol.3 (1998).

[87] Barstow, S. F., Krogstad, H. E., Lonseth, L., Mathisen, J. P., Mork, G. & Schjolberg, P. Intercomparison of sea-state and zero-crossing parameters from the wacsis field experiment and interpretation using video evidence. Journal of Offshore Mechanics and Arctic Engineering **126**, 35–42 (2004).

[88] Ingram, D. EQUIMAR, Equitable Testing and Evaluation of Marine Energy Extraction Devices in terms of Performance, Cost and Environmental Impact: D2.3 Application of Numerical Models. Tech. Rep., The Equimar Consortium (2011).

[89] Folley, M. & Whittaker, T. Analysis of the nearshore wave energy resource. Renewable Energy **34**, 1709 – 1715 (2009).

[90] NASA. Jason 1 fact sheet. ocean surface topography website of jet propulsion laboratory, california institute of technology (2001). URL http://sealevel.jpl.nasa.gov.

[91] NASA/JPL. Ocean surface topography website of jet propulsion laboratory, california institute of technology (2010). URL http://sealevel.jpl.nasa.gov/.

[92] Infoterra. http://www.infoterra.de/terrasar-x (2011).

[93] Carvalho, J. L. B. & Parente, C. E. Directional wave measurements using a slope array system. Applied Ocean Research **22**, 95 – 101 (2000).

[94] Tedd, J. Testing, Analysis and Control of Wave Dragon, Wave Energy Converter. Ph.D. thesis, Aalborg University, Department of Civil Engineering, Hydraulics and Coastal Engineering Laboratory (2007).

[95] Tsai, C.-H., Huang, M.-C., Young, F.-J., Lin, Y.-C. & Li, H.-W. On the recovery of surface wave by pressure transfer function. Ocean Engineering **32**, 1247 – 1259 (2005).

[96] Bechle, A. J. & Wu, C. H. Virtual wave gauges based upon stereo imaging for measuring surface wave characteristics. Coastal Engineering **58**, 305 – 316 (2011).

[97] Wanek, J. & Wu, C. Automated trinocular stereo imaging system for three dimensional surface wave measurements. Ocean Engineering **33**, 723 – 747 (2006).

[98] Lee, H. S. & Kwon, S. H. Wave profile measurement by wavelet transform. Ocean Engineering **30**, 2313 – 2328 (2003).

[99] Hwung, H. H., Kuo, C. A. & Chien, C. H. Water surface level profile estimation by image analysis with varying overhead camera posture angle. Measurement Science and Technology **20** (2009).

[100] Belmont, M., Horwood, J., Thurley, R. & Baker, J. Filters for linear sea-wave prediction. Ocean Engineering **33**, 2332 – 2351 (2006).

[101] Belmont, M., Horwood, J. & Thurley, R. Non-uniform sampling issues arising in shallow angle wave profiling lidar. In Proc. of the IEEE/OES Seventh Working Conference on Current Measurement Technology, 135 – 139 (2003).

[102] Rasband, W. ImageJ (2010). URL http://rsb.info.nih.gov/ij/.

[103] Aalborg University. Wavelab 2.0 (2009).

[104] Davey, T. A. D. Time Domain Stats 5 - a MATLAB tool for wave elevation-time history analysis. Internal Document (2009).

[105] Brodtkorb, P., Johannesson, P., Lindgren, G., Rychlik, I., Rydén, J. & Sjö, E. WAFO - a Matlab toolbox for the analysis of random waves and loads. In Proc. 10th International Offshore and Polar Engineering Conference ISOPE, USA, vol. 3, 343–350 (2000).

[106] Crocker, J. C. & Grier, D. G. The matlab particle tracking code repository (2007). URL http://physics.georgetown.edu/matlab/code.html.

[107] D'Errico, J. Slm - shape language modeling by john d'errico. least squares spline modeling using shape primitives. release: 1.0. MATLAB Central File Exchange (2008).

[108] WAFO group. WAFO - a matlab toolbox for analysis of random waves and loads. tutorial for wafo version 2.5. Tech. Rep., Lund FACULTY OF ENGINEERING CENTRE FOR MATHEMATICAL SCIENCES MATHEMATICAL STATISTICS (2011).

[109] Pitchai, K., Osalusi, E., Ruscoe, J., Side, J., Harris, R., Kerr, S. & Bullen, C. Overview of recent technologies on wave and current measurement in coastal and marine applications **1**, 1–10 (2010).

[110] Danisch, L. A. Bend-enhanced fiber optic sensors. Fiber Optic and Laser Sensors X **1795**, 204–214 (1993).

[111] Danisch, L., Englehart, K. & Trivett, A. Spatially continuous six degree of freedom position and orientation sensor. Sensor Review **19**, 106 – 112 (1999).

[112] Measurand Inc. ShapeTape II User Manual. Tech. Rep., Measurand Inc., Canada (2004).

[113] Mulgrew, B., Grant, P. & Thompson, J. Digital Signal Processing (Palgrave, 2003).

[114] Mathworks Inc. MATLAB Documentation: filtfilt.m. Online, Software (2009).

[115] Mitra, S. K. Digital signal processing : a computer-based approach. McGraw-Hill series in electrical and computer engineering (New York : McGraw-Hill, 1998).

[116] Hartzell, A. L., Da Silva, M. G. & Shea, H. R. MEMs Reliability. MEMS reference shelf (New York ; London : Springer, 2011).

[117] Adams, T. M. & Layton, R. A. Introductory MEMS : fabrication and applications (New York : Springer, 2010).

[118] IEC Technical Committee 70. Degrees of protection provided by enclosures (IP Code). Tech. Rep., IEC (2001).

[119] Lamberti, A. et al. Large-scale measurements of extreme wave loadings on exposed jetties. In Proc. of the HYDRALAB III Joint User Meeting, (Hannover). (2010).

[120] Benoit, M. Practical comparative performance survey of methods used for estimating directional wave spectra from heave-pifh-roll data. In Proc. 23rd International Conference on Coastal Engineering (ICCE). ASCE, vol. 1, 62–75 (1993).

[121] Dyer, C. K. Fuel cells for portable applications. Fuel Cells Bulletin **2002**, 8 – 9 (2002).

[122] Wee, J.-H. Which type of fuel cell is more competitive for portable application: Direct methanol fuel cells or direct borohydride fuel cells? Journal of Power Sources **161**, 1 – 10 (2006).

[123] Smart Fuel Cell (SFC) AG. EFOY Pro Fuel Cell (2010). URL http://www.sfc.com.

[124] Jadoo Power. Jadoo Power N-Gen Fuel Cell Engine (2010). URL http://www.jadoopower.com.

[125] Bastien, S., Sepe, R., Grilli, A., Grilli, S. & Spaulding, M. Ocean wave energy harvesting buoy for sensors. In Energy Conversion Congress and Exposition, (ECCE). IEEE, 3718 –3725 (2009).

[126] Walpert, J., Guinasso, J., N.L. & Lamonte, K. A new generation of TABS II buoy for the Texas Automated Buoy System. In Proceedings of OCEANS, 2005. MTS/IEEE., vol. 3, 2716 – 2721 (2005).

[127] Irish, J., Paul, W., Shaumeyer, J., III, C. G. & Borden, J. The next generation ocean observing buoy in support of NASA's earth science enterprise. Sea Technology **40**, 37–43 (1999).

[128] Sinha, P. et al. Design of a modular, compact, multi-role remotely operated vehicle for sheltered water operations. In Proceedings of OCEANS, 2007. MTS/IEEE., 1 –7 (2007).

[129] ADLINK Technology Inc. Embedded stackable PCI Express: a comparison of two competing standards (2008). URL http://www.adlinktech.com/.

[130] PC/104 Embedded Consortium. PC/104 embedded consortium: PCI/104 express specification (2010). URL www.pc104.org.

[131] Girard. French patent no. 349. patent (1799).

[132] Evans, D. Power from water waves. In Annual Review of Fluid Mechanics, vol. 13, 157–187 (1981).

[133] Salter, S. H. Wave power. Nature **249** (1974).

[134] House of Lords. Alternative energy sources - select committee on the european communities (1988).

[135] Falnes, J. A review of wave-energy extraction. Marine Structures **20**, 185 – 201 (2007).

[136] de O. Falcão, A. F. First-generation wave power plants: Current status and R & D requirements. Journal of Offshore Mechanics and Arctic Engineering **126**, 384–388 (2004).

[137] de O. Falcão, A. F. Wave energy utilization: A review of the technologies. Renewable and Sustainable Energy Reviews **14**, 899 – 918 (2010).

[138] Whittaker, T. Islay LIMPET wave power plant. Tech. Rep., The Queen's University of Belfast (2002).

[139] Falnes, J. Radiation impedance matric and optimum power absorption for interacting oscillators in surface waves. Applied Ocean Research **2**, 75 – 80 (1980).

[140] Valério, D., Beirão, P. & Sá da Costa, J. Optimisation of wave energy extraction with the archimedes wave swing. Ocean Engineering **34**, 2330 – 2344 (2007).

APPENDIX A

Papers Published

Peer Reviewed Conferences

Sellar, B.G., Bruce, T. & Bryden, I.
"Real-Time, Wide Area Wave Field Measurement."
In Proceedings of the 20th International Offshore and Polar Engineering Conference, Beijing, China. (2010)

Sellar, B.G., Bruce, T. & Bryden, I.
"Research within the EPSRC supergen marine energy consortium and the UKERC roadmap for wave and tidal current energy."
International Conference on Sustainable Power Generation and Supply, SUPERGEN '09, Nanjing, China. (2009)

Sellar, B.G., Bruce, T. & Wallace, A.R.
"Providing Sea Surface Elevations for Marine Energy Converters using a Novel Optical Fibre Sensor: Progress in the Flume."
In Proceedings of the 7th European Wave and Tidal Energy Conference, Oporto, Portugal. (2007)

Conferences, Articles and Presentations

Sellar, B.G.,
"Measuring Wave Fields with a Floating Sensor Array."
2nd Annual New England Marine Renewable Energy Center (MREC) Technical Conference, Cambridge, MA, USA. (2010)

Lamberti, A., Martinelli, L., Guerrero, M., Gaeta, G., Allsop, W., Alderson, J., Tirindelli, M., Shepsis, V., Hunt-Raby, A., Sellar, B.G., Bruce, T.
"Large-Scale Measurements of Extreme Wave Loadings on Exposed Jetties."
Proceedings of the HYDRALAB III Joint User Meeting, Hannover. (2010)

Sellar, B.G.,
"Progress update on Measuring Wave Fields with a Floating Sensor Array."
Supergen marine energy consortium Annual Assembly, Edinburgh. (2009)

Sellar, B.G.,
"Progress update on Measuring Wave Fields with a Floating Sensor Array."
Supergen marine energy consortium Annual Assembly, Edinburgh. (2007)

Nguyen, Anh.,
"Getting the Measure of Waves."
The Engineer. (2008)

APPENDIX B

Design and Construction of a 1/4 Scale Sensor Array

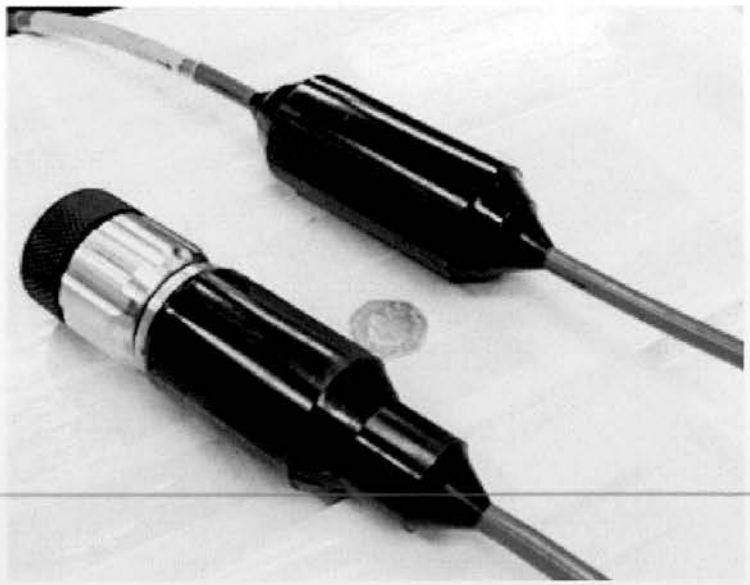

Figure B.1. Fabricated 1/4 scale, fully "marinised" sensor ribbon

B.1 Design and Construction of a 1/4 Scale Sensor Array

This appendix outlines briefly some of the development stages of a 1/4 scale sensor ribbon. Sensor fabrication was completed at the end of the research schedule and has undergone no testing other than "dry tests", including electrical and communication-bus testing, which were carried out upon delivery. It is intended that this sensor will be deployed in a large hydraulic test facility (such as the planned University of Edinburgh FloWave test tank) or open water when an opportunity arises.

When designing a ribbon at a scale greater than those tested in this thesis, and for intended deployment and operation at sea, the main design factors were:

- Survivability
- Suitable size of sensor array
- Modularity
- Remote or semi-remote powering of the array
- Communications with the array

- Manufacturability
  - Cost
  - Lead time
  - Feasibility

B.1.1 Sensor Design Process: Mechanical Design

Mechanical Design

Experience gained in the Edinburgh Flume, Aalborg and Heriot-Watt Basins and the GWK Flume shaped the subsequent 1/4 scale design process. Single cable construction (as opposed to ribbon or multi-cable) was selected. For survivability, individual waterproof canisters were replaced with directly overmoulded sensors. Structural integrity was maintained via continuation of tensile members through the encapsulated sensor regions. Customised off-the-shelf connector technology was used. Ferro-magnetic materials were avoided to allow improved operation of the magnetometer-based orientation sensors, included, as with a previous sensor array configuration, at the beginning and end of the ribbon (see Fig. B.2). Spare capacity for communications and power was included to allow the future connection of one or more sensor ribbons to the tail end of the completed unit. The custom cable, based upon the trade-offs of strength, electrical and signal properties, weight and resistance to sea-water degradation, was designed and procured from a cable manufacturer primarily operating in the oil and gas and military sector.

B.1.2 Sensor Design Process: Electrical Design

An appropriate power supply package is required in order to operate remotely a given sensor design. In order to relay surface elevation measurements to an end-user communications must also be considered. The outcome of preliminary research into these areas are included in the following sections. This preliminary technology survey was conducted with the goal of identifying any technological barriers to

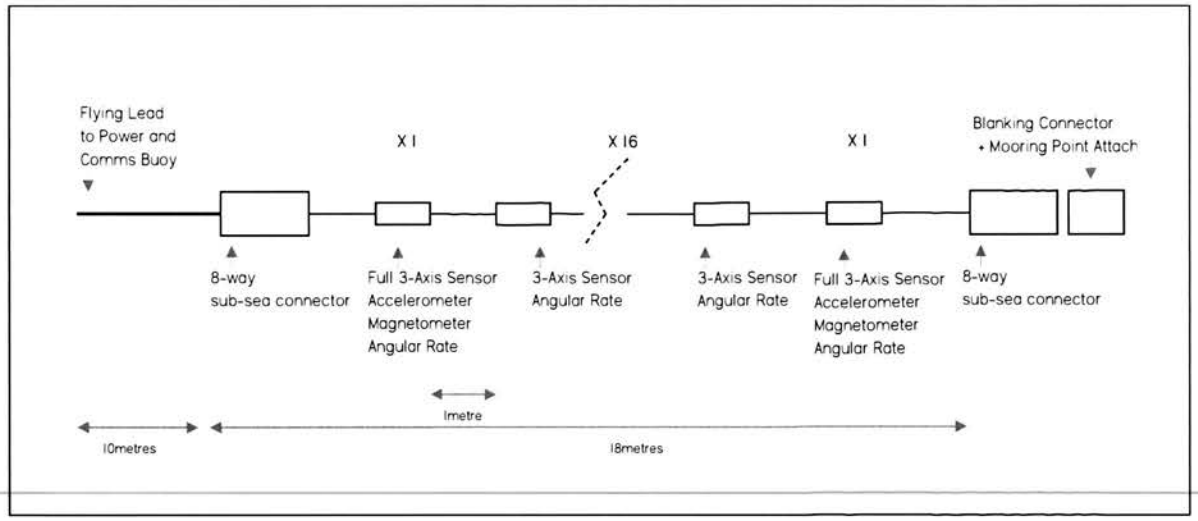

Figure B.2. Final design. 1/4 scale sensor ribbon schematic

sensor deployment, should a ribbon-like sensor array prove feasible during small-scale testing.

Power

In the proximity of a Wave Energy Converter (WEC) farm or other offshore renewable generators an electrical connection could be made to the WECs themselves or associated WEC electrical infrastructure.

For a technology benchmarking exercise or resource assessment, where no electrical infrastructure is available, the sensor array will either have to contain sufficient energy supplies or produce energy in-situ or use a combination of both.

Batteries, Fuel Cells and Small Power Buoys

Batteries

The power capacity of a floating battery pack depends on the size of the host-buoy to which the sensor array could be connected. Traditionally, lead acid batteries connected to above-surface solar panels have been used to power long term deployed ocean weather buoys. Due to the increased sensor density, sampling frequency and communications requirements it is expected that more power would be required.

It is expected that a limited duration field trial (of the order of two to four weeks) could be conducted with a reasonably sized buoy platform (of the order of 1.5 metre diameter) containing multiple lead-acid batteries. Alternatively, a seabed mounted battery pack could provide power via an umbilical to the surface sensor array. Seabed mounting removes the requirement for large-payload capable buoys for extended sensor deployments. Battery technology based on other chemicals, such as Lithium Polymer, whilst offering greater energy density, remain expensive and in some cases pose health and safety risks.

Fuel Cells

A thorough investigation was not conducted but contact was made with several fuel cell manufacturers, each using different technologies. Brief introductions to the role fuel cells could play in portable applications can be found throughout the web and in supplied references [121, 122].

Methanol fuel cells, although technologically advanced and available to consumers, were rejected due to their intolerance to the angles of motion of a buoy. Communications with the manufacturer led to the conclusion that the methanol fuel cells could operate if the excursion angle was below 20° [123]. The environmental impact of methanol fuel cells has also been raised but battery technologies have their own associated hazards, both to people, property and the environment for instance in out-gassing during charge/discharge. These hazards must be suitably managed to minimise risk.

Hydrogen fuel cells may offer benefits over traditional batteries for remote deployed sensors due to their increased energy density and "always available" nature (unlike a battery whose condition can severely degrade over time). In addition fuel cells have the ability to dramatically increase their power output when needed (for instance during an event that requires large data rate transmission hence large radio / modem-driven power loads). Jadoo Power, California, offer promising technology with several products including the N-Gen Fuel Cell Engine at an advanced stage of development and are interested in discussing research projects for remote sensor applications

with research institutions [124].

Power Buoys

Power provided by small heaving buoys is likely to be low, in the region of several Watts [125]. This was deemed inadequate for this application at this stage.

B.1.3 Sensor Design Process: Data Acquisition and Processing

In designing a field-deployable computer package the main considerations were:

- Survivability
- Power consumption
- Ease of operation and integration

The "Mark I" Deployable Computer

Ruggedized computers are commonly used in vehicles, particularly in the military sector. Several companies exist which offer near "off-the-shelf" solutions but their design specifications tend to be narrow, making integration with the sensor packages difficult. In addition, they tend to be prohibitively expensive. Various form factors exist on which to establish a custom computer package. However, after research the PC/104 form factor was selected due to its inherently rugged design and track record in similar environments, being used on various wave buoys and unmanned underwater vehicles [126, 127, 128, 129, 130]. Figure B.3 shows a PC/104 "stack" which was designed, assembled and commissioned during this research. The uppermost card is an Intel Atom 2Ghz, 2Gb ram CPU with all the functionality of a modern laptop including video out, audio, ethernet, multiple USB, PCI-Express, WiFi and built-in GPS. Whilst there are CPUs available with lower power ratings the latest Atom chipset offers the best combination of functionality, usability, integration with existing software (since it runs Windows XP) and much lower power consumption than laptop computers. The device was not tested in the field during this work but

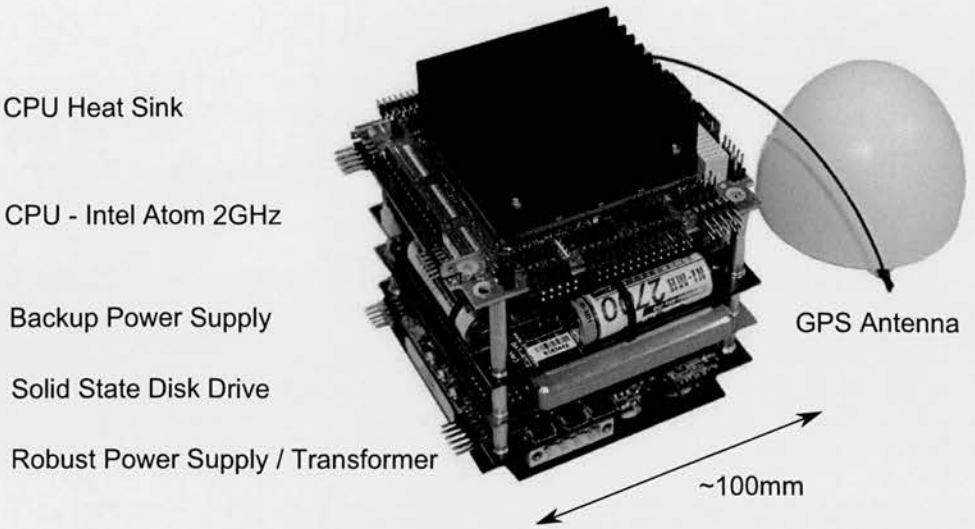

Figure B.3. PC/104 form factor remote sensor array computer

has subsequently been deployed (April 2012) on the Energy Technology Institute (ETI) funded, tidal turbine-based, ReDAPT project - on which the author is the lead researcher at the University of Edinburgh. The PC/104 based device performed well after deployment and recovery around a two month operation at a depth of 25 metres below the surface in the Fall of Warness, Orkney and whilst attached to the top of the 500KW Tidal Generation Ltd. tidal turbine. During deployment the computer acted as a data acquisition system. Images of the computer are shown in figures B.5a and B.5a during commissioning and pre-deployment.

Power Supply

One of the key elements in a ruggedized computer is the power conditioning unit. Prices for this component can typically be comparable to the CPU itself and was the case in this design. Capable of handling highly variable power inputs the transformer supplies 12V, 5V and 3.3V simultaneously to any connected equipment and maintains tight tolerances on the voltage levels. If main power fails at it's input terminals the power supply unit automatically switches over to the secondary battery input and can be set up to communicate with the CPU to provide system status.

Computer Enclosure

The PC/104 stack requires an enclosure to provide waterproofing and mechanical integrity. An "off-the-shelf" container was purchased made from extruded aluminium and machined with slots featuring rubber isolating pads to securely hold the entire PC/104 stack. This container's end-caps are ordered to a connector diagram specification to allow connections to the outside world. The container was oversized to allow for the battery pack to be installed around the PC/104 stack. The battery pack comprises eight 7.2V, 4200mAh NiMh batteries connected to output 14.4V and provide 16.8Ah.

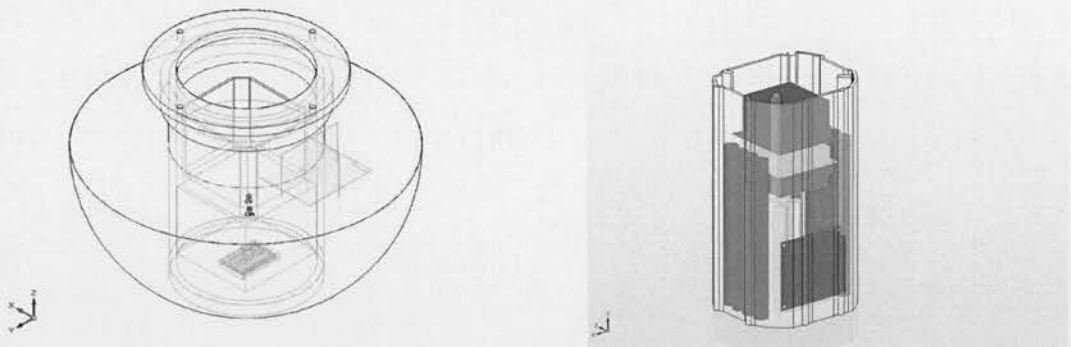

(a) CAD sketch of early design for buoy CPU enclosure

(b) CAD sketch of first concept for small buoy with customised CPU

Figure B.4. Sensor array computer package concept development.

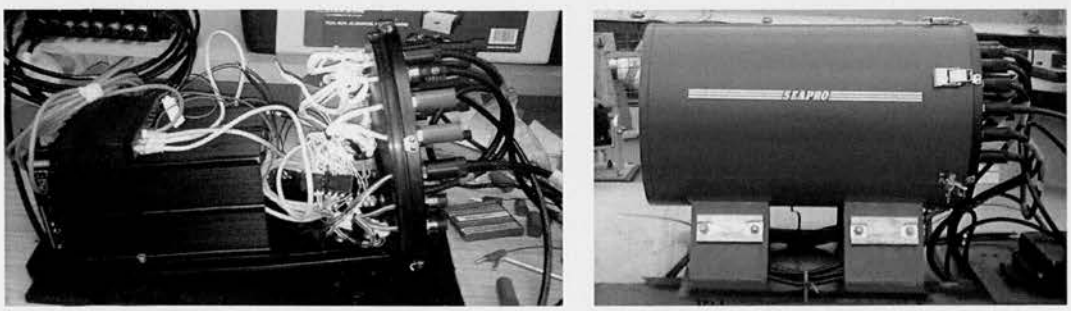

(a) Sensor array computer package configured for insertion in a subsea enclosure.

(b) Sensor array computer package enclosure mounted on tidal turbine prior to deployment, February 2012.

Figure B.5. Sensor array computer package after assembly and prior to deployment.

B.1.4 Identifying "Show Stoppers"

Early investigation of issues likely to pose a risk to the feasibility of deploying a floating sensor array based on the concepts developed in this thesis highlighted no "show stoppers" in the areas of power supply, computing and data acquisition, communication and manufacturability. Experience of data processing suggests further work is required in enabling any real-time system, due to the quantity and complexity of data acquired. In addition, much more work is required in the area of sensor array dynamics and sensor array mooring.

APPENDIX C

Wave Energy Converters: a Brief History and Summary of their Control

C.1 Wave Energy: a Brief History

It is instinctive to believe that the sea contains a large amount of energy and for hundreds of years people have been conceiving methods to harness this. In 1799 in Paris the first patent involving a device designed to extract power from the motion of sea waves was filed by Girard and his son [131]. Small, site specific installations are recorded thereafter. There is a vast array of types/classifications of wave energy devices. Each one tries to extract energy from the motions of the seas in either heave, pitch, surge, sway or a combination of these directions. Some are fixed to the sea bed, others floating and others a compromise between these two locations.

Modern day wave energy dates from the experiments in Japan of Yoshio Masuda in the 1940s in developing now commercialised navigation buoys powered by wave action forcing air through a turbine in the buoy. For an introduction to the field see [132].

(a) Early Edinburgh Wave Group WEC tank testing. 1983

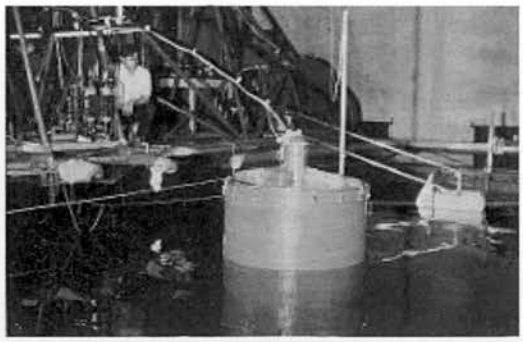

(b) Budal's Type-E Heaving Buoy. 1978

Figure C.1. Pioneering wave energy research in the 1970s and 1980s

C.1.1 The 1973 Oil Crisis

The global oil crisis of 1973 was the pre-cursor to a burst of research in to the conversion of ocean wave energy to electrical energy. Working at the University of Edinburgh, Stephen Salter's experimental research reached a worldwide audience when it was published in the journal Nature [133]. Describing a floating, pitching, cam shaped device which would become known as the Duck, Salter proposed an ambitious array several kilometres long of these devices which would generate power up in to the gigawatts. Many other devices were designed in the UK, [16], but the sudden and controversial reduction in research funding of the early 1980s throttled back the UK's involvement [134, 135]. Salter's work ran parallel to the investigations of Johannes Falnes and Kjell Budal at the Norwegian Institute of Technology in Trondheim. Coming from a background in electromagnetic and plasma physics, Falnes developed a mathematical framework that is often used when dealing with oscillating systems in the ocean environment. In 1985 a large scale prototype WEC was built at Toftestallen near Bergen, Norway based on a tapered channel created in a cliff whose amplification of inrushing waves fills a nearby reservoir. [136, 137].

C.1.2 The Resurgence - 1990 to Early 2000s

An example of one classification of device, the oscillating water column (OWC) is the LIMPET (Land Installed Marine Power Energy Transmitter) completed in 2000

and located at Claddach Farm on the Rhinns of Islay, Islay, Scotland. Developed by Wavegen and Trevor Whittaker of Queen's University Belfast the LIMPET was the world's first wave energy device connected to a national electricity network [138]. A further example is the PICO plant in the Azures (see Fig. C.2).

Ocean Power Delivery (OPD), now Pelamis Wave Power, was founded in 1998 by a group of researchers, led by Richard Yemm, who had worked with the Edinburgh Wave Power group at the University of Edinburgh. Their device development program led through small scale tank tests to trials of individual components (see Fig. C.2). By 2009 Pelamis had secured £40 million in funding and today are the World leaders in terms of deploying prototypes having connected to a national electricity grid an array of three full scale devices in Aguçadoura, Portugal in 2009 (see section C.1.3).

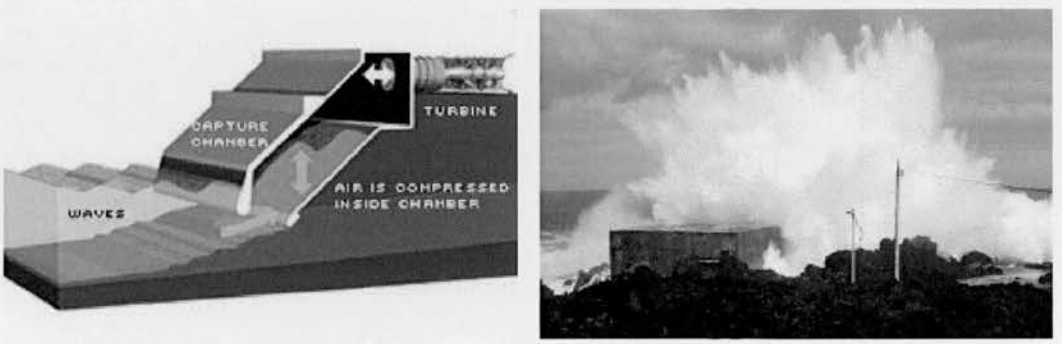

(a) LIMPET Schematic

(b) PICO in Autumn

Figure C.2. Operational and full scale WEC prototypes under construction

The situation in Europe was dramatically changed by the decision made in 1991 by the European Commission to include wave energy in their R & D program on renewable energies. The first projects started in 1992. Since then, about thirty wave energy projects have been funded by the European Commission involving a large number of teams active in Europe.

C.1.3 The State of the Art

In the UK the £28 million WaveHub project, funded by the South West Regional Development Agency, the EU (through the EU Regional Development Fund) and the UK government was completed in summer 2010. Wave Hub provides an area of

sea off the coast of Cornwall, UK, with grid connection and planning consent where arrays of devices can be operated over several years. Four berths are available.

In 2009 the Edinburgh based company Pelamis delivered a world first with the switching on of the Aguçadoura, Portugal, wave energy plant comprising Three Pelamis P1-A 750kW devices. The project was supported by feed in tariffs of approx. €0.23/kWh. Currently the next generation of device, the P2 which is designed largely around improved manufacturability, is being deployed at the European Marine Energy Centre (EMEC) in Orkney, UK (see Fig. C.3a). A further contract for four devices has completed negotiations and will be grid-connected to Orkney.

Also deployed at EMEC is the first full scale prototype of the Oyster device developed by Aquamarine Power (see Fig. C.3b). This relatively simple device is a bottom hinged flap designed to be installed in water depths of around 10m and oscillate forwards and backwards in response to the surging of coastal waves. In February 2010, Aquamarine Power were awarded £5.1m by the UK government to develop Oyster 2, and have since quickly gained ground in the industry.

(a) World's first wave farm, Aguçadoura, 5km north of Porto, Portugal comprising three Pelamis P1 750kW devices.

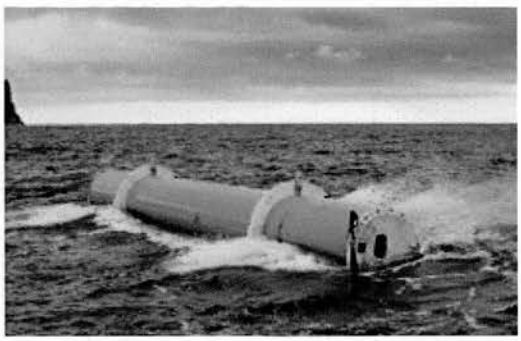

(b) Latest full scale deployment, Oyster ™ in Orkney, UK.

Figure C.3. Latest WEC developments

C.2 Control of Wave Energy Converters

In a system consisting of a water wave incident on a body the wave field can be thought of as existing as four component waves: incident, transmitted, diffracted

and radiated. The incident wave is the wave that would exist at the position of the body if the body was not present. The transmitted wave carries the energy of the incident wave that has not been absorbed. The diffracted wave occurs as a result of the presence of the body and the radiated wave is created due to the body's motions. If the sum of the transmitted, diffracted and radiated waves can be made equal to zero then all of the energy in the incident wave will have been absorbed. Therefore, controlling how the body, a Wave Energy Converter (WEC) for example, reacts to the incident wave field affects how it radiates/generates waves and in turn how much energy it is able to capture [139, 32].

Wave Energy Converters will have a frequency of oscillation at which they are resonant. When this frequency is matched by the driving frequency of incident waves the device's output power will be at a maximum. WEC design including geometry and power take off system will most likely be based around the most dominant wave frequency at the deployment site but for the majority of the time the resonant condition will not be met. As real seas comprise many different frequencies and exhibit non-linearity (as opposed to nice simple sine waves) controlling WEC mechanical behaviour in response to these varying disturbances will be necessary in order to maintain sufficient output power. The increase in efficiency or economic viability resulting from control strategies is as yet unknown. It has been estimated that improvements will be significant, [28, 29], with one author suggesting 1.5 to 3 times increased average energy production [30]. This estimated range has been corroborated with performance gains in the range of 100-330% found in a recent review of a variety of types of control strategies [31].

C.2.1 Survivability and Performance

It is easy to imagine the benefit of advanced prior knowledge of the wave field when considering survivability and reduced fatigue loading. Instructions based on this information could be delivered to the WEC to take actions to reduce the risk of damage, possibly increasing damping of the PTO or changing the relationship with the mooring system or, for example, self-submerging by the use of using buoyancy/ballast

tanks.

Defining the performance of a WEC would require a detailed investigation of the cost/benefits of a multitude of factors. However, three major considerations for being able to pinpoint an improvement in "performance" are in the cost of maintenance of a WEC, the mass of device required and in the quantity of produced electricity, or more generally (not limited to electricity) the amount of energy translated from the kinetic energy of the wave field. All of these considerations could benefit from intelligent WEC control.

A WEC can be designed to be able to change a number of parameters in order to maximise performance. The parameters a WEC may be able to change include position and orientation (and their derivatives) relative to wave field excitations, geometrical exposure to the wave field via actuated surfaces, the degrees of freedom of motion and power take off (PTO) damping force.

WECs of large horizontal size have broad bandwidths, in that they perform relatively well in terms of power captured across a range of frequencies. Point absorbers, on the other hand, whose widths are small compared to the mean wavelength tend to have narrow bandwidths and experience a rapid decay in power output when the incident wave frequency diverges from their natural resonant frequency [28]. However, if the point absorber type of WEC can be sufficiently tuned to capture energy at various frequencies then it offers advantages over it's large and heavy rivals in terms of power captured to volume of device constructed resulting in reduced construction, maintenance and mooring costs.

C.2.2 Control Strategies

Wave field information will likely improve, and in some cases enable, WEC control. Early wave energy research highlighted the potential for control strategy implementation. It is present in the original works of Budal in Trondheim, Norway and Salter in Edinburgh, UK and has continued to be an integral part of the research field [28, 32, 29]. For a more thorough introduction to WEC control strategies, their histories and their implementation good starting places can be found in the publications

of the Edinburgh Wave Power Project and the research of Falnes, Budal and Hals, Barbarit and Clement, Korde, and a recent review-led PhD Thesis on these topics by Price. [33, 34, 35, 36, 37, 38, 39, 16, 40, 41, 30, 42].

Feed-forward Control Algorithms

If the WEC/Wave system is linear (low amplitude waves, low amplitude oscillations, small body size with respect to wavelength) then the forces experienced by the WEC can be decomposed into their component parts. Linear Time Domain control can then be established and applied to irregular wave inputs. Once the linear condition breaks down alternative, more error-prone and sub-optimal techniques are required [41, 30].

In wave energy control feed-forward algorithms aim to predict the incoming exciting force (via measured parameters such as incident wave elevation upstream of the device) so that suitable changes can be made to the WECs PTO or other actuator systems [31]. Categories include complex conjugate control and phase and amplitude control. **Complex Conjugate** control, whilst theoretically "optimal", has several drawbacks including the consequences of high amplitude motions required for high efficiency, the instability it can cause and its non-causal nature: future information of at least one of the physical properties is required.

Latching is a form of *Phase Control* and is one of the easiest methods of control to visualise. Budal's latching method involves the phase of the excitations and velocity of the body being brought together by momentarily fixing or braking the WEC motion and then releasing [32]. In Budal's early experiments (see Fig. C.1b) it was noted that for any wave disturbances other than sinusoidal, advanced knowledge of the incoming wave is required in order to correctly choose the latching point and latching duration. Again, this requirement for future knowledge of wave excitation extends to other methods of control and forms the original motivation for this work [28]. In addition to tuning the phase of the device the amplitude of it's motion must also be controlled to achieve optimal results. There are various methods of achieving this. For optimal control a flexible power take off would be required, able to control the

excursions of the WEC on a wave by wave basis.

An example of *Reactive Control* is in the optimisation experiments conducted on the Salter Duck using a specially designed surging, heaving and pitching test rig. This machine was capable of holding a model Duck during exposure to waves and measuring model displacement, velocity and acceleration. These were electronically fed back having been summed together (after appropriately chosen gains) via motors thus reacting to the waves. In this case, for some of the time, power flow is in the opposite direction to the normal (the generator has been used as a motor to change the state of the device) but allows optimal tuning/control in monochromatic seas. Again without prior knowledge of future wave conditions, when moving to multi-frequency seas, this becomes sub-optimal.

This frequency domain approach (following the Falnes and Budal framework) was conducted within the Edinburgh Wave Power group with the goal of optimising a Duck's performance [33, 34, 35].

Causality

It has been shown that the response of a WEC to multi-frequency waves is non causal and that information of the future wave state is needed to properly predict the interactions , [43]. However, the impact of acausality can be diminished by the fact that moving upstream in a wave field can be thought of as moving ahead in time, i.e., the experienced perturbation is the result of a wave that can be measured some distance ahead/upstream that moves with a known velocity. Provided that at the frequencies under investigation the coherence length of the wave field is sufficient then the disturbance upstream at some starting point in time should be similar in form to the disturbance downstream some distance away at a time in the future. Here downstream is used loosely to imply that a WEC lies ahead of a measuring point and in the mean direction of the wave field [44, 40].

Many control strategies require information on the incoming excitation force which is a result of the wave field both prior, present and future. Blending this information together using a suitable algorithm should provide the excitation force and this can

be used in the control strategy. Papers published on control, as recently as 2009, whilst rigorous and geared to real world WECs, have the underlying assumption that a controller has perfect a-priori information regarding the input to the system - the excitations from the wave field.

In the recent review paper by Hals et al., it was noted that control strategies that underperformed in "future assumed known" simulations, such as latching and it's successor, clutching, when compared to reactive control strategies, performed well with imprecise (*real*) input data. Another advantage of these strategies is that by being non-reactive they do not require large, heavily over-rated energy storage/supply that can send power in reverse to the ocean to change their state [31].

C.2.3 Control Strategy in the Context of this Work

It is the author's opinion that optimal control is, at present, a distraction since a WEC exposed to any type of wave other than a perfectly linear, sinusoidal wave (which does not exist in the laboratory let alone the outside world) and in the presence of imperfect information relating to wave field, body motion and other physical quantities, will not behave in the way predicted by a model. The likely scenario of limited wave field information and body motion information, both containing a relatively large degree of error (compared to laboratory measurements), will lead to sub-optimal control algorithms being used that have been demonstrated to give an advantage to the device operators. These will likely be improved over time for a device design that has been produced in line with the multitude of real-world, external drivers including Intellectual Property rights, financial structuring, second-mover advantage and stakeholder interests etc.

More pragmatic approaches are emerging concentrating on deployment, operation and final cost per kw as opposed to maximum efficiencies and maximum theoretical controllability [45]. And the design of the Pelamis, the industry leading design puts survivability as the primary design goal [46].

> The device must be designed with survivability as the key objective, then effective ways of improving power capture must be found.
>
> Richard Yemm, Pelamis Wave Power Ltd.

Recent research on the Archimedes Wave Swing, a submerged point absorber WEC, suggests that since optimal control strategies, in real life, can not be implemented without approximations and modifications their theoretical advantages are reduced and other methods should be investigated. This research also highlights the need for improved methods of providing control strategies with wave field information. [140].

Designing a sensor array that can provide device designers and operators with improved information on the wave field in which their devices will operate could prove one stage in the process of continued improvement of WEC technology and associated control strategies.